Supercritical Water Gasification of Lignocellulosic Biomass Materials for Hydrogen Production

A Thesis Submitted to the
College of Graduate and Postdoctoral Studies
In Partial Fulfillment of the Requirements
For the Degree of Doctor of Philosophy
In the Department of Chemical and Biological Engineering
University of Saskatchewan
Saskatoon

By

JUDE AWELE OKOLIE

PERMISSION TO USE

In presenting this thesis/dissertation in partial fulfillment of the requirements for a Postgraduate degree from the University of Saskatchewan, I agree that the Libraries of this University may make it freely available for inspection. I further agree that permission for copying of this thesis/dissertation in any manner, in whole or in part, for scholarly purposes may be granted by Professor Ajay Kumar Dalai who supervised my thesis/dissertation work or, in their absence, by the Head of the Department or the Dean of the College in which my thesis work was done. It is understood that any copying or publication or use of this thesis/dissertation or parts thereof for financial gain shall not be allowed without my written permission. It is also understood that due recognition shall be given to me and to the University of Saskatchewan in any scholarly use which may be made of any material in my thesis/dissertation.

Requests for permission to copy or to make other uses of materials in this thesis/dissertation in whole or part should be addressed to:

Head of the Department of Chemical and Biological Engineering

57 Campus Drive

University of Saskatchewan

Saskatoon, Saskatchewan S7N 5A9 Canada

or

Dean

College of Graduate and Postdoctoral Studies

University of Saskatchewan

116 Thorvaldson Building, 110 Science Place

Saskatoon, Saskatchewan S7N 5C9, Canada.

ABSTRACT

The primary aim of this research is to optimize supercritical water gasification process operating conditions and develop a cost effective heterogeneous catalyst to reduce reaction temperature and improve H_2 yield. Furthermore, a detailed techno- economic feasibility study was performed to evaluate the economic feasibility of SCWG process. The work plan is divided into five phases.

In the phase one, model lignocellulosic biomass comprising of cellulose, hemicellulose and lignin were selected as the feedstock for SCWG process optimization. The objective of the study was to optimize the process conditions, propose a detailed reaction pathway for model compounds and understand how each intermediate product behaves under subcritical and supercritical conditions. The response surface methodology using the Box-Behnken design was applied for the first time to optimize the process parameters during subcritical and supercritical water gasification of cellulose. The process parameters investigated include temperature (300-500 °C), reaction time (30-60 min) and feedstock concentration (10-30 wt%). Temperature was found to be the most significant factor that influenced the yields of hydrogen and total gas yield. Among the three model compounds, hydrogen yields increased in the order of lignin (0.73 mmol/g) < cellulose (1.95 mmol/g) < xylose (2.26 mmol/g). Based on the gas yields from these model compounds, a reaction pathway of model lignocellulosic biomass decomposition in supercritical water was proposed.

The results from the first phase raised several research questions, for example, does biomass heterogeneity have an effect on product yield? How far are the batch experimental results from equilibrium values when considering a real feedstock? Lignocellulosic biomass is heterogeneous in nature and it comprises of several molecules of different compounds including

cellulose, hemicellulose, and lignin along with extractives. Lignocellulosic biomass (soybean straw and flax straw) were gasified under similar conditions as those of the model compounds in Phase two. Soybean straw exhibited superior H_2 yield (6.62 mmol/g) and total gas yield (14.91 mmol/g). Similarly, the gaseous products from soybean straw showed improved lower heating value (1592 kJ/Nm^3). The experimental results showed slight deviations from the thermodynamic models which could be as a result of temperature gradient and absence of agitation in the batch reactor.

In the third phase, several Ni-based catalysts were screened and tested for SCWG of soybean straw. The aim is to develop a cost-effective heterogeneous catalyst that could improve the gas yields towards equilibrium values and lower the reaction temperature. All experiments were performed at the desired operating conditions identified in Phase 2. A comprehensive screening of different support materials ranging from activated carbon (AC), carbon nanotubes (CNT), ZrO_2, Al_2O_3, SiO_2 and Al_2O_3-SiO_2 was performed at 10 wt% Ni loading. The effectiveness of each support in improving H_2 yield, and selectivity was in the order: ZrO_2 > Al_2O_3 > AC > CNT > SiO_2 > Al_2O_3-SiO_2. The effect of three promoters (i.e., Na, K and Ce) added to the supported Ni/ZrO_2 catalysts was evaluated. Ce promoter was found to be the best for ZrO_2 supported Ni catalysts. The performance of Ce was attributed to its high capacity for storing oxygen species which have the ability to react with the carbon deposits on the surface of the catalysts thereby preventing carbon deposition.

The objective of the fourth phase was to study the kinetics of Ni - Ce/ZrO_2 catalyzed SCWG of soybean straw. The lumped parameter kinetics method was employed with several reactions resulting from the experimental results in Phase three and the proposed reaction pathway in Phase one. The pathways were used to develop the kinetic equations. Kinetic model results were

found to correlate with experimental results. Furthermore, the kinetic model was used to predict experimental yields for long residence time. The kinetics results are also in agreement with thermodynamic predictions.

In the last phase, a detailed techno-economic evaluation and sensitivity analysis was performed for a conceptual design for hydrogen production from soybean straw gasification in SCW. The economic feasibility of hydrogen production was evaluated based on a discounted cash flow analysis. Economic analysis suggested a minimum selling price of U.S. $1.94/kg for hydrogen. The cost is relatively low when compared with that of hydrogen produced from other biomass conversion processes. Besides, the net rate of return (NRR) estimated was 37.1%. A positive NRR value indicates that the project is profitable from an economic perspective. Sensitivity analysis indicates that the minimum selling price of hydrogen is affected by the feedstock price, utility cost, tax rate and labor cost.

ACKNOWLEDGEMENTS

I would like to express my sincere appreciation to my Ph.D. supervisors, Dr. Ajay Dalai, and Dr. Janusz Kozinski, for their support and guidance during my Ph.D. studies. Their constant encouragement and mentorship ensured that I completed this thesis in due time.

My deepest gratitude goes to the members of my Ph.D. advisory committee, Dr. Catherine Niu, Dr. Venkatesh Meda, Dr. Lope Tabil and Dr. Martin Reaney and the external examiner Dr. Ramin Farnood. Their review, constructive comments and suggestions helped to improve the quality of my thesis. I would also like to thank Dr. Nanda for his guidance. Dr. Sonil helped me with the experimental set up. He also provided insightful suggestions and contributed immensely towards improving this thesis.

I would also like to extend my thanks to Mr. R. Lee Prokopishyn, Ms. Heli Eunike, Ms. Alivia Mukherjee, Mr. Girish Kamath, Ms. Rachita Rana, Dr. Venu Babu Borugadda, Dr. Philip Bohene, Dr. Epelle Emmanuel and Mr. Biswa Patra for their technical assistance at the Catalysis and Chemical Reaction Engineering Laboratory (CCREL).

Special thanks to my mother, Mrs. Anthonia Okolie and my mother-in-law, Mrs. Lorna Hanishewski for their constant support and motivation. I would like to thank Pastor Emmanuel and every member of Christ Embassy Saskatoon, for always believing in me. I would like to express my sincere gratitude to my friends Ejalonibu Hammed, Jude Dugbere, Stephen Owuamanam, Bankole Peter, Nosakhare Osemwota and Afees Ayandiran for their kindness and support.

Finally, I am grateful to the financial supporters of my research including the Natural Sciences and Engineering Research Council of Canada (NSERC) and BioFuelNet.

DEDICATION

This thesis is dedicated to:

God Almighty for his benevolence and his guidance throughout my studies.

My late father Mr. Peter Okolie, for always believing in me. He never gave up on me and my dreams.

My wife, Mrs. Brittney Okolie for her ever-present support and my son, Pete Okolie, who came to our lives with a bundle of joy.

TABLE OF CONTENTS

LIST OF TABLES

LIST OF FIGURES

LIST OF ABBREVIATIONS

AC	Activated carbon
AOE	Total annual production cost
ANOVA	Analysis of variance
ASTM	American society for testing and materials
BBD	Box - Behnken design
BET	Brunauer-Emmett-Teller method
BMC	Bare module cost
BTW	Biomass to water ratio
CCD	Central composite design
CGE	Carbon gasification efficiency
CEPCI	Chemical engineering plant cost index
CNT	Carbon nanotubes
DBEP	Discounted break-even point
DCFR	Discounted cash flow rate of return
DOE	Design of experiments
EOS	Equation of state
FCI	Fixed capital investment
FID	Flame ionization detector
FTIR	Fourier transform infrared spectroscopy
HHV	Higher heating value
HS	Hydrogen selectivity
IRR	Internal rate of return

LC	Land cost
LCA	Life cycle assessment
LHV	Lower heating value
NC	Non-conventional
NPV	Net present value
NRR	Net rate of return
ODEs	Ordinary differential equations
PBP	Payback period
RK	Redlich-Kwong
RSM	Response surface methodology
SCW	Supercritical water
SCWG	Supercritical water gasification
TCD	Thermal conductivity detector
TCI	Total investment capital
TEA	Techno-economic analysis
TG/DTG	Thermogravimetry/derivative thermogravimetry
TPR	Temperature programmed reduction
WC	Working capital
WGSR	Water gas shift reaction
XRD	X-ray diffraction

LIST OF NOMENCLATURE AND SYMBOLS

Q	Heat of decomposition, kJ
C_T	Total capital, U.S.$
ɔ	Carbon conversion, %
ΔG	Free energy of activation, $kJ.mol^{-1}$
k_1	Forward reaction rate constant for steam reforming reaction
k_2	Forward reaction rate constant for intermediate decomposition to CO
k_3	Forward reaction rate constant for intermediate decomposition to CO_2
k_4	Forward reaction rate constant for intermediate decomposition to CH_4
k_5	Forward reaction rate constant for water gas shift reaction
k_6	Forward reaction rate constant for methanation reaction
k_7	Forward reaction rate constant for the formation of liquid products
C_{Error}	Error function
C_{cal}	Calculated results from kinetics model
C_{Exp}	Experimental results used to fit the kinetic models
L_{int}	Intermediate liquid products
T	Reaction temperature, ^oC
P	Reaction pressure, MPa
rCO	Rate of generation of CO, $mmol.min^{-1}.L^{-1}$
rH_2	Rate of generation of H_2, $mmol.min^{-1}.L^{-1}$
rCO_2	Rate of generation of CO_2, $mmol.min^{-1}.L^{-1}$
rCH_4	Rate of generation of CH_4, $mmol.min^{-1}.L^{-1}$

r_{liquid}	Rate of generation of liquid products, $mmol.min^{-1}.L^{-1}$
$r_{Biomass}$	Rate of biomass decomposition, $mmol.min^{-1}.L^{-1}$
r_w	Rate of water decomposition, $mmol.min^{-1}.L^{-1}$
Yi	H_2 yield in multiple regression equation, mmol/g
C	Feedstock concentration, wt%
R_t	Reaction time, min

Chapter 1 Introduction

1.1 Introduction

Hydrogen is a clean fuel that can be processed into other fuels. The combustion of hydrogen produces water as the only end product. Hence, hydrogen utilization is widely regarded as being environmentally benign. Hydrogen is produced commercially from the electrolysis of water or through steam reforming of methane (Levin et al., 2004). Presently, steam reforming of methane is the most preferred industrial method of producing hydrogen with an estimated efficiency of about 85%; it provides up to half of the total hydrogen used industrially (Chaubey et al., 2013). Biomass is a potential source of hydrogen. However, research areas involving hydrogen production from biomass is still at its development stage as none of the technologies has been commercialized. Furthermore, the demand for hydrogen is projected to rise progressively in the future because hydrogen is used as a transportation fuels, in the refining of oil sands and the hydrotreating of crude oil containing high sulfur contents to meet the stringent environmental regulations on the maximum permissible level of sulfur in gasoline and diesel (Levin and Chahine, 2010).

Supercritical water gasification (SCWG) of biomass to produce hydrogen could help overcome the limitations of traditional biomass gasification technologies such as expensive drying requirements and low hydrogen production rate. However, the technology is not yet applied industrially because of some disadvantages such as high processing cost together with plugging and corrosion problems (Deniz et al., 2015). Therefore, extensive research effort is necessary to overcome the limitations. Several studies have reported the gasification of biomass model compounds; however, few studies have investigated the gasification of real biomass compounds. It is essential to use actual biomass compounds as feedstock for SCWG to study the effects of

biomass heterogeneity and complexity (Kumar et al., 2016). Also, the development of novel heterogeneous catalysts is important to reduce the reaction temperature and operating cost. In addition, a detailed kinetics and techno- ecocnomic analysis of SCWG process is required in order to make future decisions regarding commercialization.

To fulfill the knowledge gap, this Ph.D. research aims to propose a detailed reaction mechanism for SCWG and study the interactions between various components present in biomass compounds and the effect of their structure on gas yield. Also, novel heterogeneous catalysts will be synthesized and tested for SCWG processes. Finally, a detail techno-economic analysis and sensitivity analyis will be performed on a conceptual design of SCWG to ascertain the economic feasibility of SCWG process. Based on the literature review which is presented in chapter 2, the following knowdge gaps, hypotheses, research objectives and sub-objectives are stated.

1.2 Knowledge Gaps

A comprehensive literature review was carried out for the SCWG of several feedstocks and the knowledge gaps are outlined below.

1. Most experimental studies on SCWG are carried out using biomass model compounds because of the complex nature of real biomass. However, few studies have investigated the gasification of biomass model compounds representing cellulose, xylose and lignin over a wide range of operating conditions. Also, studies on how biomass components impact gas composition and hydrogen yield during SCWG is scarce in literature.
2. To date, studies investigating hydrogen production from the gasification of biomass such flax straw and soybean straw in supercritical water are missing from literature.

3. Studies to identify the most appropriate heterogeneous catalysts with different supports and promoters during the SCWG of flax straw and soybean straw is missing from the literature.
4. To the best of our knowledge, no study has reported a detailed kinetic and techno-economic studies of the SCWG of the above biomass.

1.3 Hypothesis

Based on the above knowledge gaps, the following hypotheses are stated:

1. SCWG of biomass model compounds such as cellulose, xylose, and lignin over a wide range of operating conditions will reflect their suitability for hydrogen production. Also, the gasification of combined model compounds to mimic real biomass could provide a clear understanding of how biomass properties impact gas yield.
2. Identification of the optimal process parameters during the gasification of flax straw and soybean straw could improve hydrogen yield. Similarly, the study of the combined effect of process parameters will help understand the interactions of operating parameters for the SCWG process.
3. Identification of the appropriate heterogeneous catalyst, together with the support and promoters could help improve the hydrogen yield, lower the reaction temperature and operating cost of the process.
4. Kinetic studies of SCWG of real biomass compounds will help in the design of a commercial SCWG process while techno – economic analysis would help to ascertain the economic feasibility of the overall SCWG process.

1.4 Research Objectives

The main research of this Ph.D. work is to evaluate the potential of different lignocellulosic biomass as feedstock for SCWG, maximize hydrogen-rich gas production from the materials and determine the economic feasibility of SCWG process. To meet the overall research objectives several research sub – objectives have been performed based on figure 1.1. The following sub – objectives of the research work in each phase are described below.

Fig 1.1 : Schematics of different research phases in this thesis.

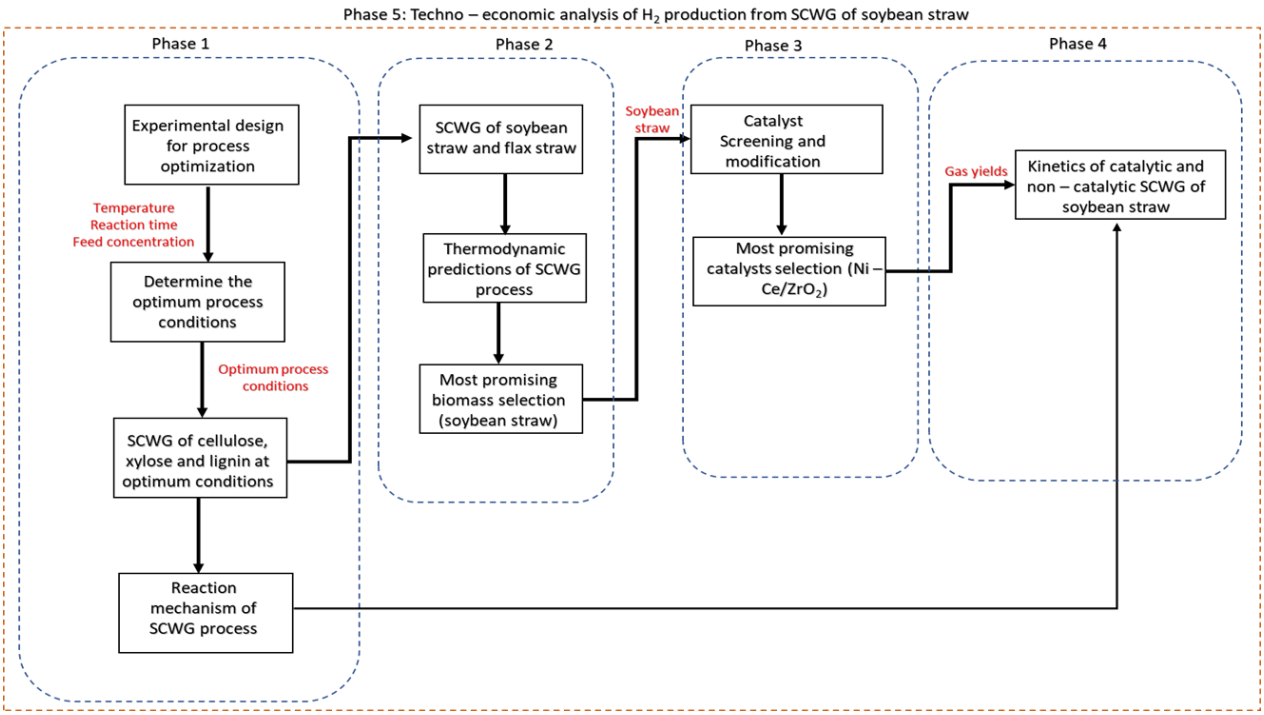

Phase 1*: To investigate how experimental factors, influence product gas composition and hydrogen yields during SCWG of model compounds representing cellulose, hemicellulose, and lignin. The factors are the experimental conditions (Temperature, reaction time, Feedstock concentration) and the interactions between them.*

- Use of Box – Behnken design to study the influence of reaction parameters on hydrogen yield.
- Comparative evaluation of product yield and decomposition behavior of cellulose, xylose, and lignin in supercritical water.

Phase 2*: To optimize hydrogen yield from SCWG of Flax straw and Soybean straw and study the effects of process parameters such as temperature, pressure BTW ratio and reaction time on hydrogen yield.*

- Characterize the biomass feedstock and correlate their performance during SCWG with their physico chemical properties.
- Compare the experimental gaseous yields with theoretical values.

Phase 3*: To identify the best heterogeneous catalyst with a comprehensive screening of different support and promoters during the SCWG of biomass with the highest hydrogen yield based on the results of phase 2.*

- Preparation and screening of a series of supported Ni catalysts (the support includes activated carbon (AC), Carbon nanotubes (CNT), ZrO_2, Al_2O_3, SiO_2 and AL_2O_3-SiO_2) and promoters (Na, K and Ce).
- Catalyst characterization and evaluation of the stability and catalytic performance during SCWG.

Phase 4*: Perform kinetics studies of a catalytic SCWG process for the best catalysts in phase 3.*

- Develop a kinetic model to predict gaseous yield during SCWG of lignocellulosic biomass and determine the evolution of the system with time.

- Determine the thermodynamic parameters and possible reaction mechanism.

Phase 5: *Perform a detailed techno – economic analysis for a heterogeneous catalyzed SCWG process for hydrogen production.*

- Design and simulate a detailed process for the conversion of the best biomass in Phase 3 to hydrogen rich syngas through SCWG process.
- Conduct a detailed techno – economic studies and sensitivity analysis of the SCWG process.

1.5 Organization of the Thesis and Manuscript Content

This thesis is organized based on the manuscript – style thesis guidelines of the College of Graduate and Postdoctoral studies at the University of Saskatchewan. The thesis starts with a general overview of the research background, introduction to the subject matter, knowledge gaps, hypothesis, and research objectives. Then, in Chapter 2, a detailed literature review based on three published review articles are provided.

Specifically, **Chapter 2** is written based on the following published articles:

- Okolie, J. A., Rana, R., Nanda, S., Dalai, A. K., & Kozinski, J. A. (2019). Supercritical water gasification of biomass: a state-of-the-art review of process parameters, reaction mechanisms and catalysis. Sustainable energy & fuels, 3(3), 578-598.
- Okolie, J. A., Nanda, S., Dalai, A. K., Berruti, F., & Kozinski, J. A. (2020). A review on subcritical and supercritical water gasification of biogenic, polymeric and petroleum wastes to hydrogen-rich synthesis gas. Renewable and Sustainable Energy Reviews, 119, 109546.

- Okolie, J. A., Epelle, E. I., Nanda, S., Castello, D., Dalai, A. K., & Kozinski, J. A. (2021). Modeling and process optimization of hydrothermal gasification for hydrogen production: A comprehensive review. The Journal of Supercritical Fluids, 105199.

Chapter 3 explains the experimental set – up and some indicators for comparing gaseous yields. Furthermore, in Chapter 3, different sources of experimental error and process safety challenges were outlined.

Chapter 4 investigates how the experimental factors influence product gas composition and hydrogen yields during SCWG of model compounds representing cellulose, hemicellulose, and lignin. This chapter is written based on:

- Okolie, J. A., Nanda, S., Dalai, A. K., & Kozinski, J. A. (2020). Optimization and modeling of process parameters during hydrothermal gasification of biomass model compounds to generate hydrogen-rich gas products. International Journal of Hydrogen Energy, 45(36), 18275-18288.

Chapter 5 compares the decomposition behaviour of real lignocellulosic feedstock (soybean straw and flax straw) in SCW. Furthermore, the experimental results were compared with theoretical values obtained from thermodynamic calculations. This chapter is written based on:

- Okolie, J. A., Nanda, S., Dalai, A. K., & Kozinski, J. A. (2020). Hydrothermal gasification of soybean straw and flax straw for hydrogen-rich syngas production: Experimental and thermodynamic modeling. Energy Conversion and Management, 208, 112545.

Chapter 6 aims to select the best heterogeneous catalysts to improve hydrogen yield and selectivity during SCWG of the most promising biomass feedstock in chapter 5. A comprehensive screening of different supports and promoters for Ni – based catalysts are performed. The chapter

is written based on a manuscript which is accepted for publication in Industrial & Engineering Chemistry Research Journal.

Chapters 7 explains the kinetics of catalytic and non – catalytic gasification of lignocellulosic feedstock in SCW. The kinetics reactions are developed based on the experimental results in chapter 6. The kinetics predictions were compared with experimental results in chapter 6 and the theoretical values. This chapter **will** be submitted for publication in a journal.

Chapter 8 proposes a conceptual design for the production of hydrogen from SCWG of lignocellulosic biomass feedstock. A detailed techno – economic studies and sensitivity analysis was performed. This chapter is written based on:

- Okolie, J. A., Nanda, S., Dalai, A. K., & Kozinski, J. A. (2021). Techno-economic evaluation and sensitivity analysis of a conceptual design for supercritical water gasification of soybean straw to produce hydrogen. Accepted for publication in Bioresource Technology.

Chapter 9 provides an overall conclusions and suggestions for future research in this field of study. The references from all the chapters are provided in the reference section. In addition, all supporting information and data used in this research are collected in the appendices section.

It should be mentioned that the original manuscripts have been modified for inclusion in this thesis. The introduction and discussion parts were simplified or extended where required.

Chapter 2 Literature Review

This section provides an overview of the SCWG technology as a means of valorizing organic waste materials for hydrogen production. The unique properties of water under supercritical conditions are also described. A review of different operating conditions affecting the SCWG technology is also outlined in this section. The contents of this chapter have been published as review articles in the following journals. Sustainable energy & fuels, Renewable and Sustainable Energy Reviews and The Journal of Supercritical Fluids.

Citation:

- Okolie, J. A., Rana, R., Nanda, S., Dalai, A. K., & Kozinski, J. A. (2019). Supercritical water gasification of biomass: a state-of-the-art review of process parameters, reaction mechanisms and catalysis. Sustainable energy & fuels, 3(3), 578-598.
- Okolie, J. A., Nanda, S., Dalai, A. K., Berruti, F., & Kozinski, J. A. (2020). A review on subcritical and supercritical water gasification of biogenic, polymeric and petroleum wastes to hydrogen-rich synthesis gas. Renewable and Sustainable Energy Reviews, 119, 109546.
- Okolie, J. A., Epelle, E. I., Nanda, S., Castello, D., Dalai, A. K., & Kozinski, J. A. (2021). Modeling and process optimization of hydrothermal gasification for hydrogen production: A comprehensive review. The Journal of Supercritical Fluids, 105199.

Contribution of the Ph.D. Candidate

Jude: Conceptualization, writing the manuscript and providing response to reviewers' comments.

Ms. Rachita Rana: Conceptualization and Manuscript writing.

Dr. Sonil Nanda: Conceptualization, reviewing the manuscript and providing response to reviewers.

Dr. Emmanuel I. Epelle: Manuscript writing and reviewing.

Dr. Daniele Castello: Manuscript writing and reviewing.

Dr. Ajay K. Dalai and Dr. Janusz A. Kozinski coordinated the manuscript preparation and provided overall supervision of the research.

2.1 Introduction

The concerns over the environmental pollution caused by fossil fuels along with their rising prices seem to be alarming. It has become imperative to explore new technologies that can aid in the production of environmentally friendly yet reliable energy resources. Organic waste residues in the form of forest and agricultural biomass, energy crops, microalgae, municipal solid wastes, sewage sludge, cattle manure etc. are abundantly available throughout the world and have tremendous potential to be used as feedstocks to produce biofuels (Nanda et al., 2015b) . These waste substrates can be converted to fuel products through biochemical technologies (e.g. fermentation and anaerobic digestion) and thermochemical technologies (e.g. pyrolysis, liquefaction, gasification and torrefaction) (Nanda et al., 2015a). Specific green fuels products are also obtained from these different technologies. For example, biomass pretreatment and fermentation mostly result in bioethanol and biobutanol using suitable bacterial or fungal species while anaerobic digestion chiefly generates methane by methanogenic bacteria. Bio-oil is the main product of interest from pyrolysis and liquefaction, whereas synthesis gas (H_2 and CO) is the chief fuel product from gasification (Ren et al., 2018).

Biomass is one of the most plentiful renewable resources on the earth and is regarded as a potential raw material to produce sustainable biofuels and value-added chemicals (Tumuluru et

al., 2011). The fuels produced from waste plant residues are considered carbon neutral because they do not lead to any greenhouse gas emission and accumulation in the atmosphere. Waste plant biomass not only provides renewable carbon for conversion to biofuels but also fixes CO_2 in the atmosphere through photosynthesis. Lignocellulosic biomass provides about 14% of the overall primary energy supply globally, although it supplements about 40–50% of the energy demand in some developing countries (Qian et al., 2007).Lignocellulosic biomass, as the name suggests, consists of three primary functional compounds with different chemical structure and weight fractions, namely cellulose (35–55 wt%), hemicellulose (20–40 wt%) and lignin (10–25 wt%) (Nanda et al., 2013). Extractives and ash are also present in smaller quantities in the lignocellulosic biomass. Extractives are the non-structural component of biomass soluble in water or neutral organic solvent (hexane and ethanol). They usually contain biopolymers such as fats, lipids, steroids, terpenoids, wax and phenolic compounds (Nanda et al., 2013).

Supercritical water gasification (SCWG) is a promising hydrothermal technology for transforming waste biomass to hydrogen-rich syngas at high temperatures and elevated pressures. The supercritical state of water exists at pressures and temperatures above the critical point of water wherein water has no distinct liquid or gaseous phase (Reddy et al., 2015). Supercritical water (SCW) possesses the dissolution properties of liquids and the diffusion properties of gases. There is no surface tension during the supercritical state of water as there is no liquid and gas phase boundary, as both the phases co-exist (Reddy et al., 2015).Water beyond its critical pressure of 22.1 MPa and critical temperature 374 ^{o}C attains improved mass transfer and solvation properties. Along with high diffusivity like gases and viscosity of a liquid, low dielectric constant is extremely favorable for the use of SCW (Basu and Mettanant, 2009; Kritzer, 2004). The viscosity and

diffusivity of SCW enhance the reaction rates and enforces particle collision thus contributing in many chemical reactions.

Hydrothermal gasification (or SCWG) is beneficial over the traditional thermochemical gasification in many ways. When biomass contains high moisture, the process of thermochemical gasification becomes inefficient as the heat of evaporation of the liquid overshadows the heat of combustion of the solid substrate. In such cases, gasification requires drying and pretreatment of biomass adding extra cost to the process economics. However, the large amount of heat required to dry the feedstock makes the entire process inefficient. The rate of reaction is rapid in the case of SCWG than other gasification treatments.

The major application of SCW is found in the gasification of waste biomass and organics to produce hydrogen. The product distribution from SCWG varies largely depending on the process variables such as temperature, pressure, residence time, feed concentration (or biomass-to-water ratio), biomass particle size, reactor configurations and presence of catalyst. Most of the reports on SCWG of biomass currently available in the literature presents scholarly work with inadequate reviews. The current chapter aims to review the impacts of these SCWG process parameters on the gas product yields, gasification efficiency, carbon conversion efficiency, hydrogen selectivity and other attributes. Moreover, most of the accessible information on catalysts involved in SCWG of biomass is scattered. This chapter also compiles the available literature on different homogeneous and heterogeneous catalysts as well as catalyst support. applied in SCWG and reviews their reaction mechanisms, performance, and activity.

2.2 Subcritical and Supercritical Water Gasification

Water above its critical temperature and critical pressure is known as supercritical water (SCW). On the contrary, subcritical water exists when the pressure is above its saturation value

while its temperature could be either near or below critical values. SCW exhibits high mass transfer and improved miscibility of the organic solvent because of its unique thermo-physical properties. The density, ionic product, viscosity, and dielectric constant of water at supercritical conditions show some special characteristics that facilitate its ability to effectively hydrolyze complex organic substrates.

Figure 2.1 shows the phase diagram of pure water. At ambient conditions (i.e., room temperature), water exists in liquid state while at its freezing point (0 °C) and boiling point (100 °C), water converts to ice and steam. However, when the temperature and pressure of water exceeds above its critical point i.e., 374.1 °C and 22.1 MPa, water forms supercritical water (SCW). On the other hand, subcritical water (SbCW) occurs at temperatures below or near the critical temperature and at a pressure above the saturation pressure (Basu and Mettanant, 2009).

At supercritical conditions, water exhibits a unique property that makes it suitable for waste biomass gasification and oxidation (Byrd et al., 2008). The physicochemical properties of water such as density, viscosity, ionic products and dielectric constant exhibit great variations at liquid and fluid state (subcritical and supercritical) as shown in Figure 2.2. At ambient condition (25 °C and 0.1 MPa), liquid water is an optimal polar solvent due to its high dielectric constant of about 80. Water can dissolve many complex organic compounds, hydrocarbons, and gases in supercritical conditions (Cheng and Ye, 2010; Yakaboylu et al., 2015).

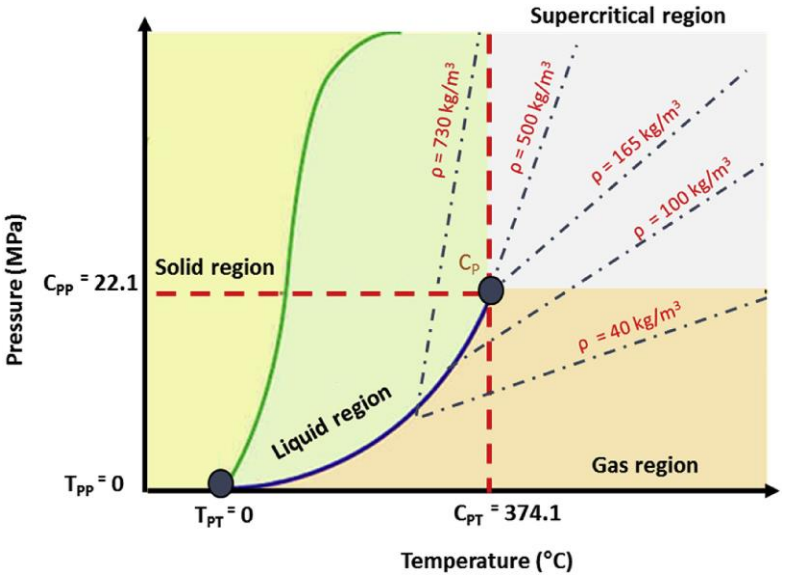

Figure 2.1: Phase diagram of pure water. TP and CP represent the triple and critical points of water, respectively. CPP and CPT are the critical pressure and temperature of water while TPP and TPT represent the triple point pressure and temperature, respectively. The density is represented by ρ. The dotted lines illustrate some isochoric curves with their respective density.

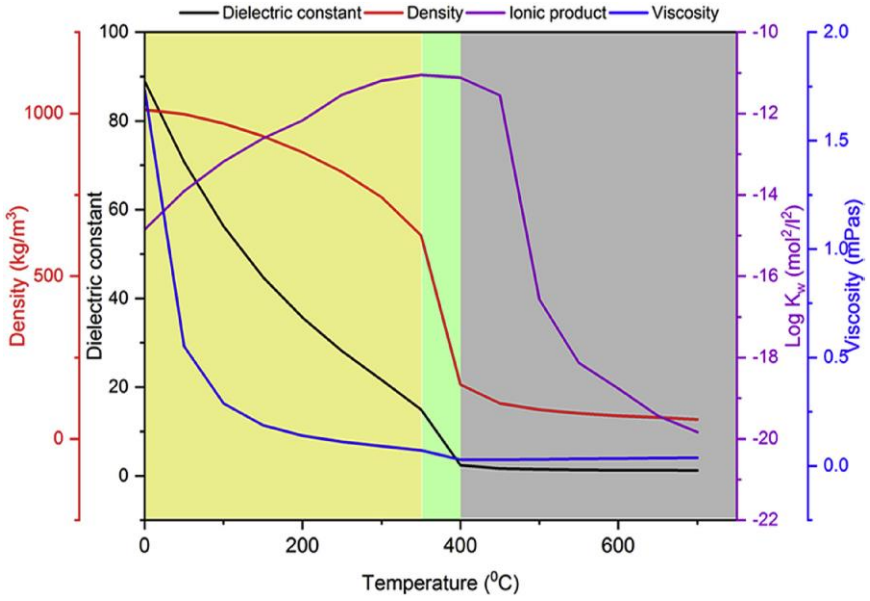

Figure 2.2: Variation in the density, dielectric constant, viscosity, and ionic product of water under supercritical conditions at constant pressure of 25 MPa. Data taken from Bandura and Lvov (2006)

Water has a maximum density of 1000 kg/m^3 at ambient temperature and pressure. However, at lower temperatures (< 250 °C), an increase in pressures can only produce a small elevation in the density of water. When the temperature rises between 270 °C and 390 °C, water density drops drastically followed by a gradual decline above 400 °C. When water enters the supercritical state, the dielectric constant, which is a measure of the hydrogen bonding, drops from 80 to 2 because of the decrease in the number of hydrogen bonds (Figure 2.2), and water begins to exhibit the behavior of a non-polar solvent. This leads to poor solubility of water in inorganic polar compounds, while at the same time, it maintains a complete miscibility with gases (e.g., CO_2, CH_4, H_2 and N_2), hydrocarbons and organic compounds. The absence of phase boundaries at supercritical conditions results in many rapid homogeneous reactions involving organic compounds. Polar inorganic compounds such as NaCl, KCl and $CaSO_4$ that are usually soluble in subcritical water and insoluble in supercritical water are easily separated from the reaction products (Peterson et al., 2008).

As it can be seen from Figure 2.2, the ionic product of water at a constant pressure of 25 MPa rises with temperature up to a maximum value of 10^{-11} at about 300 °C, after which it drops gradually until the temperature reaches the critical temperature (Bandura and Lvov, 2006). At temperatures above the critical value, there is a drastic drop in ionic product due to the decrease in density with the ionic product reaching a value of 10^{-23} at 600 °C (Bandura and Lvov, 2006). The increase in the value of ionic constant means that water can behave as an acid or base catalyst due to the greater concentration of OH^- and H_3O^+ (Yakaboylu et al., 2015). Hence, protons or hydroxyl ion catalyzed reactions could also occur in subcritical or supercritical water without the use of external acid or base catalysts. In such reactions, water itself supplies the protons and hydroxyl ions because of improved autohydrolysis or self-dissociation near the critical point.

Therefore, SCW acts simultaneously as a reaction medium, a solvent, and a catalyst. At high ionic product concentration, the main reaction pathways are ionic (Sonil Nanda et al., 2017b). However, when the ionic product formation is low, the free radical reactions are dominant, because at near-critical conditions both ionic and free radical reactions compete (Reddy et al., 2015). The free radical reaction is usually dominant under supercritical conditions, especially at high temperatures leading to improved dissolution of complex organic compounds and intermediate by-products into gases.

2.3 Supercritical water gasification of lignocellulosic biomass and organic residues

This section provides an overview of previous studies related to the SCWG of different model compounds representing cellulose, hemicellulose, and lignin as well as real biomass materials.

2.3.1 Cellulosic feedstocks

Cellulose is the main structural component of lignocellulose biomass as it typically accounts for 35–55 wt% of lignocellulosic biomass on a dry weight basis. It comprises of D-glucose monomers linked together by β-1,4 glycosidic bonds. The polymer exists in two forms i.e. amorphous disorganized structure and the ordered crystalline structure (Hendriks and Zeeman, 2009; Nanda et al., 2015c). Cellulose has been a preferred model biomass compound for SCWG for two major reasons. Firstly, glucose is the main product of cellulose hydrolysis and a direct monomer. Secondly, glucose is entirely homogeneous, making it easy to study the reaction kinetics and degradation pathway during SCWG.

Resende et al. (2007) reported the non-catalytic SCWG of cellulose in a metal-free quartz reactor at 500 ^{o}C with 9 wt% feed concentrations for 20 min of reaction time. The gas yields

obtained were compared with that of another study by Hao et al. (2005) who used a stainless-steel reactor under the same reaction conditions. The gas yield obtained from the metal-free quartz reactor (8.2 mmol g^{-1}) was lower than that from the stainless-steel reactor (18.5 mmol g^{-1}) . They attributed the increase in gas yield to the reactor wall acting as heterogeneous catalyst, thereby increasing the yield (Hao et al., 2005.; Resende et al., 2007). It is important to note that the contribution of cellulose to H_2 production is more than that of hemicellulose and lignin (Yoshida and Matsumura, 2001). Therefore, the valorization of real biomass feedstock with high cellulose content for H_2 production in SCW is invaluable (Yoshida et al., 2004). Table 2.1 shows the list of a few biomass that have been gasified in SCW.

Other biomasses with high cellulosic content that have been explored as some potential feedstocks for SCWG includes wheat straw (Cao et al., 2011), fruit shells (Demirbas, 2004) and rice shell (Lu et al., 2008). Demirbas (2004) studied the SCWG of five different varieties of fruit shells and suggested that the H_2 yield largely depends on the cellulose content of the biomass. The yield of H_2 from different fruit shells as reported can be arranged as almond shell > sunflower shell > coconut shell > hazelnut shell > walnut shell.

Table 2.1: List of different lignocellulosic and organic feedstocks used in supercritical water gasification.

Biomass	Optimal reaction conditions	Key findings	Reference
Alkaline black liquor from wheat straw	600 ^{o}C, 25 MPa and 12.4 min	• Maximum H_2 yield obtained was 11.3 mol kg^{-1} • Maximum chemical oxygen demand (COD) removal of 88.7%	Cao et al. (2011)
Cellulose and pinewood	550 ^{o}C, 1: 7 biomass-to-water ratios and 30 min	• For SCWG of pure cellulose and pinewood, the maximum H_2 yield without and with catalyst was 1.16 and 0.83 mmol g^{-1} respectively. • H_2 yield increased with the use of KOH catalyst to 9.09 mmol g1 of cellulose and 5.55 mmol g^{-1} of pinewood.	Ding et al. (2014)
Cellulose, xylan and lignin mixtures	350 ^{o}C and 26 – 29 MP	• Presence of lignin affected the gas yield and composition. • No interaction between cellulose and xylan was observed. • Lignin interacted with other Components.	Yoshida and Matsumura (2001)
Fruit shells (almond, cotton, hazelnut, sunflower and walnut)	476 ^{o}C, 48 MPa and 60 min	• H_2 yield: walnut shell < hazelnut shell < cotton shell < sunflower shell < almond shell • A correlation was established between temperature and H_2 yield, pressure and H_2 yield as well as cellulose content and H_2 yield.	Demirbas (2004)
Fruit waste and agro-food residues	600 ^{o}C, 45 min, 1 : 10 biomass-to water ratio and 23–25 MPa	• H_2 yield: coconut shell > sugarcane bagasse > Aloe vera rind > orange peel > pineapple peel > lemon peel > banana peel.	Nanda et al. (2016)

		• Coconut shell showed high yields of H_2 (4.78 mmol g^{-1}) and CH_4 (3.1 mmol g^{-1}) using 2 wt% K_2CO_3.	
Kraft lignin	651 °C, 25 MPa and 3.9 biomass-to water ratio	• Coconut shell had high total gas yields (15 mmol g^{-1}) and H_2 selectivity (45.8%) due to its high lignin content. • Central Composite Design (CCD) was used to optimize H_2 yields. • Maximum H_2 yield was 1.60 mmol g^{-1} of lignin.	Kang et al. (2015)
Sawdust, rice straw, cellulose, and lignin	400 °C, 25 MPa and 20 min	• Strong interactions between high temperature and water-to-biomass ratio were observed. • Possible catalyst deactivation by tarry products. • Maximum gas and H_2 yield from sawdust (6 mmol g^{-1}) and rice straw (8 mmol g^{-1}) using 0.04 g of Ni catalyst.	Yoshida et al. (2004)
Xylose	600 °C, 21 MPa and 3600 s	• Different lignin reagents exhibited different gasification behavior in SCW. • Maximum H_2 yield without catalyst was 15 mol kg^{-1}.	Gokkaya et al. (2016)
Timothy grass	650 °C, 23–25 MPa, 1 : 8 biomass-to - water ratio and 45 min	• K_2CO_3 improved the carbon gasification efficiency (86%) and H_2 yield (18 mol kg^{-1}). • Maximum gas yield was 17.2 mol Kg^{-1} and H_2 yield was 5.15 mol kg^{-1} without catalyst. • 3 wt% KOH catalyst increased H_2 and total gas yields up to 8.91 and 30.6 mol g^{-1} respectively. • Catalyst performance for H_2 and total gas yields increased as Na_2CO_3 < NaOH < K_2CO_3 < KOH	Nanda et al. (2016)

2.3.2 Hemicellulosic feedstocks

Hemicelluloses is a mixture of C_5 and C_6 sugars as well as sugar acids including mannose, glucose, xylose, arabinose, galacturonic acid and methylglucuronic acid (Nalbant et al., 2007). Hemicelluloses occur in amorphous form in plants and are the second most abundant component of biomass after cellulose (Nanda et al., 2015a). Pure xylan is often used as a model compound of hemicellulose to study the decomposition mechanism and behavior under supercritical conditions as shown in Table 1.1 although the propensity of its SCWG studies is lesser compared to that of cellulose.

Timothy grass is a perennial grass variety found predominantly in Canadian prairies with high and almost equivalent cellulose and hemicellulose contents (i.e., 34 wt% cellulose, 30 wt% hemicellulose and 18 wt% lignin) (Nanda et al., 2013). Nanda et al. (2016) stated that timothy grass is a dedicated energy crop for SCWG due to its high H_2 yields of 5.2 mol kg^{-1} without catalyst and 8.9 mol kg^{-1} in the presence of 3% KOH catalyst. Similarly, the total gas yields increased from 17.2 mol kg^{-1} in non-catalytic SCWG to 30.6 mol kg^{-1} in KOH-catalyzed SCWG (Nanda et al., 2016c). The residues from corn contain 45 wt% cellulose, 35 wt% hemicellulose and 15 wt% lignin (Prasad et al., 2007). Yanik et al. (2007) investigated the potential candidacy of corncob as feedstock for H_2 production via SCWG. The experiments were carried out in a batch autoclave reactor at 500 ^oC at a heating rate of 3 ^oC min1 for an hour. Their findings showed H_2 yield of 2.09 mol kg^{-1}in SCW (Yanik et al., 2007).

2.3.3 Ligneous feedstocks

Lignin is an essential component of lignocellulosic biomass, which comprises of a branched cross-linked phenyl propane polymer of guaiacyl, syringyl and p-hydroxyphenyl units.

Many researchers have reported the SCWG of biomass compounds with high lignin content (Table 2.1). Nanda et al. (2016) reported the SCWG of coconut shell and other agro-food residues at an optimal temperature of 600 ^{o}C with 1: 10 biomass-to-water (BTW) ratio and 45 min of reaction time. Compared to other agro-food residues studied (e.g. banana peel, lemon peel, pineapple peel, orange peel, sugarcane bagasse and Aloe vera rind) coconut shell gave a H_2 and total gas yields of 2.15 mmol g^{-1} and 7.85 mmol g^{-1} , respectively without a catalyst (Nanda et al., 2016d). With 2 wt% K_2CO_3 catalyst, coconut shell also produced the highest yields of H_2 (4.8 mmol g^{-1}) and total gases (15 mmol g^{-1}) owing to its high lignification.

In a contrasting study, Yoshida and Matsumura (2001) examined the subcritical water gasification of cellulose, xylan and lignin mixtures at 350 ^{o}C and 25 MPa to understand the interactions among the three main constituents of lignocellulosic biomass. They showed that there is least interaction between cellulose (C_6 sugar) and xylan (C_5 sugar), although the contribution of cellulose towards H_2 production is more significant than hemicellulose (xylan). Interestingly, the presence of lignin in the mixture inhibited the H_2 and gas yields in subcritical water. In subcritical water, the decomposition of lignin proceeds with the initial hydrolysis of its branched primary structures into phenolic compounds (e.g., phenol, catechol and guaiacol), aldehydes (form aldehyde) and other low molecular weight compounds. These intermediate compounds undergo crosslinking and re-polymerization to yield high molecular weight compounds such as tars and aromatic chars at moderate temperatures and longer reaction time (Nanda et al., 2016e).

2.4 Reaction pathways of biomass in supercritical water.

For optimizing and enhancing the efficiency of a SCWG process, it is important to understand the decomposition behavior and reaction pathways for each biomass component in SCW. Hydrolysis is the first degradation reaction during hydrothermal processing of

lignocellulosic biomass. Because of hydrolysis, cellulose breaks down to glucose, hemicelluloses to xylose and glucuronic acid, and lignin to phenolics.

SCWG involves some important sub-reactions to enhance the thermal degradation of biomass into H_2. A few of such reactions include water–gas shift reaction (WGSR), methanation reaction, steam reforming reaction, hydrogenation, dehydration, decarbonylation, decarboxylation and Boudouard reaction. The reactions are illustrated with equations shown below (Nanda et al., 2017b).

Water-gas shift reaction (WGSR):

$$CO + H_2O \rightarrow CO_2 + H_2 \quad (2.1)$$

Steam reforming:

$$CH_xO_y + (1 - y)\, H_2O \rightarrow CO + (1 - y + 0.5\, x)\, H_2 \quad (2.2)$$

Methanation reaction for CO

$$CO + 3H_2 \rightarrow CH_4 + H_2O \quad (2.3)$$

Methanation reaction for CO_2

$$CO_2 + 3H_2 \rightarrow CH_4 + H_2O \quad (2.4)$$

Eq. 5 represents the overall chemical equation obtained by combining steam reforming and water-gas shift reaction.

$$CH_xO_y + (2 - y)\, H_2O \rightarrow CO_2 + (2 - y + 0.5\, x)\, H_2 \quad (2.5)$$

Where *x* and *y* represent the elemental molar ratios H/C and O/C in biomass, respectively (Gökkaya et al., 2016; Kritzer, 2004).

Hydrogenation reaction

$$CO + 2H_2 \rightarrow CH_4 + 0.5\, O_2 \quad (2.6)$$

Boudouard reactions

$$2CO \rightarrow C + CO_2 \quad (2.7)$$

$$CO_2 \rightarrow O_2 + C \quad (2.8)$$

As represented in Equation (2.1), the WGSR reaction involves a reaction between CO and water to produce CO_2 and H_2. The reaction is favorable at high temperatures and low feed concentrations (Nanda et al., 2017b). Steam reforming is also another major reaction that occurs during the SCWG of biomass to produce H_2, CO_2 and CO (Equation (2)). Hydrogenation and methanation reactions are perceived to be secondary reactions that requires longer residence time and mostly utilizes H_2, CO_2 and CO to produce CH_4 as illustrated in Equations (2.3), (4) and (6).17,53 In contrast, Boudouard reaction produces carbon in the form of char or coke from CO and CO_2 (Equations (7) and (8)).

2.5 Parametric studies of biomass gasification in supercritical water

2.5.1 Temperature

Temperature is one of the most significant parameters that affects the product yield during SCWG of biomass, especially when the reaction occurs in the absence of catalyst. The operating temperature in SCWG can be grouped into two zones, namely low temperatures (350–500 ^oC) and high temperature (500–700 ^oC). There is an increase in CO and CH_4 yields in low temperature SCWG, while H_2 and CO_2 formation is favored at high temperature SCWG (Nanda et al., 2015b). The ionic product mechanism is promoted at low temperature SCWG, whereas the free-radical mechanism is enhanced at high temperature SCWG (Kruse, 2008). The concentration of ionic products of water (H^+ and OH^-) increase as the SCWG temperature increases, reaching a maximum around 300 ^oC (subcritical regime) further which they decrease (Savage, 2009). The splitting of water into ionic products is an endothermic process. Hence, the ionic product mechanism is favored with a rise in temperature. Therefore, subcritical water is a good medium for acid-

catalyzed and base-catalyzed reactions. On the contrary, high temperature SCW supplies more hydronium ions ($H3O^+$) for acid-catalyzed reactions, thereby reducing its pH compared to liquid water. As the pH of SCW medium lowers, the free radical mechanisms are enhanced at high temperatures. The free radical mechanism leads to efficient dissolution of complex organic compounds and their intermediate degradation components to gases (Chuntanapum and Matsumura, 2010).

Several researchers have studied the effects of temperature on the gasification yield from both model and real biomass compounds. Many studies have also reported an increment in H_2, and CO_2 yields as well as carbon gasification efficiency with the increase in SCWG temperature (Chuntanapum and Matsumura, 2010; Nanda et al., 2015f, 2016e, 2016d). Lee et al. (2002) investigated the gasification of glucose in SCW and studied the effects of temperature on H_2 yield. They observed an increase in H_2 yield with temperature above 660 ^oC alongside a decrease in CO yield. The increase in H2 yield at high temperatures is due to WGSR and the reduction of CO is due to its consumption as the WGSR reactant (Lee et al., 2002) .A similar study by Promdej and Matsumura (2011) on the SCWG of glucose also supported the findings. The researchers grouped the reaction mechanism of glucose degradation into ionic and free radical reactions based on the temperature and kinetic reaction rates (Promdej and Matsumura, 2011).

Reaction temperature is a very significant parameter during the hydrothermal gasification of biomass. However, high temperature requirement is also a crucial concern to determine the economics of the SCWG process. The need for high temperature and pressure during SCWG process requires specialized reactor materials that can withstand these extreme reaction conditions. This in turn increases the overall process cost due to the high-energy consumption and durable material requirement. High temperature could reduce reactor plugging and char formation, which

are significant problems in SCWG (Yoshida and Matsumura, 2009). High temperature and pressure demand in SCW technologies are challenging issues that requires further attention. A cost effective SCWG technology relies on the following attributes: (i) recovery of waste heat for cogeneration, (ii) development of stable reactor materials that can withstand high-temperature and high-pressure conditions, and (iii) development of novel homogeneous and heterogeneous catalyst to minimize the temperature requirements of the process.

2.5.2 Pressure

The effects of pressure on SCWG process are not clearly understood. According to Le Chatelier's principle, pressure favors the side with the least sum of molecules. To explain the pressure effects, it is essential to consider other competing chemical reactions involved in SCWG. The steam reforming, methanation and WGSR as described earlier are the three main competing reactions in SCWG (Guo et al., 2007). A rise in the pressure will shift the methanation reaction to the right, thereby enhancing the formation of CH_4 with the subsequent consumption of CO, CO_2 and H_2. A rise in pressure could lead to an increase in the water density, ionic product and dielectric constant of water (Basu and Mettanant, 2009). As the density of water changes with pressure, ionic and free radical reactions are in direct competition. However, as stated by Buhler et al. (2002) the ionic reaction is dominant at high pressure due to ionic stabilization at high density of water. Therefore, the rate of ionic reactions increases with pressure while that of free radical reactions decreases (Bühler et al., 2002).

Gadhe and Gupta (2005) investigated the gasification of methanol to produce H_2 in SCW. Their experimental and equilibrium calculations showed that an increase in the pressure favors methanation reaction, which culminates into a subsequent decrease in H_2 yield. From the equilibrium calculations, the H_2 yield decreases from 2.75 to 1.5 mol mol^{-1} with an increase in

pressure from 3.4 to 25.6 MPa. Similarly, there was also a decline in CO and CO_2 yields from 0.9 to 0.3 mol mol^{-1} and 1.0 to 0.6 mol mol^{-1}, respectively. As expected, CH_4 yield increased from 0.03 to 0.24 mol mol^{-1} under the condition of pressure increase from 3.4 to 25.6 MPa. Therefore, there is an overdependence of individual gas yield on pressure (Gadhe and Gupta, 2005).

Demirbas (2004) reported a significant increase in H_2 yield with pressure during the SCWG of fruit waste shells. The H_2 yield percent rose from 5.9 to 12.6% as the pressure heightened from 23 to 48 MPa. On the contrary, Lu et al. (2008) observed a slight increase in H_2 yield from 15 to 17 mol kg^{-1} when with a rise in pressure from 17.5 to 30 MPa because of the preference of WGSR at higher pressures. Similarly, Byrd et al. (2008) noted a negligible effect of pressure on H_2 yield. In their study, 10 wt% of ethanol was gasified in SCW at 700–800 ^oC with 1.92 g of Ru/Al_2O_3 catalyst and a residence time of 2 s. Though the H_2 yield increased linearly with temperature, the same was not noticed with pressure. H_2 yield increased from 2.6 to 4.5 mol mol^{-1} of ethanol as the reaction temperature elevated from 700 to 800 ^oC. On the contrary, H_2 yield almost remain unchanged (2.6 to 2.7 mol mol^{-1} of ethanol) as the pressure increased from 22.1 to 27.6 MPa.

2.5.3 Reaction time

Reaction time also known as residence time refers to the duration for which the reactants stay inside the reactor. At longer residence times and high temperatures, the gas yields are usually high from SCWG through enhanced thermal cracking reactions. With longer residence times, usually the concentration of CO is reduced because it is consumed as a reactant for many reactions Consequently, the concentrations of H_2 and CO_2 are higher in the gas phase as they are the main products of WGSR, whereas CH_4 yields are also higher from methanation and hydrogenation reactions(Nanda et al., 2016e).

Many researchers have studied the temporal effect on the gas yield from SCWG of biomass and organic waste matter. Guo et al. (2012) noticed an increase in H_2 yield during the SCWG of glycerol from 0.35 to 1.35 mol mol^{-1} as well as a rise in gasification efficiency from 8 to 42% as the residence time was prolonged from 5.2 to 9 s (Guo et al., 2012). Similarly, Lu et al. (2006) observed an increase in the yields of H_2 (from 14.5 to 17.5 mol kg^{-1}), CO_2 (from 16 to 20 mol kg^{-1}) and CH_4 (from 4 to 8 mol kg^{-1}) during SCWG of wood sawdust as the residence time increased from 9 to 46 s.

Residence time is also dependent on the type of biomass. For instance, for maximum conversion, long-chain hydrocarbons are expected to spend longer time in the reactor compared to short-chain or oxygenated hydrocarbons (Anikeev and Fan, 2014). Susanti et al. (2010) studied the effect of residence time on the SCWG of isooctane at a constant temperature of 632 ^{o}C, pressure of 25 MPa and 15.25 wt% feed (isooctane) concentration. As the residence time was extended from 6 to 33.3 s, the gas yield increased from 1.1 to 2.9 L g^{-1}. Since isooctane is a long-chain hydrocarbon, its complete conversion required a longer residence time (Susanti et al., 2010).

2.5.4 Biomass particle size

A few studies have investigated the effects of biomass particle size on the gas yield via hydrothermal gasification. The low mass transfer resistance of SCW could also negate the impacts of biomass particle size, although the latter affects both heat and mass transfer. Moreover, it cannot be denied that smaller particle size biomass provides higher surface area for higher degradation and solubility by SCW. To explain the influence of particle size on gas yield during SCWG, it is important to consider the effect of surface area per unit mass of biomass feedstock. Biomass with smaller particles size exhibits larger surface area per unit mass, which makes them exposed to the reaction environment and enhance the heat and mass transfer between the particles. This could

increase the efficiency of the Gasification reactions and improve the hydrothermal decomposition and subsequent gas yields. However, to obtain the optimal particle size, the cost of energy utilization during biomass size reduction should also be considered.

There are not many studies that report the effect of biomass particle size on hydrothermal gasification of biomass. However, ample amount of information is available in the literature on the effects of biomass particle size on pyrolysis, liquefaction, torrefaction, and thermochemical gasification. Therefore, it is important to understand the biomass behavior with different particle sizes in SCWG to optimize the process conditions and maximize gasification efficiency. Lu et al. (2006) compared hydrothermal gasification results at 650 ^{o}C, 25 MPa with 2 wt% rice straw and sodium carboxymethylcellulose for 30 s and varying biomass particle sizes of 40–80 mesh. Biomass with smaller particle sizes, i.e., <80 mesh size produced higher H_2 yield of 17 mol kg^{-1} compared to larger biomass particle size of 40–80 mesh that produced H_2 yield of 13.7 mol kg^{-1}.

2.5.5 Feed concentration or biomass to water ratio

Since the feedstock in SCWG reactor comprises of biomass and water, the feedstock concentration is also referred as the biomass to water or water-to-biomass ratio. When the biomass-to-water ratio is high, it means the amount of water is low compared to the quantity of biomass. Therefore, H_2 and CO yield would decrease. At low feed concentration or low biomass-to-water ratio, there is usually an increase in the yields of H_2 and CO_2 because of higher biomass to-gas conversion efficiency caused by the higher amount of water than the feedstock. High concentration of water than the biomass quantity results in its improved solvation properties in SCW. In a SCW system, the interactions between high temperatures and low feed concentrations are characterized by a reduction in water density, dielectric constant and ionic product formation as well as an elevation in the solubility potential and free radical formation (Resende et al., 2007). At low feed

concentration, the low density of water together with less moles of biomass lead to the superior thermal cracking of the organic compounds into gases.

Nanda et al.(2015d) varied the concentration of fructose from 4 to 10 wt% during SCWG using a continuous flow tubular reactor at an optimal temperature of 700 ^{o}C and pressure of 25 MPa and residence time of 60 s. The total gas yield and carbon gasification efficiency decreased from 1.04 to 0.83 L g^{-1} and 88 to 76%, respectively with an increase in feed concentration from 4 to 10 wt%. The H_2 and CO_2 yields decreased from 3.37 to 2.52 mol mol^{-1} and 3.25 to 1.95 mol mol^{-1}, respectively with an increase in fructose concentration. They suggested that a reduced activity of WGSR at high feedstock concentration is the main reason for the drop in H_2 and CO_2 yield. The impaired WGSR at high feed concentration results in maximum amount of CO remaining unreacted. However, methanation reaction is promoted at high feed concentration leading to higher concentration of CH_4 (Nanda et al., 2016e).

2.5.6 Heating rate

Heating rate is another important parameter that influences gas yield during SCWG process. Some intermediate reactions might occur during reaction warm up time, therefore heating rate could influence the product distribution during SCWG (Azadi et al., 2012b).

A few studies have investigated the effects of heating rate on the gaseous yield during SCWG. Fang et al., (2004) used a diamond anvil cell reactor to visualize and study the influence of heating rate on the decomposition of cellulose in SCW. Their findings show that higher heating rate (1.3–2.3 K/s) promotes homogeneous reaction while lower heating rate (0.18 K/s) leads to heterogeneous reaction with interference of char and dissolved compounds (Fang et al., 2004).

Sinag et al., (2004) performed experiments with glucose in SCW at two different heating rates (1 and 3 K/min) with and without K_2CO_3 catalyst. The authors observed an elevation in gas

yields with heating rate. Studies by Matsumura et al. (2007) also confirmed that higher heating would lead to an improved carbon gasification efficiency.

2.6 Catalysts for supercritical water gasification

The section presents an overview of different homogeneous and heterogeneous catalysts used to improve gas yields during SCWG.

2.6.1 Homogeneous catalysts

SCWG is an energy-intensive process requiring high temperature and pressure, which could possibly lead to high processing cost. Catalysts are used in SCWG to improve the gas yield at the same time minimize the heat requirements. Homogeneous catalysts mostly include the alkali and hydroxide catalysts such as K_2CO_3, Na_2CO_3, KOH and NaOH. Alkali homogeneous catalysts have an ability to break the C–C bonds and promote the WGSR (Guo et al., 2007; Kruse, 2008). Homogeneous catalysts are beneficial because of their low cost, higher and faster conversion rates and flexibility for use in batch and continuous gasification processes (Juan et al., 2011). Although homogeneous catalysts are more effective than the heterogeneous catalyst, in some cases they pose serious challenges such as contributing to reactor plugging and corrosion problems (Kang et al., 2017). Moreover, it is relatively difficult to recycle and reuse homogeneous catalysts after a SCWG experiment. Conversely, heterogeneous catalysts offer a few ways for recovery and reuse with additional expenditures.

Nanda et al.(2016a) evaluated the SCWG efficiency of timothy grass as an energy crop using four alkali homogeneous catalysts, especially carbonates (Na_2CO_3 and K_2CO_3) and hydroxide catalysts (NaOH and KOH). SCWG of timothy grass at 650 ^oC and 45 min of reaction time with 1: 8 biomass-to-water feed ratios gave high yields of H_2 (5.15 mol kg^{-1}) and total gases

(17.2 mol kg^{-1}). The application of alkali catalysts significantly improved the H_2 yields in the following order: KOH (8.91 mol kg^{-1}) > K_2CO_3 (7.84 mol kg^{-1}) > NaOH (6.68 mol kg^{-1}) > Na_2CO_3 (6.39 mol kg^{-1}) > no catalyst (5.15 mol kg^{-1}). It is affirmed that alkali catalysts, especially KOH and K_2CO_3 helps to catalyze the WGSR, thereby producing H_2 and CO_2 instead of CO. On the other hand, Na_2CO_3 causes decarboxylation of formic acid (HCOOH), which is an intermediate product of WGSR, thereby increasing the H_2 yields (Kruse et al., 2005; Xu et al., 2009). Additionally, Na_2CO_3 forms precipitated particles in SCW that subsequently provide larger surface area for many catalytic reactions. In contrast, NaOH promotes CH_4 yields by favoring methanation reaction even at subcritical conditions (Nanda et al., 2016c). Hydrolysis of biomass by NaOH produces sodium acetate (CH_3COONa) as an intermediate product, which further decomposes to CH4 and sodium bicarbonate ($NaHCO_3$) (Onwudili and Williams, 2009).

Trona ($NaHCO_3.Na_2CO_3.2H_2O$), red mud, borax ($Na_2B_4O_7.10H_2O$) and dolomite [$CaMg(CO_3)_2$] are a few other homogeneous catalysts used to improve gas yield during SCWG of lignocellulosic biomass. Yanik et al. (2007) showed that trona exhibited similar catalytic activity with K_2CO_3 during SCWG of lignocellulosic materials. In another study, Madenoˇglu et al.(2014) compared the catalytic activity of three different homogeneous catalysts (e.g. Borax, dolomite and trona) during the hydrothermal gasification of hard-shell nut residues at temperatures of 300–600 ^oC .The activities were in the following order: trona > borax > dolomite (Madenoɨlu et al., 2014).

2.6.2 Heterogeneous catalysts

Heterogeneous catalysts can be classified into metal oxides and transition metal catalysts. One main advantage of heterogeneous catalysts is the ability to recover and reuse while reducing the cost of catalyst development at the same time adding cost to their recovery. The catalysts are also preferred because of their selectivity and inertness to reside inside the reactor or on the support

material. However, deactivation, poisoning and sintering of heterogeneous catalysts due to the presence of sulfur, nitrogen, coke, or any other compounds containing heteroatom is still a big challenge. Moreover, the metal cations are transformed into oxides and their corresponding salts during SCWG while elements such as S and Cl are easily oxidized into their corresponding organic acids, which stay in the aqueous phase after the completion of the reaction (Azadi et al., 2012b).

As mentioned earlier, the transition metal catalyst could be either nickel or other novel metal catalyst. The examples of novel metal catalysts that have been used for SCWG include Pb, Pt, Rh and Ru. Ni-based catalysts are mostly used in SCWG because of its low cost compared to other novel metal catalysts. Although the use of nickel could possibly lead to high total gas yields and improved carbon gasification efficiency, the H_2 production is subdued due to the consumption in hydrogenation reaction. Nickel also catalyzes methanation reaction and demonstrating high selectivity towards CH_4 in SCWG (Fang et al., 2008; Nanda et al., 2017a).

The main issue with nickel catalyst is the unavoidable problem of sintering and catalyst deactivation by tar-forming products. Lu et al. (2014) reported that the char layer could be avoided by co-precipitation of Ni-Mg-Al catalyst during the SCWG of glucose. They synthesized and tested a series of Ni-Mg-Al catalysts with different molar ratios of Mg/Al. An increase in both H_2 yield from 1.7 to 12 mmol/g and H_2 selectivity from 25 to 70% was obtained at a Ni-Mg-Al ratio of 1:0.6:1.9. Additionally, the presence of Mg could increase the longevity of the catalyst and enhance the anti-carbon formation by the Ni-Al catalyst, thereby hindering graphite formation (Lu et al., 2014c).

The metal catalysts used in SCWG are either in the supported or unsupported form. A suitable catalyst support could increase the catalytic activity and provide better stability. Supporting material is very important for heterogeneous catalyst due to the strident nature of the

SCW environment. The commonly used catalyst support in hydrothermal gasification includes alumina, silica, molybdenum, olivine, metal oxides, activated carbon, carbon nanotubes, graphite, etc. Some studies have also reported lignocellulosic biomass as the support material and reactant in hydrothermal gasification studies (Fang et al., 2008; Kang et al., 2017; Lu et al., 2014c; Nanda et al., 2017a). In such studies, catalytic metal nanoparticles were impregnated or synthesized in the biomass's cell wall at varying the metal concentrations and doping conditions (e.g. temperature, pH, agitation, duration, and additives).

Tailoring the catalyst by varying the supporting material is an alternative way to increase the catalytic activity, stability, and gas yields. Several studies have reported the use of different types of catalysts support to enhance hydrogen yield during the SCWG of biomass model and real compounds. For instance, Azadi et al. (2012) evaluated the performance of five different catalysts (e.g., Ru/C, Ru/γ-Al_2O_3, Ni/γ-Al_2O_3, Ni/hydrotalcite and Raney-Ni catalyst) during the SCWG gasification of glucose, cellulose, fructose, xylan, pulp, lignin and bark. Their results showed that Ni/hydrotalcite and Ni/γ-Al_2O_3 exhibited the best catalytic activity and high H_2 selectivity compared to other catalysts tested in the study. They suggested that the behavior of the catalyst was because of their low nickel dispersions and Ni-defect sites compared to other catalysts.

Kang et al. (2016) tested five different supports (e.g., Al_2O_3, activated carbon or AC, TiO_2, ZrO_2 and MgO) and three promoters (e.g., Co, Cu and Ce) for Ni-based catalyst. The synthesized catalysts were screened for their performance in the SCWG of lignin. They found that catalytic activity of Ni varied in the order of its support materials as Al_2O_3 > TiO_2 > AC > ZrO_2 > MgO. Likewise, the catalytic activity of Ni-based catalysts for SCWG of lignin using different promoters was in the order of Ce > Co > Cu. The authors reported that Ce improved H_2 yield because of its ability to promote Ni dispersion, thereby debilitating the Ni–Al_2O_3 interaction (Kang et al., 2016a).

Tushar et al. (2016) studied the use of dual metals (Ni and Ru) and dual supports (Al_2O_3 and ZrO_2) to improve the H_2 yield from SCWG of biocrude obtained from hydrothermal liquefaction of cattle manure at 500-700°C, 10-20 g/L carbon concentration and 25 MPa pressure. Glucose was also gasified as a model compound to test the catalytic activity of different synthesized novel catalysts. The synthesized 10%Ni-0.08%Ru/Al_2O_3-ZrO_2 catalyst revealed the highest H_2 yield (1.01 mol mol^{-1} of biocrude and 1.34 mol mol^{-1} of glucose) and maximum carbon gasification efficiency (92% for biocrude and 88% for glucose). The dual catalyst 10%Ni-0.08%Ru/Al_2O_3-ZrO_2 was found to be highly stable for up to 20 h.

Carbon materials derived from natural sources such as coal and plants residues can be treated through carbonization and activation under high-temperature inert gas, CO_2 and/or steam to modify their properties for use as a catalyst or catalyst support for hydrothermal gasification. The physical and chemical properties of treated carbon are dependent on the treatment method and the precursor biomass. Activated carbon is an activated form of char produced from pyrolysis or carbonization followed by chemical or physical activation. Activated carbons (AC) have high surface area (~1500 m^2), which is nearly 50 times greater than that of the char (Nanda et al., 2016a). The highly microporous morphology of activated carbons makes them suitable for use as a catalyst or catalyst support (Nanda et al., 2016a; Xu et al., 1996). Xu et al. (1996) studied the effects of four different carbon catalysts (e.g. spruce wood charcoal, macadamia shell charcoal, coal AC and coconut shell AC) on the gasification of glucose, glycerol, cellobiose, sewage sludge and other biomass waste. The use of 0.6 g of coconut shell activated carbon catalyst decreased the amount of CO produced from 3.18 to 0.79 mol/mol of feed and increased the carbon gasification efficiency from 80 to 103%. In contrast H_2 yield rose from 0.56 to 2.24 mol/mol of feed with the use of carbon catalyst. However, catalyst deactivation occurred after 4 h of reaction time.

Carbon nanotubes (CNT) have also been viewed as a promising catalytic support for SCWG. CNT are known for their high heat conductivity, open structure, large surface area and most notably their physical and chemical stability (DeVlieger et al., 2012; Taylor et al., 2009).Taylor et al.(2009) explored the use of Ni catalyst supported by CNT for the SCWG of cellulose in a batch reactor. The synthesized Ni/CNT catalyst produced approximately the same H_2 yield (~8 mmol/g) compared to two commercial alumino-silicates supported Ni catalysts. A study by De Vlieger et al. (2012) revealed the highly stable behavior of Pt/CNT in SCW.

The recovery and reuse of heterogeneous catalyst during SCWG is a significant issue that requires further attention. Catalyst recovery and reuse is important from both environmental and economic perspectives. Catalyst deactivation during SCWG can also occur mainly due to the deposition of carbon materials in form of fine char, thereby blocking the active sites of the catalyst. Therefore, even after recovery of the catalyst during SCWG, effective regeneration is required to restore the catalyst activity.

Hossain et al. (2018) performed catalyst deactivation and regeneration studies on AC catalyst during the hydrothermal gasification of oleic acid. The deactivation of AC catalyst during SCWG was attributed to the deposition of impurities that precedes the decarboxylation reaction and participation in steam reforming reaction during decarboxylation (Hossain et al., 2018).The spent AC catalyst was regenerated by thermal treatment with KOH. The procedure involved mixing the catalyst with KOH followed by heating at 750°C and 0.5°C/min for 3 h under inert atmosphere. KOH was further neutralized with a diluted solution of HNO_3 and washing with water to remove the remaining KOH before drying for 12 h. The regenerated and fresh AC catalyst were found to exhibit similar surface properties and product selectivity. It was proposed that thermal treatments with KOH is a low-cost and effective approach for regeneration of carbonaceous catalysts.

2.7 Optimization of process parameters in hydrothermal gasification

2.7.1 Univariate (one variable at a time) approach

The univariate approach is a common and traditional method used to investigate the influence of experimental factors on gas yield during the hydrothermal gasification process. This technique involves changing the level of a single parameter and studying the effects on the response while keeping other parameters constant. Several authors have used this technique to study the effects of process parameters during hydrothermal gasification of biomass (Lu et al., 2008; Nanda et al., 2016d). The most useful application of a univariate approach is found in batch hydrothermal gasification studies to investigate the influence of temperature, residence time and feed concentration on gas yields.

Ding et al. (2014) used the univariate method to study the influence of temperature (400-550°C), catalysts (e.g., Ni/CeO_2/Al_2O_3, KOH, calcined dolomite, and calcined olivine) and water-to-biomass ratio during hydrothermal gasification of cellulose and pinewood. An increase in the reaction temperature and water-to-biomass ratio favored H_2 yields. For the non-catalytic gasification of cellulose, a maximum H_2 yield of 1.2 mmol/g was obtained at 550°C with a water-to-biomass ratio of 7:1. On the other hand, the KOH catalyst elevated H_2 yield to 2 mmol/g under similar conditions (Ding et al., 2014).

The univariate approach has also been used to optimize catalyst composition and examine the effects of different catalyst supports and catalyst synthesis methods in hydrothermal gasification studies. Kang et al. (2017) studied the influence of different catalyst preparation methods (i.e., co-precipitation and wet impregnation) on H_2 yield during the SCW gasification of lignin at 650°C and 26 MPa with a water-to-biomass mass ratio of 5. Their results indicated the co-precipitation method to be more efficient than wet impregnation for catalysts preparation. It should be noted that the univariate approach is flexible and easy to apply. However, it cannot be

used to study the interactions between the operating parameters. The interactions could play a significant part in the process. Moreover, their effects on the response can even exceed the effects of individual process parameters.

2.7.2 Factorial method (full and fractional factorial)

Compared to the univariate approach, the factorial designs can study the influence of more than one factor and levels simultaneously. Factorial designs typically include different combinations of factors and levels, which enable the screening and identification of the factors that have the highest effect on the response. Such methods are useful for preliminary studies or to perform initial optimization steps (Tarley et al., 2009). Factorial designs can be performed by using either coded factor levels or the real factor levels. The coded factor levels are mostly preferred because they provide a uniform framework to study the influence of a factor on the response in an experiment. Furthermore, the model coefficients for coded factor levels are dimensionless. Therefore, they are directly comparable. This makes it effective for the determination of the relative size of the factor effect (Wang and Wan, 2009).

Factorial design can be grouped into two categories, namely full factorial design and fractional factorial design (Wang and Wan, 2009). The full factorial design involves the complete testing of all possible combinations of each factor level. The number of experimental runs required for a full factorial design with n-factors and p-level is denoted with p^n. For example, factorial design with two-levels and four factors, denoted by 2^4, requires a total number of sixteen experimental runs.

Hendry et al. (2011) applied the 2^3 factorial methods to study the effect of temperature (750-800°C), reaction time (4-6.5 s) and feed concentration (10-15 wt%) on the gas yields during SCW gasification of glucose in a continuous reactor. A maximum H_2 yield of 59.5 wt% was

obtained at 800°C in 4 s with 10 wt% feed concentration. Owing to the large number of experimental runs required for the full factorial design, this method can be tedious and time-consuming during the hydrothermal gasification process. On the other hand, fractional factorial is preferred when many factors are involved as it minimizes the total number of experiments required (Hendry et al., 2011).

Miller et al. [128] used the 2^{3-1} fractional design to study the effect of temperature (550 and 600°C), feed concentration (17.5 and 25 wt%) and residence time (4 and 9 s) on product yield during SCW gasification of Spirulina algae in a continuous reactor. Four experimental runs were required for the fractional design compared to eight experiments needed for a full factorial design with similar factors and levels. Among the three factors studied, temperature and residence time had the most statistically significant effects on gasification efficiency (Miller et al., 2012).

The fractional factorial design provides a feasible alternative when the number of experimental runs required for the full factorial is too large. Therefore, the influence of certain variables on a response can be obtained under cost-effective, time-efficient, and feasible conditions. It is important to note that both full and fractional factorial designs permit free interaction with data and the opportunity to make comparisons, seek similarities, trends, differences, etc. (Tarley et al., 2009). Moreover, the full factorial designs are rotatable. Hence, it cannot accurately predict the space that is equidistance from the center. The Taguchi, central composite, Box-Behnken and Plackett-Burman designs have embedded fractional design functions (Wang and Wan, 2009).

2.7.3 Taguchi method

The Taguchi method is an experimental design approach used for process optimization studies and the design of high-quality systems. Such a design can minimize the total number of

experiments while providing accuracy and consistency to the process. It is a factorial-based method that uses the orthogonal array (i.e. series of experiments under different situations) to assign the factors selected for an experiment (i.e. variables). Taguchi method is a relatively simple, efficient, and systematic optimization technique (Thamizhmanii et al., 2007).

According to the Taguchi method, the process or product optimization should be performed in a three-step approach comprising of the system, parameters, and tolerance design (Nalbant et al., 2007). The system design involves the use of scientific and engineering knowledge to produce a functional prototype design. It comprises the product and process design stage. On the contrary, the parameter design aims to optimize the process variables to enhance the process performance and identify the combination of process variables that can produce optimum output. Therefore, the parameter design is the most important step in achieving quality while reducing the cost in the Taguchi design.

The Taguchi design recommends the use of a loss function, which is further transformed into a signal-to-noise (S/N) ratio for measuring the deviation between the experimental and the desired values. The S/N ratio is defined as the ratio of the mean value of quality characteristics of the response to the corresponding standard deviation. It can be used to determine the level of each factor that could optimize the response. In the analysis of the S/N ratio, three categories of performance characteristics are inherent i.e. lower-the-better, higher-the-better and nominal-the-better (Nalbant et al., 2007; Thamizhmanii et al., 2007). It is important to note that a statistical analysis using analysis of variance (ANOVA) is usually carried out to evaluate the statistically significant variables. Therefore, a Taguchi design coupled with ANOVA analysis could help to determine the optimum conditions for a process.

Only a few studies have reported the use of the Taguchi method to optimize process variables during the SCW gasification process (Kang et al., 2016b). Kang et al. (2016b) used the $L_{18} = 2^1 \times 3^3$ Taguchi method to study the influence of temperature, catalysts loading, biomass type and catalyst type on H2 yield during SCW gasification of cellulose, lignin, and waste biomass. The L_{18} design comprised of a mixture of a three-factor three-level design and one-factor two-level design with eighteen experiments. In terms of H_2 yield, the authors reported the importance of each parameter in the following order: temperature > catalyst loading > catalyst type > biomass type.

2.7.4 Response surface methodology

The response surface methodology (RSM) is a very popular statistical technique used to model and optimize a process where the output (i.e., response) is sensitive to various parameters. The RSM approach helps in evaluating the influence of various parameters and their interactions on the response. It uses empirical statistical methods to model the relationship between process variables and the response. The variables that affect the process (i.e., factors) can also be called the independent variables while the response (i.e., output) is known as the dependent variable.

In comparison to the univariate approach, RSM offers the following advantages. Firstly, RSM can study the interactive effects of the variables on the response. Secondly, RSM can develop a mathematical equation as a function of the variables and the response. The equation can be used to predict the response results for future observations. Moreover, RSM can save the process expenditures by minimizing the number of experiments, labor and resources involved. In the RSM methodology, the experimental data are usually fitted with a polynomial model at the second level (Silva, 2018). Compared to the factorial design, the second-order polynomial is suitable for systems where the relationship between the factors and response exhibits a curvature.

Figure 2.3 shows the sequential steps that should be applied when using the RSM for optimization studies. RSM starts with the problem description and identification of important factors and responses. In some cases, when several factors (> 6) are involved, a screening experiment could be performed to select the most important factors for further analysis followed by the selection of appropriate design. Finally, model evaluation and validation are carried out. Central composite design (CCD) and Box-Behnken (BBD) are the two most common RSM approaches used for optimization studies. The CCD approach is a factorial or fractional factorial design that contains a center point augmented with a group of star points or axial points. These points enable the estimation of curvatures in the model. The CCD method is suitable for sequential experiment designs where experiments with many factors can follow a screening to select the most significant factors. The CCD approach has an embedded factorial design whose results can be modified to include axial and center points as shown in Figure 2. 4. On the contrary, the BBD approach does not include an embedded fractional or full factorial design. Instead, the design points fall at combinations of the high- and low-factor levels and their center (mid) points (Minitab manual, 2019). Compared to the CCD method, the BBD approach does not have axial points. Therefore, the BBD method is useful for performing experiments that are feasible to operate beyond the safe operating limits. In the case of CCD design, the axial points could drift outside the cube (Figure 2.4), thus the design points could exceed the initial levels.

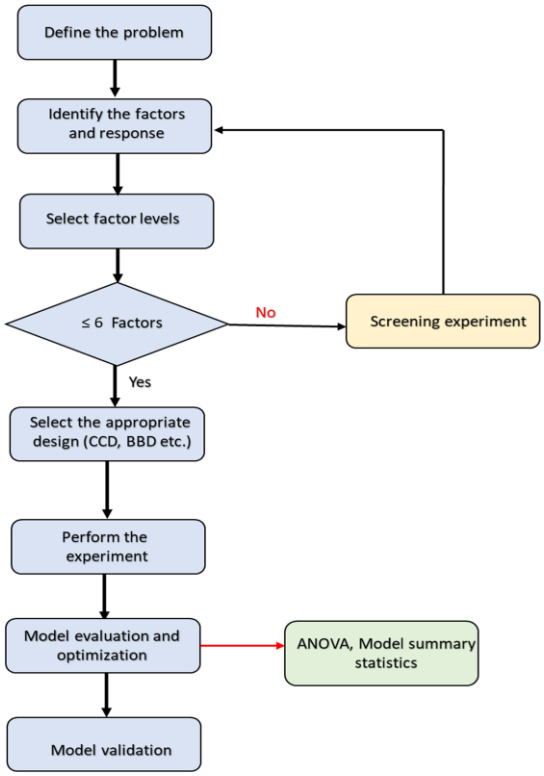

Figure 2.3:Sequential steps during the response surface methodology analysis.

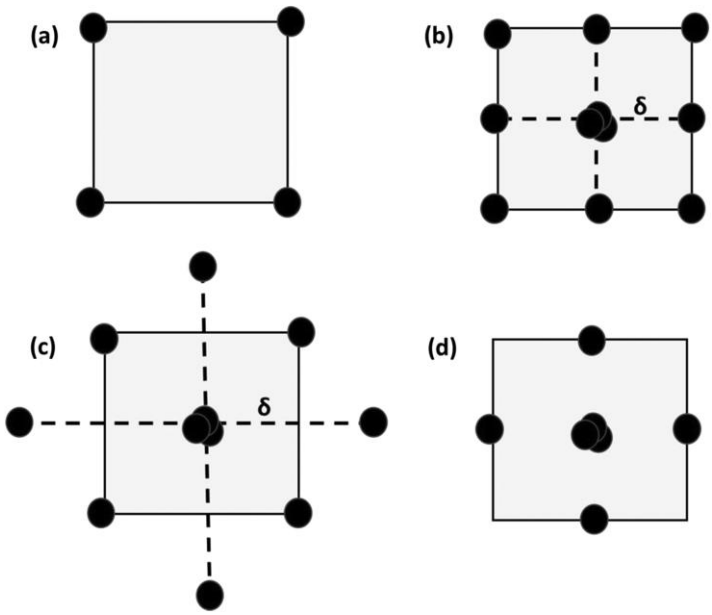

Figure 2.4: A 2D representation of different experimental designs: (a) factorial design, (b) central composite design with $\delta = 1$, (c) central composite design with $\delta > 1$, and (d) Box-Behnken design. δ represents the coded axial-point distance.

The CCD design has been applied to optimize SCW gasification studies by a few researchers. Yang et al. (2013) used the CCD method to optimize the gas yield by varying the reaction temperature (300-600°C), feed concentration (1-7 wt%) and KOH catalyst loading (0.61-2.39 mol/L) during the hydrothermal gasification of glycerol. Kang et al. (2015) used the CCD method to study the interactions between different process conditions and their influence on H_2 yield during the SCW gasification of lignin in a batch reactor. Their results show a strong interaction between water-to-biomass ratio and higher temperatures (>525°C) on H_2 yield. On the contrary, the changes in pressure did not affect H_2 yield drastically.

2.8 Modeling of hydrothermal gasification

2.8.1 Thermodynamic modeling

The application of thermodynamic models in hydrothermal gasification can help to predict the yield and composition of gas products, which is important for reactor design, unit operations, process optimization, energy recovery, techno-economic analysis and lifecycle assessment (De Blasio and Järvinen, 2017). In the field of hydrothermal gasification, thermodynamic models are generally applied for the prediction of thermodynamic equilibrium, which represents the state in which a system does not change its composition over time. Equilibrium of a system is a point when all the kinetics constraints are removed. Ideally, this condition would be reached when time tends to infinite.

Thermodynamic equilibrium models can be grouped into two main categories: non-stoichiometric and stoichiometric models. The stoichiometric approach involves the explicit definition of a system of chemical reactions converting reactants into products, while non-stoichiometric models only need the definition of a set of chemical compounds that are expected

at equilibrium. Despite the two classes of models have a radically different mathematical implementation, it can be proved that, if certain conditions are met, they are equivalent in terms of results (Fiori and Castello, 2014).

The stoichiometric approach involves defining a series of independent reactions comprising different species present in SCW gasification products. For each of these reactions, it is thus possible to calculate an equilibrium constant, which is a function of the equilibrium concentration of each chemical species, and that can be related to other thermodynamic properties (e.g. temperature and pressure) through the standard chemical potential. Therefore, by writing all these mathematical relations, along with element conservation equations, a system of algebraic equations is obtained, whose solution allows calculating the equilibrium composition. A detailed explanation of the implementation of stoichiometric models can be found elsewhere (Fiori and Castello, 2014).

Although stoichiometric models result in a relatively simple mathematical formulation (i.e. algebraic systems), they have not been widely utilized in the literature. The preferred approach to thermodynamic modeling is represented by the non-stoichiometric approach. This kind of model is based on the fact that the equilibrium composition of the system corresponds to a minimum of the system's Gibbs energy. To set a non-stoichiometric model, it is necessary to define a list of chemical species that are expected at equilibrium. Then, the model needs to calculate which distribution of the defined chemical compounds allows reaching the minimum Gibbs energy, provided that mass conservation is respected. From a mathematical point of view, a non-stoichiometric model is a non-linear constrained minimization problem, which can be solved numerically using commercial software (e.g., Matlab, Aspen Plus, etc.). The non-stoichiometric

method is widely used due to its flexibility and the fact that it prevents the omission of important reactions.

2.8.2 Kinetic modeling

Kinetic models describe the composition of syngas as a function of temperature and residence time, which is one of the key limitations of the thermodynamic equilibrium models. With the help of a kinetic model, it is possible to predict the evolution of the system over time and, therefore, calculate the dynamic mass and energy balances. This is fundamental to design reactors and equipment in general. The development of accurate kinetic equations for SCW gasification of biomass requires determining the reaction pathway and mechanism. However, this can be quite difficult due to the intrinsic high complexity of biomass feedstock and the formation of many intermediate degradation products at variable temperatures, reaction times, feed concentrations, as well as catalysts type and loading (Chen et al., 2019). Most of the kinetics models in SCW gasification are focused on calculating the kinetic parameters and predicting the total feedstock conversion. A few researchers have also explored the prediction of syngas yield and composition, which is crucial for practical applications (Jin et al., 2015a).

In summary, kinetics models provide information about the reaction rates for different possible reaction pathways during SCW gasification. Several kinetics models proposed in the literature have been observed to show reasonable agreement with experimental values. Kinetics parameters are important for the design and predict the product distribution with time during the SCW gasification process. Through the kinetics models, it is possible to show which reaction route or pathway is responsible for the production of a particular gaseous product. For example, reactions such as methanation and water-gas shift occur during SCW gasification. The former produces CH4. However, it is unsure if all the CH4 derived from the product yield is obtained

from methanation reaction or other reaction routes. Such questions could be answered with the aid of reliable kinetic models in combination with CFD.

2.8.3 Computational fluid dynamics

Computational fluid dynamics (CFD) modeling is based on fluid mechanics principles and the use of numerical methods to solve fluid flow equations (Lu et al., 2014a). The model can simulate fluid (i.e. liquid and gas) interactions whose surfaces are defined by a specific boundary condition. CFD modeling has been widely used to simulate several biomass conversions processes such as thermochemical gasification (Xue and Fox, 2014), pyrolysis (Papadikis et al., 2009), and liquefaction (Verma et al., 2015). However, it is rare to find the application of CFD models to study fluid behavior during hydrothermal gasification. The CFD approach can provide a clear understanding of the SCW gasification process and reactor upgrading or retrofitting. However, CFD modeling encounters certain challenges in hydrothermal gasification because of the complex transport and thermodynamic properties of subcritical and supercritical water. It is also difficult to select the most reliable turbulent heat-transfer models (Jin et al., 2016).

Goodwin and Rorrer (2011) used a CFD model to simulate SCW gasification of xylose in a microchannel reactor and study the influence of residence time on the gasification process. The model suggested that the endothermic gasification of xylose has minimal influence on the reaction temperature. Furthermore, the average fluid residence time was found to be dependent on the reacting fluid temperature and reactor configuration. The CFD model predicted the gas composition accurately except for the CH_4 yield (Goodwin and Rorrer, 2011).

Azadi et al. (2011) proposed a semi-theoretical model based on the numerical simulations of the SCW gasification process. The model was used to evaluate the heating time constant as a function of process conditions in an SCW gasification reactor. The authors also studied the effects

of various process parameters on the heating length of the SCW gasification reactor and heating time. The heating length was observed to be sensitive to flow rate while the external temperature and pressure showed little influence on the heating time constant (Azadi et al., 2011).

2.8.4 Process modeling

Compared to thermodynamic modeling approaches, process modeling provides insights about an entire hydrothermal gasification process by simulating the behavior and performance of each equipment and unit operation in a processing plant. This is valuable for process optimization and techno-economic analysis. Process modeling requires specialized software such as Aspen Plus (Aspen Technology, Inc., Massachusetts, USA), which is a problem-oriented input program to simulate an entire chemical process. It facilitates the development of small and complex reactions with built-in property data banks containing different stream properties.

Fiori et al. (2012) performed process simulation for SCW gasification of substrates such as glycerol, microalgae, sewage sludge, grape marc, and phenol to assess H2 production and energetic self-sustainability of the process. Their simulation results indicated that a minimum of about 15-25 wt% feedstock concentration is required for the process to be energetically self-sustainable. Moreover, for an SCW gasification reactor operating at 500°C, 30 MPa and 10 wt% feed concentration, the calculated thermal energy required for the microalgae process is about 0.6 MJ (Fiori et al., 2012).

Ortiz et al. (2011) used AspenPlusTM for process simulation of SCW gasification of glycerol. The predictive Soave-Redlich-Kwong equation of state was used to study the influence of process parameters on H_2 yield. The authors reported that pressure did not influence H_2 yield during the SCW gasification of glycerol. However, temperature affected the H_2 yields. The

maximum yield of H_2 was obtained at 900°C with 1 mol% of glycerol feed concentration (Ortiz et al., 2011).

In general, process modeling and CFD are wider contexts to apply thermodynamics and kinetics models, respectively. In process modeling, the overall aim is to estimate the cost of the process (reactor is often modeled with RGibbs, although it is not a requirement). In CFD modeling, the primary objective is designing the reactor, which requires consideration of a detailed fluid dynamics study. Furthermore, some kinetic studies should be incorporated into such an analysis.

2.9 Summary

SCWG technology is more promising than other thermochemical and biochemical technologies. Nevertheless, some limitations still exist that hinder the commercialization of this process. The feedstocks used for SCWG are those with extremely high disposal cost or hazardous nature to be treated by other conventional methods. Majority of the processing cost comes from the high-temperature and high-pressure requirements. Therefore, there has been several attempts to reduce the temperature requirements by using a suitable catalyst.

The catalysts used in SCWG can be homogeneous or heterogeneous. Homogeneous catalysts are more effective than heterogeneous catalyst, but their recovery and reuse are still the issues that limits their largescale industrial applications. Most of the research areas that involves the use of homogeneous catalysts focus mainly on their performance and product selectivity. Deactivation of heterogeneous catalysts during SCWG is another challenge limiting their usage . Catalyst deactivation could be caused by the following reasons: (i) inorganic compounds such as salt and mineral precipitation, which causes catalyst fouling; (ii) unwanted side reactions leading to coke and tar formation, which deposit on the catalyst surface; and (iii) poisoning of the active site of the catalyst by sulfur-containing compounds, and (iv) sintering of metallic catalysts.

Inorganic precipitation and coke formation can also lead to plugging problems during SCWG process. On the other hand, the harsh environment created by SCW medium facilitates the decline in the surface area of metallic catalysts and some changes in their surface structure, a phenomenon known as catalyst sintering.

We attempt to bridge the gap between the past research progress and the future perspectives. Regarding the commercialization of SCWG several economic issues and knowledge gaps are outlined below: (i) Most of the studies carried out on SCWG involved the use of biomass model compounds. However, more research on real biomass is required to understand their decomposition behavior in aqueous environment and foresee the challenges in large scale operations. Such studies could provide detailed understanding of the issues of real biomass complexity. (ii) In low-temperature catalytic SCWG, there has been enormous progress in the use of homogeneous catalysts, especially alkali carbonates to improve gas yields. However, the recyclability of homogeneous catalyst is still an issue that needs further attention. (iii) High-temperature and high-pressure requirement of SCWG means that there are many concerns associated with the process such as material corrosion and durability as well as waste heat generation. Recovery of waste heat during SCWG and its reuse within the processing plant or for power generation can considerably supplement the all-inclusive process expenditures relating to energy input. In conclusion, SCWG has immense potential towards the conversion of waste biomass to produce biofuels. Further research and development related to SCWG should continue to overcome the limitations associated with the technology.

Chapter 3 Hydrothermal Gasification Experimental setup and gas yield calculations

3.1 Hydrothermal gasification tubular batch reactor setup

All the hydrothermal gasification experiments in this thesis were performed in a in a tubular fixed-bed batch reactor made of stainless steel SS316 (length: 40 cm, outer diameter: 13 mm and inner diameter: 9 mm). Figure 3.1 shows a schematic representation of the gasification setup.

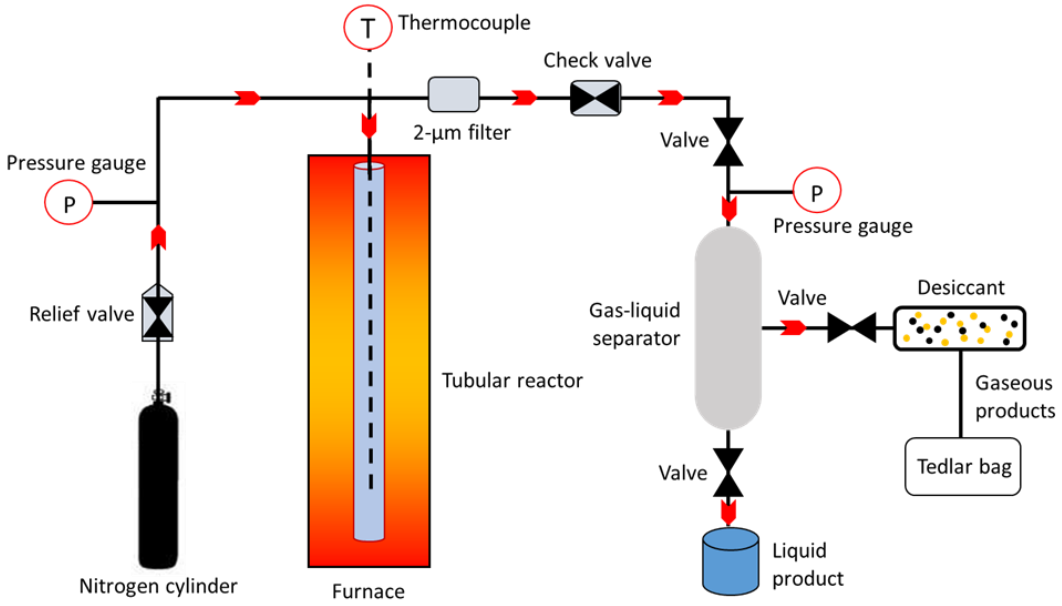

Figure 3.1: Schematics of the tubular hydrothermal gasification reactor.

The gasification assembly consisted of SS316 materials purchased from Swagelok (Swagelok Central Ontario, Mississauga, Ontario, Canada). The setup comprised of a tubular reactor enclosed inside an ATS Series 3210 furnace (Applied Test Systems, Butler, Pennsylvania, USA), thermocouples, pressure gauges, pressure relief valves, check valves, 2-µm filters, a gas-liquid separator, a desiccator, and a temperature controller system. For hydrothermal gasification

experiment, the desired feed material was loaded into the reactor together with the desired amount of water depending on the feedstock concentration. Prior to gasification experiment, a leak detection test was carried out to ensure safety relating to high-pressure and high-temperature operations. After the reactor assembly was sealed tightly, any trace amount of air was removed from the reactor by using a vacuum pump. Nitrogen gas was then used to purge the reactor, create an inert atmosphere, and supply the initial pressure required for the experiments i.e. 5–10 MPa. In the next step, the split furnace was used to heat the reactor to the desired temperature. The Omega type-K thermocouples (Spectris Canada Inc., Laval, Quebec, Canada) were used to continuously monitor and record the reactor temperature. Once the gasification reaction was completed, the furnace was switched off and the reactor was cooled by spraying cold water. The gas products, volatiles and vapors entered the gas-liquid separating cylinder where the gases were collected using Tedlar bags and the liquid products were collected after condensation. The desiccator trapped the moisture from the gas products before injecting into a gas chromatography system. Finally, the solid biochar product was recovered after cooling the reactor.

3.2 Indicators for comparing the gas yields.

The following indicators were used to quantify and evaluate the product gas yield during SCWG.

3.2.1 Individual gas yields and total gas yields

The gas yield of each product gas component was expressed in Equation 3.1 as the moles of each gas per gram of biomass feedstock used in the experiment (mmol g^{-1}) (Guo et al., 2007; Nanda et al., 2019a). The total gas yield was expressed as the sum of individual gas yield expressed in mmol g^{-1}.

$$\text{Gas yield } (\text{mmol/g}) = \frac{\text{Moles of individual gases}}{\text{Mass of biomass loaded into the reactor}} \qquad \text{Equation (3.1)}$$

3.2.2 Hydrogen selectivity

The hydrogen selectivity is calculated as the ratio of the moles of hydrogen to the sum of moles of other gaseous products excluding hydrogen. (Equation 3.2) (Nanda et al., 2015f).

Hydrogen selectivity (HS):

$$\text{HS } (\%) = \frac{\text{Moles of } H_2}{\text{Sum of moles of CO, } CO_2, \text{ } CH_4 \text{ and } C_1 - C_4} \qquad \text{Equation (3.2)}$$

3.3.3 Carbon gasification efficiency

The carbon gasification efficiency (CGE) is expressed in Equation 3.3 as the ratio of the number of carbons in the product gas from hydrothermal gasification to the carbon present in the feedstock. The CGE is expressed in percentage.

Carbon gasification efficiency (CGE):

$$\text{CGE } (\%) = \frac{\text{Sum of the number of moles of carbon in CO,} CO_2 \text{ and } CH_4}{\text{Number of moles of carbon in the feedstock}} \qquad \text{Equation (3.3)}$$

3.3.4 Lower heating values (LHV) and higher heating values (HHV)

The lower heating value (LHV) which is also defined as the net calorific value of a fuel is the quantity of heat released during the combustion of a specific amount of fuel material initially at room temperature and returning the temperature of the product of combustion to 150 ^{o}C . The LHV does not consider the latent heat of vaporization of water from the reaction products. The LHV values is calculated from Equation 3.4.

Lower heating value (LHV):

$$\text{LHV (kJ/Nm}^3) = 4.2 \times (30.3 \times \text{CO} + 25.8 \times \text{H}_2 + 85.4 \times \text{CH}_4 + 151.3 \times \text{C}_n\text{H}_m)$$

Equation (3.4)

The values of H_2, CO, CH_4 and C_nHm depict the molar concentration of the gaseous products.

The higher heating values (HHV) which considers the latent heat of vaporization of the water in the combustion products is calculated from Equation 3.5 (Friedl et al., 2005).

Friedl's formula:

$$\text{HHV (KJ/kg)} = (3.55 \times \text{C}^2) - (232 \times \text{C}) - (2230 \times \text{H}) + (51.2 \times \text{C} \times \text{H}) + (131 \times \text{N}) + 20600$$

Equation (3.5)

Where C, H and N represents the mole of carbon, hydrogen and nitrogen obtained from the ultimate analysis of the fuel.

3.3 Experimental error

The fixed bed batch reactor used in all experimental studies is prone to some inevitable experimental errors as outlined below:

- Some technical challenges were encountered during product collection thereby causing unaccounted product losses. For example, some fine char particles remained trapped in the gas-liquid separator during product collection before being entrained in the liquid effluents, thus creating some inaccuracies in measuring the mass of hydrochars.

- The weight percent of the gaseous product was estimated from the total gas yield, which may contain C_2-C_4 hydrocarbons. Adding these compounds to gas yield measurements could elevate the product yield.
- It is very challenging to control the pressure in the fixed bed reactor, therefore the desired pressure was pre – determined based on the reaction temperature.

3.4 Process safety analysis

Hydrothermal gasification experiment is performed under supercritical conditions (high temperature, > 350 ^oC and high pressure, 22 – 26 MPa. Therefore, the following safety procedures were considered during the experiments:

- All experiments were performed in a fume hood which is tightly covered with a sash to prevent the escape of dangerous gases and ensures the safety of the operator in case of unexpected accident.
- The reaction should only proceed if the leak detection test is positive.
- The reactor temperature was continuously monitored during each experimental run.
- After each experimental run, the batch reactor was allowed to cool down to room temperature before detaching from set up.
- The nitrogen cylinder was closed, and the pressure gauge was set to the lowest reading when not in us.
- A pressure relief valve was installed close to the reactor to ensure that the pressure does not exceed its maximum allowable limit. Furthermore, if at any point the pressure exceeds 27 MPa, the system is shut down immediately.

Chapter 4 Optimization and Modeling of Process Parameters During Hydrothermal Gasification of Biomass Model Compounds to Generate Hydrogen-Rich Gas Products

The content of this chapter has been published in the International Journal of Hydrogen Energy cited below and presented in the following conferences:

Citation :

Okolie, J. A., Nanda, S., Dalai, A. K., & Kozinski, J. A. (2020). Optimization and modeling of process parameters during hydrothermal gasification of biomass model compounds to generate hydrogen-rich gas products. International Journal of Hydrogen Energy, *45*(36), 18275-18288.

Conference Proceedings:

Okolie, J. A., Nanda, S., Dalai, A. K., & Kozinski, J. A. (2018). "Optimization and modeling of process parameters during hydrothermal gasification of biomass model compounds to generate hydrogen-rich gas products." Oral presentation at 68th Canadian Chemical Engineering Conference, Toronto, Ontario, Canada.

Contribution of the Ph.D. Candidate

Jude Okolie did the following: (1) Sample preparations and performing SCWG experiments; (2) Performing the characterization of gaseous, liquid, and solid products; (3) analyzing the experimental results; and (4) Writing the manuscript and provide responses to reviewers' comments. Dr Sonil Nanda helped with the experimental design and reviewed the manuscript. Dr. Ajay K. Dalai and Dr. Janusz A. Kozinski examined the research results, coordinated the manuscript preparation, and provided overall supervision of the research.

Contribution of this chapter to the overall PhD research

The first phase of the research is addressed in this chapter: To investigate how experimental factors, influence product gas composition and hydrogen yields during SCWG of model compounds representing cellulose, hemicellulose, and lignin. The factors are the experimental conditions (Temperature, reaction time, Feedstock concentration) and the interactions between them. This section proposes a reaction mechanism for lignocellulosic feedstock in SCW.

4.1 Abstract

Hydrothermal gasification in subcritical and supercritical water is gaining attention as an attractive option to produce hydrogen from lignocellulosic biomass. However, for process optimization, it is important to understand the fundamental phenomenon involved in hydrothermal gasification of synthetic biomass or biomass model compounds, namely cellulose, hemicellulose and lignin. In this study, the response surface methodology using the Box-Behnken design was applied for the first time to optimize the process parameters during hydrothermal (subcritical and supercritical water) gasification of cellulose. The process parameters investigated include temperature (300–500 °C), reaction time (30–60 min) and feedstock concentration (10–30 wt%). Temperature was found to be the most significant factor that influenced the yields of hydrogen and total gases. Furthermore, negligible interaction was found between lower temperatures and reaction time while the interaction became dominant at higher temperatures. Hydrogen yield remained at about 0.8 mmol/g with an increase in the reaction time from 30 min to 60 min at the temperature range of 300–400 °C. When the temperature was raised to 500 °C, hydrogen yield started to elevate at longer reaction time. Maximum hydrogen yield of 1.95 mmol/g was obtained from supercritical water gasification of cellulose alone at 500 °C with 12.5 wt% feedstock concentration in 60 min. Using these optimal reaction conditions, a comparative evaluation of the

gas yields and product distribution of cellulose, hemicellulose (xylose) and lignin was performed. Among the three model compounds, hydrogen yields increased in the order of lignin (0.73 mmol/g) < cellulose (1.95 mmol/g) < xylose (2.26 mmol/g). Based on the gas yields from these model compounds, a possible reaction pathway of model lignocellulosic biomass decomposition in supercritical water was proposed.

4.2 Introduction

Over the past few years, biofuel economy is perceived as one of the most promising alternatives to mitigate the challenges of greenhouse gas emissions and unmatchable reliance on fossil fuels (Nanda et al., 2015b). Hydrogen (H_2) is a clean and efficient energy source, which can be used as a direct fuel or converted into other hydrocarbon fuels and chemicals through Fischer-Tropsch catalysis. Since the product of combustion of H_2 is water, its utilization is widely regarded as being environmentally benign. Hydrogen finds many industrial applications in the upgrading of conventional petroleum, production of ammonium and desulfurization of heavy oils to meet stringent environmental regulations (Levin et al., 2004). Commercial H_2 is produced from the steam reforming of methane (Bej et al., 2017; Singh et al., 2018) due to its low production cost of US$ 1.5–3.7 per kg (Reddy et al., 2016). Only a small fraction of the global supply of H_2 gas is obtained from electrolysis of water due to the high energy requirement of the process (Rodriguez Correa and Kruse, 2018a). To reduce the over dependency on fossil fuels such as methane and reduce greenhouse gas emissions, the use of alternative resources for H_2 production such as lignocellulosic biomass is highly plausible.

Non-edible plant residues (i.e. lignocellulosic biomass) are renewable, plentiful, and widely regarded as an inexpensive source for renewable energy generation (Azargohar et al., 2019; Nanda et al., 2014) . Hydrogen can be produced through several thermochemical and biochemical

methods. The thermochemical technologies for H_2 generation include steam reforming, autothermal reforming, partial oxidation, gasification, and pyrolysis, whereas the biological technologies involve the participation of photosynthetic microorganisms such as photoheterotrophic bacteria and photoautotrophic algae (Nanda et al., 2017). Subcritical and supercritical water gasification are promising alternatives routes for producing H_2 from high moisture containing biomass.

Supercritical water (SCW) exists at temperatures and pressures beyond the critical point of pure water (374 °C and 22.1 MPa). Biomass is efficiently solubilized in SCW to produce gases consisting of H_2, CO_2, CO, CH_4 and smaller amounts of C_{2+} components (Kruse et al., 2005). SCW exhibits gas-like viscosity and liquid-like density, which makes it act like a green solvent to dissolve highly recalcitrant organic compounds to permanent gases (Basu and Mettanant, 2009). In addition, there is a significant reduction in the dielectric constant of water under supercritical conditions, which increases its ability to dissolve non-polar compounds (Kumar et al., 2018). The syngas (mostly H_2 and CO) obtained at high pressures from supercritical water gasification (SCWG) also reduces the compression costs for industrial applications.

Numerous studies have been published on the SCWG of different biomass compounds (Castello et al., 2015; Nanda et al., 2019a; Norouzi et al., 2017; Rana et al., 2019). However, the high heterogeneity and complexity of real biomass compounds still pose a significant challenge for conducting experimental studies to understand the fundamentals of SCWG process and its reaction pathway (Castello and Fiori, 2011). Therefore, it is essential to understand the decomposition behavior of individual biomass model compounds (e.g., cellulose, hemicellulose, and lignin) and their interactions under supercritical conditions. These model compounds can

imitate the composition of real biomass, thereby making it easier to explore the reaction pathways during SCWG.

Cellulose, hemicellulose, and lignin as the three main functional compounds in lignocellulosic biomass (Nanda et al., 2013). Extractives, also present as the non-structural components in lignocellulosic biomass, are readily soluble in water or neutral organic solvents. There are a few studies that report SCWG of biomass model compounds such as glucose (Lee et al., 2002), xylan (Pińkowska et al., 2011) and lignin (Kang et al., 2015). In addition, SCWG of fructose (Nanda et al., 2015f) and lactose (Nanda et al., 2015e) have also been reported as the model compounds of waste fruits and dairy products. Yoshida and Matsumura (2001) examined the combined gasification of cellulose, xylan, and lignin mixtures to understand the interactions among the three main constituents of lignocellulosic biomass. They showed that there was no signification interaction between cellulose and xylan. However, the presence of lignin in the feedstock significantly lowered H_2 and total gas yield, which suggested an interaction between lignin and holocellulose (cellulose and hemicellulose).

Despite the vast amount of literature available for the gasification of several biomass using SCW, only a few studies have investigated the decomposition patterns and behavior of the biomass model compounds. Moreover, studies on the effect of experimental conditions (i.e., temperature, reaction time and feedstock concentration) and their interactions on H_2 yield during SCWG is scarce in the literature. A lucid understanding of the effect of different experimental conditions and their interactions during SCWG could be useful for determining the process economics and optimization. Most studies in SCWG applies the univariate approach to study the influence of experimental conditions. Such procedures involve investigating the effect of a single process parameter while maintaining the other variables constant. Such approaches can discount the

interrelated effects among other significant parameters, thereby shedding their actual impacts on gas yields. If these parameters were altered together, and not individually, their combined impacts on syngas yields can be easily elucidated. Statistical models can be applied to study the interaction effects among each parameter. Kang et al. (2015) reported a central composite design (CCD) to optimize H_2 yields from non-catalytic gasification of lignin in SCW. At 600 °C, they observed a strong interaction between temperature and water-to-biomass ratio.

In the current work, we investigated the interactions among the process parameters (e.g., temperature, reaction time and feedstock concentration) on the product gas composition during hydrothermal gasification of biomass model compounds. In addition, this study also considered the interrelated effects between cellulose, hemicellulose, and lignin as well as the above-mentioned process parameters on the overall gas yields during SCWG. To study the effects of experimental conditions and the interactions between the biomass model compounds, the response surface methodology (RSM) based on the Box-Behnken design (BBD) was implemented in the present study.

The traditional "one variable at a time" (univariate) approach is often used by many researchers to optimize a process and study the effects of various factors on the response. The method involves testing the effect of a single variable on a response by keeping other variables constant (Kang et al., 2015). Although promising results have been achieved using this approach, the information about the actual interactions among the variables is not explained. However, the RSM incorporates a set of statistical techniques that are used for modeling and model exploitation (Muthukumar et al., 2003). Through a meticulous design of experiments, the RSM attempts to establish the relationship that exists between a set of measured dependent variables (responses) and the controlled independent variables (experimental factors). This approach allows the

development of mathematical models to predict the responses and study the statistical significance of the different factors of interest (Ferreira et al., 2007). Moreover, the interaction effects between the factors can be evaluated with minimal experimental runs, which is an added advantage.

To the best of our knowledge, this is the first study to implement BBD design for optimizing and studying the effects of process parameters including temperature, reaction time and feedstock concentration (biomass-to-water ratio) for maximum H_2 yield during SCWG of synthetic biomass comprising of cellulose, xylose and lignin. Initially, H_2 yields from hydrothermal gasification of cellulose was optimized following which the optimal reaction conditions were used to study the decomposition patterns and gaseous product distribution for other model compounds such as xylose and lignin. Cellulose was used for process optimization because in most of the available lignocellulosic biomasses, cellulose exhibits the largest composition compared to hemicellulose and lignin. Overall, lignocellulosic biomass consists of 30–60 wt% cellulose, 20–40 wt% hemicellulose and 15–25 wt% lignin on dry basis (Nanda et al., 2014). Finally, considering all the experimental results, a generic reaction pathway for synthetic biomass gasification in SCW was proposed. This study could provide a comprehensive knowledge useful for the identification of suitable biomass species and process conditions optimal for H_2-rich syngas production through hydrothermal gasification.

4.3 Materials and Methods

4.3.1 Feedstock collection and preparation

Three different biomass model compounds (i.e., cellulose, hemicellulose, and lignin) were used to represent the synthetic lignocellulosic biomass. The model compounds such as cellulose, xylose (hemicellulose) and Kraft lignin were purchased from Sigma-Aldrich (Oakville, ON, Canada). All model compounds were in high purity and in the form of dry powder. Nitrogen which

was used as the inert gas was purchased from Praxair Canada Inc. (Saskatoon, SK, Canada). The details of the hydrothermal gasification setup used for the experimental studies has been meticulously described in chapter 3. It should be mentioned that xylose was selected as hemicellulose model compound because it is a direct hemicellulose monomer. Furthermore, xylose has been used as a model compound to study the decomposition behaviour of hemicellulose in SCW by several authors (Gökkaya et al., 2016; Goodwin and Rorrer, 2011)

4.3.2 Feedstock and product characterization

The ultimate analysis of the model biomass compounds (cellulose, xylose, and lignin) was performed to estimate the proportions of carbon, hydrogen, nitrogen, sulfur, and oxygen using an Elementar Vario EL III CHNS analyzer (Elementar Analysensysteme, Hanau, Germany). The product gas composition from hydrothermal gasification of biomass model compounds was analyzed by an Agilent GC 7820A gas chromatograph (Agilent Technologies, Santa Clara, USA). The GC was equipped with a thermal conductivity detector (TCD) together with one capillary column and three packed columns. Ultimetal HayesepQ T 80/100 mesh column was used to measure the concentrations of H_2, CH_4 and CO while Ultimetal Hayesep T 80/100 mesh column was used to estimate the concentrations of CO_2 and C_2–C_4 gases. Argon was used as the carrier gas. The column and detector temperatures were maintained at 60 °C and 50 °C, respectively.

The yield of each product gas component was expressed as the moles of each gas per gram of biomass feedstock used in the experiment (mmol/g). On the other hand, the total gas yield was defined as the sum of individual gas yields expressed in mmol/g of feedstock. A detailed explanation of different indicators used for comparing gas yields have been provided in section 3.2 of chapter 3.

4.3.3 Design of experiments for modeling and optimization studies

In this work, the RSM approach using a 3-level and 3-factor Box-Behnken design was used to optimize H_2 yields and study the influence of different process variables on the gas yield during the SCWG of cellulose. The independent process variables selected for the experimental studies are temperature (300–500 °C), reaction time (30–60 min) and feedstock concentration (10–30 wt. %). H_2 yield expressed in mmol/g of feedstock was the dependent variable. Table 4.1 shows the investigated factors and levels for the BBD. The center values selected for the experimental design were temperature (400 °C), reaction time (45 min) and feedstock concentration (20 wt%). The number of experiments required for the Box-Behnken design was calculated using Equation 4.1, where k is the number of factors and C_0 is the number of center points.

$$N = 2k^2 - 2k + C_0 \quad (4.1)$$

Table 4.1: Box- Behnken experimental design factors and factor levels used for hydrothermal gasification of cellulose.

Factor	**Low level (-1)**	**Medium Level (0)**	**High Level (+1)**
Temperature, T (^oC)	300	400	500
Reaction time, R_t (min)	30	45	60
Feedstock concentration, C (wt %)	10	20	30

For this study, fifteen experimental runs containing triplicates at the center points were used. The experimental error was obtained using the center points. Design-Expert® Software version 8.0.7.1 (Stat Ease, Inc., Minneapolis, Minnesota, USA) was used to perform the experimental design and the runs were designed in a random order. The Box-Behnken design

procedure includes carrying out the statistically planned experiments and a regression equation resulting from the fitting of the data to different models. The best model was selected based on the sequential sum of squares (p-value and F-value) and the model summary statistics (R^2 i.e. coefficient of determination), adjusted R^2, predicted R^2 and standard deviation). The equation was used to approximate the relationship between the factors and their responses as well as for predicting the responses. The BBD is advantageous because it requires that all factors be run at only three levels and they are rotational or almost rotational (Yetilmezsoy et al., 2009). Moreover, there is a reduction in the number of experimental runs required for the design when compared to the 3-factors and 3-levels complete factorial design or the central composite design as reported by Kang et al. (2015).

4.4 Results and Discussion

4.4.1 Feedstock characterization

The ultimate analysis of cellulose, xylose and lignin used as the model compounds of the synthetic feedstock is shown in Table 4.2. Lignin had highest carbon content (47.4 wt%) followed by cellulose (42.5 wt%) and xylose (39.9 wt%). Cellulose did not show the presence of nitrogen and sulfur. On the contrary, lignin contained 0.1 wt% nitrogen and 3.9 wt% sulfur, while xylose had 0.1 wt% sulfur. Although, the present study does not involve the use of catalyst, it should be noted that for catalytic reactions, the presence of sulfur in the lignin could deactivate the catalyst. Lignin also showed the lowest oxygen content (43.8 wt%) because of its lower degree of oxidation compared to cellulose and xylose. Moreover, xylose had the lowest carbon content (39.9 wt%) and the highest oxygen content (54.2 wt%). Lignin is a phenylpropane polymer consisting of highly branched and cross-linked C–H groups as opposed to cellulose (containing long chain glucose

monomers) and hemicellulose (containing short chain pentose and hexose sugars) (Nanda et al., 2014).

Table 4.2: Ultimate analysis of cellulose, xylose and lignin.

Feedstock	**Carbon (wt %)**	**Hydrogen (wt %)**	**Nitrogen (wt %)**	**Sulfur (wt %)**	**Oxygen (wt%)**
Cellulose	42.5 ± 0.33	5.7 ± 0.83	0	0	51.7
Xylose	39.9 ± 0.07	5.9 ± 1.01	0	0.1 ± 0.11	54.2
Lignin	47.4 ± 0.12	4.8 ± 0.71	0.1 ± 0	3.9 ± 0.07	43.8

Note: Oxygen wt% composition was calculated by the difference of C, H, N, S wt%

4.4.2 Hydrothermal gasification of synthetic biomass

The reaction conditions, H_2 yield and total mass balance for the products obtained from hydrothermal gasification of cellulose in subcritical and supercritical conditions are reported in Table 4.3. The total mass balance ranged from 84.9 wt% to 95.6 wt%. The loss in mass could be due to the difficulties encountered during product collection leading to certain product losses as described in chapter 3. Ding et al. (2014) reported a mass balance of 53–59.8 wt% during SCWG of cellulose. Similarly, Kang et al. (2015) obtained a mass balance between 85.9 wt% and 93.5 wt% during SCWG of lignin.

As seen in Table 4.3 (experimental run 3), the maximum H_2 yield of 1.94 mmol/g was obtained from cellulose gasification under supercritical conditions (500 °C, 20 wt% feedstock concentration and 60 min). In contrast, lowest yield of H_2 was obtained from cellulose gasification under subcritical conditions (300 °C, 30 wt% feedstock concentration and 45 min) (Table 4.3, experimental run 7). The H_2 yield increased with temperature from 300 °C (subcritical water gasification) to 500 °C (supercritical water gasification) due to enhanced water-gas shift reaction (WGSR) and steam reforming reaction (Nanda et al., 2016b). Water-gas shift reaction is a reaction

between water vapor and CO to produce CO_2 and H_2. The reaction is favored at high temperatures (Equation 2.1).

Lee et al. (2002) gasified glucose as a model compound of cellulose in SCW at a temperature range of 470–750 °C under a constant pressure of 28 MPa. The authors observed a rapid increase in H_2 yields with temperature above 660 °C with a subsequent decrease in CO yield. The carbon gasification efficiency also approached 100% at about 700 °C. Therefore, greater SCW temperature of 500 °C was found to be optimal for maximum H_2 yields in this study.

4.4.3 Statistical evaluation and determination of regression model

As mentioned earlier, 15 experimental runs were carried out in triplicates in this study and regression analysis was used to estimate the coefficients of the model. To obtain the optimum conditions for H_2 yield and investigate the effect of process conditions, the experimental runs were performed in accordance with the experimental design in Table 4.1. The regression equation for understanding the relationship between H_2 yield and temperature, reaction time and feedstock concentration was obtained by fitting of the data to different models such as linear, quadratic, interactive and cubic. The adequacy of the models was determined by the sequential model sum of squares and the model summary statistics (Swamy et al., 2014), after which a multiple regression was performed to estimate the coefficients present in the mathematical model. The obtained model, which was used to predict H_2 yield was compared with the experimental yield as shown in Table 4.3.

Table 4.3: Experimental conditions, experimental and predicted hydrogen yields and mass balance from hydrothermal gasification of cellulose.

	Temperature (^{0}C)		Reaction time (Mins)		Feedstock Concentration (wt %)		Hydrogen Yield (mmol/g)		Overall mass balance (%)
Experimental number	**T (Coded)**	**T (Uncoded)**	**Rt (Coded)**	**Rt (Uncoded)**	**C (Coded)**	**C (uncoded)**	**Experimental Value**	**Predicted Value**	
1	0	400	1	60	10	-1	1.18	1.20516	88.7
2	0	400	0	45	20	0	0.88	0.90511	95.2
3	1	500	1	60	20	0	1.94	1.89447	91.6
4	-1	300	-1	30	20	0	0.64	0.69276	93.9
5	1	500	-1	30	20	0	1.36	1.34865	92.4
6	-1	300	0	45	10	-1	0.69	0.65307	94.9
7	-1	300	0	45	30	1	0.56	0.52691	87.4
8	0	400	-1	30	30	1	0.90	0.87594	87.7
9	0	400	0	45	20	0	0.99	0.90511	94.8
10	0	400	0	45	20	0	0.85	0.90511	89.9
11	1	500	0	45	10	-1	1.44	1.47303	94.8
12	1	500	0	45	30	1	1.49	1.52556	84.9
13	-1	300	1	60	20	0	0.72	0.73175	91.7
14	0	400	-1	30	10	-1	0.72	0.70228	94.4
15	0	400	1	60	30	1	0.94	0.90	95.6

The results of the model adequacy verification are presented in Table 4.4 and Table 4.5 . From the sequential model sum of squares table, it should be noted that a model with a low p-value (probability value) and high F-value are said to be significant. In addition, a model with non-significant lack of fit (p-value > 0.05) is also desirable. The F-value provides an indication of how each controlled factor affects the tested model. It can be defined as the ratio of regression mean square and mean of the real error (Swamy et al., 2014). On the other hand, the associated p-value evaluates whether the F-value is large enough to demonstrate statistical significance. The non-significant lack of fit confirms that the model fits properly with the response and the data can be used to interpret the model adequately (Dahmoune et al., 2014). From the lack of fit test, the quadratic model was observed to be highly insignificant with p-value of 0.5912 and was suggested as the best model.

Table 4.4: Model adequacy verification for the Box-Behnken design: Sequential model sum of squares for hydrogen yield during hydrothermal gasification of cellulose.

Source	**Sum of squares**	**Degree of freedom**	**Mean square**	***F*-value**	***p*-value**	**Remark**
Linear	0.29	9	0.032	5.87	0.1539	
2FI	0.17	6	0.028	5.17	0.1709	
Quadratic	0.013	3	4.44E-03	0.82	0.5912	Suggested
Cubic	0	0				Aliased
Pure Error	0.011	2	5.43E-03			

Abbreviations: *p*-value (Probability > *F*); 2-Factor interaction (2FI)

Table 4.5: Model adequacy verification for the Box-Behnken design: Model Summary Statistics for hydrogen yield during hydrothermal gasification of cellulose.

Source	**Standard deviation**	**R^2**	**Adjusted R^2**	**Predicted R^2**	**Remark**
Linear	0.16	0.8593	0.8209	0.7214	
2FI	0.15	0.9153	0.8518	0.6446	
Quadratic	0.07	0.9886	0.968	0.8878	Suggested
Cubic	0.074	0.9949	0.9641	+	Aliased

Abbreviations: 2-Factor interaction (2FI)

The model summary statistics was also used to verify the model adequacy based on the values of R^2 (coefficient of determination), adjusted R^2, predicted R^2 and standard deviation (Table 4.5). The quadratic model had the maximum adjusted R^2 (0.968), predicted R^2 (0.8878) (Table 4.5). The adjusted R^2 is the value of R^2 that has been adjusted to account for different number of predictors in a model. Furthermore, the quadratic model exhibited the lowest standard deviation of 0.07. The standard deviation, which is a measure of variability indicates the deviation of the model data from the mean. The lower the standard deviation, more closely the data points are arranged to the mean. It should be noted that although the cubic model had the highest R^2 value (0.9949) compared to the quadratic model (0.968), the quadratic model was suggested based on the adjusted R^2 value and standard deviation. Based on the results from the sequential sum of squares and model summary statistics, the quadratic model was selected to represent the relationship between H_2 yield and process conditions (i.e. temperature, reaction time and feedstock concentration). By using multiple regression analysis, the second-order equation obtained including the linear, square and interaction terms in coded factors is represented in Equation 4.2. On the other hand, the equation for the actual factor that can be used to predict the response is presented in Equation 4.3.

$$\mathrm{Y_i} = 0.91 + 0.45\mathrm{T} - 0.018\mathrm{C} + 0.15R_t + 0.045\mathrm{TC} + 0.13\mathrm{T}R_t - 0.1\mathrm{CR_t} + 0.18\mathrm{T}^2 - 0.048\mathrm{C}^2 + 0.074\mathrm{R_t}^2 \quad \text{(Equation 4.2)}$$

$$Y_i = 3.36 - 0.014858T + 0.030083C - 0.039333R_t + 0.000045TC + 0.0000833333TR_t - 0.0007CR_t + 0.0000184167T^2 - -0.000458333C^2 + 0.00032963R_t^2$$

(Equation 4.3)

where, Yi denotes H_2 yield; T, C and R_t denotes the dimensionless hydrothermal gasification temperature feedstock concentration and reaction time respectively for equation 4.2. On the other hand, in equation 4.3 the units T, C and Rt denotes the hydrothermal gasification temperature (^oC), feedstock concentration (wt.%) and reaction time (min) respectively. In addition, TC, TR_t and CR_t represent the process interactions such as temperature-feedstock concentration, temperature-reaction time, and feedstock concentration-reaction time, respectively. On the other hand, T^2, C^2 and R_t^2 signify the square term of the model. The predicted response for H_2 yield using the quadratic model correlates well with the experimental results as shown in Table 4.3.

The analysis of variance (ANOVA) was used to ascertain whether each independent variable and its interactions were significant. The value of alpha (α), used to evaluate the statistical significance in this study, is 0.05. A p-value ≤ 0.05 means that the model and all the terms associated with it are statistically significant (Soni et al., 2012). Similarly, a large F-value means that the model equation can explain the variation in the response adequately. Other descriptive statistics used to further assess the goodness of fit for the model include R^2, adjusted R^2, predicted R^2, sum of squares, coefficient of variation and the mean sum of squares. The ANOVA results presented in Table 4.6 show that the model has an F-value of 48.1 and p-value of 0.0003, which imply that the model is highly significant. For each individual term of the model, a p-value < 0.05 means that they are significant. The most significant parameter that affects H_2 yield is temperature with a p-value < 0.0001. The reaction time was also significant with p-value of 0.0019.

The interaction effects, especially TRt (temperature-reaction time) and CRt (feedstock concentration-reaction time) together with the square term for temperature (T^2) and reaction time (Rt^2) were also found to be significant. In general, two interaction terms and two square terms were found to be significant. The F-value of 0.82 and p-value of 0.5912 imply that the lack of fit is insignificant with respect to the pure error. Non-significant lack of fit is preferable for the model fit. To determine how well the model fits, R^2 and adjusted R^2 values were assessed. The value of R^2 (0.9886) implies that 98.9% of the variation in the response can be explained by the model (Table 4.6). On the other hand, the adjusted R^2 value of 0.9680 further confirms the significance of the model (Sadoun et al., 2018). The adjusted R^2 is the modified value of R^2 that has been adjusted to compare models with different number predictors since R^2 value increases whenever a predictor is added to a model. Therefore, the adjusted R^2 is suggested to be a better criterion. For new observations, the predicted R^2 helps to evaluate how well the model can predict the response. The predicted R^2 value of 0.8878 is in good agreement with the adjusted R^2 value. The results in Table 4.6 confirms that the equation is an actual representation of the relationship between the experimental conditions (factors) and H_2 yields (response).

To show the correlation between the experimental and predicted values, a parity plot is presented in Figure 4.1. The parity plot exhibits a satisfactory correlation between the observed and predicted values of H_2 yield. The data points are found to cluster around the straight line, which implies that there is a good agreement between the observed and predicted values. The normality of the dataset was also verified using the normal probability plot of the residuals as shown in Figure 4.2.

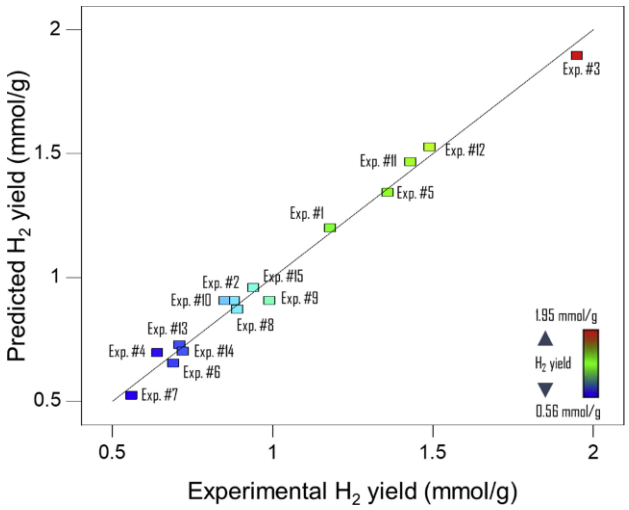

Figure 4.1: Parity plot showing the comparison between the experimental and predicted H_2 yield from different experimental runs during hydrothermal gasification of cellulose at 300–500 °C with 10–30 wt% feed concentration in 30–60 min.

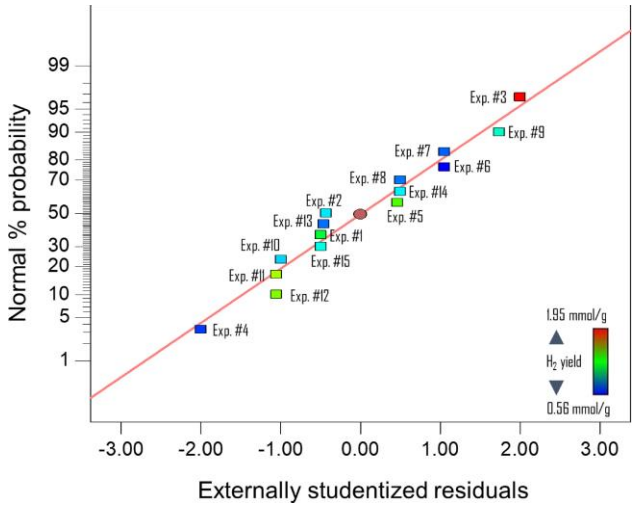

Figure 4.2: Normal probability plots of the residuals for H_2 yield from different experimental runs during hydrothermal gasification of cellulose at 300–500 °C with 10–30 wt% feed concentration in 30–60 min.

The residuals indicate the variation between the observed value of the response (H_2 yield) and the value obtained under the theoretical model. The normality plot is a useful diagnostic tool

that is used to identify and explain the deviations from the assumptions that the errors are normally distributed, their variances are consistent, and they are independent of each other [43]. As seen in Figure 4.2, the data points are reasonably close to the straight line, which shows that the data are normally distributed.

Table 4.6: Analysis of variance (ANOVA) and regression analysis of the models used to predict hydrogen yield from hydrothermal gasification of cellulose.

Source	**Sum of squares**	**Degree of freedom**	**Mean square**	***F*-value**	***p*-value**
Model	2.09	9	0.23	48.1	0.0003
Temperature, T (°C)	1.65	1	1.65	340.43	< 0.0001
Feed concentration, C (wt%)	2.45E-03	1	2.45E-03	0.51	0.5085
Reaction time, R_t (min)	0.17	1	0.17	35.37	0.0019
TC	9.03E-03	1	9.03E-03	1.87	0.2302
TR_t	0.068	1	0.068	13.97	0.0135
CR_t	0.042	1	0.042	8.69	0.0320
T^2	0.13	1	0.13	25.88	0.0038
C^2	8.63E-03	1	8.63E-03	1.78	0.2394
R_t^2	0.02	1	0.02	4.2	0.0958
Residual	0.024	5	4.84E-03		
Lack of fit	0.013	3	4.44E-03	0.82	0.5912
Pure error	0.011	2	5.43E-03		
Standard deviation	0.070	R^2	0.9886		
Mean	1.02	Adjusted R^2	0.9680		
CV	6.83	Predicted R^2	0.8878		
PRESS	0.24		24.144		

4.4.4 Effects of experimental factors and their interactions on hydrogen yield

Hydrothermal gasification of cellulose was performed at pressure ranges of 23–25 MPa to study the impacts of temperature (300–500 °C), reaction time (30–60 min) and feedstock concentration (10–30 wt%). The 3D response surface plots and 2D contour plots are useful in

understanding the influence of experimental factors and their interactions on the responses and obtain the optimal values of the variables within the study range. The plots are usually expressed as a function of two factors while the other factors are kept constant. Therefore, the 3D response surface plots and 2D contour plots were used in this study to investigate the influence of temperature, feedstock concentration and reaction time on H_2 yield. Since there are only three factors used for the regression model, one of the variables was kept constant at the center point for each of the plots. The 3D response surface plots as a function of two experimental variables (reaction time and temperature) with one variable fixed (feedstock concentration) at the center point and 2D contour plots are presented in Figure 4.3. In Figure 4.4, the reaction time was kept constant while the feedstock concentration and temperature were varied.

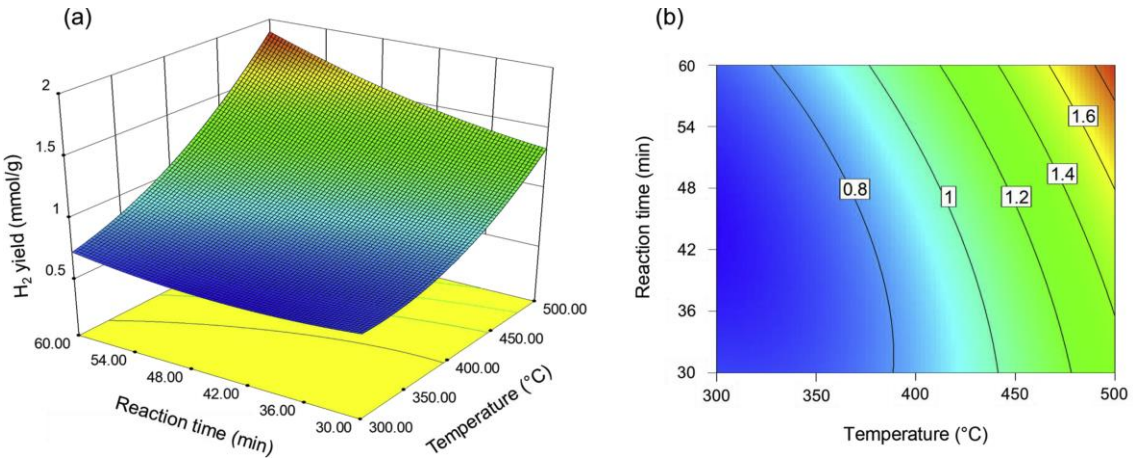

Figure 4.3: (a) 3D response surface plot and (b) 2D contour plot showing the influence of reaction time and temperature on H_2 yield from hydrothermal gasification of cellulose.

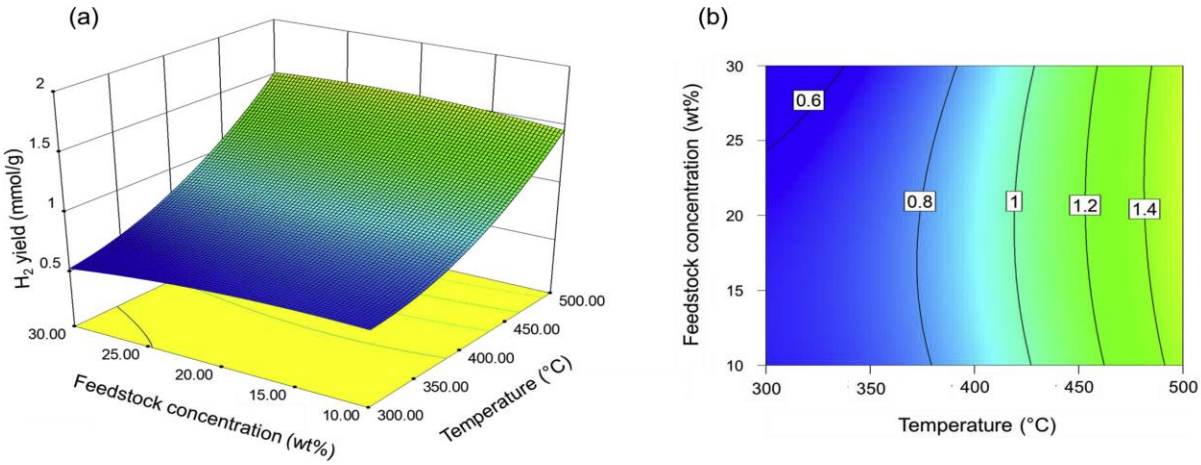

Figure 4.4: (a) 3D response surface plot and (b) 2D contour plot showing the influence of feedstock concentration and temperature on H_2 yield from hydrothermal gasification of cellulose.

It is evident from Figures 4.3 and 4.4 that H_2 yield increases with temperature and reaction time. As the temperature increases from 300 °C (subcritical conditions) to 500 °C (supercritical condition), two reaction pathways are inherent, i.e. the ionic pathway and free radical pathway (Kruse, 2008). The ionic pathway is dominant at subcritical conditions, whereas the free radical pathway is favorable at supercritical conditions. As the temperature elevates from 300 °C to 500 °C, the ionic product concentration i.e. K_w (H^+ and OH^-) also increases up to a maximum value at around 300 °C before decreasing at higher temperatures (Kumar et al., 2018). The initial increase in ionic concentration provides more hydronium ions (H_3O^+), thereby facilitating acid-catalyzed reactions. Besides, the decrease in K_w at higher temperatures from subcritical to supercritical water gasification is attributed to a decrease in the density of water. This also leads to enhanced free radical mechanisms as low water density is preferable for free radical reactions (Nanda et al., 2015e). The free radical mechanisms play a major role in improved solvation of organic compounds, thereby leading to enhanced gas yields. Like temperature, an increase in reaction time from 30 to 60 min led to a subsequent rise in H_2 yields. In the present study, an increase in H_2 yield with temperature and reaction time was observed during the SCWG of cellulose. Keeping the other

parameters constant, H_2 yield elevated from 0.56 mmol/g at 300 °C (experimental run 7) to 1.94 mmol/g at 500 °C (experimental run 3) (Table 4.3). In the same way, as the reaction time prolonged from 30 min to 60 min, the H2 yield increased from 0.64 mmol/g (experimental run 4) to 1.94 mmol/g (experimental run 3).

Longer reaction time leads to improved H_2 yields by enhancing the primary reactions taking place under supercritical conditions (Rana et al., 2019). The primary reactions occurring under high temperature in supercritical conditions include bond cleavage, dehydration, decarboxylation, deamination and depolymerization (Toor et al., 2011). Regarding the interactions between reaction time and temperature, it should be mentioned that the effect of increasing reaction time on H_2 yield at supercritical conditions was more pronounced than at subcritical conditions. For instance, at 300 – 400 °C, the interactions between reaction time and temperature was weaker. The H_2 yield remained at about 0.8 mmol/g with an increase in reaction time from 30 min to 60 min at the temperature range of 300–400 °C (Figure 4.3b). This shows that an increase in reaction time from 30 min to 60 min had an insignificant increase in H_2 yield. When the temperature increased up to 500 °C, the interaction between H_2 yield and temperature became significant as the H_2 yield starts to increase with longer reaction time. This behavior could be a result of the formation of char and tar from partially decomposed biomass at low temperatures in subcritical conditions (Gong et al., 2017a, 2017b).

Char and tar are polymeric compounds that are highly challenging to breakdown even at longer reaction time restricting further degradation of the feedstock intermediates and gas formation (Gong et al., 2017a; Sivasangar et al., 2015). Similar results was obtained by Tiong et al. (2016) during the SCWG of microalgae *Chlorella vulgaris* and *Scenedesmus quadricauda*. The amount of gas yield remains almost the same by increasing the reaction time more than 30 min at

385 °C and 26 MPa (Tiong et al., 2016). A recent study by Samiee-Zafarghandi et al. (2016) also reported a similar trend. They investigated the gasification of microalgae in SCW at a temperature range of 355–405 °C, reaction time of 15–45 min and biomass loading of 1–8 wt%. By increasing the reaction time from 15 min to 45 min at 405 °C (supercritical conditions), the H_2 yield improved from 13.3 mol% to 20.9 mol%. However, at 355 °C (subcritical conditions), the increase in H_2 yield was insignificant (1.1–1.2 mol%) (Samiee-Zafarghandi et al., 2018).

Concerning the influence of the feedstock concentration on H_2 yield, a negative effect occurs on H_2 yield at higher feedstock concentration. A negative coefficient of feedstock concentration (represented as C in Equation 4.2) in the regression model presented in Equation (4.2) also confirms the negative effect. Furthermore, the interaction between feedstock concentration and temperature is insignificant (Table 4.6). Therefore, an increase in the feedstock concentration means a decrease in water molecules compared to the amount of feedstock. Similarly, a reduction in feedstock concentration translate into higher amount of water molecules compared to the feedstock. The high amount of water molecules leads to enhanced solvation properties in SCW, better solvation of biomass and improved gas yields. Since a majority of the H_2 produced from SCWG is supplied by water acting as a reactant , it is imperative to have excess amount of water to achieve high H_2 yield from biomass. The excess amount of water can be provided at low feedstock concentration.

Fig.4.4a shows that at supercritical conditions (temperature of 500 ^{o}C) there is a slight increase in hydrogen yield with feedstock concentration. The increasing hydrogen yield could be attributed to the interactive effects between feedstock concentration and reaction temperature at supercritical conditions. This is also confirmed by the ANOVA results in Table 4.6. The p- value

for the interactive term between temperature and feedstock concentration is significant with a value less than 0.05.

4.4.5 Optimization of hydrogen yield

In the present study, the Box-Behnken design with 3-factors and 3-levels were employed to obtain the best combination of experimental conditions (i.e., temperature, feedstock concentration and reaction time) to produce the maximum H_2 yield. The numerical optimization function in Design-Expert® software was used for the process optimization. All the variables are set within the experimental limits, i.e., temperature ranges: 300–500 °C, feedstock concentration: 10–30 wt% and reaction time ranges of 30–60 min (Figure 4.5). According to the 3D surface plot in Figures 4.3 and 4.4, at 500 °C, 60 min and 20 wt% feedstock concentration, the highest H_2 yield obtained was 1.89 mmol/g. Therefore, the value of H_2 yield in the optimizer was set to be greater than or equal to 1.9 mmol/g in the Design-Expert® software. The numerical optimization produced a maximum H_2 yield of 1.92 mmol/g at optimal reaction conditions of 500 °C, 60 min and 12.5 wt% feedstock concentration. By using the obtained reaction conditions, a test experimental run was carried out to validate the model. The value of H_2 yield obtained from the experimental run at optimal conditions (temperature: 500 °C, reaction time: 60 min and feedstock concentration: 12.5 wt%) was 1.95 mmol/g. The percentage error between the experimental and predicted values was calculated using Equation 4.5. The percentage error between the experimental and predicted result was found to be less than 2%.

$$\text{Percent Error} = \frac{(\text{Experimental value of } H_2 \text{ yield} - \text{Predicted value of } H_2 \text{ yield})}{\text{Experimental value of } H_2 \text{ yield}} \times 100$$

(Equation 4.3)

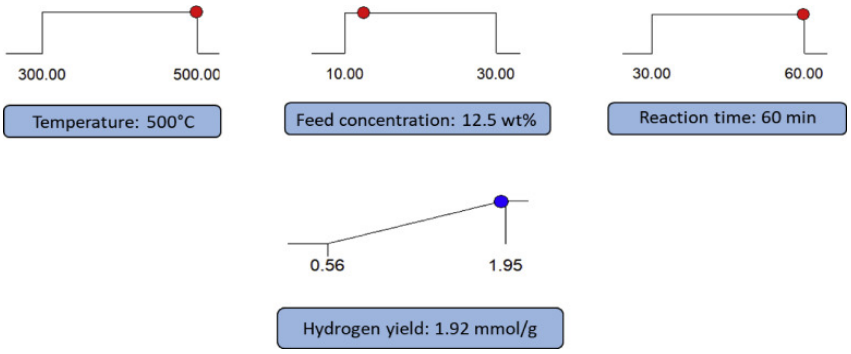

Figure 4.5: Experimental limits set for each process conditions and the response (H_2 yield) together with their optimal values.

4.4.6 SCWG of biomass model compounds

The model compounds representing cellulose, xylose and lignin were gasified at optimal conditions (temperature: 500 °C, feedstock concentration: 12.5 wt% and reaction time: 60 min) to compare their gas yield and understand the behavior of each component under supercritical conditions. The distribution of the gaseous products was useful for the prediction of reaction mechanism of model compounds and their decomposition patterns. Figure 4.6 shows the gaseous product distribution of the SCWG of biomass model compounds at optimal reaction conditions. As seen in Figure 4.6, gases produced during the gasification of lignocellulosic model compounds are CO_2, H_2, CH_4, CO and C_2–C_4 hydrocarbons. Almost half of the H_2 is supplied by the WGSR while CH_4 production is attributed to methanation and hydrogenation reactions (Azadi et al., 2012a). However, it should be noted that since H_2 is the desired product of SCWG, methanation reaction should be suppressed while enhancing the water-gas shift reaction, which is achieved through the application of selective catalysts.

The product gas distribution varies for all the model compounds, which indicates that properties such as functional groups and chemical linkages influence biomass decomposition and gas evolution under SCW conditions (Samiee-Zafarghandi et al., 2018). Cellulose demonstrated

highest CO_2 (3.24 mmol/g), CO (0.17 mmol/g) and CH_4 (1.79 mmol/g) yields (Figure 4.6). Furthermore, from Figure 4.6, H_2 yield decreases in the order of xylose (2.26 mmol/g) > cellulose (1.95 mmol/g) > lignin (0.73 mmol/g). Similar trend was obtained by Sivasangar et al. (2015). They stated that the highest H_2 yield was obtained from the model compound representing hemicellulose. This could be because of the decomposition of formic acid produced during the hydrolysis of xylose to form CO_2 and H_2 under SCW conditions. Highest H_2 selectivity was also found in the case of xylose (57.9%) as shown in Table 4.7. Cellulose demonstrated highest CO_2 (3.24 mmol/g), CO (0.17 mmol/g) and CH_4 (1.79 mmol/g) yields (Figure 4.6).

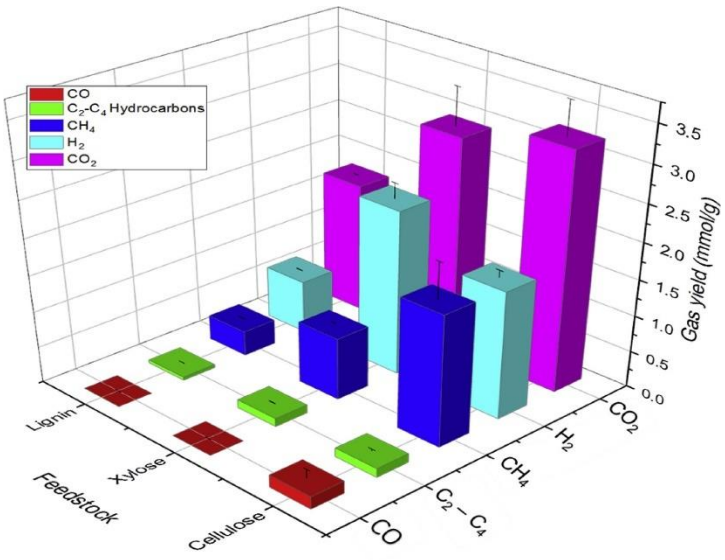

Figure 4.6: Gas yields from supercritical water gasification of cellulose, xylose and lignin at optimal process conditions (temperature: 500 °C, feedstock concentration: 12.5 wt% and reaction time: 60 min).

Table 4.7: Total gas yields, hydrogen selectivity and lower heating value of gas products obtained from SCWG of biomass model compounds at optimal conditions (temperature: 500 °C, feedstock concentration: 12.5 wt% and reaction time: 60 min).

Model Compound	Total gas yield (mmol/g)	Hydrogen selectivity (%)	LHV (kJ/Nm$^{3)}$
Cellulose	5.97	32.82	935.73
Xylose	6.16	57.91	626.10
Lignin	2.92	33.32	231.67

The molecular weights of cellulose, hemicellulose (xylose) and lignin are 342 g/mol, 150 g/mol and 1514 g/mol (Nanda et al., 2015d). Moreover, the degree of polymerization of cellulose is 1510–5500, whereas for hemicellulose it is 50–200 (Hu and Ragauskas, 2012). Each cellulose polymer comprises of long-chain polysaccharide with 7000–15,000 glucose monomers, whereas each short-chain polysaccharide in hemicellulose consists of 500–3000 glucose monomers. In addition, cellulose is mostly present in both crystalline and amorphous forms while hemicellulose is amorphous and easily hydrolysable. Owing to the relatively lower degree of polymerization and lower molecular weight and short-chain nature, hemicellulose (xylose) is easily hydrolyzed and gasified in hydrothermal gasification compared to cellulose and lignin, which require more intense reaction conditions for near-complete conversion.

The gases such as CO and CO_2 are produced because of the cleavage of functional groups such as carboxyl and carbonyl groups that are present in the basic subunits of lignocellulosic biomass (Sivasangar et al., 2015). However, CO is consumed during the WGSR, which explains the lowest amount of CO compared to all gases produced in the model compounds. Another explanation for the high concentration of CO and CO_2 in cellulose compared to xylose and lignin could be because cellulose has a higher amount of carbonyl and carboxyl functional groups in its

chemical structures (O'Sullivan, 1997). Cellulose is a polymer of glucopyranose linked together by β-1,4 d-glucose subunits and rich in C–O and O–H groups compared to hemicellulose and lignin (Sivasangar et al., 2015; Yang et al., 2007). The hydrothermal cleavage of such functional groups presents in cellulose results in the production of high concentrations of CO and CO_2.

Among all the model compounds, the total gas yield decreased as xylose (6.16 mmol/g) > cellulose (5.97 mmol/g) > lignin (2.92 mmol/g) (Table 4.7). Furthermore, the gaseous products from cellulose exhibited the highest LHV of 935.7 kJ/Nm^3 followed by xylose (626.1 kJ/Nm^3) while the gaseous products from the SCWG of lignin had the lowest LHV of 231.7 kJ/Nm^3. An increase in the LHV of the gaseous products from cellulose compared to those from other model compounds was due to the superior concentrations of CO, CH_4 and $C_2 – C_4$ hydrocarbons found in the gas products obtained from SCWG of cellulose.

4.4.7 Proposed reaction pathway for hydrothermal gasification of lignocellulosic biomass

Based on our experimental observations, a possible pathway for the hydrothermal gasification of lignocellulosic biomass in subcritical and supercritical water was proposed (Figure 4.7). Lignocellulosic biomass is a complex mixture that consists of three main functional groups, namely cellulose, hemicellulose and lignin. During SCWG, two reaction mechanisms are inherent such as the ionic mechanism, which occurs at low subcritical temperatures and the free radical mechanism, which occurs at higher supercritical temperature (>500 °C). At temperature and pressure above the critical point of water, there is a decrease in density, ionic product, and dielectric constant of water, which leads to enhanced free radical mechanisms at the same time inhibiting ionic mechanism (Kumar et al., 2018). Under subcritical temperatures, lignocellulosic biomass initially undergoes hydrolysis reaction to produce hydrolyzed products. Carbohydrates

such as cellulose and hemicellulose degrade into monomeric pentose and hexose sugars (e.g., glucose, xylose, arabinose, mannose, rhamnose, etc.), whereas lignin decomposes into phenolic compounds and formaldehydes (e.g. guaiacol, cathecol, syringol and cresol).

The hydrolysis products of cellulose and hemicellulose are further converted via intermediate degradation into furfurals and hydroxymethylfurfural. These intermediate products further dissociate into permanent gases (e.g., CO_2, CO, H_2, CH_4 and $C_2 - C_4$ gases) via ionic mechanisms. The phenolic compounds generated during the hydrolysis of lignin have the tendency to react and polymerize into heavier molecular weight compounds such as tar and char at longer reaction times. On the contrary, when free radical mechanisms dominate, the carbohydrates and organic acids produced during the hydrolysis of cellulose undergo secondary hydrolysis to produce aldehydes, phenolics and aromatics to further degrade into product gases. The concentration of product gases is dependent on the reaction temperature, reaction time, feedstock concentration and the interactions between these parameters. These parameters influence gasification reactions e.g. WGSR, methanation, hydrogenation and Boudouard reactions (Rodriguez Correa and Kruse, 2018a). Boudouard reaction results in char and coke formation with the consumption of CO as shown in Equations 2.7 and 2.8.

As mentioned earlier, during SCWG, water could act as an organic solvent by producing free radicals that take part in the decomposition of organic components. SCW also behaves as a catalyst and the reaction medium, thereby promoting the degradation of lignocellulosic biomass into mostly combustible gases. However, the high temperature requirements for SCWG is still a concern, due to the cost involved, challenges in selecting a suitable reactor material to withstand harsh conditions and the potential risks of char/tar-induced plugging issues. Therefore, various

homogeneous and heterogeneous catalysts are used to improve gas yield and reduce char/tar formation while simultaneously decreasing temperature requirements.

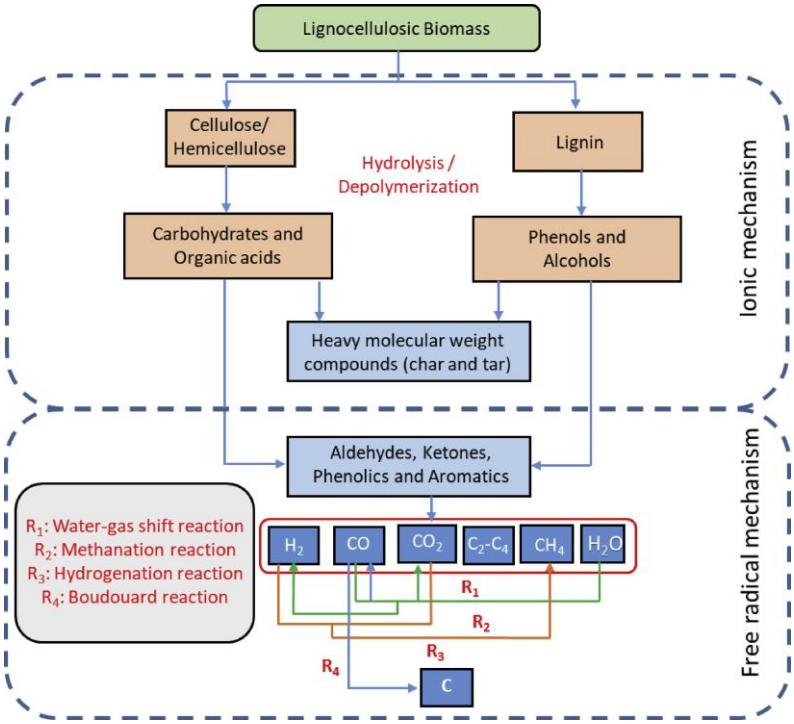

Figure 4.7: Reaction pathway during hydrothermal gasification of lignocellulosic biomass.

4.5 Conclusions

The RSM method based on the Box-Behnken design was applied to study the hydrothermal gasification of cellulose as a lignocellulosic biomass model compound for the first time. The parameters studied were temperature (300–500 °C), reaction time (30–60 min) and feedstock concentration (10–30 wt%). Maximum H_2 yield of 1.95 mmol/g was obtained at 500 °C with 12.5 wt% feedstock concentration in 60 min of reaction time. A comparative evaluation of the SCWG of biomass model compounds representing cellulose, xylose and lignin shows that xylose had the highest H_2 yield of 2.26 mmol/g. Lignin had the lowest H_2 yield (0.73 mmol/g), which is

attributed to its highly polymeric and recalcitrant chemical structure difficult to decompose even at supercritical conditions. The disparity in product gas composition between the model compounds signifies that chemical linkages and functional groups influence the decomposition patterns and the gaseous products formed during SCWG process. The reactant water through the water-gas shift reaction supplies majority of the H_2 in the syngas. The total gas yields for the model compounds decreased in the following order: xylose (6.16 mmol/g) > cellulose (5.97 mmol/g) > lignin (2.92 mmol/g). Based on the experimental observations, many important reactions involved in product gas formation during SCWG such as water-gas shift reaction, steam reforming reaction, methanation, hydrogenation and Boudouard reaction were identified. These reactions are useful during the stoichiometric thermodynamic analysis to predict gas yield and composition.

Chapter 5 Hydrothermal Gasification of Soybean Straw and Flax Straw for Hydrogen-Rich Syngas Production: Experimental and Thermodynamic Modeling

The content of this chapter has been published in the Energy conversion and management journal cited below and presented in the following conferences:

Citation :

Okolie, J. A., Nanda, S., Dalai, A. K., & Kozinski, J. A. (2020). Hydrothermal gasification of soybean straw and flax straw for hydrogen-rich syngas production: Experimental and thermodynamic modeling. Energy Conversion and Management, 208, 112545.

Conference Proceedings:

Okolie, J. A., Nanda, S., Dalai, A. K., & Kozinski, J. A. (2019). Hydrothermal gasification of soybean straw and flax straw for hydrogen-rich syngas production: Experimental and thermodynamic modeling. Poster presentation at the first EGCC poster competition, University of Saskatchewan, Canada.

Contribution of the Ph.D. Candidate

Jude A. Okolie: (1) Sample preparations and performing SCWG experiments and thermodynamic modeling (2) Performing the characterization of gaseous, liquid, and solid products (3) analyzing the experimental results (4) Writing the manuscript and provide responses to reviewers' comments. Dr Sonil Nanda helped with the experimental design and reviewed the manuscript. Dr. Ajay K. Dalai and Dr. Janusz A. Kozinski examined the research results, coordinated the manuscript preparation, and provided overall supervision of the research.

Contribution of this chapter to the overall PhD research

The second phase of the research is addressed in this chapter: To optimize hydrogen yield from SCWG of Flax straw and Soybean straw and study the effects of process parameters such as temperature, pressure BTW ratio and reaction time on hydrogen yield. The experimental results were compared with theoretical values to determine if the SCWG batch reaction results approach equilibrium values.

5.1 Abstract

Biofuels produced from lignocellulosic feedstocks are gaining popularity because of the elevating energy demand, increasing greenhouse gas emissions, escalating fuel prices, and dwindling fossil fuel resources. Therefore, it has become important to seek alternative energy resources from renewable waste biomass. In this study, agricultural crop residues such as soybean straw and flax straw were gasified in subcritical water (300 °C) and supercritical water (400 and 500 °C) for H_2 production. To maximize the non-catalytic process, the impacts of temperature (300–500 °C), biomass-to-water ratio, BTW (1:5 and 1:10), biomass particle size (0.13 mm and 0.8 mm) and residence time (30–60 min) on H_2 production were studied at a pressure range of 22–25 MPa. Maximum H_2 yield and total gas yields of 6.62 mmol/g and 14.91 mmol/g, respectively were obtained from soybean straw at the highest temperature (500 °C), lower feed concentration (1:10 BTW), smaller particle size biomass (0.13 mm) and longer residence time (45 min). To evaluate the drift in the experimental H_2 yield from the theoretical values, thermodynamic modeling using Gibbs free minimization method was performed. The experimental results showed slight deviations from the thermodynamic models due to the temperature gradient and absence of agitation in the tubular batch reactor. However, the KOH catalyst was found to elevate the H_2, CO_2

and CH_4 yields for soybean straw and flax straw. The findings suggest that supercritical water gasification could be an efficient green technology for H_2 production from waste biomass.

5.2 Introduction

In the present day, the world encounters problems due to rising energy demands, which arise mostly because of rapid industrialization and urbanization due to population growth. Fossil fuels are predominantly used to quench the increasing energy demand. However, their consumption is constrained by the rising fuel prices, exhausting finite resources, greenhouse gas emissions, global warming and pollution issues associated with their extraction, processing, and utilization (Nanda et al., 2016f). Therefore, there is a need to develop alternative energy sources that are reasonable, sustainable, reliable and environmentally benign such as biofuels (e.g. bio-oil, biodiesel, bioethanol, biobutanol, biomethane and biohydrogen) (L. Zhang et al., 2010). Additionally, these energy resources should have the potential to complement fossil fuels and mitigate the environmental challenges associated with fossil fuel consumption (Parparita et al., 2015).

Hydrogen (H_2) is widely seen as a promising energy carrier and alternative fuel in the energy sector. In the last decade there has been a progressive increase in the demand for H_2 production for use as transportation fuels, hydrotreating (hydrodesulfurization, hydrodenitrogenation and hydrodeoxygenation), heavy oil upgrading and fuel cells (Levin et al., 2004). Recently, lignocellulosic biomass (e.g. energy crops, agriculture residues and forestry biomass) has received immense attention for biofuel production due to its abundant availability, low cost, and the ability to reduce atmospheric CO_2 through photosynthesis (Fougere et al., 2016). Furthermore, they do not pose any “food versus fuel” issues unlike the starch-based feedstocks (e.g. oilseeds, grains, corn, potato, cassava, etc.), which are associated with the risk of diverting

large farmlands and food crops for fuel production (Fougere et al., 2016). Hydrogen produced from lignocellulosic biomass is widely considered as a green fuel for combined heat and power generation due to its high-energy content. Compared to other conventional fuels, H_2 has a very high-energy content of 120–142 MJ/kg. Moreover, the combustion product of H_2 is pure water, which makes it a much cleaner fuel.

Presently, catalytic steam reforming of methane is the most preferred industrial method of producing H_2 with an estimated efficiency of about 85% (Shafiqah et al., 2020). Nonetheless, steam reforming is a process that uses large quantities of hydrocarbons, thereby generating enormous amounts of greenhouse gas emissions (Abatzoglou and Fauteux-Lefebvre, 2016). Renewable H_2 production through different biological (e.g. photo-fermentation and dark fermentation) and thermochemical conversion (e.g. gasification and pyrolysis) of waste biomass offer the possibility of reducing or eliminating the greenhouse gas emissions while improving the process economics. Among the biomass conversion methods, hydrothermal gasification is emerging as a promising method for H_2 production from a wide variety of waste resources such as lignocellulosic biomass, sewage sludge and municipal solid wastes (Okolie et al., 2020a). Moreover, hydrothermal gasification can effectively convert biomass containing high moisture content, which otherwise requires expensive pretreatment and drying steps before thermochemical conversion, thus imparting additional processing costs. The thermochemical conversion of wet biomass becomes inefficient because the heat of liquid evaporation usually exceeds the heat of combustion of the biomass (Okolie et al., 2019).

Water at a temperature and pressure above its critical point (T_c > 374 °C and P_c > 22.1 MPa) is known as supercritical water (SCW) (Reddy et al., 2014b). In contrast, subcritical water (SbCW) exists at temperatures and pressures below the water's critical points (T_c < 374 °C and

Pc < 22.1 MPa). SCW exhibits a gas-like viscosity and liquid-like density that makes it an excellent candidate for biomass conversion through gasification, liquefaction, and oxidation (Reddy et al., 2015). SCW gasification results in a hydrogen-rich syngas product that also contains certain levels of CO, CO_2, CH_4 and C_{2+} gases (Elif and Nezihe, 2016). Furthermore, the use of high pressures in SCWG eliminates the requirement for gas compression and downstream shift reactor (Lu et al., 2008).

Soybean (*Glycine max*) has gained popularity as an agricultural product after corn and wheat with about 42% of the 324 million tons/year production from North America alone (Abdulkhani et al., 2017). The common residues left behind after soybean harvesting and processing include straw, hulls, and fibers (Felfli et al., 2011). Similarly, massive amounts of flax straw are obtained after harvesting flaxseeds from flax plants (*Linum usitatissimum*). Although with high potentials, the straw residues generated from agricultural practices have fewer practical applications. A portion of accumulated straw is used for fodder or bedding material for cattle, while the remaining ones are used for briquetting, biocomposites manufacturing and fuel pellet production (Azargohar et al., 2018). In some developing countries where the arable lands are scarce, the straw residues are burnt in the farmlands, which emit huge amounts of smoke, particulate matter, and greenhouse gas emissions. On the other hand, the straws could be harnessed to produce renewable energy, thereby mitigating the problems of disposal. On the contrary, the agricultural straw residues contain a substantial amount of lignin, cellulose, hemicellulose, carbohydrates, proteins, and lipids, which can be converted to biofuels and biochemicals. Soybean straw is reported to contain 34.1 wt% cellulose, 16.1 wt% hemicellulose and 21.6 wt% lignin (Wan et al., 2011). On the other hand, flax straw typically contains 53.8 wt% cellulose, 17.1 wt% hemicellulose and 23.3 wt% lignin (Buranov and Mazza, 2008).

Soybean straw and flax straw are of particular interest in this study because of the limited literature available on their hydrothermal gasification to produce H_2-rich syngas. Furthermore, in our previous study in phase 1, we showed that lignin model compound is very difficult to degrade compared to cellulose and xylose (hemicellulose) (Okolie et al., 2020b). Therefore, it would be interesting to evaluate the gasification of real biomass feedstocks with high lignin contents.

Qing et al. (2017) performed different acid and alkaline pretreatment for enzyme hydrolysis of soybean straw and the hulls to produce fermentable sugars (Qing et al., 2017). Xu et al. (2007) performed enzymatic hydrolysis of soybean straw for bioconversion. Harry et al. (2014) conducted liquefaction of flax straw in SbCW to produce furfural as an industrial chemical precursor. Soybean straw and flax straw have both been used as precursors for producing activated carbon for a wide variety of applications such as removal of heavy metals from contaminated water (Grishina et al., 2016; Harry et al., 2014; Melia et al., 2018; Qing et al., 2017; Xu et al., 2007).

A clear understanding of the thermal degradation of soybean straw and flax straw could help in improving their effective management and valorization. Furthermore, the identification of important process parameters and thermodynamic modeling could aid in the design and optimization of the hydrothermal conversion process, energy recovery potential, lifecycle assessment and techno-economic analysis. Therefore, the current study aims to investigate the decomposition of soybean straw and flax straw in SbCW and SCW. The effects of different process parameters, temperature (300–500 °C), biomass-to-water ratio (1:5 and 1:10), biomass particle size (0.13 mm and 0.8 mm) and residence time (30–60 min) on H_2 production at a pressure range of 22–25 MPa were studied. The experimental results were also compared with the theoretical values obtained from thermodynamic models. To the best of our knowledge, this is the first study

to report the experimental and thermodynamic modeling of hydrothermal gasification of soybean straw and flax straw.

5.3 Materials and Methods

5.3.1 Biomass and catalysts preparation

Soybean straw and flax straw were the two agricultural residues used as the feedstocks in this study. Both the straw varieties were procured from a local farm in Saskatoon, Canada. The straws were chopped, air-dried, and brushed to remove any soil particles before pulverizing. The chopped straws were crushed using an IKA MF 10 Basic S1 grinder (ThermoFisher Scientific Inc., Mississauga, Ontario, Canada) to obtain two different average particle sizes of 0.13 mm and 0.8 mm. The pulverized straw particles were stored in a clean and dry airtight container at room temperature before characterization and hydrothermal gasification. Potassium hydroxide, KOH (purity: 99.995%), purchased from Sigma-Aldrich Canada Co. (Oakville, Ontario, Canada) was used as the catalyst in hydrothermal gasification.

5.3.2. Biomass and product characterization

The amount of moisture, ash, volatile and fixed carbon (proximate analysis) of soybean straw and flax straw were determined using the standard ASTM procedures (ASTM, 2004; ASTM E871-82, 2006; D3175-11, 2011). For moisture determination, about 1 g of biomass sample was weighed in a crucible and heated for 2 h inside a muffle furnace at 105 ± 3 °C. The weight difference of the samples placed in the crucible after drying indicates the amount of moisture present. Following the same procedure, the ash and volatile matter contents were determined as the difference in the weight when 1 g of the sample was heated at 575 ± 10 °C for 4 h and 950 ± 10 °C for 7 min, respectively. The fixed carbon content was calculated as the difference of moisture, ash, and volatile matter.

An Elementar Vario EL III CHNS analyzer (Elementar Analysensysteme, Hanau, Germany) was used for ultimate analysis to measure the elemental composition (i.e. carbon, hydrogen, nitrogen, sulfur, and oxygen contents) in soybean straw, flax straw and their derived hydrochars. Oxygen content was calculated as the difference between the amounts of carbon, hydrogen, nitrogen, sulfur, and ash. The experimental higher heating value (HHV) of soybean straw, flax straw and hydrochars were measured using a 6400 Automatic Isoperibol Calorimeter (Parr Instrument Company, Moline, Illinois, USA). The theoretical HHV was evaluated using the Friedl's formula in Equation 3.5.

The gaseous products (i.e., H_2, CO_2, CO, CH_4 and C_1 - C_4 hydrocarbons) obtained from hydrothermal gasification were analyzed using an Agilent GC 7820A gas chromatograph (Agilent Technologies, Santa Clara, USA). The gas chromatography system was equipped with a capillary column, three packed columns and a thermal conductivity detector. The carrier gas was argon with the detector and column temperature kept at 50 °C and 60 °C, respectively. The concentrations of CO, CH_4 and H_2 were measured with the Ultimetal HayesepQ T 80/100 mesh column, while the concentrations of other gases such as CO2 and C_2 - C_4 were evaluated with the Ultimetal Hayesep T 80/100 mesh column.

The thermogravimetric analysis (TGA) and differential thermogravimetric analysis (DTA) for soybean straw and flax straw were conducted using a TGA Q500 instrument (TA Instruments – Waters LLC, New Castle, DE, USA). The TGA-DTA analysis was studied under a nitrogen atmosphere with a flow rate of 60 mL/min to determine the devolatilization behavior of the agricultural residues. About 10–15 mg of the biomass samples was heated up to 800 °C at a heating rate of 10 °C/min. The pattern of weight loss with elevating temperature was observed to determine the thermal stability of the feedstock and the fraction of the volatile components.

The gas chromatography-mass spectrometry (GC–MS) analysis of the liquid effluents produced from the hydrothermal gasification reaction was performed with a Trace 1310 Gas Chromatograph and a TSQ Duo Mass Spectrometer (Thermo Fisher Scientific, Waltham, USA) to determine the group of organic compounds. The temperature of the source was at 250 °C with helium as carrier gas at a flow rate of 1.2 mL/min. To prepare the test samples for GC–MS analysis, each liquid effluent sample was dissolved in acetone with 1:10 vol/vol. Nearly, 1 μL of the prepared sample was precisely injected into the system at an initial oven temperature of 40 °C for a minute holding time using a split ratio and split flow of 50:1 and 60 mL/min, respectively. The temperature was then programmed for an increase up to 150 °C at a flow rate of 5 °C/min, followed by a final rise to 320 °C at 10 °C/min for 5 min holding time. The mass spectra of the liquid effluents were obtained from 50 to 650 m/z with the peaks identified using the standard NIST (National Institute of Standards and Technology) library. Chromeleon™ 7.2 Chromatography Data System (CDS) software was used for all the analysis and comparison.

5.4 Thermodynamics model analysis

5.4.1 Thermodynamic modeling

In this study, the experimental product composition was compared with theoretical equilibrium values from thermodynamic modeling. This is important to ascertain how far the experimental product composition, especially in terms of H_2 yield deviates from the theoretical values. Consequently, it is easier to define a research gap related to catalyst design, process optimization and simulation for scale-up (Adamu et al., 2017). Additionally, thermodynamic equilibrium is important in energy evaluations and to determine whether a particular chemical process is energetically sustainable (Castello and Fiori, 2011). In this field, there are two

approaches to thermodynamic modeling, namely stoichiometric and non-stoichiometric. While the stoichiometric approach requires that the different reactions taking place should be identified, the non-stoichiometric approach is in contrast (Castello and Fiori, 2011). The latter is based on the Gibbs free energy minimization method (GFMM). Since hydrothermal gasification involves a series of complex reactions with the formation of several intermediates, the GFMM method was selected because it does not require the identification of intermediate reactions. This method requires that each product species should be identified following, which the calculations are made to determine the distribution of products for ensuring that the chemical reaction approaches a minimum Gibbs free energy value (Okolie et al., 2020b).

The GFMM method was used for thermodynamic modeling in this study for the following reasons. Firstly, SbCW and SCW gasification are complex processes comprising several intermediate steps, which often makes it difficult to identify all the involved chemical reactions and intermediate reactions. Furthermore, several researchers used this approach and reported good agreement with experimental values (Castello et al., 2015; Fiori et al., 2012; Fiori and Castello, 2014; Yakaboylu et al., 2015). The Aspen Plus software v7.3 (AspenTech, Bedford, USA) was used for thermodynamic modeling. Aspen Plus is a commercial chemical process simulator widely used in most process simulation. The program operates on a steady state with a built-in array of physical properties database that is very useful during thermodynamic calculations. Flowsheet can be designed in Aspen Plus by using the unit operation blocks while specifying each component present in the reaction (Han et al., 2017).

5.4.2 Aspen Plus process description

In the Aspen Plus program, there is no readymade model relating to hydrothermal gasification; therefore, it is important to simulate the entire process into different unit

operations. The schematics of the hydrothermal gasification process design flowsheet developed using Aspen Plus is shown in Figure 5. 1. The flowsheet is designed in a simple format to make provision for adjustments and scale up in the future. The flowsheet represents a typical description of a model experimental set-up that has been utilized in a few previous studies in this field with slight modification (Louw et al., 2016; Withag et al., 2012; R. Zhang et al., 2010). The description of the blocks included in the flowsheet and their block ID is provided in Table 5.1. Two blocks used to simulate the hydrothermal gasification reactor are the RYield and RGibbs blocks. Aspen Plus defines lignocellulosic biomass as a non-conventional stream containing heterogeneous solid with no identified molecular weight. To include such stream in the model, the RYield reactor block was used to decompose the biomass ($CH_\mu O_\alpha Cl_\beta N_s S_\infty$ $(ASH)_z$ $(H_2O)_k$) into its conventional components (C, H_2, O_2, N_2, Cl_2, H_2O, ash and S) based on the proximate and ultimate analyses (Equation 5.1).

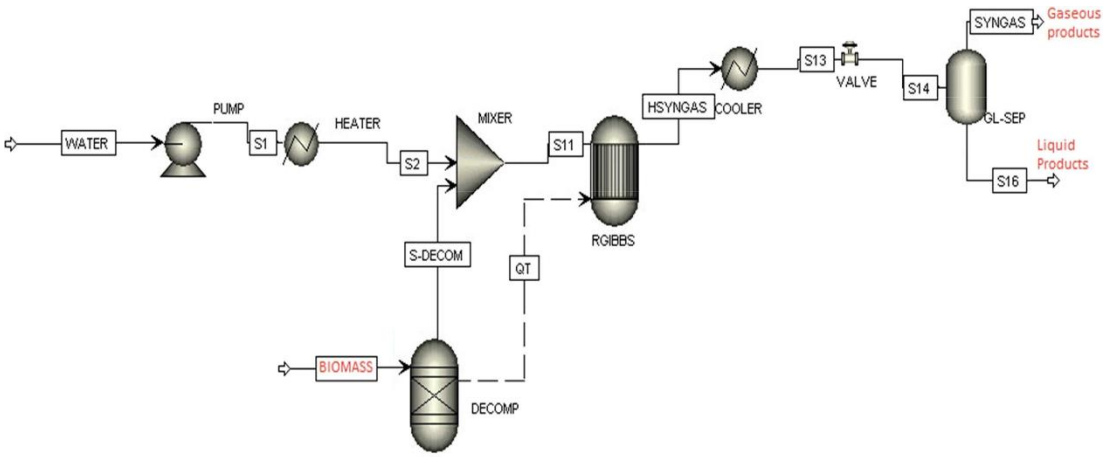

Figure 5.1: Schematics of process description for the proposed hydrothermal gasification process designed using Aspen Plus program.

$$CH_{\mu}O_{\alpha}Cl_{\beta}N_{s}S_{\infty}\,(ASH)_{z}\,(H_2O)_{k} = ɜ\,C + \mu/2\,H_2 + \alpha/2O_2 + \beta/2\,Cl_2 + s/2\,N_2 + \infty S + z\,(ASH) + (1 - ɜ)\,C + kH_2O + Q \quad \text{(Equation 5.1)}$$

Where, ɜ and Q are the carbon conversion (in %) and heat of decomposition, respectively.

Table 5.1: Description of the Aspen Plus blocks using in the thermodynamic modeling.

Default ID in Aspen Plus	**Assigned unit operations for block ID in the flowsheet**	**Unit operation description**
Pump	PUMP	Increases the pressure of the water stream to the pressure of the RGibbs reactor.
Heater	HEATER	Heats water to the temperature of the Gibbs reactor before mixing with the products from the RYield reactor.
Mixer	MIXER	Mixes water with elements from the RYield reactor.
RYield	DECOMP	It helps to thermally degrade the lignocellulosic biomass into components (C, H_2, O_2, Cl_2, N_2 and S). A calculator block is used to determine the composition of the products leaving the reactor. In this reactor, the reaction stoichiometry and kinetics are unknown and not relevant. However, the product yield distribution is estimated from the proximate and ultimate analyses of the biomass fed.
RGibbs	RGIBBS	RGibbs reactor performs the non-stoichiometric Gibbs free minimization method calculations. This reactor was used in modeling the hydrothermal gasification reactor. Furthermore, for systems that do not attain a complete equilibrium, RGibbs reactor can permit restricted equilibrium calculations.
Cooler	COOLER	Reduces the temperature of the hot gases leaving the RGibbs reactor to room temperature and removes any moisture present.
Valve	VALVE	Reduce the pressure of the incoming cold gas leaving the RGibbs reactor to atmospheric pressure.
Sep	GL-SEP	Separates liquid products from the gaseous products. The liquid product is collected from the bottom of the gas-liquid separator, whereas the gas products are collected from the top potion.

A calculator block is included in the RYield block, and the function was carried out through a programmed FORTRAN subroutine statement. It should be mentioned that the enthalpy from the outlet stream (S-DECOM) is not the same as that of the entering stream (BIOMASS) because of the splitting of chemical bonds (Figure 5.1). Therefore, the heat stream 'Q_T' was added between the RYield and RGibbs to balance the enthalpy. The stream 'S-DECOM' was then mixed with incoming preheated water (S2) in the MIXER before being sent to the RGibbs block (S11 stream) where the calculations of Gibbs free minimization is carried out at a specified temperature and pressure. 'S' represents the material stream while 'Q' signifies the heat stream. The product species leaving the RGibbs reactor (HSYNGAS) consisted of gases such as CO, CO_2, CH_4, H_2, H_2O and C_2-C_4 hydrocarbons (Wan, 2016). The product stream (HSYNGAS) is cooled (COOLER) to ambient temperature, after which the pressure is reduced to atmospheric pressure in an expansion valve. The gas-liquid separator (GL-SEP) helps to separate the liquid and gaseous products. Table 5.2 summarizes the assumptions made in the model, operating conditions and property packages used in the model. A water feed flow rate of 100 kg/h was assumed. However, to specify the required BTW ratio another calculator block (C2) was defined. The details of the calculator block and the FORTRAN subroutine code can be found in the appendices section.

The Peng-Robinson (PR) equation of states was used in this study for the thermodynamic modeling. Usually, high-pressure systems (> 21 MPa) used during hydrothermal processes restrict the use of activity co-efficient methods, thus preferring the PR equation of states. Hydrothermal gasification occurs in two regions based on the reaction temperature and pressure, i.e. subcritical region (< 375°C) and supercritical region (> 375°C). In each of these regions, the dielectric constant and the properties of water vary from being

non-polar to polar. Therefore, the PR equation of states is suitable in capturing the varying polar behavior of water under hydrothermal conditions. Moreover, the PR equation of states has been used by several authors for simulating hydrothermal gasification of biomass feedstocks (Fiori et al., 2012; Louw et al., 2016; Tang and Kitagawa, 2005).

Table 5.2: List of assumptions, operating conditions and property packages used in the thermodynamic model.

Attributes	**Conditions/specifications**
Thermodynamic package	Peng-Robinson equation of state
Stream class	MIXCINC
Enthalpy mode	HCOALGEN
Density mode	DCOALIGT
Hydrothermal gasification process temperature	300-500°C
Hydrothermal gasification process pressure	22-25 MPa
Biomass-to-water ratio	1:5 and 1:10
Biomass	Specified using its proximate and ultimate analyses
Assumptions: • Steady-state operation is assumed throughout the simulation. • The RGibbs reactor is operated isothermally. • The pressure drop in the reactor is neglected. • The ash produced from the biomass is inert and assumed not to react with any other component. • Carbon conversion efficiency was assumed 90% and biomass particle size effects are negligible.	

5.5 Results and Discussion

5.5.1 Product distribution from hydrothermal gasification

Soybean straw was hydrothermally gasified at temperatures of 300–500 °C with BTW of 1:5 and 1:10, residence times of 15–60 min under a pressure range of 22–25 MPa. Table 5.3 shows the mass balance for the gaseous, liquid, and solid products obtained from SbCW and SCW gasification of soybean straw. It can be seen from Table 5.3 that the gas yield increases with temperature while a decline in the yield of solid (hydrochars) and liquid products was observed.

This shows a progression of gasification reaction with temperature. It should be mentioned that the relatively higher yield of liquid products is because of water, which acts as the reaction medium and a solvent.

Table 5.3: Product yields from the hydrothermal gasification of soybean straw with 1:5 BTW ratio, particle size A (0.8 mm), residence time of 45 min and pressure of 23 MPa.

Gasification temperature	Solid product (wt%)	Liquid product (wt%)	Gaseous product (wt%)
300°C	8.13 ± 0.30	75.46 ± 0.64	3.14 ± 0.16
400°C	7.26 ± 0.22	64.63 ± 1.43	3.33 ± 0.02
500°C	6.28 ± 0.33	57.92 ± 1.41	4.54 ± 0.01

The total mass balance observed during the gasification experiments ranged from 68.8 to 86.7 wt%. The mass balance was susceptible to some inevitable experimental errors because of the technical challenges encountered during product collection, which could lead to some unaccounted product losses. The challenges during product collection have been mentioned in Chapter 3. Furthermore, the weight percent of the gaseous product was estimated from the total gas yield, which may contain C_2 - C_4 hydrocarbons. Adding these compounds to gas yield measurements could elevate the product yield. Similar challenges in mass balance calculations have been reported in the literature. For instance, mass balance ranges of 52.4–59.8 wt%, 84.9–95.6 wt%, 74–83 wt% and 85.9–93.5 wt% have been reported during the hydrothermal gasification of glucose (Ding et al., 2014), cellulose (Okolie et al., 2020b), pinecone (Sonil Nanda et al., 2017a) and lignin (Kang et al., 2015), respectively.

5.5.2 Physicochemical characterization of biomass and hydrochar

The proximate composition of soybean straw and flax straw is presented in Table 5.4. Flax straw demonstrated higher contents of volatile matter (83.3 wt%) and moisture (9.3 wt%) compared to soybean straw. In contrast, soybean straw had higher ash content (4.6 wt%) and fixed carbon (8.9 wt%) than that of flax straw. Soybean straw and flax straw both had a relatively high volatile matter and low ash content, which makes them good candidates for energy production through different thermochemical conversion processes.

Table 5.4: Proximate analysis of soybean straw and flax straw.

Component	**Soybean Straw**	**Flax straw**
Moisture (wt%)	5.2	9.3
Ash (wt%)	4.6	2.6
Volatile matter (wt%)	81.3	83.3
Fixed carbon (wt%)	8.9	4.8

The thermogravimetric analysis of soybean straw and flax straw is given in Figure 5.2a. The thermal decomposition of the agricultural residues occurs in three different stages related to their weight losses (Huang et al., 2016). The thermal decomposition of agricultural residues begins at 80–210 °C, which corresponds to the removal of moisture and light volatile matter due to the hygroscopic behavior of the agricultural residues (Damartzis et al., 2011). The second stage, which is the main decomposition step, involves the degradation of hemicellulose and cellulose at 210–400 °C. The final step is observed as lignin decomposes at 400–800 °C (Damartzis et al., 2011). The devolatilization pattern of soybean straw and flax straw appeared quite similar as illustrated in Figure 2a.

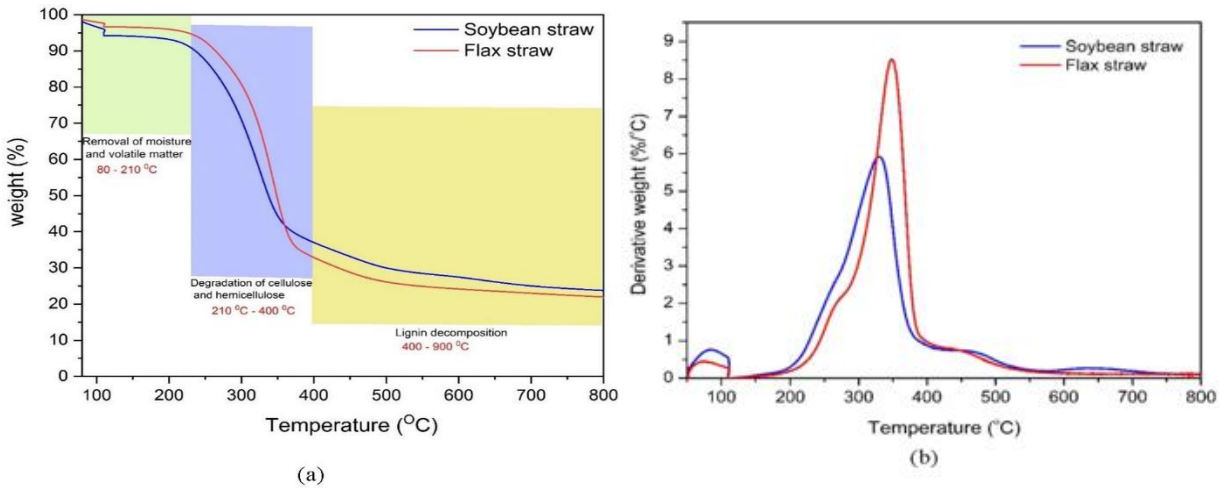

Figure 5.2: (a) Thermogravimetric and (b) differential thermogravimetric analyses of soybean straw and flax straw.

The differential weight loss patterns for soybean straw and flax straw is illustrated in Figure 5.2b. The relative intensities of the peaks in the differential thermogravimetric (DTG) curves could be attributed to the cellulose, hemicellulose, and lignin contents. Three main peaks were identified from the DTG curves of flax straw and soybean straw. The major peaks in the temperature ranges of 200–300 °C, 250–350 °C and 200–500 °C corresponded to the thermal degradation of hemicelluloses, cellulose, and lignin, respectively (Carrier et al., 2011). According to the DTG profile of flax straw, there is the main peak at 360 °C, which is preceded by a very small hump at 270 °C, these correspond to two different degradation sub-regions of hemicellulose and cellulose. Similar peaks were found for soybean straw at 340 °C and 240 °C, respectively. Additionally, the presence of a shoulder peak at 410–520 °C could be attributed to the presence of lignin. Huang et al. (2016) studied the pyrolysis kinetics of soybean straw using the thermogravimetric analysis under an argon atmosphere at different heating rates of 5–30 K/min. The maximum weight loss of the straw due to pyrolysis decomposition of hemicellulose and cellulose was observed at 453–673 K (Huang et al., 2016).

The ultimate analysis of soybean straw and flax straw along with the hydrochars derived from SbCW (300 °C) and SCW (400–500 °C) gasification of soybean straw are presented in Table 5.5. Between the two agricultural residues, flax straw had higher C, H and N contents of 47.78, 5.37 and 0.84 wt%, respectively. Soybean straw contained 41.98 wt% C, 5.05 wt% H, 0.46 wt% N and 0.45 wt% O. The C content of soybean hydrochars increased from 53.75 wt% at 300 °C to 80.56 wt% at 500 °C. Maximum C content in biochar at higher temperatures is due to the enhanced dehydration and decomposition reactions such as dehydration, decarboxylation, decarbonylation, which lead to aromatization of biochar (Azargohar et al., 2014). Thus, the hydrochars obtained at increased temperature SCW conditions are perceived to be more carbonaceous and stable.

Moreover, the experimental HHV also increased with temperature in the following order soybean straw (16.4 MJ/kg) < flax straw (17.33 MJ/kg) < soybean straw hydrochar-300 °C (19.56 MJ/kg) < soybean straw hydrochar-400 °C (24.01 MJ/kg) < soybean straw hydrochar-500 °C (29.98 MJ/kg) (Table 5.5). The higher HHVs of hydrochars were also reflected in the van Krevelen diagram (Figure 5.3). This diagram reveals that the agricultural residues and their hydrochars at low temperatures had higher atomic ratios O/C and H/C compared to the hydrochars produced at high temperatures (SCW conditions). Through hydrothermal gasification at high temperatures, the composition of the hydrochars resembles that of coal by becoming more carbonaceous with respect to lower oxygen and hydrogen contents. Therefore, the hydrochars obtained at high-temperature SCW conditions could undergo further processing to produce activated carbon, which has many industrial applications (Nanda et al., 2016a).

Table 5.5: Ultimate analysis of soybean straw and flax straw together with soybean straw hydrochars derived from hydrothermal gasification (BTW ratio: 1:5 BTW; Residence time: 45 min; Particle size A: 0.8 mm; Pressure: 22–25 MPa).

Parameter	**Soybean straw**	**Flax straw**	**Soybean straw hydrochar-300°C**	**Soybean straw hydrochar-400°C**	**Soybean straw hydrochar-500°C**
C (wt%)	41.98	47.78	53.75	65.88	80.56
H (wt%)	5.05	5.37	3.39	3.35	2.71
N (wt%)	0.46	0.84	0.38	0.83	0.91
S (wt%)	0.45	0.21	0.19	0.06	0.05
O (wt%)	47.46	43.22	42.29	29.88	15.77
Atomic ratios					
H/C	1.44	1.35	0.76	0.61	0.4
O/C	0.93	0.72	0.59	0.34	0.15
N/C	0.009	0.015	0.006	0.011	0.01
Empirical formula	$CH_{1.44}O_{0.93}N_{0.009}$	$CH_{1.35}O_{0.72}N_{0.015}$	$CH_{0.76}O_{0.59}N_{0.006}$	$CH_{0.61}O_{0.34}N_{0.011}$	$CH_{0.4}O_{0.15}N_{0.01}$
Experimental HHV (MJ/kg)	16.4	17.33	19.56	24.01	29.98
Theoretical HHV (MJ/kg)	16.77	16.51	20.27	24.69	30.2

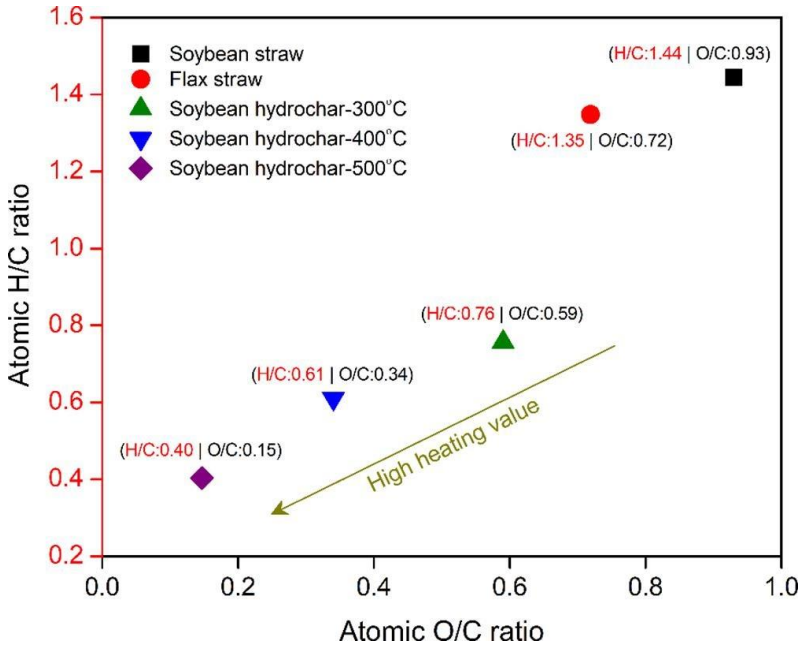

Figure 5.3: van Krevelen diagram for soybean straw, flax straw and soybean straw hydrochars derived from hydrothermal gasification at 300–500 °C for 45 min with 1:5 BTW ratio and 22–25 MPa pressure.

5.5.3 Parametric studies during hydrothermal gasification of biomass

To investigate the influence of temperature (300–500 °C) on the SbCW and SCW gasification of soybean straw, a fixed particle size A (0.8 mm), BTW ratio of 1:5 BTW ratio, residence time of 45 min and pressure range of 22–25 MPa were selected. As can be seen in Figure 5.4a, that elevated temperature favored the hydrothermal gasification of soybean straw. As the temperature rose from 300 °C (SbCW) to 500 °C (SCW), the yield of CH_4, H_2, CO_2 and C_2 - C_4 hydrocarbons increased. H_2 yield elevated from 0.99 mmol/g at 300 °C to 3.39 mmol/g at 500 °C. Similarly, the yield of CH_4, CO_2 and C_2 - C_4 hydrocarbons also increased at 500 °C to 1.73 mmol/g, 4.61 mmol/g and 0.38 mmol/g, respectively. In contrast, the yield of CO decreased slightly at higher temperatures. Based on the higher gas yields, the desired gasification temperature selected in this study is 500 °C (i.e. SCW condition).

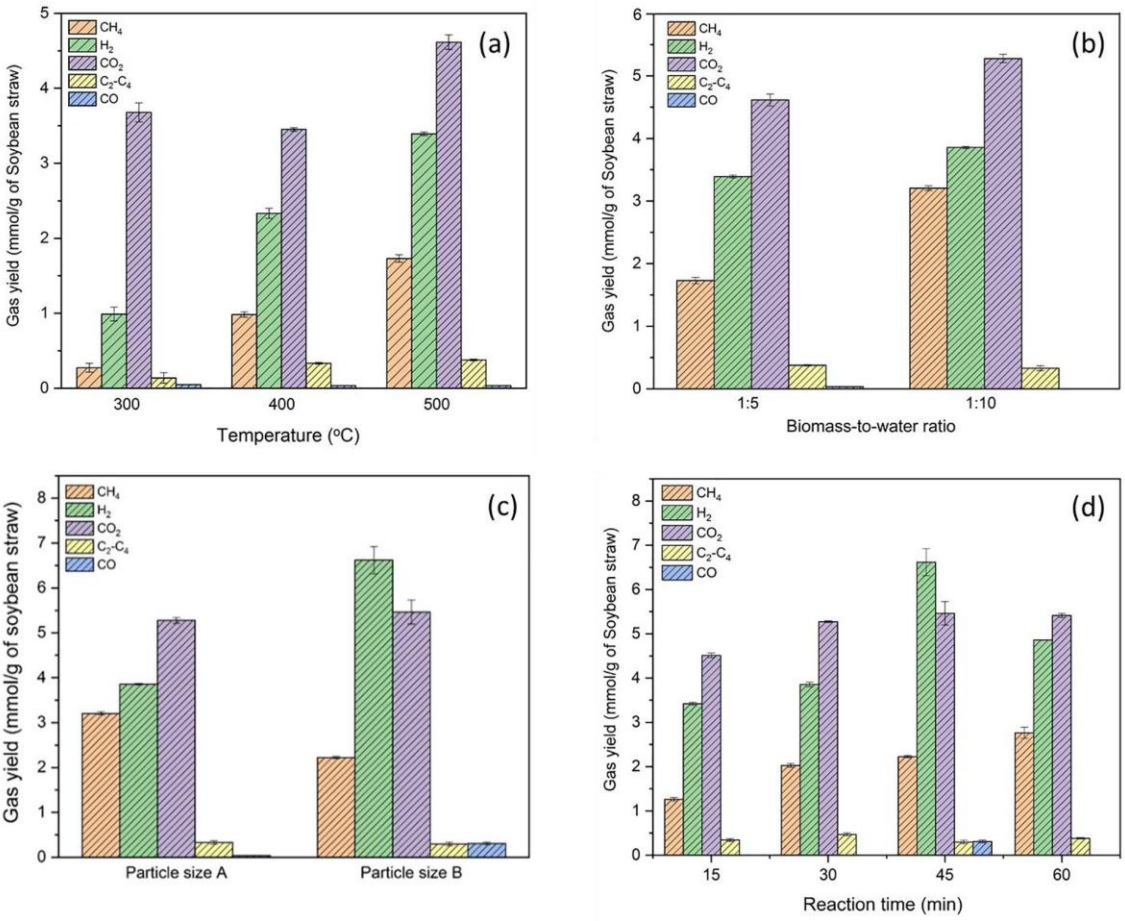

Figure 5.4: Parametric studies during the hydrothermal gasification of soybean straw. (a) Effect of temperature at 1:5 BTW ratio, Particle size A (0.8 mm), 22–25 MPa pressure and 45 min of residence time. (b) Effect of BTW ratio at 500 °C, Particle size A (0.8 mm), 22–25 MPa pressure and 45 min of residence time. (c) Effect of biomass particle size at 500 °C, 1:10 BTW ratio, 22–25 MPa pressure and 45 min of residence time. (d) Effect of residence time at 500 °C, 1:10 BTW ratio, Particle size B (0.13 mm) and 22–25 MPa pressure.

At supercritical conditions, two main reactions are inherent such as water-gas shift reaction and steam reforming reactions. The consumption of CO during water-gas shift reaction and the production of H_2 and CO_2 could be responsible for the elevated CO_2 and H_2 yields at higher temperatures. Nanda et al. (2018) have reported similar findings during hydrothermal gasification of wheat straw as they observed an increase in H_2 (0.26 to 2.98 mmol/g), CH_4 (0.27 to 1.42

mmol/g) and CO_2 (1.10 to 5.30 mmol/g) yield with a rise in temperature from 300 to 550 °C (Nanda et al., 2018).

Table 5.6 shows the total gas yield, CGE, LHV and H_2 selectivity. An increment in the individual gas yield with temperature led to an upsurge in the total gas yield by a factor of almost two (5.1 mmol/g at 300 °C to 10.1 mmol/g at 500 °C) in the case of soybean straw. Likewise, the H_2 selectivity also increased with temperature from 300 °C (24.2%) to 500 °C (50.4%). Greater values of LHV (1229 kJ/Nm^3) and CGE (17.1 %) were observed at 500 °C in comparison to 300 °C (LHV: 239 kJ/Nm3 and CGE: 9.87 %). The increase in total gas yields with rising temperatures further highlights its influence during hydrothermal gasification and shows the superiority of SCW over SbCW in terms of gas yield and gasification efficiency. At SbCW, ionic mechanisms are dominant while free radical ions are favorable at SCW gasification conditions (Chowdhury et al., 2018). The free radical mechanism helps to improve the dissolution of organic compounds and reactants in SCW, thereby escalating the gas yields. The rise in LHV values with temperature could be because of the elevated concentrations of C_2 - C_4 hydrocarbons and CH_4 at high temperatures.

After finding the desired temperature that produced the maximum gaseous yield, the effect of two BTW ratios were examined at a constant temperature (500 °C), Particle size A (0.8 mm), residence time (45 min) and pressure range of 22–25 MPa (Figure 5.4b). The total gas yield (12.6 mmol/g), CGE (21.9 %) and LHV (1764 kJ/Nm^3) were relatively higher during 1:10 BTW ratio of soybean straw gasification (Table 5.6). However, the H_2 selectivity was lower (43.8 %) for the BTW 1:10 ratio compared to the 1:5 BTW ratio (50.4 %). Furthermore, the yields of H_2 (3.86 mmol/g), CH_4 (3.2 mmol/g) and CO_2 (5.28 mmol/g) were higher for 1:10 BTW ratio (Figure 5.4b). On the contrary, the CO yield declined at a 1:10 BTW ratio. The superior gas yield at 1:10 BTW ratio could be attributed to the function of water in hydrothermal gasification. Since water is known

to act as a reactant, catalyst and solvent during hydrothermal gasification, an increment in the amount of water could favor the formation of desired products and gasification efficiency (Reddy et al., 2014a).

Table 5.6: Total gas yield, carbon gasification efficiency, lower heating value and hydrogen selectivity of the gas products obtained from hydrothermal gasification of soybean straw and flax straw at 22–25 MPa.

Gasification conditions		**Total gas yield (mmol/g)**	**Carbon gasification efficiency (%)**	**Lower heating value (kJ/Nm^3)**	**Hydrogen selectivity (%)**
Biomass: Soybean straw BTW ratio: 1:5 Residence time: 45 min Particle size A: 0.8 mm	300°C	5.1	9.9	239	24.2
	400°C	7.1	12.1	796	48.9
	500°C	10.1	17.1	1229	50.4
Biomass: Soybean straw Temperature: 500°C Residence time: 45 min Particle size A: 0.8 mm	1:5 BTW	10.1	17.1	1229	50.4
	1:10 BTW	12.6	21.9	1764	43.8
Biomass: Soybean straw Temperature: 500°C Residence time: 45 min BTW ratio: 1:10	Particle size A (0.8 mm)	12.6	21.9	1764	43.8
	Particle size B (0.13 mm)	14.9	20.2	1592	63.0
Biomass: Soybean straw Temperature: 500°C BTW ratio: 1:10 Particle size B: 0.13 mm	15 min	10.0	15.5	1094	53.0
	30 min	11.2	19.9	1400	45.6
	45 min	14.9	20.2	1592	63.0
	60 min	13.4	21.6	1798	56.8
Temperature: 500°C Residence time: 45 min BTW ratio: 1:10 Particle size B: 0.13 mm	Soybean straw	14.9	20.2	1592	63.0
	Flax straw	12.1	20.7	1506	61.9

Note: All results are presented in triplicates with a standard deviation of <3%.

The effect of biomass particle size during hydrothermal gasification of soybean straw at a fixed temperature of 500 °C, 1:10 BTW ratio, residence time of 45 min and pressure range of 22–25 MPa is shown in Figure 5.4c. Reducing the biomass particle size influenced the gas yields and product composition. H_2 yield increased from 3.86 mmol/g (with Particle size A: 0.8 mm) to 6.61 mmol/g (with Particle size B: 0.13 mm). Similarly, the CO_2 and CO yields also elevated with a decrease in the biomass particle size. On the contrary, the CH_4 yield declined from 3.2 to 2.26 mmol/g with a decrease in particle size. The influence of biomass particle size can be explained by considering the surface area of smaller and larger particles. Smaller particles contain a large surface area per unit mass, which exposes them to the reaction vicinity efficiently (Okolie et al., 2019). Therefore, the heat and mass transfer are greatly enhanced to facilitate the solubility and degradation of biomass particles during hydrothermal gasification.

Lu et al. (2006) reported comparable results on the influence of biomass particle size on hydrothermal gasification. The authors gasified 2 wt% rice straw and sodium carboxymethylcellulose with biomass particle sizes passing through 40–80 mesh and < 80 mesh at 650 °C and 25 MPa for 30 s. Biomass with smaller particle size resulted in higher H_2 yield (17 mol/kg) compared to biomass with larger particle size (13.7 mol/kg) (Lu et al., 2006). Regardless, the additional cost of energy consumption during biomass grinding should also be accounted for during feedstock processing.

The influence of residence time (15–60 min) for soybean straw with biomass Particle size B (0.13 mm) at temperature of 500 °C and BTW ratio of 1:10 was investigated (Figure 5.4d). It is clear that H_2 yield elevated from 3.42 mmol/g (at 15 min) to 6.62 mmol/g (at 45 min) followed by a decline to 4.85 mmol/g (at 60 min). Similarly, CO_2 yield also increased from 4.51 mmol/g (at 15 min) to 5.46 mmol/g (at 45 min) with a slight decrease to 5.41 mmol/g (at 60 min). Moreover, CO

yield enhanced from 0.02 mmol/g (at 15 min) to 0.31 mmol/g (at 45 min) after which it declined to 0.04 mmol/g (at 60 min). In contrast, CH_4 yield increased steadily with residence time from 1.26 mmol/g (at 15 min) to 2.76 mmol/g (at 60 min) indicating methanation reaction.

The CGE and LHV are also favored at longer residence times. The CGE amplified from 15.5% (at 15 min) to 21.6% (at 60 min) while the LHV augmented by 39% with an increase in residence time (Table 5.6). In contrast, H_2 selectivity increased up to a maximum value of 63% at 45 min after which it decreased to 56.8% at 60 min. Similarly, the total gas yield amplified to 14.9 mmol/g (at 45 min) followed by a decline to 13.42 mmol/g (at 60 min). Longer residence time could favor hydrogenation and methanation reactions by consuming CO and H_2 to produce CH_4 thereby reducing the yields of H_2 and CO as well as H_2 selectivity (Nanda et al., 2019b).

Based on the observation from the parametric studies, the desired reaction conditions for hydrothermal gasification of soybean straw were: Temperature, 500 °C; BTW, 1:10; Biomass particle size B (0.13 mm) and residence time, 45 min. Flax straw was also hydrothermally gasified using the above-mentioned maximum conditions to make a comparison of its performance with those of soybean straw. As can be seen from Figure 5.5, soybean straw had the highest H_2 (6.62 mmol/g), CO (0.31 mmol/g) and CO_2 (5.42 mmol/g) yields compared to that of flax straw. On the other hand, flax straw had H_2, CO and CO_2 yields of 3.82, 0.1 and 5.52 mmol/g, respectively. The CH_4 (2.43 mmol/g) and C_1 - C_4 hydrocarbon (0.34 mmol/g) yields were higher for flax straw. The total gas yield (14.9 mmol/g), H_2 selectivity (63%) and LHV (1592 kJ/Nm^3) were higher for soybean straw (Table 5.6). The superior H_2, CO and CO_2 for soybean straw could be attributed to its low lignin content compared to flax straw. The better performance of soybean straw could be because of the higher ash content (4.6 wt%), which is almost 1.7 times higher than that of flax straw (Table 5.4). Ash from herbaceous biomass is known to contain some alkali minerals such as

Ca, Mg, Na, P and K, which have catalytic effects during pyrolysis, liquefaction, or gasification (Cai et al., 2017; Mohanty et al., 2013).

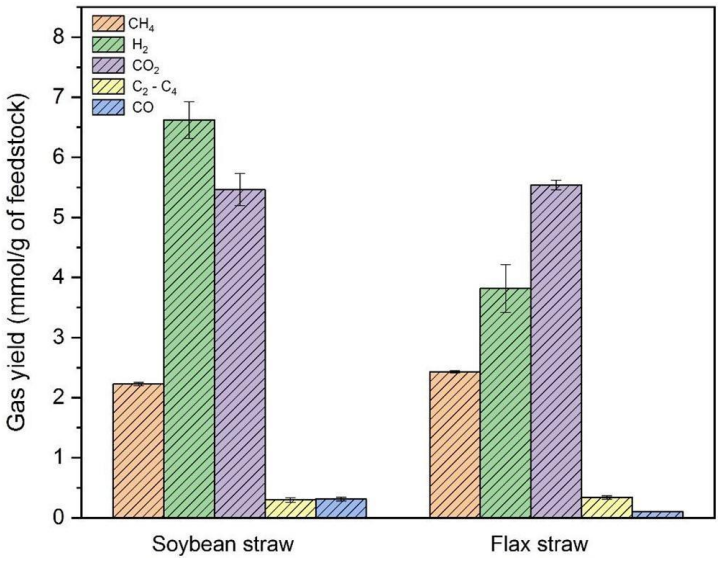

Figure 5.5: Gas yields from the hydrothermal gasification of soybean straw and flax straw at optimal process conditions (temperature: 500 °C, BTW 1:10, residence time of 45 min and biomass particle size B (0.13 mm).

5.5.4 Thermodynamic equilibrium predictions

Thermodynamic equilibrium predictions of the hydrothermal gasification of soybean straw at 300–500 °C and 1:10 BTW ratio was compared with the experimental results under similar conditions (Figure 5.6). In the present study, higher molecular weight C_2 - C_4 hydrocarbons were assumed negligible in our thermodynamic predictions owing to their insignificant theoretical values from the thermodynamic models. Therefore, the experimental yield was analyzed and compared with thermodynamic predictions for the H_2, CH_4, CO and CO_2. As can be seen in Figure 5.6 that the non-catalytic hydrothermal gasification of soybean straw exhibited a large deviation from theoretical yields for CH_4, CO_2 and H_2 yields at the temperature range of study with CO_2 exhibiting the largest deviation. On the other hand, the CO yield correlates with the theoretical

yield. However, it should be noted that the experimental observations did not exceed the theoretical values obtained from thermodynamic models.

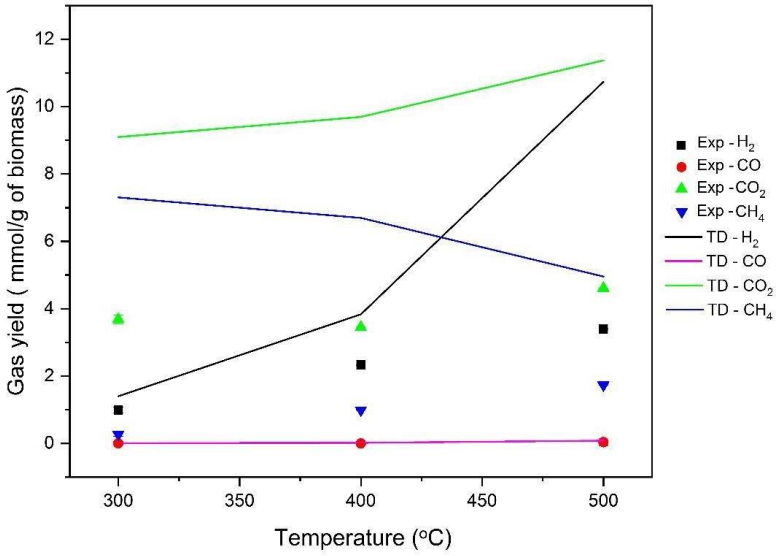

Figure 5.6: Experimental and theoretical equilibrium yields from hydrothermal gasification of soybean straw at the temperature of 300–500 °C, 1:5 BTW ratio for 45 min with 22–25 MPa.

To estimate the extent to which our experimental yield deviates from the theoretical yield obtained from thermodynamic predictions, a new term R_{Dev} was introduced. It is defined as the ratio of the experimental yield to the theoretical yield (expressed in percentage). The R_{Dev} values approaching 100% signifies that the experiments attain equilibrium and the yield obtained is the maximum theoretical yield. The R_{Dev} values of CH_4, CO_2 and H_2 yields for the non-catalytic gasification of soybean straw at 500 °C were estimated as 17.9 %, 27 % and 57.6 %, respectively. Similarly, for the non-catalytic gasification of flax straw under the same experimental conditions, R_{Dev} values of CH_4, CO_2, and H_2 yields were calculated as 16 %, 27.1 % and 37.4 %, respectively.

The deviations between experimental observations and thermodynamic yields have been documented in literature as shown in Table 5.7.

Table 5.7: Comparison of R_{Dev} values obtained during the hydrothermal gasification of soybean straw and flax straw in this study with literature values.

Feedstock	Reactor	Operating conditions	Catalyst	R_{Dev} value (%) H_2	CH_4	CO_2	Reference
Primary paper sludge	Batch reactor	Temperature: 450°C Residence time: 60 min Feed concentration: 10 wt%	Non-catalytic	21.2	6.7	28.0	Louw et al. (2016)
Glycerol and methanol mixture	Continuous reactor	Temperature: 600°C Pressure: 25 MPa Residence time: 45 s Feed concentration: 10 wt% Glycerol-to-methanol ratio: 1:1	Non-catalytic	73.1	82.9	80.6	Reddy et al. (2016)
Glucose	Stirred tank batch reactor	Temperature: 500°C Pressure: 28 MPa Residence time: 120 min Feed concentration: 0.25 M	Ni-La_2O_3/Al_2O_3	93.0	49.8	90.9	Chowdhury et al.(2018)
Glucose	Batch reactor	Temperature: 400°C Pressure: 25 MPa Residence time: 30 min Feed concentration: 0.25 M	$Ni/La_2O_3/Al_2O_3$	61.5	23.1	80.0	Adamu et al.(2017)
Fruit pulp	Batch reactor	Temperature: 400°C Pressure: 25 MPa Residence time: 30 min Feed concentration ratio: 2.5%	Non-catalytic	54.1	50.0	90.2	Eliz and Nezihe (2016)
Soybean straw	Fixed bed tubular batch reactor	Temperature: 500°C Pressure: 23-25 MPa Residence time: 45 min BTW ratio: 1:10 Biomass particle size: 0.13 mm	Non-catalytic	57.6	17.9	27.0	This work
Soybean straw	Fixed bed tubular batch reactor	Temperature: 500°C Pressure: 23-25 MPa Residence time: 45 min BTW ratio: 1:10	KOH	66.6	21.2	31.4	This work

Flax straw	Fixed bed tubular batch reactor	Biomass particle size: 0.13 mm Temperature: 500°C Pressure: 23-25 MPa Residence time: 45 min BTW ratio: 1:10	Non-catalytic	37.4	16.0	27.1	This work
Flax straw	Fixed bed tubular Batch reactor	Biomass particle size: 0.13 mm Temperature: 500°C Pressure: 23-25 MPa Residence time: 45 min BTW ratio: 1:10	KOH	58.7	18.3	30.6	This work

Note: R_{Dev} values were calculated based on the ratio of experimental to the thermodynamic equilibrium yields. Some values used in the calculations of R_{Dev} from published literature were extrapolated from the figures presented.

The deviations in experimental and thermodynamic equilibrium predictions in this study at longer residence times of 45 min could be attributed to the following reasons:

(i) The experiments were performed in a batch reactor without reactor mixing. The absence of agitation or mixing could restrict heat and mass transfer by reducing the contact between the biomass particles and water molecules.

(ii) The presence of temperature gradient in the reactor could also be responsible for the deviation from equilibrium prediction results. Some lighter intermediate compounds formed could stay trapped in the cooler zones of the reactor. These compounds are prevented from participating in further reactions (Zöhrer and Vogel, 2013).

(iii) There is no preheater installed in the reactor, the biomass and water mixture are introduced into the reactor to polymerize into heavy molecular weight compounds (e.g. char and tar) (Barbier et al., 2011; Sinağ et al., 2004). The heavy molecular weight compounds may require longer residence time to decompose into gases.

(iv) Longer residence time could enhance the decomposition of intermediates into products (Nikoo et al., 2015).

As can be seen from Table 5.7 that most of the studies on SCWG have been performed in the batch reactor because of its simplicity and the ability to effectively gasify solid feedstocks (Reddy et al., 2014b). The heterogeneity of lignocellulosic biomass and their insolubility in water makes it challenging to utilize continuous reactors. Most studies that reported the use of continuous or semi-continuous reactor either operate on biomass model compounds or real biomasses that are soluble in water (Okolie et al., 2019). Moreover, continuous reactors are usually prone to plugging and non-uniform mixing of biomass in the water.

To enhance the gas yields towards equilibrium the hydrothermal gasification of soybean straw and flax straw was carried out at maximum operating conditions in the presence of KOH catalyst (Figure 5.7 and Figure 5.8). Alkali homogeneous catalyst (KOH) was selected in this study because of its ability to enhance the WGSR and methanation reaction leading to improved H_2, CH_4 and CO_2 yield. During hydrothermal reactions, KOH undergoes initial hydrolysis to form potassium acetate (CH3COOK), which is further decomposed into potassium bicarbonate ($KHCO_3$) and CH_4 (Nanda et al., 2016c). Furthermore, a recent exergy analysis study reported the catalytic activity of different homogeneous catalysts during hydrothermal gasification to be in the order: Na_2CO_3 < NaOH < K_2CO_3 < KOH (Zhang et al., 2019).

As illustrated in Figure 5.7 and Figure 5.8, KOH catalyst elevated the yield of H_2, CO_2 and CH_4 close to equilibrium values. For soybean straw, H_2, CO_2 and CH_4 yields increased by approximately 15 % (7.64 mmol/g), 17 % (6.37 mmol/g) and 18 % (2.62 mmol/g), respectively.

Similarly, flax straw demonstrated an increase in H_2 (57 % or 5.99 mmol/g), CO_2 (13 % or 6.24 mmol/g) and CH_4 (15% or 2.78 mmol/g) with KOH catalyst. Similar to the gas yields (of H_2,

CO_2 and CH_4), there was also an increase in the R_{Dev} values with the use of catalysts as indicated in Table5. 7. R_{Dev} values for soybean straw elevated from 56.7 % to 66.6 % for H_2, 17.9 % to 21.2 % for CH_4 and 27 % to 31.4 % for CO_2. Likewise, for catalytic gasification of flax straw, the R_{Dev} values were found to be 58.7 % for H_2, 18.3 % for CH_4 and 30.6 % for CO_2. The improvement in R_{Dev} values signifies that the KOH catalyst drives the reaction towards equilibrium.

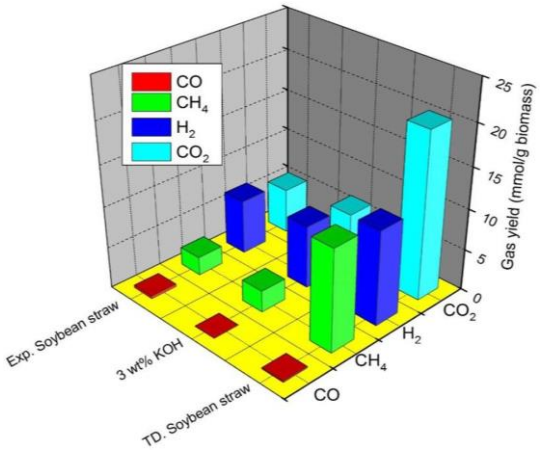

Figure 5.7: Experimental and thermodynamic predictions gas yields from catalytic SCW gasification of soybean straw at optimal conditions (Temperature: 500 °C; BTW ratio: 1:10; Biomass particle size B: 0.13 mm; Residence time: 45 min).

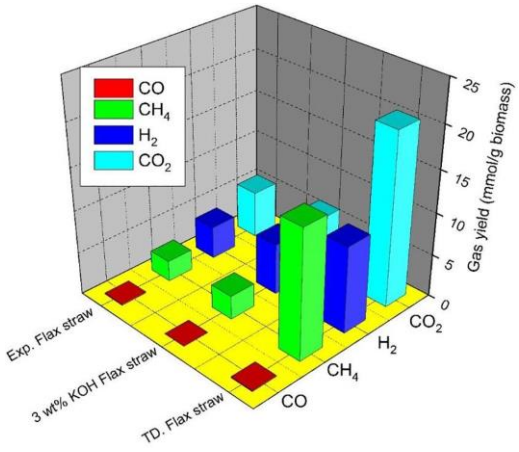

Figure 5.8: Experimental and thermodynamic predictions gas yields from catalytic SCW gasification of flax straw at optimal conditions (Temperature: 500 °C; BTW ratio: 1:10; Biomass particle size B: 0.13 mm; Residence time: 45 min).

5.5.5 Compositional analysis of liquid products

The compositional analysis of liquid effluents obtained from the non-catalytic hydrothermal gasification of soybean straw at 300–500 °C, 45 min of residence time with 1:10 BTW ratio and 22–25 MPa pressure was performed through GC–MS. Table 5.8 summarizes the identified compound from the GC–MS analysis of the liquid effluent obtained from hydrothermal gasification of soybean straw. The main products identified in the liquid effluents were grouped into alcohols, organic acids, furans, phenolic derivatives, ketones, aldehydes, aromatics, and other compounds with a relative area <1% of the total integrated area. The percentage area of each compound identified is defined as the ratio of each identified compound chromatographic area to the total area expressed in percentage (Sun et al., 2011).

As can be seen in Figure 5.9 that with a rise in temperature from 300 °C (SbCW) to 400 °C (SCW), there was a decrease in the concentration of aromatics, alcohols, and organic acids. On the other hand, the levels of phenols and aldehydes were utmost at 400 °C. However, with a further elevation in temperature to 500 °C, the concentrations of aldehydes, phenols, acids decreased while that of alcohols and ketones increased. Cellulose and hemicellulose present in the straw undergo hydrolysis at SbCW temperatures 300 °C due to ionic mechanisms to produce organic acids, whereas lignin produces phenols, aldehydes and aromatics at SCW temperatures (> 400 °C) due to free radical mechanisms (Okolie et al., 2020a). The lowering of acids, phenols, and aldehydes at 500 °C indicates their thermal cracking and decomposition to produce gases and lighter hydrocarbons during gasification.

Table 5.8: Qualitative GC–MS analysis of liquid effluents obtained from hydrothermal gasification of soybean straw at 300–500 °C, 1:5 BTW ratio, 45 min of residence time with particle size A (0.8 mm) and pressure of 22–25 MPa.

Compound name	**Molecular formula**	**Area (%)**		
		300°C	**400°C**	**500°C**
(2E)-2-Hexenyl hexanoate	$C_{12}H_{22}O_2$	ND	1.56	1.44
1,3,5-Trimethyl-1H-pyrazole	$C_6H_{10}N_2$	4.44	3.44	3.63
1-Isocyanato-octadecane	$C_{19}H_{37}NO$	ND	ND	1.01
2,3-Dimethyl-phenol	$(CH_3)_2C_6H_3OH$	ND	3.99	3.54
2,5-Dimethyl-furan	C_6H_8O	3.69	1.31	2.83
2,5-Dimethyl-phenol	$C_8H_{10}O$	2.69	ND	ND
2-Biphenylcarboxylic acid	$C_{13}H_{10}O_2$	1.83	ND	ND
2-Ethyl-2-butenal	$C_6H_{10}O$	ND	1.14	1.05
2-Hydroxy-3-methyl-2-cyclopenten-1-one	$C_6H_{10}O_3$	ND	12.64	ND
2-Methoxy-4-methyl-phenol	$C_8H_{10}O_2$	1.27	1.07	ND
2-Methoxy-phenol	$C_7H_8O_2$	6.68	7.94	7.68
2-Methyl-phenol	$CH_3C_6H_4OH$	4.83	5.05	3.90
3-Ethyl-phenol	$C_8H_{10}O$	4.64	ND	ND
3-Furaldehyde	$C_5H_4O_2$	ND	2.20	ND
3-Methyl-phenol	$CH_3C_6H_4OH$	9.45	ND	ND
4-Hydroxy-4-methyl-2-pentanone	$C_6H_{12}O_2$	2.27	2.17	2.53
4-Hydroxy-4-methyl-2-pentanone	$C_6H_{12}O_2$	4.42	4.32	7.01
4-Methyl-phenol	C_7H_8O	ND	9.93	9.14
Bis(2-ethylhexyl) phthalate	$C_{24}H_{38}O_4$	ND	ND	1.06
Diphenyl ether	$C_{12}H_{10}O$	1.55	1.09	1.91
Furfural	$C_5H_4O_2$	13.02	17.86	15.85
Methyl-2-furoate	$C_6H_6O_3$	ND	ND	1.08
Phenol	C_6H_6O	10.33	1.08	9.92

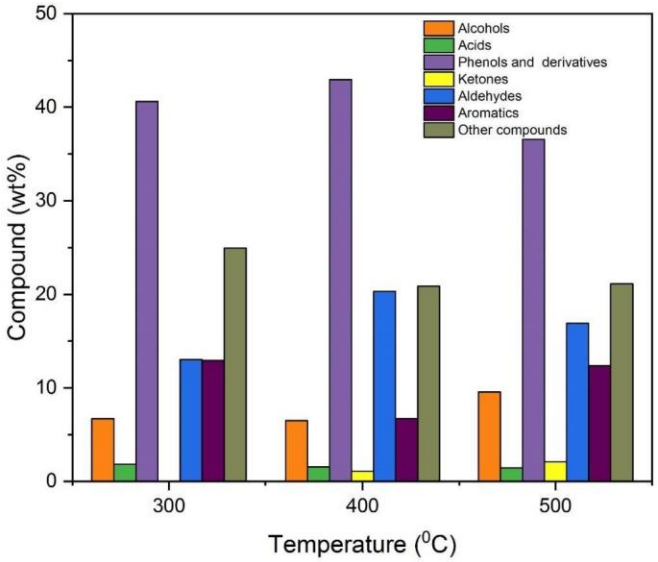

Figure 5.9: GC–MS analysis of liquid effluents obtained from hydrothermal gasification of soybean straw at 300–500 °C, 1:5 BTW ratio, 45 min of residence time with particle size A (0.8 mm) and pressure of 22–25 MPa.

5.6 Conclusions

This study explores for the first time the subcritical and supercritical water gasification of soybean straw and flax straw. The effects of temperature (300–500 °C) BTW (1:5 and 1:10), biomass particle size (Particle size A: 0.8 mm and Particle size B: 0.13 mm) and residence time (30–60 min) on the gas yields and composition were investigated. The major products obtained during the hydrothermal gasification of soybean straw and flax straw were H_2, CO_2, CO, CH_4 and C_1 - C_4 hydrocarbons. The desired temperature, BTW ratio, biomass particle size and residence time were found to be 500 °C, 1:10, Particle size B and 45 min, respectively. The gasification of soybean straw at the aforementioned conditions resulted in H_2, CO_2, CO, CH_4 and C_2 - C_4 yields of 6.62, 5.46, 0.31 and 0.30 mmol/g, respectively. At the same experimental conditions, the total gas yield of 14.9 mmol/g, CGE of 20.2 % and H_2 selectivity of 63 % was obtained from soybean straw gasification. A comparative evaluation of gasification efficiency between the two

agricultural crop residues showed that soybean straw exhibited superior product yield and gasification efficiency. The thermodynamic estimations show that the experimental observations are far from equilibrium values. However, the use of the KOH catalyst in our study significantly improved the gas yield close to the theoretical observations. The insights from the thermodynamic predictions could provide information that can be useful for catalyst development, process optimization and scaling up. In summary, the findings from this study suggest that soybean straw and flax straw could serve as possible feedstocks to produce H_2-rich syngas through hydrothermal gasification. Based on the results from this Chapter, Soybean straw was selected for the most promising lignocellulosic material. Therefore, the next chapter will aim to develop a stable heterogeneous catalyst that can improve the gaseous yield towards the theoretical values.

Chapter 6 Catalytic supercritical water gasification of soybean straw: Effect of catalyst supports and promoters.

The content of this chapter has been accepted for publication in the Industrial & Engineering Chemistry Research Journal cited below:

Citation :

Okolie, J. A., Mukherjee, A., Nanda, S., Dalai, A. K., & Kozinski, J. A. (2021). Catalytic supercritical water gasification of soybean straw: Effect of catalyst supports and promoters. Industrial & Engineering Chemistry Research (Accepted).

Contribution of the Ph.D. Candidate

Jude: (1) Sample and catalyst preparations and performing SCWG experiments (2) Performing the characterization of gaseous, products and the catalysts (3) analyzing the experimental results (4) Writing the manuscript and provide responses to reviewers' comments. Dr Sonil Nanda and Alivia Mukherjee helped with the experimental design and reviewed the manuscript. Dr. Ajay K. Dalai and Dr. Janusz A. Kozinski examined the research results, coordinated the manuscript preparation, and provided and provided overall supervision of the research.

Contribution of this chapter to the overall PhD research

The third phase of the research is addressed in this chapter: To identify the most promising supports and promoters for Ni based catalysts during the SCWG of soybean straw. The supports evaluated are activated carbon (AC), carbon nanotubes (CNT), ZrO_2, Al_2O_3, SiO_2 and Al_2O_3-SiO_2. Three different promoters (Ce, Na and K) were also screened.

6.1 Abstract

Supercritical water gasification is a hydrothermal process to gasify complex organic biomass to produce hydrogen-rich syngas. This study reports the catalytic performance and

hydrogen selectivity of several Ni-based catalysts during supercritical water gasification of soybean straw. All experiments were performed at a temperature, biomass particle size, feedstock/water ratio and residence time 500 °C, 0.13 mm, 1:10 and 45 min, respectively. A comprehensive screening of different support materials ranging from activated carbon (AC), carbon nanotubes (CNT), ZrO_2, Al_2O_3, SiO_2 and Al_2O_3-SiO_2 was performed at 10 wt.% Ni loading. The effectiveness of each support in improving H_2 yield, and selectivity was in the order: ZrO_2 > Al_2O_3 > AC > CNT > SiO_2 > Al_2O_3-SiO_2. The effects of three promoters (i.e., Na, K and Ce) in addition to the supported Ni/ZrO_2 and Ni/Al_2O_3 catalysts were evaluated. In terms of H_2 yield, the performance of each promoter for Ni/ZrO_2 catalysts was in the order: Ce (10.9 mmol/g) > K (10.3 mmol/g) > Na (9.5 mmol/g). Ce showed better performance in promoting H_2 yield and minimizing coke deposition on the support. The addition of K, Na and Ce promoters elevated Ni dispersion and the metallic surface area, thus improving H_2 yields.

6.2 Introduction

The increasing world population has led to elevating energy demands. With the world population predicted to exceed 8 billion by 2030, the energy consumption level is estimated to increase beyond 42 % of its current value (i.e., 695 quadrillion British thermal units) (Okolie et al., 2020a). Fossil fuels and petrochemicals are used to complement the rising energy demand and industrial manufacturing worldwide. However, fossil fuels are prone to fluctuations in their cost and cause environmental issues such as pollution and global warming.

A hydrogen-based energy system is viewed as a possible solution to elevating energy demand and the overdependence on fossil fuels (Okolie et al., 2021). Besides, a high energy density of 120 MJ/kg, its ability to burn without any toxic emission while releasing water makes it a superior and clean biofuel. Some practical applications of hydrogen include automobile

engines, petroleum upgrading, hydrogen fuel cells and ammonia production (Abdalla et al., 2018). A major challenge in the utilization of hydrogen in addressing the global energy demand is its sustainable production. About 95 % of the hydrogen used today is obtained from petroleum resources via steam reforming reaction while the other 5 % is from other production sources such as electrolysis and biomass (Okolie et al., 2021). Although the consumption of hydrogen does not emit any greenhouse gases directly, its production from petroleum resources generates a considerable amount of greenhouse gas emissions.

Supercritical water gasification (SCWG) is an attractive technology for the sustainable production of hydrogen from waste materials under aqueous conditions. During SCWG, feedstock drying is not a prerequisite, unlike other thermochemical technologies, since the process can thermally crack wet biomass, thereby reducing the overall process expenditures (Okolie et al., 2019).

A wide variety of feedstock can be used to produce hydrogen through SCWG technologies, a few of which include forestry biomass, agricultural crop residues, algae, energy crops, invasive crops, municipal solid waste, food waste, livestock manure, sewage sludge, polymeric waste, waste plastics, petroleum residues and industrial effluents (Elif and Nezihe, 2016; Lu et al., 2006; Nanda et al., 2019b, 2018). Agricultural crop residues constitute a major proportion of lignocellulosic biomass that require effective management to reduce volume, prevent greenhouse gas emissions from natural microbial decomposition and valorize the inherent cellulose, hemicellulose, and lignin. One of the examples is soybean straw, which is obtained in large quantities (324 million tons per annum) in North America because of soybean (*Glycine max*) cultivation (Abdulkhani et al., 2017).

In our previous study in phase 2 of this research work, we valorized soybean straw for hydrogen-rich syngas production through SCWG and compared the experimental results with theoretical yield (Okolie et al., 2020c). The experimental results were found to be less than the theoretical values indicating incomplete gasification of soybean straw. Furthermore, the results indicated that the SCWG process has high activation energy. Therefore, to effectively produce hydrogen from SCWG and attain maximum conversion of biomass while decreasing the activation energy, it is imperative to develop catalysts with high hydrogen selectivity and high stability under harsh supercritical water (SCW) conditions. Therefore, catalysts are also used to reduce the reaction temperature required to attain the desired product yield.

Heterogeneous catalysts are the focus of this research because of their advantages in terms of their recovery, recyclability and modifications via supports and promoters (Kang et al., 2017). On the other hand, homogeneous catalysts are challenging to recover and reuse combined with their ability to cause reactor corrosion (Sun et al., 2020). Heterogeneous catalysts used in SCWG can be broadly classified into metal oxides, activated carbon and transition metal catalysts (Okolie et al., 2019). Ni-based catalysts are preferred heterogeneous catalysts used in SCWG due to their low cost and efficient catalysis when compared with other metal catalysts (Ru, Pt and Rh) (Kang et al., 2016a). However, Ni-based catalysts are characterized by the challenges of sintering and catalyst deactivation due to coke deposition on the metallic support (Okolie et al., 2019). In this regard, many researchers have comprehensively studied the modification of Ni-based catalysts with different supports and promoters (Azadi et al., 2012a; Chowdhury et al., 2018; Sun et al., 2020).

Chowdhury et al. (2018) noted that the modification of Ni-Al_2O_3 catalyst by doping with La could enhance hydrogen selectivity and reduce catalyst deactivation. Kang et al. (2016)

screened five different supports including activated carbon (AC), TiO_2, Al_2O_3, MgO and ZrO_2, together with the promoters Cu, Co, and Ce for Ni-based catalysts during hydrothermal gasification of lignin. The activity of the catalysts in terms of hydrogen yield was in the following order: MgO < ZrO_2 < AC < TiO_2 < Al_2O_3. On the other hand, the Ce promoter showed the highest activity for hydrogen yield. Recently, Sun et al. (2020) screened Ni-based catalysts with different supports such as Al_2O_3, spent bleaching clay ash (SBC) and SiO_2 as well as Co-promoter for cellulose gasification in subcritical water. The effectiveness of the supports towards hydrogen yield was in the order of Al_2O_3 > SBC > SiO_2. Moreover, the addition of 6 wt.% Co increased the hydrogen yield by 1.4 times.

High-temperature and high-pressure conditions during SCWG necessitate the requirement for catalyst support that shows chemical stability, high surface area and ability to effectively disperse the metal particles on its surface. Several supports such as Al_2O_3, ZrO_2, MgO, AC and carbon nanotubes (CNT) have been widely investigated. Ni/ZrO_2 catalyst was used to improve the carbon gasification efficiency of SCWG of diesel (Kou et al., 2018). Al_2O_3 is widely used as catalyst support for steam reforming of methane (Singh et al., 2018). Ni/SiO_2 catalyst elevated H_2 yield by 57 wt.% during subcritical water gasification of glucose (Sun et al., 2020). Ni/Al_2O_3-SiO_2 catalysts showed promising results during the SCWG of lignin (Guan et al., 2014). AC has been proven to elevate the carbon gasification efficiency of glucose in SCW by catalyzing water-gas shift reaction (Lee and Ihm, 2009). On the other hand, CNT exhibits high surface area, favorable physical and chemical stability coupled with their high heat conductivity in SCW (DeVlieger et al., 2012).

The addition of promoters in heterogeneous catalysts even at low concentrations could affect the stability, selectivity, and performance of a catalyst. Promoters could modify the number

of active sites on the catalyst surface and alter the chemical nature of a particular site (Rocha et al., 2014). Alkali metals such as K and Na are used as promoters for alcohol production by increasing product selectivity while minimizing hydrocarbon production (Simeonov et al., 2014; Tavasoli et al., 2016). Besides, Cu/γ-Al_2O_3 catalysts are promoted by 2.5 wt.% K has shown to improve H_2 selectivity by 54 % during SCWG of sugarcane bagasse (Tavasoli et al., 2016). As a promoter, cerium (Ce) has a high capacity for storing oxygen, thereby releasing a large quantity of active oxygen species (Roh et al., 2002). In addition, Ce has been reported to effectively promote Ni/Al_2O_3 catalysts during the SCWG of lignin (Kang et al., 2017).

Most of the literature reported on the screening of catalysts are performed with biomass model compounds such as glucose (Azadi et al., 2012a), or lignin (Kang et al., 2016a). However, little is known about the effectiveness of such catalysts for actual lignocellulosic biomass owing to its structural complexity and compositional heterogeneity. Moreover, the effect of alkali metal promoters (e.g., K and Na) on gas yield during SCWG is scarce in the literature. Therefore, in the current study, a systematic screening of six different supports ranging from metal oxides and carbon-based materials (e.g., ZrO_2, Al_2O_3, Al_2O_3-SiO_2, SiO_2, AC and CNT) for Ni-based catalysts were carried out. The catalysts were tested for the SCWG of soybean straw with the results compared with those from homogeneous catalysts KOH and non-catalytic reactions. Furthermore, the screening of three different promoters (e.g., K, Na and Ce) for Ni-based catalysts was carried out. To the best of the authors' knowledge, this is the first study to systematically evaluate different carbon and metal oxides supports for Ni-based catalysts together with understanding the effects of alkali metal promoters on hydrogen yield and gasification efficiency.

6.3 Materials and Methods

6.3.1 Materials and catalysts

Soybean straw was obtained from a local farm in Saskatoon, SK, Canada. The straw was chopped followed by pulverization with an IKA MF 10 Basic S1 grinder (ThermoFisher Scientific Inc., Mississauga, Canada) t to obtain ground samples with an average particle size of 0.13 mm. The crushed biomass samples were stored in a clean and airtight container before SCWG experiments. The proximate and ultimate analyses of soybean straw have been reported in our previous studies in phase 2 (Okolie et al., 2020c). Soybean straw contains 42 wt.% carbon, 5.1 wt.% hydrogen, 0.5 wt.% nitrogen and 47.5 wt.% oxygen, respectively. On the other hand, the moisture, volatile matter, ash, and fixed carbon contents of soybean straw were 5.2 wt.%, 81.3 wt.%, 4.6 wt.% and 8.9 wt.%, respectively.

The metal precursors including nickel (II) nitrate hexahydrate [Ni $(NO_3)_2{\cdot}6H_2O$], cerium(III) chloride hexahydrate ($CeCl_3{\cdot}6H_2O$), sodium carbonate (Na_2CO_3) and potassium nitrate (KNO_3) were purchased from Sigma–Aldrich (Oakville, Canada). The catalyst support including aluminum oxide (Al_2O_3) in pellet form, silicon dioxide (SiO_2), silica-alumina (Al_2O_3-SiO_2) and zirconium dioxide (ZrO_2) were procured from Alfa Aesar (Haverhill, USA).

The activated carbon support was prepared by using coffee waste precursors. Slow pyrolysis of the coffee residue was performed in a fixed bed reactor made of Inconel having a length of 870 mm, an internal diameter of 22 mm and an external diameter of 25.4 mm. The Inconel reactor was placed inside an electronically heated Applied Test Systems (ATS) split furnace connected to an ATS temperature controller system (Applied Test Systems, Butler, Pennsylvania, USA). The pyrolysis system consists of an Omega Type-K thermocouple (Spectris Canada Inc., Laval, QC, Canada), pressure gauges, pressure relief valve, check valve, 2-μm filters and a condenser placed inside an ice bath. Pyrolysis experiments were performed in the presence of

industrial-grade nitrogen gas at a flow rate of 100 mL/min and steam produced with a steam generator at 150 ± 5 °C. The reaction temperature was maintained at 400 °C with a heating rate of 5 °C/min for 1 h of holding time.

After pyrolysis, the produced biochar was physically activated using steam as the activating agent. The activation procedure has been described in a previous publication from our research group (Shahkarami et al., 2015). The activation was carried out in a similar reactor. A boiler was connected to the experimental setup for steam generation. The boiler consists of a 6.35 mm SS316 tube enclosed inside an insulated aluminum block. Water was injected into the boiler with a metering pump (A-60-S, Eldex Laboratories Inc., Napa, USA) while the unreacted steam was condensed in an ice bath. For steam activation, about 20 g of biochar produced from the pyrolysis of coffee residue was loaded into the reactor and heated up to 700 °C at a heating rate of 3 °C/min using N_2 as a carrier gas at a flow rate of 140 mL/min. Steam was continuously injected into the reactor at a steam-to-carbon mass ratio of 1.06 for 1.4 h after which the reactor was cooled down to room temperature under an inert atmosphere. The produced activated carbon had a surface area, pore volume and pore diameter of 722 m^2/g, 0.25 cm^3/g and 4.15 nm, respectively. The carbon, hydrogen, nitrogen, sulfur, and oxygen contents of the produced activated carbon were 83.7 wt.%, 2.3 wt.%, 5.2 wt.%, 0.04 wt.% and 6.2 wt.%, respectively. Furthermore, the average particle size of the activated carbon was 463 µm.

M.K. Impex Corp. (Mississauga, Canada) supplied commercial carbon nanotubes (CNT). About 5 g of the CNT was functionalized using a mixture of 4 M HNO_3 and 10 M H_2SO_4 in a 1:3 ratio to obtain a 200 mL solution (Thi Mai Hoa, 2018). The acid solution was refluxed through CNT for 5 h at 90 °C (Santangelo et al., 2012). The dried CNT was treated with $KMnO_4$ solution for surface modification. The CNT was washed with deionized water to remove any traces of acid.

Further washing with deionized water was carried out until its pH reached neutrality (Rana et al., 2020). The CNT sample was dried at 100 °C for 6 h before its use as catalyst support.

6.3.2 Catalysts synthesis

Catalysts were synthesized by incipient wetness impregnation and co-impregnation method (when two metal precursors were involved) as shown in Figure 6.1. Approximately 10 wt.% of Ni loading was used for all the catalysts with the catalysts denoted by 10 Ni/Y (catalysts without promoter) and 10Ni-aX/Y (catalysts with promoter). Where Y, X and a represents the support material, promoter, and promoter loading, respectively. The amount of metal precursors used were evaluated based on the desired catalyst composition.

The synthesis procedure started by dissolving the metal precursor in water followed by the impregnation onto the support using a 1 mL syringe. The mixture was aged for 2 h and dried in an oven at 105 °C for 6 h to obtain a solid catalyst sample. The sample was ground to powder form and calcined in a furnace at 650 °C for 8 h under air except for AC and CNT supports, which were calcined under nitrogen atmosphere. The catalysts were reduced at 550 °C using a 10 % mixture of H_2/N_2 (1:1 vol/vol ratio) for 3 h (Sun et al., 2020). It is important to note that carbonaceous support materials are not calcined under airflow because of the chances of decomposition to CO_2. However, N_2 creates an inert atmosphere preventing oxidation of carbon.

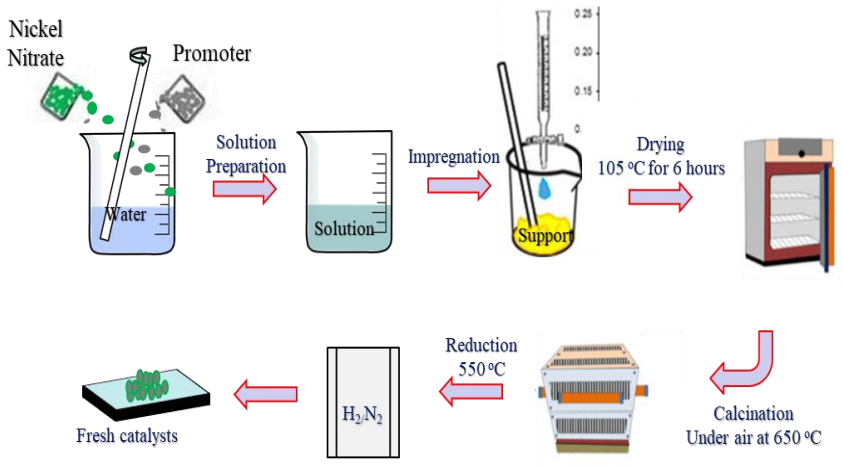

Figure 6.1: Schematic representation for catalyst preparation by incipient wet impregnation method

6.3.3 Physicochemical characterization of catalysts and gasification products

The gases produced from SCWG of soybean straw were analyzed using an Agilent 7820A gas chromatograph (GC) (Agilent Technologies, Santa Clara, California, USA). The GC system is equipped with a thermal conductivity detector, three packed columns and one capillary column. H_2, CH_4 and CO were measured by Ultimetal HayesepQ T 80/100 mesh column. On the other hand, CO_2 and C_2-C_6 gases were quantified by Ultimetal Hayesep T 80/100 mesh column. The column and detector were operated at temperatures of 50 °C and 60 °C, respectively with argon as the carrier gas.

Brunauer–Emmett–Teller (BET) surface area and porosimetry analyses of the catalysts were performed using a Micrometrics ASAP 2020 instrument (Norcross, USA). The BET method was used to determine the surface area while the pore size analysis was obtained from the Barrett–Joyner–Halenda (BJH) method. The BET assumes that the surface is homogeneous, and all sites are equal. However, for most mesoporous materials, the surface of the pore has a certain amount of curvature and most of the surface is within its pores. Since BET analysis does not take the geometry into account, the BHJ method was used to determine the pore size. This approach has

been used by several authors in the literature (Badoga et al., 2020; Lee and Ihm, 2009; Lu et al., 2014c). The samples were first degassed at 300 °C for 4 h under 0.5 mm Hg pressure, before the nitrogen adsorption and desorption analysis was carried out at −196 °C.

X-ray diffraction (XRD) of the calcined catalysts was performed using a Bruker D8 ADVANCE device equipped with CuKα radiations (Bruker AXS, Karlsruhe, Germany). Hydrogen-temperature-programmed reduction (TPR) of the catalysts was performed using a Micromeritics AutoChem 2950 HP chemisorption analyzer (Norcross, USA). The TPR analysis was performed with a 10 v/v% H_2/Ar mixture at a flow rate of 50 mL/min. The heating rate was set at 10 °C/min while the temperature ranged from 35 °C to 800 °C. For CO chemisorption, 100 mg of catalyst placed in a quartz tube was degassed. Pure H_2 was used to reduce the samples at 350 °C for 2 h followed by cooling under vacuum to 35 °C. The chemisorption analysis was performed by passing pulses of CO gas.

Thermogravimetric (TGA) analysis of the spent catalysts was conducted in a PerkinElmer Pyris Diamond instrument (Waltham, USA) to study the carbon formation. TGA analysis was performed under an N_2 flow rate of 60 mL/min until a final temperature of 600 °C at a heating rate of 10 °C/min. The weight loss pattern with increasing temperature was observed to determine the coke formation in the spent catalyst.

6.4 Results and discussion

6.4.1 Characterization of catalysts and screening of supports.

In the present study, six different materials ranging from ZrO_2, Al_2O_3, SiO_2, Al_2O_3-SiO_2, AC and CNT were investigated as support for Ni-based catalysts. The aim was to screen and identify the most effective support for Ni-based catalysts based on H_2 yield and selectivity during SCWG of lignocellulosic biomass. The XRD patterns of supported Ni catalysts are shown in

Figure 6.2. XRD aids in the determination of the crystallographic structure of the active metals present in heterogeneous catalysts as well as understanding the correlation of catalysts' properties with their performance (Badoga et al., 2020).

As illustrated in Figure 6.2, for the supported Ni-catalysts, the presence of NiO was characteristic to the 2θ peaks at 37°, 43°, 52°, 62.5° and 76°(Lu et al., 2014c). For Ni/Al_2O_3 catalyst the characteristics 2θ peak at 66.7° corresponds to the presence of crystalline γ-Al_2O_3 (Kang et al., 2016a). The diffraction peaks corresponding to 2θ values of 30.5°, 50.6° and 60.3° were ascribed to the presence of ZrO_2 in Ni/ZrO_2 catalyst (Lu et al., 2014c). The 2θ peak located at 42° in Ni/CNT catalyst could be due to the graphitic crystalline moieties typical to carbon nanotubes (Rana et al., 2020). The 2θ diffraction peak at 52° was accredited to the formation of the hexagonal $Ni(OH)_2$ phase (Rana et al., 2020). The XRD patterns showed little variation in the peak locations among the catalysts, which could be because of the difference in interactions between the active metal (Ni) and the support materials. Moreover, the intensities of the peaks at the same position are also different. It is important to note that NiO peaks with high intensities could be attributed to the poor dispersion of Ni on the support material. For example, NiO peaks at 37° for Ni/SiO_2 showed high intensities when compared with peaks at a similar position. Furthermore, for Ni/CNT and Ni/AC catalysts, high-intensity peaks of NiO were also observed at 76°.

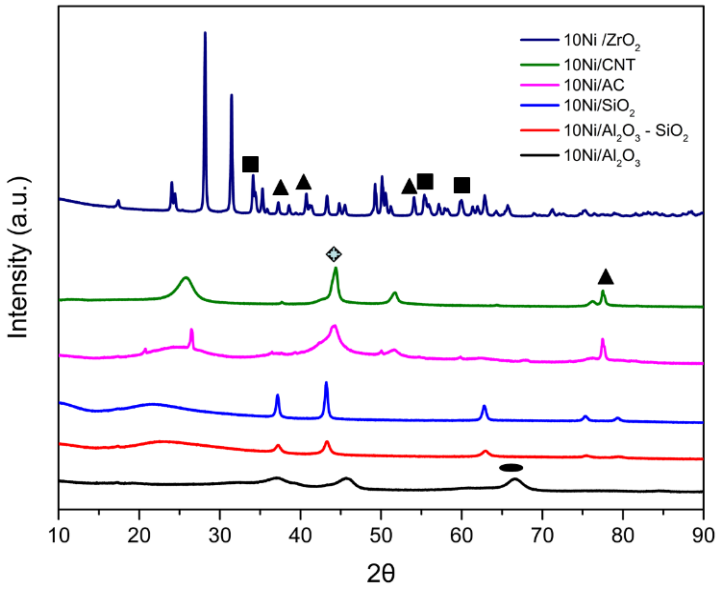

Figure 6.2: XRD profile for Ni-based catalysts with different supports. The symbols are represented as NiO (▲), ZrO_2 (■), crystalline γAl_2O_3 (⬬) and graphite crystalline moieties (◈)

The surface properties of supported Ni catalysts together with their influence on total gas yields, H_2 yields, H_2 selectivity and LHV are shown in Table 6. 1. The product yield obtained from catalytic SCWG of soybean straw using supported Ni-based catalysts was compared with the non-catalytic and KOH-assisted gasification. Key results on non-catalytic and KOH-assisted SCWG of soybean straw presented in Table 6.1 were adapted from our previous report in phase 2 (Okolie et al., 2020c). All the catalysts performed differently in terms of product gas yields, H_2 selectivity and LHV of the resulting gases. $10Ni/ZrO_2$ showed the highest H_2 yield (8.1 mmol/g) and H_2 selectivity (88.2 %) while $10Ni/Al_2O_3$-SiO_2 presented the lowest H_2 yield (3.5 mmol/g) and H_2 selectivity (35.3 %). Compared to non-catalytic SCWG, the use of $10Ni/ZrO_2$ catalyst resulted in an increase in H_2 selectivity from 63 % to 88.2 %. When compared to homogeneous catalysts (KOH), $10Ni/ZrO_2$ showed better performance in terms of H_2 yield and selectivity. In terms of H_2 yield, the effectiveness of the supports was in the following order: $10Ni/ZrO_2$ (8.1 mmol/g) >

$10Ni/Al_2O_3$ (7 mmol/g) > 10Ni/AC (6.7 mmol/g) > 10Ni/CNT (5.6 mmol/g) > $10Ni/SiO_2$ (5.1 mmol/g) > $10Ni/Al_2O_3$-SiO_2 (3.5 mmol/g). On the contrary, the gaseous products obtained from $10Ni/Al_2O_3$ showed the highest LHV of 2743 kJ/Nm^3 while $10Ni/Al_2O_3$-SiO_2 produced the least LHV (i.e. 1256 kJ/Nm^3). The relatively lower LHV of the gaseous products obtained from $10Ni/Al_2O_3$-SiO_2 could be attributed to reduced yields of CO, C_2-C_4 and CH_4.

The specific surface area, porosity and catalysts activity were correlated to understand the influence of catalyst properties on SCWG product yields. As shown in Table 6.1, the specific surface area of catalysts determined through BET analysis decreased in the following order: $10Ni/Al_2O_3$-SiO_2 (596 m^2/g) > 10Ni/AC (368 m^2/g) > $10Ni/Al_2O_3$ (320 m^2/g) > $10Ni/SiO_2$ (239 m^2/g) > 10Ni/CNT (235 m^2/g) > $10Ni/ZrO_2$ (6 m^2/g). Furthermore, the pore volume decreased in the following order: $10Ni/SiO_2$ (1.48 cm^3/g) > 10Ni/CNT (0.95 cm^3/g) > $10Ni/Al_2O_3$-SiO_2 (0.69 cm^3/g) > 10Ni/AC (0.63 cm^3/g) > $10Ni/Al_2O_3$ (0.61 cm^3/g) > 10Ni/ ZrO_2 (0.02 cm^3/g). Ni/Al_2O_3-SiO_2 showed the highest surface area and pore volume. However, its activity was lower than that of $10Ni/Al_2O_3$ with a relatively smaller surface area. 10Ni/AC catalysts with a surface area of 368 m^2/g also performed poorly when compared to $10Ni/Al_2O_3$ (surface area of 320 m^2/g). Some factors that could be responsible for the reduction in the catalytic activity of 10Ni/AC catalysts could be catalyst sintering or coke formation under SCW conditions. Similar observations were reported by Zhang et al.(2011) during glucose gasification in SCW. The lower catalytic activity of Ni/AC was attributed to the poor nickel dispersion onto the support (Zhang et al., 2011a).

Table 6.1: BET analysis of Ni-based catalysts together with H_2 yields, total gas yields, H_2 selectivity and lower heating values of gases obtained from SCWG of soybean straw at optimal conditions.

Catalysts	**Specific surface area (m^2/g)**	**Total pore volume (cm^3/g)**	**Pore diameter (nm)**	**H_2 yields (mmol/g)**	**Total gas yields (mmol/g)**	**H_2 selectivity (%)**	**LHV (kJ/Nm^3)**
*No catalyst	-	-	-	6.6	14.9	63.0	1592
*KOH (homogeneous catalyst)	-		-	7.7	16.6	85.2	1810
10Ni/ZrO_2	6	0.02	13	8.1	17.4	88.2	1861
10Ni/Al_2O_3	320	0.61	8	7.0	24.1	41.0	2743
10Ni/Al_2O_3-SiO_2	596	0.69	4	3.5	10.9	48.0	1256
10Ni/AC	368	0.63	7	6.7	18.6	55.9	2197
10Ni/SiO_2	239	1.48	25	5.1	19.7	35.3	2546
10Ni/CNT	235	0.95	16	5.6	14.9	50.9	2021

*Selected data adapted from Okolie et al. (2020d). Note: All experiments are carried out at temperature (500 °C), biomass/water ratio (1:10), biomass particle size (0.13 mm) and residence time (45 min). The experiments were performed in duplicates with a standard deviation of less than 4 %.

In the current study, the lower activity of catalysts such as 10Ni/CNT (5.6 mmol/g), 10Ni/SiO_2 (5.1 mmol/g) and 10Ni/Al_2O_3-SiO_2 (3.5 mmol/g) could be due to the poor nickel dispersion onto the support as confirmed by the XRD results in Figure 4.2. Another factor that could be responsible for the decline in H_2 yields with the use of such catalysts is their ability to promote some parallel reactions that consume hydrogen. Examples of such reactions are hydrogenation and methanation reactions. Enhancing such reactions could lead to a reduction in the yield of H_2 when compared to non-catalytic reactions.

Based on the product gas yields obtained from different catalysts with distinctive textural properties, it is observed that for the catalytic SCWG of soybean straw, high surface area and porosity are beneficial. However, they do not always exhibit the highest catalytic activity. Some other factors such as metal support interactions or metal dispersion, coke formation and the ability

of the catalysts to participate in intermediate reactions could influence the catalytic activity. Besides, the two most effective catalysts in terms of H_2 yield and selectivity, $10Ni/Al_2O_3$ and $10Ni/ZrO_2$ were selected for further modification with promoters.

6.4.2 Performance of promoters for SCWG of soybean straw

$10Ni/Al_2O_3$ and $10Ni/ZrO_2$ were selected for further modification with the addition of K, Na and Ce promoters based on the results of catalysts screening. Since CH_4 and C_2-C_4 hydrocarbons are some of the main products obtained from SCWG of soybean straw, it is important to select promoters that reduce their yields while enhancing H_2 yield and selectivity. To compare the performance of the selected promoters, SCWG of soybean straw was performed at optimal conditions using the corresponding Ni-based catalysts with the addition of 1 wt.% promoter (K, Na and Ce). The total gas yield, CGE, H_2 selectivity and H_2 yield of the promoted Ni-based catalysts are shown in Table 6.2. In terms of H_2 yields, the performance of each promoter for $10Ni/ZrO_2$ catalyst was in the following order: $10Ni\text{-}1Ce/ZrO_2$ (10.9 mmol/g) > $10Ni\text{-}1Na/Al_2O_3$ (10.8 mmol/g) > $10Ni\text{-}Ce/Al_2O_3$ (10.6 mmol/g) > $10Ni\text{-}1K/ZrO_2$ (10.3 mmol/g) > $10Ni/1Na\text{-}ZrO_2$ (9.5 mmol/g) > $10Ni\text{-}1K/Al_2O_3$ (8.7 mmol/g) > $10Ni/ZrO_2$ (8.1 mmol/g) > $10Ni/Al_2O_3$ (7 mmol/g). It was observed that the addition of 1 wt.% Ce, K and Na promoters to the Ni/ZrO_2 catalysts elevated H_2 yield. 1 wt.% Ce led to an increase in H_2 yield and total gas yields from 8.1 mmol/g to 10.9 mmol/g and 17.4 mmol/g to 24.3 mmol/g, respectively. On the other hand, the addition of K elevated the H_2 yield and total gas yields from 8.1 mmol/g to 10.3 mmol/g and 17.4 mmol/g to 21.2 mmol/g, respectively. Compared to Ce and K promoters, the effect of Na addition to Ni/ZrO_2 is not well pronounced. The addition of Na led to a slight increase in H_2 yield from 8.13 mmol/g to 9.5 mmol/g and total gas yields from 17.4 mmol/g to 20.6 mmol/g. The CGE also increased by 45.8 %, 25.6 % and 56.3 % with the addition of K, Na and Ce promoters, respectively.

Table 6.2: H_2 yields, total gas yields, carbon gasification efficiency and lower heating value of gases obtained from SCWG of soybean straw at optimal conditions using ZrO_2 and Al_2O_3 supported Ni-based catalysts and catalysts modified with K, Na and Ce promoters.

Catalysts	**H_2 yields (mmol/g)**	**Total gas yields (mmol/g)**	**CGE (%)**	**LHV (kJ/Nm^3)**
*No catalyst	6.6	14.9	20.2	1592
*KOH (homogeneous catalyst)	7.7	16.6	21.4	1810
10Ni/ZrO_2	8.1	17.4	21.5	1861
10Ni/Al_2O_3	7.0	24.1	22.5	2743
10Ni-1K/ZrO_2	10.3	23.1	31.3	2419
10Ni-1K/Al_2O_3	8.7	21.4	31.6	2266
10Ni-1Na-ZrO_2	9.5	20.6	27.0	2116
10Ni-1Na/Al_2O_3	10.8	22.3	29.1	2664
10Ni-1Ce/ZrO_2	10.9	24.3	33.5	2884
10Ni-Ce/Al_2O_3	10.6	24.1	33.0	2734

*Selected data adapted from Okolie et al. (2020d). Note: All experiments are carried out at temperature (500 °C), biomass/water ratio (1:10), biomass particle size (0.13 mm) and residence time (45 min). The experiments were performed in duplicates with a standard deviation of less than 4 %.

The addition of 1 wt.% promoter to Ni/Al_2O_3 catalysts also elevated H_2 and total gas yields. Surprisingly, 10Ni-1Na/Al_2O_3 (10.8 mmol/g) showed a superior H_2 yield compared to 10Ni-Ce/Al_2O_3 (10.6 mmol/g) and 10Ni-1K/Al_2O_3 (8.7 mmol/g). On the other hand, 10Ni-Ce/Al_2O_3 catalyst showed a superior CGE (33 %) when compared with 10Ni-1K/Al_2O_3 (31.6 %) and 10Ni-1Na/Al_2O_3 (29.1 %). Therefore, K appears to be a better promoter than Na to improve CGE during SCWG of soybean straw. However, in terms of CGE, the effectiveness of the promoters was in the order of Na < K < Ce. Based on the catalyst screening results, 10Ni-1Ce/ZrO_2 was found to be the most effective for SCWG of soybean straw in terms of H_2 yield and CGE.

It should be emphasized that the CGE values ranged from 20.2 % for the non-catalytic reaction to 21.5 % with 10Ni/ZrO_2 catalysts. However, the addition of 1 wt.% Ce promoter

elevated the CGE to 33.5 %. Soybean straw is a lignocellulosic feedstock containing cellulose (34.1 wt.%), hemicellulose (16.1 wt.%) and lignin (21.6 wt.%) as well as extractives, and ash (Okolie et al., 2020c). The high lignin content makes it difficult for the complete gasification of soybean straw leading to low gasification efficiency. Lignin has a complex structure containing three-dimensional phenyl propane monomeric compounds joined by ester linkage (Okolie et al., 2020d). Therefore, it is challenging to hydrolyze lignin into phenolic compounds and the subsequent conversion into catalysts in the absence of a catalyst. Moreover, the presence of a catalyst helps to facilitate intermediate reactions that promote lignin degradation leading to an improved CGE.

To understand the effect of the promoters on hydrocarbon conversion and competing reactions (e.g. WGSR and methanation), the product gas yield was evaluated as shown in Figure 6.3. The addition of 1 wt.% K and Na promoters to the supported Ni-based catalysts led to an increase in the yields of H_2, CO_2, CH_4 and a decline in the C_2-C_2 hydrocarbons and CO yield decreased. The decline in the yields of light hydrocarbons with the addition of alkali metal promoters could be a result of their ability to reduce the production of hydrocarbon gases (Tavasoli et al., 2016). On the other hand, K tends to adsorb CO, thereby inhibiting its complete reduction while preventing the production of lighter hydrocarbon gases. A decline in CO yield and an increase in the yields of H_2 and CO_2 could be a result of the ability of K and Na to promote WGSR during SCWG of soybean straw.

The addition of the Ce promoter led to an increase in H_2, CO_2, CH_4 and C_2–C_6 hydrocarbons while there is a decline in CO yield (Figure 6.3). Ce can weaken the interactions between a catalyst and the support, thereby leading to high reducibility and stronger nickel dispersion (Wang and Lu, 1998). Ce could also influence the gas yield by promoting steam

reforming reactions and inhibiting carbon deposition due to its ability to oxidize carbon deposits on the catalyst surface (Kang et al., 2016a). For future applications, it is invaluable to understand the properties of the aforementioned catalysts and correlate them with their performance.

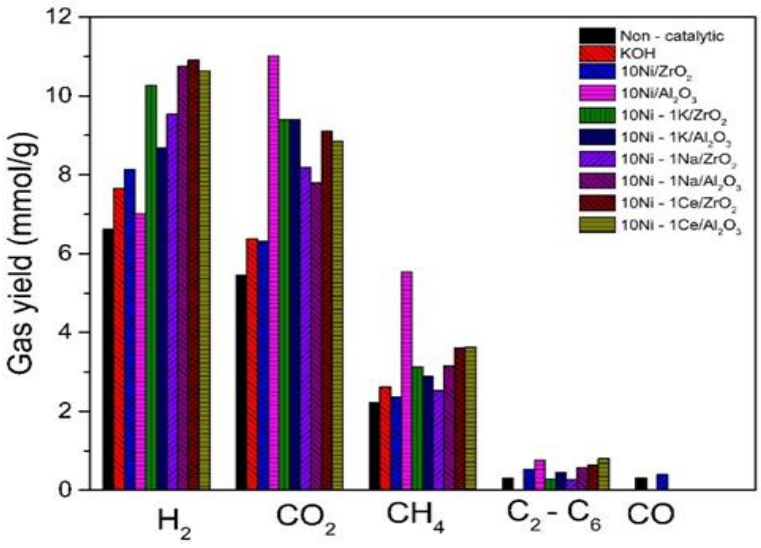

Figure 6.3: Product gas yields from supercritical water gasification of soybean straw with different heterogeneous catalysts. All experiments are carried out at 500 °C with a 1:10 biomass/water ratio, biomass particle size of 0.13 mm and residence time of 45 min.

6.4.3 Textural properties of promoted catalysts

The textural properties of promoted catalysts including their surface area, pore volume and pore diameter are shown in Table 6.3. The addition of promoters to $10Ni/Al_2O_3$ and $10Ni/ZrO_2$ catalysts led to a decrease in their surface area, pore diameter and pore volume. The exceptions are applied to $10Ni\text{-}1Na/Al_2O_3$ and $10Ni\text{-}1Ce/ZrO_2$ catalysts where the addition of Na and Ce elevated the pore diameter. For example, the pore diameter for $10Ni\text{-}1Ce/ZrO_2$ (16 nm), $10Ni\text{-}1Na/Al_2O_3$ (11 nm) and $10Ni\text{-}1Ce/Al_2O_3$ (10 nm) were relatively higher in contrast to that of their unpromoted counterparts i.e. $10Ni/ZrO_2$ (13 nm) and $10Ni/Al_2O_3$ (8 nm).

Table 6.3: Textural properties of supported Ni-based catalysts and catalysts modified with K, Na and Ce promoters.

Catalysts	**Specific surface area (m^2/g)**	**Total pore volume (cm^3/g)**	**Pore diameter (nm)**
$10Ni/ZrO_2$	6	0.02	13
$10Ni/Al_2O_3$	320	0.61	8
$10Ni\text{-}1K/ZrO_2$	5	0.02	13
$10Ni\text{-}1K/Al_2O_3$	269	0.63	7
$10Ni\text{-}1Na/ZrO_2$	2	0.02	6
$10Ni\text{-}1Na/Al_2O_3$	351	0.67	11
$10Ni\text{-}1Ce/ZrO_2$	4	0.02	16
$10Ni\text{-}1Ce/Al_2O_3$	299	0.59	10

The decline in the surface area and pore volume of promoted catalysts was because of the saturation of the empty pores with Na, K and Ce promoters. This also indicates a change in the pore structure. Pierella et al. (2005) reported a slight decline in the surface area of ZSM-5 zeolite catalyst with the addition of Mo and Zn promoters. The decline in the surface area was attributed to the blockage of the catalyst pores by Mo and Zn metals (Pierella et al., 2005). In the present study, Ni is the active metal. Although the addition of promoters might cause pore blockage, it could also make the nickel more accessible by increasing the metal dispersion. Besides, the promoters could also act as a cleavage site to split water into H^+ and OH^- ions. These atoms could spill over nickel metals, thereby contributing to an increase in the overall reaction. This phenomenon could be responsible for the elevation in H_2 yield and CGE with the addition of K, Na and Ce promoters despite the slight decline in the surface area, pore diameter and pore volume.

From Table 3, the percentage decline in surface area for the promoted $10Ni/ZrO_2$ catalysts was in the following order: $10Ni\text{-}1Na/ZrO_2$ (66.7 %) > $10Ni\text{-}1Ce/ZrO_2$ (33.3 %) > $10Ni\text{-}1K/ZrO_2$ (16.7 %) for. It is important to note that the dissimilarity in the decline of the textural properties of each catalyst could be a result of the difference in the degree of the metal-metal interactions.

6.4.4 Temperature programmed reduction

One of the potential roles of a promoter during catalytic SCWG is to ease the reduction of NiO. Although, the extent of reduction is reliant on the type of promoters and their quantity added to the catalyst. TPR analysis was carried out to investigate the reducibility of nickel metal in Ni/ZrO_2 since its metallic form is the active phase of the catalysts (Zhang et al., 2011a). It should be mentioned that the reduction of Ni might occur *in situ* inevitably since a large amount of H_2 is produced during SCWG. In addition, since the maximum temperature for SCWG experiments in this study is 500 °C, the reduction peak above this temperature was not considered.

The H_2-TPR spectra of $10Ni/ZrO_2$ promoted catalysts are presented in Figure 6.4. Besides, the peak temperature and H_2 uptake are also presented in Table 6.4. Compared to the unpromoted $10Ni/ZrO_2$ catalyst, the addition of promoters increased the H_2 uptake in the following order: 10Ni-$1Na/ZrO_2$ (3.3 mmol/g_{cat}) > 10Ni-$1Ce/ZrO_2$ (1.9 mmol/g_{cat}) > 10Ni-$1K/ZrO_2$ (1.3 mmol/g_{cat}) > $10Ni/ZrO_2$ (0.7 mmol/g_{cat}). An elevation in H_2 uptake shows that there is an increase in the number of available sites for the reaction. The Ni-supported catalysts, peaks that appear at low temperatures are assigned to the reduction of relatively free NiO particles (Kang et al., 2016a). On the other hand, the peaks that appear at high temperatures are attributed to the reduction of the complex NiO species, which is in contact with the oxide support (Roh et al., 2002). From the H_2-TPR spectra, the first reduction peaks for Ni/ZrO_2, 10Ni-$1Na/ZrO_2$, 10Ni-$1Ce/ZrO_2$ and 10Ni-$1K/ZrO_2$ catalysts were at 349 °C, 338 °C, 342 °C and 350 °C, respectively (Figure 6.4). Second reduction peaks for $10Ni/ZrO_2$ and 10Ni-$1Na/ZrO_2$ catalysts appeared at 578 °C and 536 °C, respectively. The reduction peaks at temperatures above 500 °C correspond to the reduction of complex NiO species (Roh et al., 2002). However, these peaks are not considered in this study because the maximum temperature of the reaction is 500 °C.

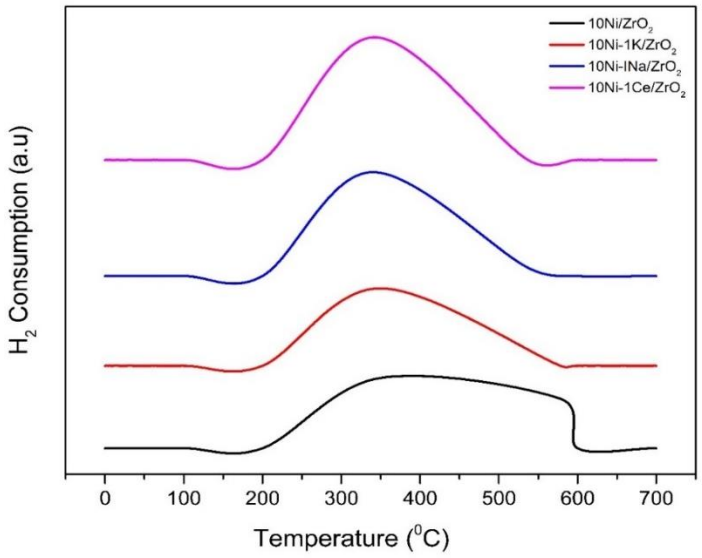

Figure 6.4: H_2 TPR profile for Ni-based catalysts and catalysts modified with K, Na and Ce promoters.

Table 6.4: CO chemisorption results for supported Ni-based catalysts modified with K, Na and Ce promoters.

Catalysts	**First TPR peak temperature (°C)**	**Second TPR peak temperature (°C)**	**H_2 consumption in TPR (mmol/g_{cat})**
10Ni/ZrO_2	348.9	578.3	0.7
10Ni-1K/ZrO_2	349.7	-	1.3
10Ni-1Na/ZrO_2	338.6	536.9	3.3
10Ni-1Ce/ZrO_2	342.3	-	1.9

6.4.5 CO chemisorption

The portion of nickel (active metal) in the catalyst that is available for the reaction was determined with CO chemisorption. Table 6.5 illustrates the CO chemisorption results with metal dispersion, metallic surface area and crystallite size. Metal dispersion is defined in terms of the fraction of the total amount of Ni atoms that is exposed to the catalyst surface. As indicated in Table 6.5, the addition of Ce and K promoters led to an elevation in the metallic surface and metal

dispersion. While the crystallite size declines with the addition of K and Ce promoters. The metal dispersion was in the following order: 10Ni-1Ce/ZrO_2 (6.6 %) > 10Ni-1Na/ZrO_2 (3.1 %) > 10Ni-1K/ZrO_2 (2.7 %) > 10Ni/ZrO_2 (2.7 %) > 10Ni/Al_2O_3 (1.1 %). This trend is similar to the ease of reducibility obtained from the H_2-TPR studies.

Table 6.5: CO chemisorption results for supported Ni-based catalysts modified with K, Na and Ce promoters.

Catalyst	**Metallic surface area (m^2/g)**	**Metallic surface area (m^2/g)**	**Metal dispersion (%)**	**Crystallite size (nm)**
10Ni/ZrO_2	18.1	1.8	2.7	31.1
10Ni/Al_2O_3	7.5	0.8	1.1	88.1
10Ni-1K/ZrO_2	18.3	1.8	2.7	30.7
10Ni-1Na/ZrO_2	15.0	1.9	3.1	25.1
10Ni-1Ce/ZrO_2	26.0	0.6	6.6	15.0

It is important to note that higher active metal (Ni) dispersion is preferable while finely dispersed active metal particles produce an improved sintering resistance (Zhang et al., 2011a). As shown in Table 6.5, better dispersion could also lead to smaller particle size, thereby enhancing coke resistance of the catalyst. Based on the chemisorption results, it can be deduced that the addition of 1 wt.% K, Ce and Na promoters to 10Ni/ZrO_2 catalysts increased the active metal dispersion and metallic surface area while producing a smaller crystallite size, thus elevating the H_2 yields.

6.4.6 Thermogravimetric analysis of the spent catalysts

Thermogravimetry analysis (TGA) was performed for the spent catalysts obtained from SCWG of soybean straw at optimal conditions obtained in phase 2 (i.e., temperature: 500 °C, feedstock particle size: 0.13 mm, feedstock/water ratio: 1:10, residence time: 45 min and pressure: 23-25 MPa). TGA was used to analyze and quantify the coke deposition on the catalyst surface.

The anti-coking ability of catalysts used in SCWG is essential for regeneration and practical use (Zhu et al., 2019). As noted by Lu et al. (2014b) some factors that could lead to catalysts deactivation during SCWG include coke deposition, sintering and the phase change of the support. However, coke deposition is one of the most severe problems of Ni-based catalyst during the SCWG of biomass (Lu et al., 2014b).

The TGA profiles of spent 10Ni/ZrO_2 catalysts modified with Na, Ce and K promoters are given in Figure 6.5. It is important to note that two important factors influence the changes in the weight of the spent 10Ni/ZrO_2 catalysts when measured with TGA analysis (Lu et al., 2014b; Zhu et al., 2019). The first factor is the sample weight increase because of nickel oxidation, whereas the second factor is sample weight decline due to the oxidation of the deposited carbon. The weight loss of unpromoted spent 10Ni/ZrO_2 catalyst was 25 %. However, when promoter was added to the catalysts the weight loss decreased in the following order: 10Ni-1Na/ZrO_2 (14 %) > 10Ni-1K/ZrO_2 (11 %) > 10Ni-1Ce/ZrO_2 (6 %). The results imply that the addition of promoters minimizes coke accumulation in the catalysts. Furthermore, Ce shows the lowest accumulation of coke. The superior performance of Ce in reducing coke accumulation could be a result of the improved Ni dispersion as confirmed by the CO chemisorption findings (Table 6.5).

The amount of deposited coke on the surface of the catalyst was also calculated from the weight loss curve with the values expressed in the mass of coke accumulated per mass of catalysts. Figure 6.6 shows the correlation between coke accumulation (g/g_{cat}) with H_2 yield (mmol/g) and CGE (%). An elevation in the amount of coke accumulation led to a rapid decrease in H_2 yield and CGE. Therefore, coke formation in a catalyst could influence the H_2 yield and CGE. High resistance of 10Ni-1Ce/ZrO_2 towards coke formation and its improved catalytic activity towards H_2 yield could be linked to the redox properties of Ce (Lu et al., 2014b). CeO_2 - based materials

possess relatively high oxygen mobility and storage capacity because of their improved reduction/oxidation ability. The reversible reaction of CeO_2 with oxygen enables rapid uptake and release of oxygen (Equation 6.1).

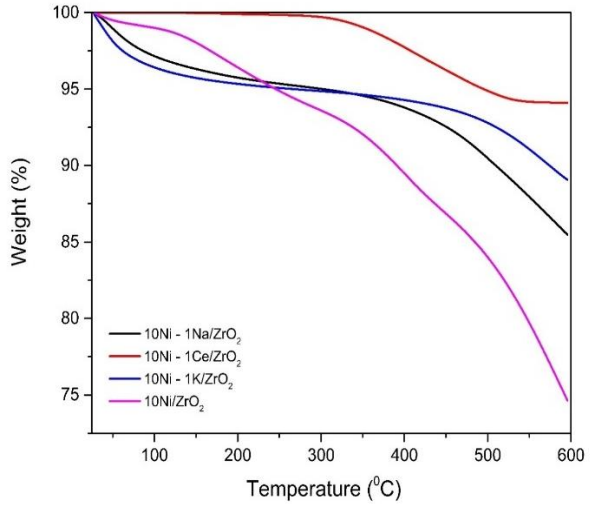

Figure 6.5: TGA profile of spent ZrO_2 supported Ni catalysts and catalysts modified with K, Ce and Na promoters.

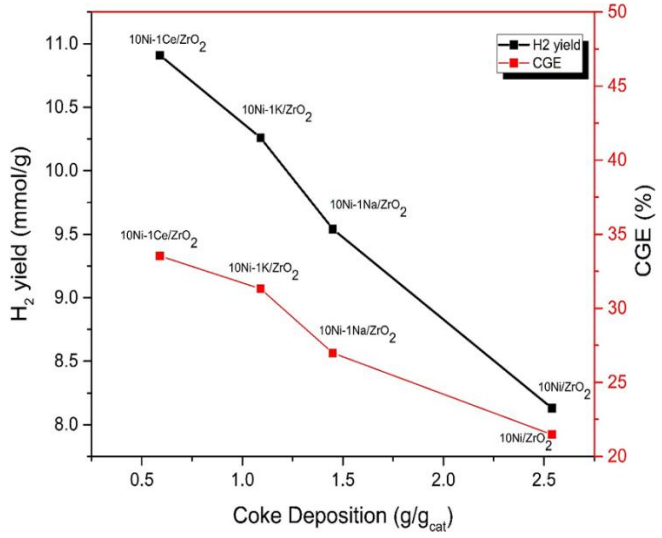

Figure 6.6: Relationship between coke deposition on the catalyst surface, H_2 yield and carbon gasification efficiency during supercritical water gasification of Soybean straw.

$$CeO_2 \leftrightarrow CeO_{2-x} + O_x \qquad (6.1)$$

Where, O_x represents the lattice oxygen on the CeO_2 surface. Oxygen can react or be adsorbed by CO on the surface of a Ce-based catalyst to produce CO_2 (Equation 6.2). Furthermore, the solid carbon is oxidized to CO (Equation 6.3), thus leading to a reduction in carbon deposition (Li et al., 2006; Roh et al., 2002; Zhu et al., 2019).

$$CO + O_x \leftrightarrow CO_2 + O_{x-1} \quad (6.2)$$

$$C + O_x \leftrightarrow O_{x-1} + CO \quad (6.3)$$

It is important to note that Ni could also interact with CeO_2 for catalysts prepared by the co-impregnation method leading to the improvement in catalysts performance (Lu et al., 2014b). Moreover, NiO could also react with the reduced site Ce (O_{x-1}) and it is reduced to active metal nickel while maintaining its activity for the SCWG process (Kumar et al., 2008). The performance of the alkali metal promoters (i.e. Na and K) in minimizing coke formation could be linked to their ability to neutralize acidic sites and suppress polymerization and cracking reactions (Lu et al., 2014b).

6.4.7 X-ray diffraction analysis

The crystalline properties of promoted Ni/ZrO_2 catalysts were analyzed by XRD analysis (Figure 6.7). All the catalysts showed the same characteristic peaks at 30.5°, 35.2°, 50.6° and 60.3° corresponding to tetragonal ZrO_2 (Kou et al., 2018).[19] The diffraction peaks corresponding to 2θ values of 29.1°, 31.6°, 40.6°, 51.9°, 71.4° and 76.6° show the presence of Ni. This indicates the reduction of Ni^{2+} to Ni°.

The XRD profile for Ni/ZrO_2 showed broad and small 2θ peaks at 71.4° and 76.6°. However, with the addition of promoters, the peaks were not visible. Furthermore, the intensity of

2θ peaks at 31.6°, 40.6° and 51.9° also decreased with the addition of promoters. Lower peak intensity means improved dispersion of nickel. Therefore, the addition of promoters helped in increasing the metal dispersion. A similar trend was observed from the chemisorption results. It is interesting to note that there is no apparent change in the XRD patterns upon the addition of promoters, thus indicating that the active phase of the catalyst remains intact.

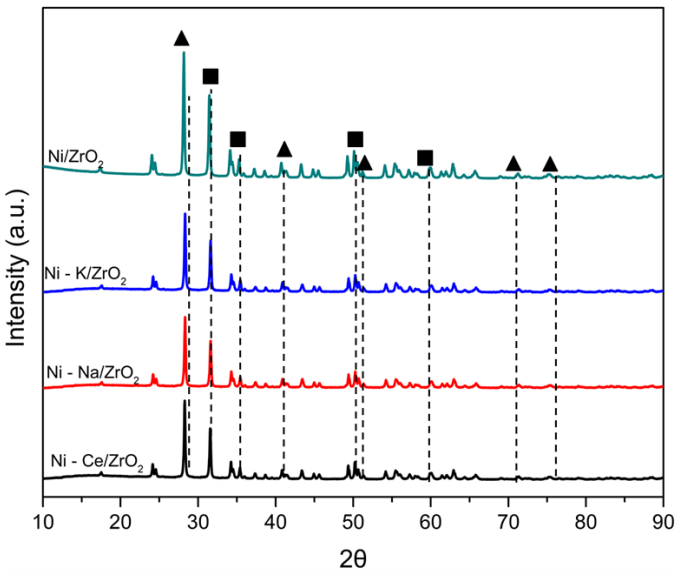

Figure 6.7: XRD profile for ZrO_2 supported Ni catalysts and catalyst modified with K, Ce and Na promoters. The symbols are represented as ZrO_2 (■) and Ni (▲).

6.4.8 Catalytic cycle study

The catalytic stability of 10Ni/ZrO_2 and 10Ni-1Ce/ZrO_2 catalysts were evaluated during the SCWG of soybean straw. After the first catalytic run, the catalyst was recovered and used for the next experiments. Three catalytic cycles were tested in the study. After the third cycle, the catalysts were calcined at high temperature (650°C) and activated (reduced in a tubular reactor at 550°C using a 10% mixture of H_2/N_2 i.e., 1:1 vol/vol ratio for 3 h). The regenerated catalysts were tested under similar operating conditions and the results compared with that of the fresh catalysts.

The results of the stability test for 10Ni/ZrO_2 and 10Ni-1Ce/ZrO_2 catalysts are shown in Figure 6.8 and Figure 6.9, respectively. As can be seen from Figure 6.8, the use of recycled 10Ni/ZrO_2 catalyst led to a decline in H_2 yield from 8.1 mmol/g to 7.4 mmol/g (8.6% decrease) when the catalyst was reused for the first time. H_2 yield decreased to 5.9 mmol/g the second time (20.3% decrease). On the contrary, there was a dramatic increase in CO_2 yield from 6.3 mmol/g to 10.4 mmol/g when the catalyst was reused for the first time. CO_2 yields decreased slightly when the catalyst was reused the second time. CH_4 also showed a similar trend with CO_2. With the reuse of 10Ni/ZrO_2 catalyst for the first time, the CH_4 yield escalated from 2.4 mmol/g to 2.9 mmol/g followed by a decline to 2.5 mmol/g with the second cycle.

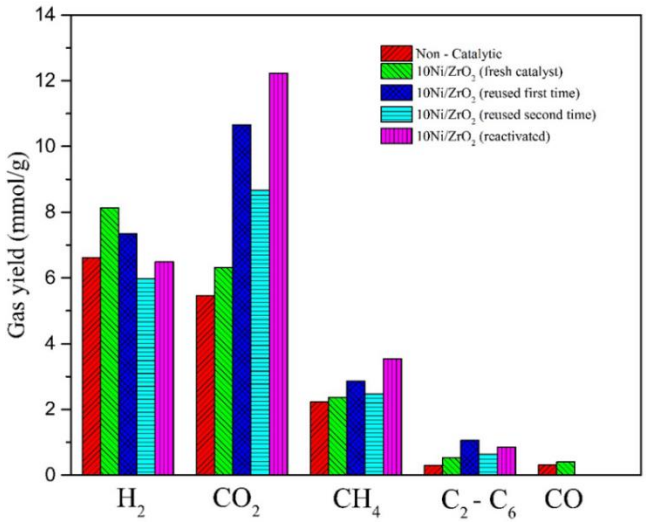

Figure 6.8: Product gas yields from supercritical water gasification of soybean straw with used Ni/ZrO_2 catalysts. All experiments are carried out at 500 °C with a 1:10 biomass/water ratio, biomass particle size of 0.13 mm and residence time of 45 min.

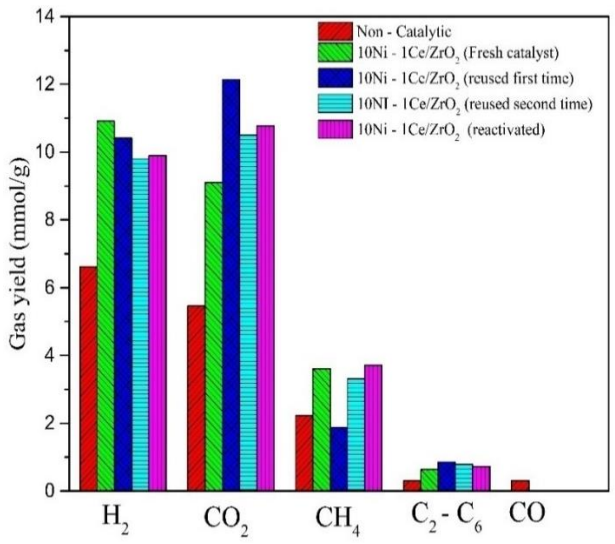

Figure 6.9: Product gas yields from supercritical water gasification of soybean straw with used Ni-Ce/ZrO_2 catalysts. All experiments are carried out at 500 °C with a 1:10 biomass/water ratio, biomass particle size of 0.13 mm and residence time of 45 min.

Compared to the 10Ni/ZrO_2 catalyst, recycled 10Ni-1Ce/ZrO_2 catalyst showed a slight decline in H_2 yield when reused the first time and the second time (Figure 6.9). H_2 yield decreased by 4.6% and 5.9% when the catalyst was reused the first and second time, respectively. The results demonstrate the great advantages of Ce promoter in improving the stability of Ni/ZrO_2 catalyst under SCW conditions.

The significant decrease in H_2 yield (20.3%) upon the reuse of 10Ni/ZrO_2 catalyst for the second time indicates a severe deactivation after the SCWG reaction. However, there are several factors responsible for the catalyst deactivation under SCW conditions as stated in the previous section. The most common ones include catalyst poisoning, sintering or coke formation (Lu et al., 2019). Coke is found to block the active sites of a catalyst and in some extreme situations, its deposition leads to the physical blockage of the pore entrance leading to the active site (Li et al., 2019). If the deactivation of the catalyst is a result of coke formation covering the active site, then high-temperature calcination and reduction should be able to recover the catalyst activity. From

the experimental results presented in Figure 6.8 and Figure 6.9. However, high-temperature calcination and reduction did not increase the gas yields. Therefore, it can be inferred that the active site was not regained. This indicates that the blockage of the active site of the catalysts because of coke formation was not the only reason responsible for the catalyst deactivation. The other possible reason could be an irreversible catalyst deactivation caused by sintering.

Catalyst sintering also known as thermal deactivation is common for high-temperature catalytic processes such as SCWG. It leads to agglomeration and a decline in the surface-to-volume ratio of the catalyst (Hansen et al., 2013). Sintering could be due to the movement of particles on the support surface (e.g., Brownian-like motion) and the subsequent coalescence to cause particle growth. It could also be from the migration of mobile atoms (adsorbed atoms). The migration is due to the difference in free energy and concentrations of adsorbed atoms on the support surface (Hansen et al., 2013). The results from this study show that the 10Ni/ZrO_2 catalyst is prone to sintering. However, the addition of 1 wt.% Ce helped to improve its stability. Ce could help to prevent the collision of the migrating crystallites, thereby improving the stability of the catalyst (Li et al., 2011).

6.4.9 Correlation between catalyst properties and performance

In the present study, we try to correlate the properties of the catalyst with its performance during the SCWG of soybean straw at optimal conditions obtained in phase 2 (i.e., temperature: 500 °C, feedstock particle size: 0.13 mm, feedstock/water ratio: 1:10, residence time: 45 min and pressure: 23-25 MPa). The catalyst properties such as reducibility defined using H_2 uptake during TPR analysis and metal dispersion were plotted against H_2 yields and selectivity as shown in Figure 6.10 and Figure 6.11. An elevation in H_2 yield with H_2 uptake was observed. On the contrary, there is a slight decline in the H_2 selectivity with increasing H_2 uptake. It is also important

to note that the addition of promoters led to an increase in H_2 uptake for the ZrO_2 supported Ni-based catalysts with Ce promoters exhibiting the highest uptake and the maximum H_2 yield and selectivity.

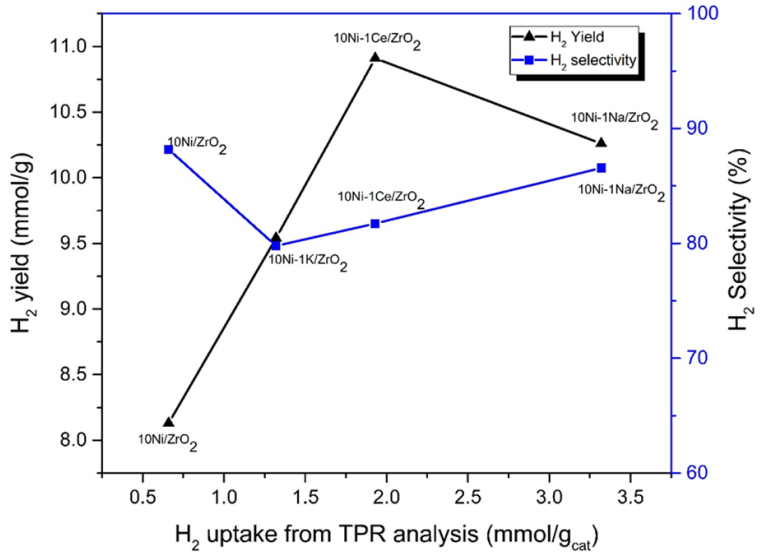

Figure 6.10: Correlation between catalyst properties from TPR analysis and performance in terms of H_2 yield and selectivity.

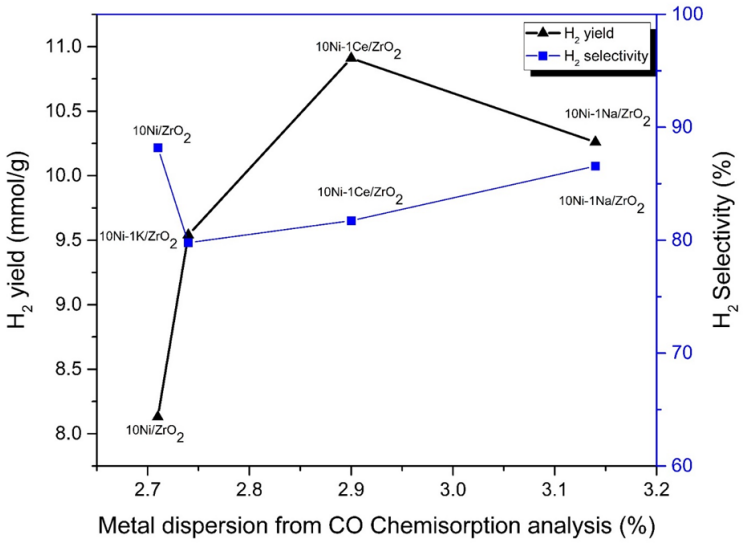

Figure 6.11: Correlation between metal dispersion and catalyst performance in terms of H_2 yield and selectivity.

In terms of metal dispersion from CO chemisorption analysis, the H_2 yield increased with a rise in metal dispersion. On the other hand, a rise in metal dispersion due to the addition of 1

wt.% K, Na and Ce promoters produced a slight decrease in H_2 selectivity. The XRD analysis in Figure 6.7 also confirms that the addition of promoters improved the Ni dispersion, which in turn improved the H_2 yield. Among all the catalysts evaluated in this study, 10Ni -Ce/ZrO_2 catalysis with the maximum H_2 uptake and metal dispersion produced the highest H_2 yield and selectivity. 10Ni-Ce/ZrO_2 also showed the lowest coke deposition among all the catalysts studied. Based on the above observations, it can be stated that the properties of the catalysts are well correlated with their performance. Thus, 10Ni-Ce/ZrO_2 improved the H_2 yield (6.6 mmol/g without a catalyst to 10.9 mmol/g with catalyst) and H_2 selectivity (from 63 % without a catalyst to 81.7 % with catalyst) during the hydrothermal gasification of soybean straw. Such observations are due to the properties of the catalysts including the surface area, ease of reducibility, improved metal dispersion and the oxidative ability of Ce.

6.5 Conclusions

In this study, various catalysts support materials ranging from ZrO_2, Al_2O_3, SiO_2, Al_2O_3-SiO_2, AC and CNT were screened for the application of Ni-based catalysts during SCWG of soybean straw. All the catalytic SCWG experiments were performed in a fixed bed tubular reactor at temperature (500 °C), feedstock/water ratio (1:10), biomass particle size (0.13 mm) and residence time (45 min). The performance of the catalysts was evaluated in terms of H_2 yield, H_2 selectivity and CGE. The performance of each support in improving H_2 yield was in the order of ZrO_2 (8.1 mmol/g) > Al_2O_3 (7 mmol/g) > AC (6.7 mmol/g) > CNT (5.6 mmol/g) > SiO_2 (5.1 mmol/g) > Al_2O_3-SiO_2 (3.5 mmol/g). On the other hand, the H_2 selectivity was in the order of ZrO_2 (88 %) > AC (56 %) > CNT (51 %) > Al_2O_3-SiO_2 (48 %) > Al_2O_3 (41 %) > SiO_2 (35 %). Moreover, the experimental results indicate the importance of the high surface area of catalysts during SCWG. However, some other properties such as coke formation, active metal dispersion and metal-support

interactions could play a more important role in improving product yield and selectivity. The variation in H_2 yield and selectivity could be attributed to catalyst properties and nickel interactions with the support materials.

Ni/ZrO_2 showed the highest H_2 yield and selectivity. Therefore, it was selected for further modification with three different promoters (K, Na and Ce) together with Ni/Al_2O_3 catalysts. All the promoters improved H_2 yield while reducing coke formation. The performance of cerium was attributed to its high capacity for storing oxygen species, which can react with the carbon deposits on the catalyst surface, thereby preventing carbon deposition. When all the three promoters used in this study were compared in terms of CGE, their effectiveness was in the order of Na < K < Ce.

Chapter 7 Kinetics of Soybean Straw Gasification in Supercritical Water in the Presence of Ni – Ce/ZrO_2 Catalysts

A version of this section will be submitted for publication in a journal.

Contribution of the Ph.D. Candidate

Experiment and Modeling including coding in Matlab were carried out by Jude Okolie. The manuscript was also drafted by Jude. Dr. Sonil Nanda helped with the experimental set up and reviewed the manuscript. Dr. Ajay K. Dalai examined the research results, coordinated the manuscript preparation, and provided overall supervision of the research. Dr. Janusz A. Kozinski examined the research results, coordinated the manuscript preparation, and assisted in designing the work.

Contribution of this chapter to the overall PhD research

This section provides the kinetics studies of Ni – Ce/ZrO_2 catalytic and non – catalytic gasification of soybean straw in SCW to produce H_2. The kinetic model was used to study the dynamic behavior of SCWG system with time. The results provide a basic understanding of the reaction mechanisms influencing the catalytic gasification of soybean straw in SCW.

7.1 Abstract

Supercritical water gasification is a novel thermochemical technology that can be used to effectively convert the lignocellulosic feedstock into hydrogen rich syngas, thereby eliminating the issues of overdependency on petroleum resources. Moreover, a clear understanding of the kinetics of biomass gasification in supercritical water is invaluable for reactor design and process optimization. Therefore, a novel kinetic model for the gasification of soybean straw in supercritical water was proposed in this study. Experimental data for soybean straw gasification with Ni – Ce/ZrO_2 catalysts and without the catalyst were used to fit the kinetics model at 500 ^oC, 1:10

biomass to water ratio and biomass particle size of 0.13 mm for 45 min at a pressure range of 22 – 25 MPa. The kinetics predictions showed correlates with experimental findings and the non – stoichiometric thermodynamic predictions. The proposed kinetic model is also able to predict gaseous yield outside the experimental study range Compared to the non – catalytic studies, the addition of a catalysts increased the rate constants for steam reforming reactions, pyrolysis reactions and water gas shift reaction.

7.2 Introduction

The present world is faced with increasing population and rapid industrialization which has led to an exponential increase in energy demand. Moreover, it is predicted that by the year 2040, the global energy consumption would rise by 20 – 30% of its current value (Sarker et al., 2021). Fossil fuel resources are predominantly used to sustain the global energy consumption. On the other hand, the petroleum resources have been used globally in developing and underdeveloped countries for the production of value-added chemicals, as a direct fuel and in the transportation sector. However, the issues of climate change, environmental pollution and price instability of petroleum resources have led to a growing interest in alternative energy sources that are renewable and sustainable (Li et al., 2011).

Biomass valorization to produce energy through thermochemical or biochemical pathways is one of the pathways for the sustainable production of energy supply. Lignocellulosic biomass is renewable and readily available for the production of sustainable fuels and chemicals. Furthermore, their availability is non – seasonal and their utilization for biofuel production creates immense socioeconomic advantage. Lignocellulosic biomass originates from non – edible plant materials such as the energy crops, forestry biomass and agricultural residues. As a result, the

utilization of lignocellulosic materials for the second-generation biofuels production does not create the food against fuel debate created by the first generation biofuels (Sarangi et al., 2018).

The thermochemical conversion of lignocellulosic biomass to biofuels offers an attractive pathway for their effective utilization compared to the biological pathways. The thermochemical processes offers improved conversion efficiency, short reaction time and it has the ability to handle different types of feed materials (Okolie et al., 2020a). Gasification, pyrolysis, torrefaction, carbonization, and liquefaction are notable examples of thermochemical conversion pathways. On the other hand, the biochemical pathways includes anaerobic digestion, butanol fermentation and syngas formation (Brethauer and Studer, 2015).

Supercritical water gasification (SCWG) is an attractive technology for the effective valorization of lignocellulosic biomass to produce hydrogen rich syngas. SCWG process employs the unique features of water under supercritical conditions (temperature > 374.1 ^{o}C and pressure > 22.1 MPa) to decompose biomass into syngas (Rodriguez Correa and Kruse, 2018b). Supercritical water (SCW) has the tendency to act as a reaction medium and also behave like a green solvent and catalysts due to a significant change in its thermo – physical properties when compared to water at ambient temperature (Resende and Savage, 2010).

Since the pioneering work of SCWG by Modell (Modell et al., 1978), several research areas has been explored and developed, thereby leading the technology on the path to commercialization. A wide varieties of feedstocks such as food waste (Nanda et al., 2016d), sewage sludge (Gong et al., 2017b), wheat straw (Nanda et al., 2018), microalgae (Miller et al., 2012) and Petrochemical residues (Rana et al., 2020) have been studied as potential feed materials for hydrogen rich syngas production from SCWG in both batch and continuous experimental system. On the other hand, some researchers have also studied the effect of several homogeneous

and heterogeneous catalysts to improve product yield during SCWG (Kou et al., 2018; Lu et al., 2014d; Zhang et al., 2011b). However, due to the complex reaction mechanisms of SCW and the presence of several intermediate reactions occurring simultaneously during SCWG, the kinetics of the reaction is least understood.

Kinetics models of SCWG helps to describe the system evolution with time and subsequently determine the dynamic mass and energy balance. This is very useful during reactor design and process optimization of a SCWG system. In our previous study, it is shown that Soybean straw is a viable feedstock for hydrogen rich syngas production from SCWG (Okolie et al., 2020c). The result of the study indicates that the experimental results did not approach the theoretical values. One of the reasons that could be responsible for the deviation is that a long residence time could promote the decomposition of intermediates into products (Nikoo et al.2015). Therefore, it is imperative to develop kinetics models that can predict the system behavior with time.

Several authors have proposed the kinetic model of different lignocellulosic model feedstock in SCW (Y. Chen et al., 2020; Guan et al., 2012; Jin et al., 2015b; Resende and Savage, 2010; Tushar et al., 2015, 2020). However, most of the proposed kinetic models in literature are mostly to determine the kinetic parameters and predict the gasification efficiency. On the other hand, few researchers have also studied the prediction of different gaseous yield and composition during SCWG. This is invaluable, especially for studying the system evolution with time and for practical applications of SCWG.

Resende and Savage (2010) proposed a kinetic model for the gasification of cellulose in SCW. Their model was used to effectively predict the effect of biomass loading and density of water on gaseous yield. Guan et al. (2012) proposed a kinetic model for algae gasification in SCW.

The model was able to effectively predict the gaseous yield and decomposition behavior of algae in SCW. Cao et al. (2018) studied the kinetics of sugarcane bagasse in SCW with the presence of homogeneous catalysts Na_2CO_3. The experimental data were fitted to a homogeneous model with the assumption that the reaction is Pseudo-first-order reaction (Cao et al., 2018). The kinetic model was able to predict the gasification efficiency and activation energy. However, the individual gaseous products cannot be predicted by the model. To fill the knowledge gap, this study proposes a kinetic model for catalytic and non – catalytic gasification of soybean straw in SCW. The objective of this study is to develop models that could predict the behavior of SCWG system with time. The experimental results from our previous study were used to fit the model based on several intermediate reactions related to SCWG. To the best of the authors knowledge, this is the first study to propose a detailed kinetics models for lignocellulosic biomass (soybean straw) gasification in SCW. Furthermore, it is important to note that the gasification of real biomass material which is heterogeneous in nature is different from those of the model compounds. Therefore, a detailed kinetics study of real biomass feedstock is important for its effective valorization.

7.3 Kinetics studies

The reaction of Soybean straw is complicated with several intermediate reactions taking place simultaneously. A generalized reaction pathway for the gasification of lignocellulosic biomass in SCW has been proposed in our previous studies (Okolie et al., 2020b). The pathway is illustrated in Figure 4.7. However, one of the most important reaction is steam reforming reactions. Soybean straw reacts with water to produce CO and H_2, and most of the soybean straw is consumed in the reaction. Some other intermediate reactions that produce gases are also considered in the kinetic models.

During SCWG process, soybean straw undergoes rapid hydrolysis and depolymerization reactions to produce carbohydrates, organic acids, phenols, and alcohols. The unique properties of water under supercritical conditions ensures that a homogenous environment is created, therefore the reaction rate is assumed to be first order. The stoichiometric equations used in developing the kinetic model are based on the reaction pathway in Figure 4.7. It is important to note that the production of solid chars and tars are not considered in the stoichiometric equations because SCWG occurs at high temperature above the critical point of water with fast hydrolysis and polymerization of organic molecules taking place leading to low formation of chars and tars.

Another important concept in the kinetic model is the use of the lumped parameter technique to represent reaction intermediate. The lumped parameter method was employed for the following reasons. First, it is very difficult to quantitatively represent all the intermediates involved in a complex reaction such as SCWG. Second, our reaction is concerned with modeling individual gaseous products rather than identification of the intermediates involved. Third, this approach has been employed by several researchers during the kinetic modeling of biomass gasification in hydrothermal medium (Guan et al., 2012; Guo et al., 2013; Resende and Savage, 2010).

In order to balance the stoichiometric equations, soybean straw was assumed to possess one carbon atoms with a molecular formular of $CH_{1.44}O_{0.93}$ which is consistent with the elemental composition of Soybean straw reported in our previous studies (Okolie et al., 2020c). It should be noted that S and N atoms were neglected because the product gases do not detect compounds containing those atoms. Although, the elemental composition of Soybean straw ($CH_{1.44}O_{0.93}N_{0.009}$) shows that it contains N atoms, we assume that majority of the N atoms appears as nitrogen containing compounds such as NH_3 and moves to the aqueous phase after the reactor is cooled at room temperature in the SCWG reactor.

Based on the proposed reaction mechanism for biomass gasification in SCW and the assumption that all intermediate produced are lumped together as lumped intermediates (L_{int}), gaseous products obtained are proposed to proceed through the following reaction pathway.

Reaction pathway 1 (Steam reforming reaction): The first reaction involves the steam reforming of soybean straw to produce CO and H_2 (Equation 7.1).

$$2CH_{1.44}O_{0.93} + 0.14H_2O \xrightarrow{k_1} 2CO + 1.58H_2 \quad (7.1)$$

Reaction pathway 2 (Biomass pyrolysis): Soybean straw pyrolysis also occurs to produced CO, CO_2 and CH_4 respectively as shown in Equations 7.2, 7.3 and 7.4.

$$CH_{1.44}O_{0.93} \xrightarrow{k_2} L_{int\,1} + CO \quad (7.2)$$

$$CH_{1.44}O_{0.93} \xrightarrow{k_3} L_{int\,2} + CO_2 \quad (7.3)$$

$$CH_{1.44}O_{0.93} \xrightarrow{k_4} L_{int\,1} + CH_4 \quad (7.4)$$

Reaction pathway 3 (Methanation and Water gas shift reaction): The produced gases from steam reforming reactions and biomass pyrolysis reacts with one other via WGSR, methanation, hydrogenation and Boudouard reactions.

The water gas shift reaction and methanation reaction occur to produce CO_2, H_2, CO and CH_4 (Equations 7.5). On the other hand, the methanation reaction is shown in Equation 7.6.

Water gas shift reaction

$$CO + H_2O \xleftrightarrow{k5} CO_2 + H_2 \quad (7.5)$$

Methanation reaction

$$CO + 3H_2 \overset{k6}{\leftrightarrow} CH_4 + H_2O \quad (7.6)$$

Equilibrium calculations shows that reactions such as hydrogenation and Boudouard reaction do not take place to an extent in supercritical conditions therefore they are not considered as part of the stoichiometric equations. The methanation and water gas shift reactions are both reversible reactions. However, the reverse reactions of water gas shift reaction and methanation reactions are neglected because their reverse reactions rates are very small as a result of a very large equilibrium constants of methanation and water gas shift reactions (Guo et al., 2013; Jin et al., 2015b). The equilibrium constant was calculated form the Gibbs free energy minimization method. Similar approach was used in our previous study (Okolie et al.,2020).

Reaction pathway 4 (formation of liquid products). The non - pyrolyzed intermediates are converted into liquid phases as shown in Equation 7.7:

$$CH_{1.44}O_{0.93} \overset{k_7}{\rightarrow} L_{int\ i\ (L)} \quad (7.7)$$

It should be emphasized that although soybean straw also undergoes liquefaction to produce liquid products which can also be gasified into condensable gases. However, some liquid products once formed, they are very difficult to gasify. Therefore they are lumped together into intermediates in Equation 7.7 (Guo et al., 2013). The reaction rate in Equation 7.7 is referred to as the liquid forming reactions that is opposing gas production. Therefore, the value of the rate constant, k_7 should be small enough to allow the production of gases.

Kinetics of soybean gasification in supercritical water was evaluated through the pseudo-first order reaction in the absence mass transfer (internal and external). The pseudo-first order

system assumes that the reaction is first order and that the catalyst surface is at a pseudo homogeneous state. This implies that the concentration of each species present at various locations on the catalyst surface remains constant. Therefore, the adsorption terms for each species are not accounted for. The kinetic expressions for the pseudo – homogeneous reactions are represented in equations 7.8 -7.14. The concentration of each the species present in the reaction are represented by C_{H2} (hydrogen), C_{int1}(Lumped intermediates 1, C_{int2} (lumped intermediates 2), C_{CO} (carbon monoxide), C_{CO2} (carbon dioxide), C_{CH4} (methane), C_w (water), $C_{Biomass}$ (Soybean straw), C_{liquid} (liquid products). It should be noted that the concentration of soybean straw and that of the lumped intermediates are calculated as the ratio of the number of moles of the carbon atoms present in each individual species to the volume of the experimental set up used to obtain the gaseous yield. The concentration of each rection species is expressed in mmol/g of dry soybean straw.

$$r_{co} = 2k_1 C_{Biomass}C_w + k_2 C_{Biomass} - k_5 C_{co}C_w - k_6 C_{co}C_{H_2} \quad (7.8)$$

$$r_{H_2} = 1.58k_1 C_{Biomass}C_w + k_5 C_{co}C_w - 3k_6 C_{co}C_{H_2} \quad (7.9)$$

$$r_{co_2} = k_3 C_{Biomass} + k_5 C_{co}C_w \quad (7.10)$$

$$r_{CH_4} = k_4 C_{Biomass} + k_6 C_{co} C_{H_2} \quad (7.11)$$

$$r_{liquid} = k_7 C_{Biomass} \quad (7.12)$$

$$r_{Biomass} = -2k_1 C_{Biomass}C_w - k_2 C_{Biomass} - k_3 C_{Biomass} - k_4 C_{Biomass} - k_7 C_{Biomass} \quad (7.13)$$

$$r_w = 1.58k_1 C_{Biomass}C_w - k_5 C_{co}C_w + k_6 C_{co} C_{H_2} \quad (7.14)$$

7.3.1 Determination of the rate constant

The experimental data obtained in phase 4, from catalytic (Ni-Ce/ZrO_2 catalysts) and non – catalytic gasification of Soybean straw in supercritical water were used to fit the model. The time

dependent variables fitted are CO, H_2, CO_2, CH_4,$C_{Biomass}$, $C_{int,}$ and C_W. The overall procedure used to estimate the rate constants is illustrated in Figure 7.1.

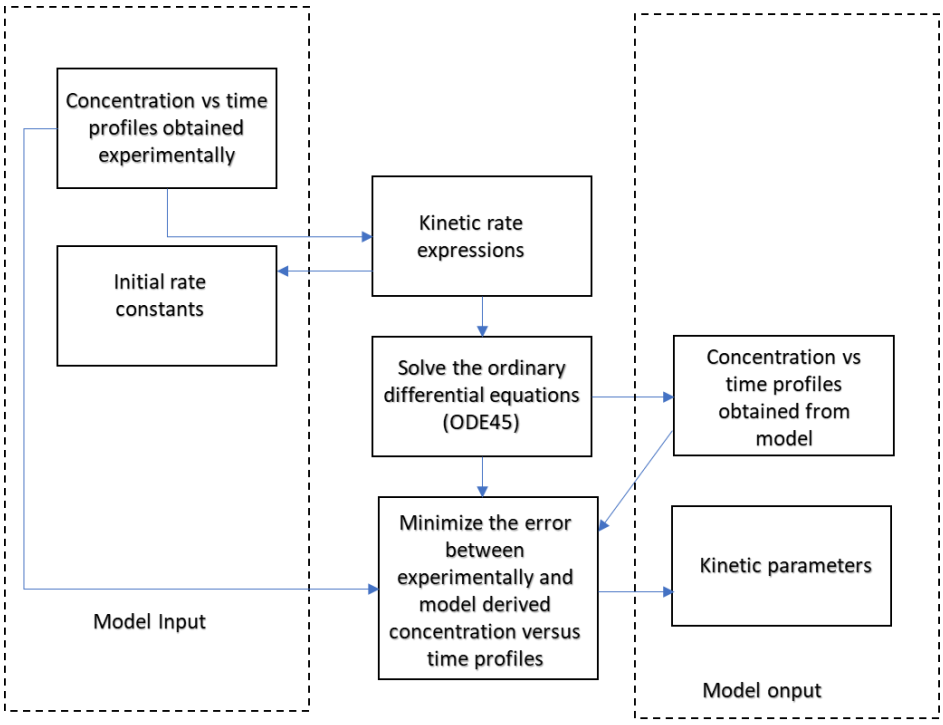

Figure 7.1: Methodology used to determine the kinetics parameters.

First, the concentration of each reaction products is plotted against the residence time. Then the slope is estimated at any arbitrary time constant. Then the slope and concentration values are substituted into the rate constant equations (Equation 8 -14) to get the initial rate constants. The determined rate constant values together with the initial concentration were used as initial guess in solving the kinetic equations.

The kinetics equations which were written in the form of ordinary differential equations (ODEs) were solved using the ODE45 command in MATLAB R 2018a software (MathWorks, Inc. Santa Clara, California, USA). The MATLAB software is licensed by the University of

Saskatchewan. The MATLAB built in ODE45 uses the 4th and 5th order Runge-Kutta formula to solve the ODEs. The concentration of each species as a function of time was obtained after solving the ODEs. An error function 'err' was defined as the square of the difference between the experimental values for each individual species and the model values. The function was denoted as C_{Error} and was expressed by Equation 7. 15 (Issariyakul and Dalai, 2012).

$$C_{Error} = [C_{Cal} - C_{exp}]^2 \quad (7.15)$$

Where C_{Exp} and C_{Cal} represents the experimental and model results respectively.

To determine the rate constants for each individual reactions the "*fminsearch*" command in MATLAB was used to minimize the error function. The command uses the initial guess of rate constant and returns a value that minimizes the error by changing the rate constant.

7.4 Results and discussions

7.4.1 Kinetics parameters estimation and model validation

Catalytic and non -catalytic gasification of soybean straw in SCW was performed at temperature 500 ^{0}C, pressure range of 22 – 25 MPa, 1:10 biomass to water ratio and biomass particle size of 0.13 mm with a residence time range of 15 – 45 mins. The kinetic rate constants were determined from the methodology in Figure 7.1, and they are presented in Table 7.1.

Generally, the addition of a catalysts enhanced the hydrolysis and dissolution of soybean straw in SCW thereby increasing the rate constants for steam reforming reactions, pyrolysis reactions and WGSR. As a result, the yields of H_2, CO_2 and CH_4 are increased with the addition of a catalyst. On the other hand, CO is consumed during the WGSR and methanation reactions. Therefore, there is a decline in CO yields with the addition of a catalyst.

Table 7.1: The estimated rate constants for the non – catalytic and Ni – Ce/ZrO_2 catalyzed reactions.

Rate constant	Unit	Non catalytic reaction	Catalytic reaction (Ni – Ce/ZrO_2 catalysts)
k_1	$Lmol^{-1}min^{-1}$	1.1×10^{-3}	2.90
k_2	min^{-1}	4.62×10^{-2}	1.62×10^{-1}
k_3	min^{-1}	1.28×10^{-1}	1.53×10^{-1}
k_4	min^{-1}	9.52×10^{-2}	1.95×10^{-1}
k_5	$Lmol^{-1}min^{-1}$	1.10×10^{-1}	3.76×10^{-1}
k_6	$Lmol^{-1}min^{-1}$	4.10×10^{-7}	1.03×10^{-5}
k_7	min^{-1}	1.40×10^{-3}	9.2×10^{-8}

The concentrations against time profiles for CO, H_2, CO_2 and CH_4 obtained from the kinetic models were fitted against the experimental values with reaction time ranging from 15 – 45 mins at 500 ^{0}C and the results are presented in Figure 7.2. It is observed that most of the experimental points fall on the model prediction lines which indicates that there is a good correlation between them. From Figure 7.2, it can be seen that the yields of H_2 ,CO_2 and CH_4 increase with residence time within the study range. Since H_2 is the desired product during SCWG it is important to design the process within operating conditions that improves H_2 yield.

Long residence time in SCWG can be achieved by increasing the length of the reactor. Moreover, increasing the reactor length would lead to additional processing cost, therefore adequate optimization between increasing the reactor length and cost savings should be carried out

.

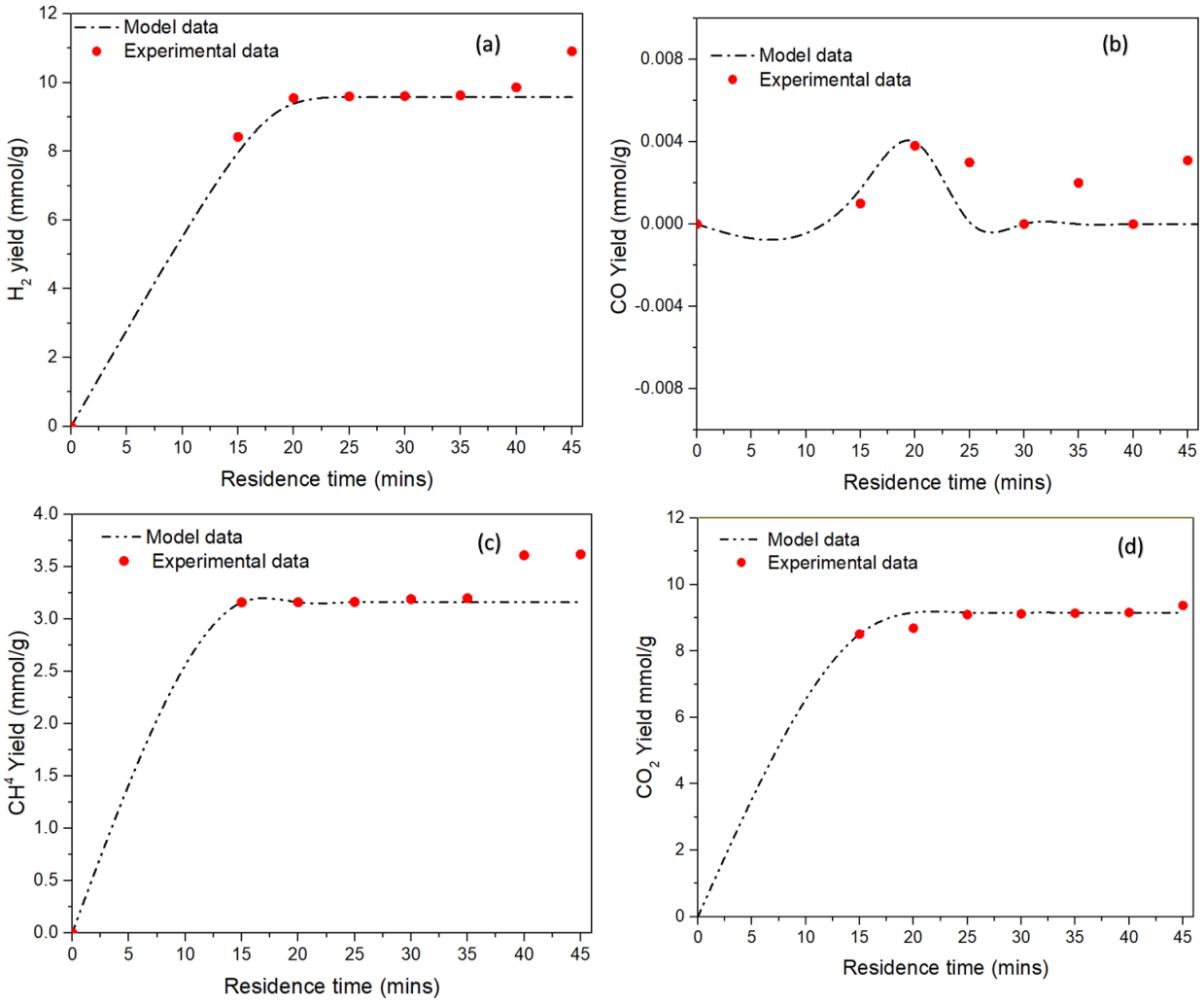

Figure 7.2: Fitting of soybean straw gasification kinetics results with experimental values. The experiments were performed at temperature = 500 ^{0}C, pressure of 22 – 25 MPa, biomass particle size of 0.13 mm, 1:10 BTW and the presence of Ni – Ce/ZrO_2 catalysts. (a) H_2(b) CO(c) CH_4(d) CO_2

In order to determine the validity of the kinetics model and evaluate if the model could be useful in predicting experimental results that are outside the study range, a parity plot is presented in Figure 7.3. The values of H_2, CO, CO_2 and CH_4 from different experimental conditions were predicted by the model and the results were compared with experimental values. The results from the kinetics model fits well with the experimental observations at all points on the diagonal line.

The data points were all observed to cluster around the diagonal line indicating a good correlation. Furthermore, the correlation coefficient, R^2 is 0.98 which shows that the kinetic model is able to describe the experimental data.

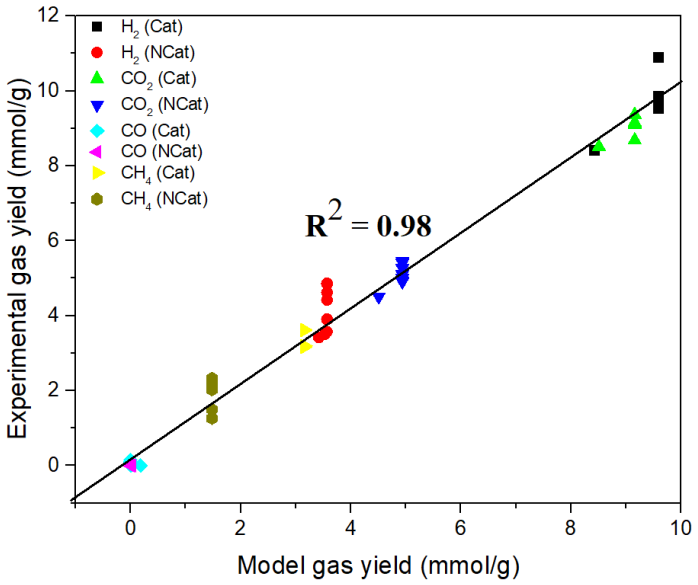

Figure 7.3: Parity plots for the experimental versus model yields during the Ni – Ce/ZrO_2 catalyzed and non – catalytic gasification of Soybean straw in supercritical water at 500 ^oC, 1:10 BTW ratio, 0.13 mm biomass particle size and residence time of 15 – 45 mins. NCat and Cat represents the yields from the non – catalytic and catalytic reactions respectively.

7.4.2 Comparison with thermodynamic equilibrium yields

The thermodynamic equilibrium yields obtained from the SCWG of soybean straw at 500 ^oC, 1:10 BTW ratio, 0.13 mm biomass particle size and residence time of 45 mins were calculated with ASPEN plus using the RGibbs reactor. Details of the ASPEN plus calculation has been provided in our previous study in chapter 5 and published by Okolie et al. (2020d). The thermodynamic predictions results were compared with the kinetics and experimental yields and are shown in Figure 7.4. For the experimental, thermodynamic, and kinetic yields, the major products include H_2, CO_2 and CH_4 with small amounts of CO. Furthermore, the kinetics model

nearly matches the experimental and thermodynamic equilibrium yields for CO, H_2 and CO_2. However, there is a large deviation in the kinetics and thermodynamics equilibrium values for CH_4 yield. The deviation in the CH_4 yield between thermodynamic equilibrium values and kinetics predictions could be as a result of some CH_4 forming intermediate reactions that is not captured by the kinetics models. Regardless, the close correlation between the equilibrium yields and kinetics predictions for CO, H_2 and CO_2 indicates that model is able to accurately predict equilibrium yields.

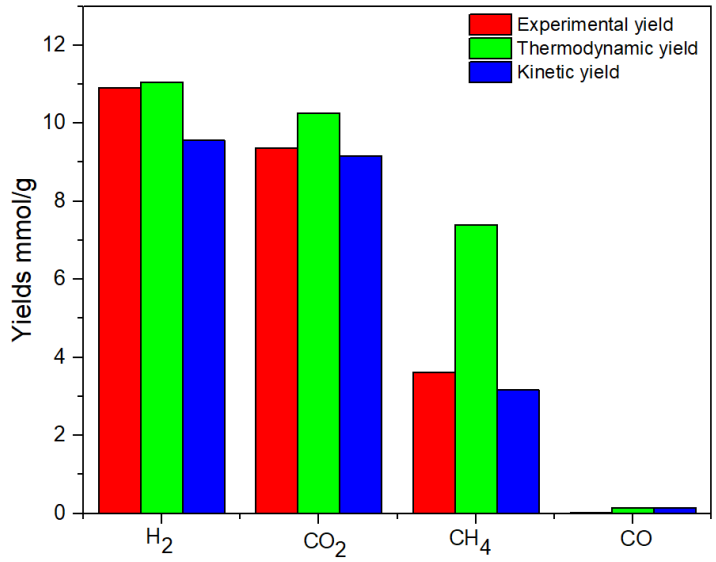

Figure 7.4: Comparison between experimental. Kinetics and thermodynamics yields during SCWG of soybean straw at 500 ^{0}C, 0.13 mm biomass particle size, 1:10 BTW ratio for 45 min residence time at pressure ranges of 22 – 25 MPa.

7.4.3 Parametric studies

Since H_2 is the desired product during SCWG of soybean straw, it is important to evaluate if the kinetic model is able to predict H_2 yield beyond the experimental conditions studied. Therefore, a parametric study was performed to study the kinetics predictions at temperatures of

300 – 500 ^{o}C and feed concentration of 10 – 30 wt.% at residence time of 45 mins, biomass particle size of 0.13 mm and pressure ranges of 22 – 25 MPa.

As can be seen in Figure 7.5a, there is a close correlation between the experimental and model results of hydrogen yield at temperature range of 300 – 500 ^{o}C Furthermore, the trend for the change in hydrogen yield with temperature for both experimental and model yield is similar. With an elevation in temperature from 300 – 500 ^{o}C, the predicted hydrogen yield rose from 3.89 to 9.56 mmol/g. The increasing temperature favors free radical mechanism leading to improved WGSR thereby contributing to the elevated hydrogen yield (Okolie et al.,2019). Moreover, the free radical mechanisms also provide improved solvation of organic compounds and several intermediate decompositions to enhance hydrogen yield.

Figure 7.5b shows the effects of feed concentration on hydrogen yield for both experimental and model predictions. It is important to note that feed concentration in this study is defined as the mass ratio of biomass to water. Therefore, the 10 wt.% feed concentration corresponds to 1:10 BTW ratio. As illustrated in figure 7.5b, the hydrogen yield declines from 9.56 mmol/g to 9.01 mmol/g with an elevation in feed concentration from 10 to 30wt.%. A rise in the concentration of feedstock indicates that there is a decline in water concentration when compared to the amount of soybean straw. On the other hand, a decline in feed concentration means that the amount of water concentration has increased. Moreover, high water concentration could lead to improved hydrogen yield by enhancing the dissolution properties of supercritical water. On the other hand, since most of the hydrogen produced comes from water molecules through the WGSR (Okolie et al.,2020d), decrease in water molecules due to the increasing feed concentration would decrease the hydrogen yield.

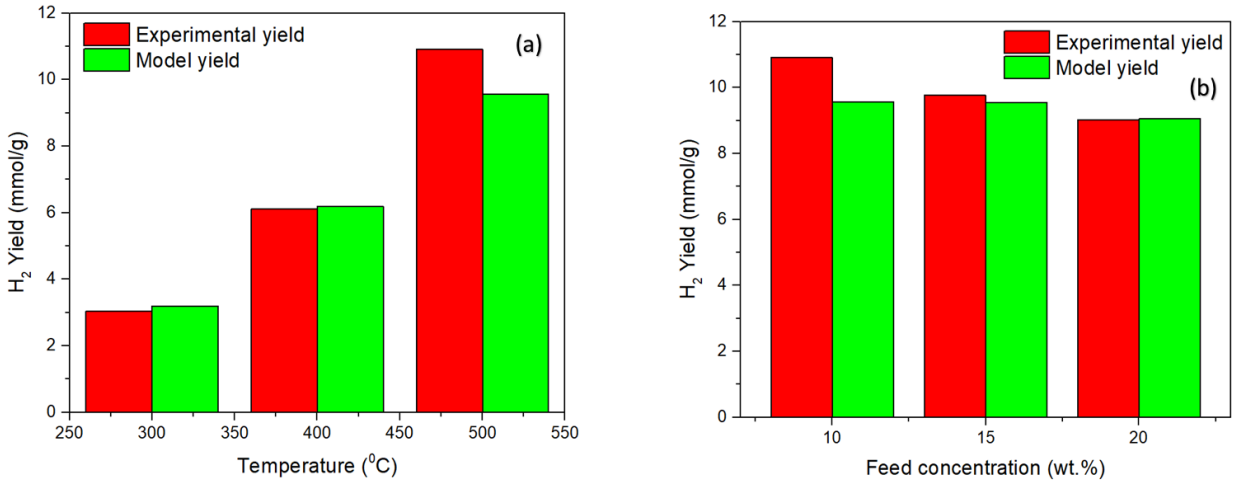

Figure 7.5: Parametric studies showing the effect of reaction parameters during the supercritical water gasification of soybean straw (a) Effect of temperature (300 -500 ^{0}C) at constant residence time of 45 min, feed concentration of 10 wt.%, biomass particle size of 0.13 mm and pressure range of 22 – 25 MPa (b) Effect of feed concentration (10 -20 wt.%) at constant residence time of 45 min, temperature of 500 ^{0}C, biomass particle size of 0.13 mm and pressure range of 22 – 25 MPa.

7.4.4 Determination of reaction routes

A comparison between the kinetics and experimental results in the previous section shows that the kinetic model can predict the gaseous product yields and their composition during the SCWG of soybean straw. However, several reactions were used for the kinetic model as indicated in Equations 7.1 – 7.7. Therefore, it is imperative to determine the reactions that are responsible for the production of different gases. Identification of the contribution of each reaction towards the formation of different gases would help to understand the reaction pathway of lignocellulosic biomass in SCW. Additionally, the relative importance of each independent reaction could be determined.

The kinetic model was used to evaluate the rate of reaction as a function of the batch holding reaction time, after which they were compared with each other to determine their

respective contribution towards the production of gases. The rate of formation or consumption of H_2, CO, CO_2 and CH_4 as a function of reaction time is shown in Figures 7.6 – 7.9. The rate of formation or consumption of H_2 as a function of reaction time is shown in Figure 7.6. Three different reactions contributed to H_2 formation or consumption are identified in Figure 7.6.

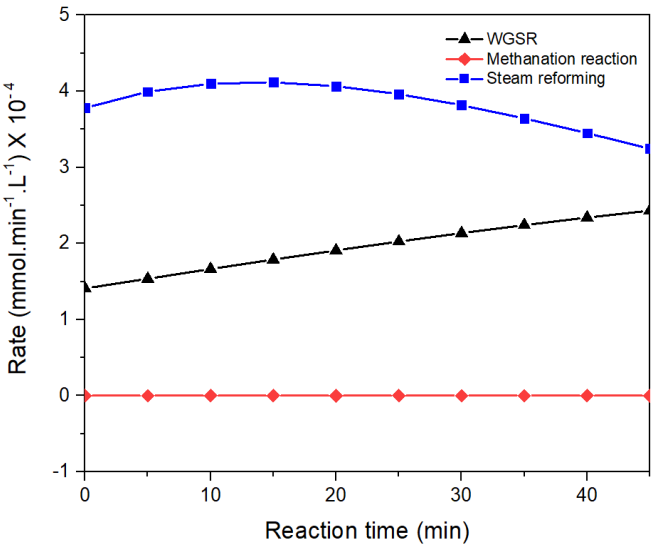

Figure 7.6: Rates of formation and consumption of H_2 during the SCWG of soybean straw at 500 ^{0}C, 0.13 mm biomass particle size, 1:10 BTW ratio for 45 min residence time at pressure ranges of 22 – 25 MPa.

The WGSR and steam reforming reactions are responsible for H_2 formation while the methanation reaction consumes H_2. Furthermore, it can be seen that the contribution of WGSR towards hydrogen formation increases steadily with reaction time. On the other hand, the contribution of methanation reaction towards H_2 formation increases with reaction time from 0 – 20 min, followed by a small decrease. It is worth emphasizing that although the methanation reaction is responsible for H_2 consumption, it does not alter H_2 concentration much even at longer reaction time for up to 45 min.

The rate of formation or consumption of CO_2 as a function of reaction time is shown in figure 7.7. Two main reactions are responsible for the formation of CO2 during the SCWG of soybean straw (intermediate reaction 2 and WGSR). However, it should be noted that the WGSR is responsible for most of the CO_2 formed while the decomposition of intermediates produces very little concentrations of CO_2.

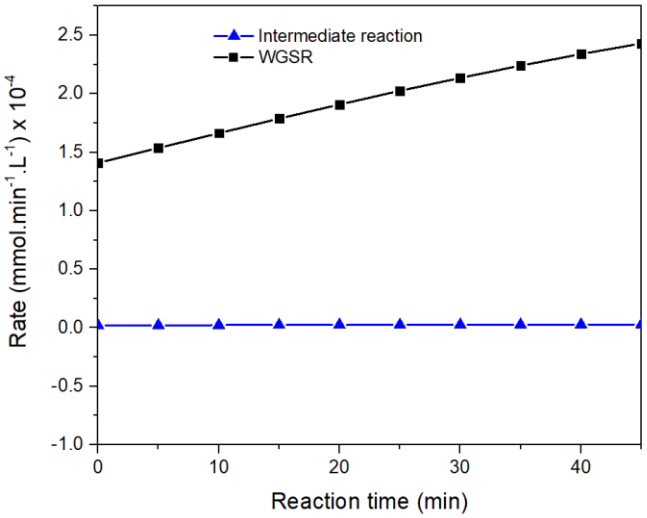

Figure 7.7: Rates of formation of CO_2 during the SCWG of soybean straw at 500 ^{0}C, 0.13 mm biomass particle size, 1:10 BTW ratio for 45 min residence time at pressure ranges of 22 – 25 MPa.

Figure 7.8 shows the rate of formation of CH_4 during SCWG of soybean straw. The methanation reaction and intermediate decomposition reactions are both responsible for CH_4 formation. However, the rate of CH_4 production from the methanation reaction is much slower when compared with that of the decomposition reaction. In addition, the rate of CH_4 production from both reactions increases slightly with time.

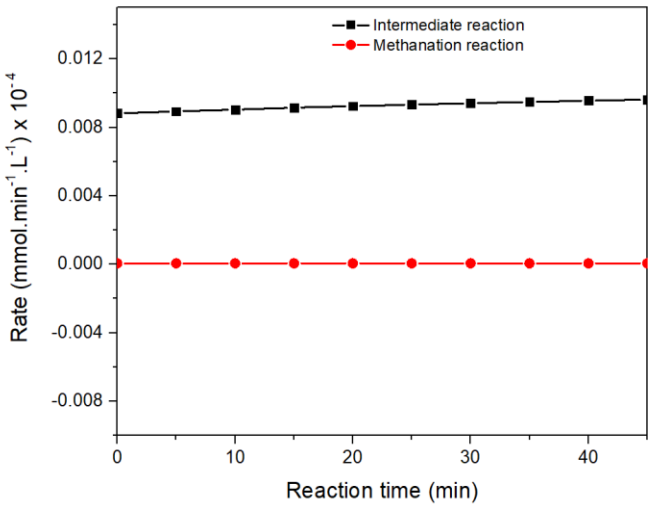

Figure 7.8: Rates of formation of CH_4 during the SCWG of soybean straw at 500 ^{0}C, 0.13 mm biomass particle size, 1:10 BTW ratio for 45 min residence time at pressure ranges of 22 – 25 MPa.

The four reactions including the WGSR, steam reforming, methanation and decomposition reactions that are responsible for the production or consumption of CO are illustrated in figure 7.9. Most of the CO were produced by steam reforming reaction, while decomposition reaction also produces smaller amounts of CO. On the other hand, the methanation reaction and the WGSR consume CO. It should be mentioned that the rate of CO production from steam reforming reaction increases up to a maximum value at 20 min before it declines slightly. For the WGSR, the rate of CO formation declines with residence time. This also signifies a progression in WGSR leading to the consumption of CO to produce more H_2.

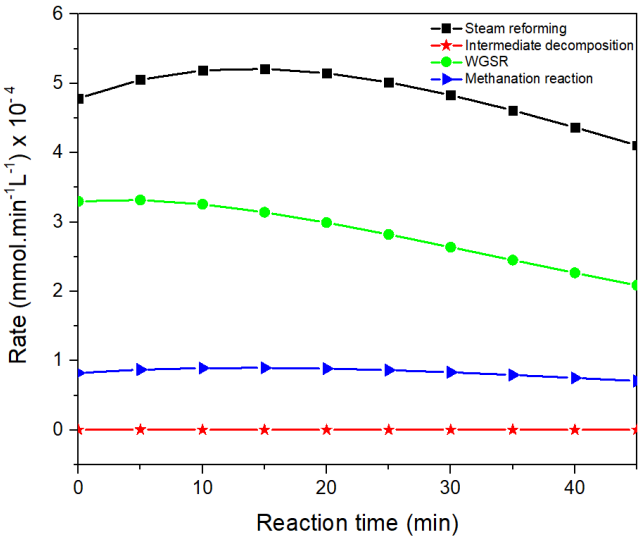

Figure 7.9: Rates of formation or consumption of CO during the SCWG of soybean straw at 500 ^{o}C, 0.13 mm biomass particle size, 1:10 BTW ratio for 45 min residence time at pressure ranges of 22 – 25 MPa.

7.5 Conclusions

This study proposes a novel kinetic model for the gasification of soybean straw in supercritical water. Experimental results from the Ni – Ce/ZrO2 catalyzed and non – catalytic gasification of soybean straw at 500 ^{o}C, 0.13 mm biomass particle size, 1:10 BTW ratio for 45 min residence time at pressure ranges of 22 – 25 MPa were used to fit the model. Seven different independent reactions including the steam reforming, WGSR, methanation, decomposition and liquid formation reactions were used to describe the kinetic model. The proposed model was used to predict the concentration of gaseous species such as H_2, CO, CO_2 and CH_4. The predicted concentrations were compared with experimental results and thermodynamic predictions from the non – stoichiometric Gibb's energy method. Kinetics models were observed to correlate with experimental and thermodynamic predictions even at long residence time. The results indicate that the model could be used to study the behaviour of SCWG system with time.

A comprehensive analysis of the reaction routes involved in the formation or consumption of each gaseous products was also studied to understand their respective contributions. The results indicate that most of the produced H_2 was from the steam reforming and WGSR. On the contrary, the methanation reaction is responsible for H_2 consumption. The proposed kinetic models would be invaluable for the optimization and techno economic evaluation of SCWG process involving lignocellulosic materials.

Chapter 8 Techno-economic evaluation and sensitivity analysis of a conceptual design for supercritical water gasification of soybean straw to produce hydrogen rich syngas production.

The content of this chapter has been published in the Bioresource Technology journal cited below.

Citation :

Okolie, J. A., Nanda, S., Dalai, A. K., & Kozinski, J. A. (2021). Techno-economic evaluation and sensitivity analysis of a conceptual design for supercritical water gasification of soybean straw to produce hydrogen. Bioresource Technology, p.125005.

Contribution of the Ph.D. Candidate

Jude: (1) Performed the process economic evaluation and sensitivity analysis studies (2) Writing the manuscript and provide responses to reviewers' comments. Dr Sonil Nanda helped with the conceptualization, and he also reviewed the manuscript. Dr. Ajay K. Dalai examined the research results, coordinated the manuscript preparation, and provided overall supervision of the research. Dr. Janusz A. Kozinski assisted in designing the work and provided overall supervision of the research.

Contribution of this chapter to the overall PhD research

A preliminary economic evaluation is required before the commercial implementation of SCWG technology. This chapter helps to evaluate the economic feasibility of the SCWG technology and also to determine the sensitivity of hydrogen price to several parameters.

8.1 Abstract

This paper proposes a conceptual design for the catalytic supercritical water gasification of soybean straw. The design consists of four process units for pretreatment, gasification, separation, purification, and combustion. The economic feasibility of hydrogen production was evaluated

based on a comprehensive cash flow analysis. The economic analysis suggested a minimum selling price of U.S. $1.94/kg for hydrogen. The cost is relatively low when compared with that of hydrogen produced from other biomass conversion processes. Besides, the net rate of return (NRR) estimated was 37.1 %. A positive NRR value indicates that the project is profitable from an economic perspective. Sensitivity analysis indicates that the minimum selling price of hydrogen is affected by the feedstock price, utility cost, tax rate and labor cost. Moreover, feedstock price and labor cost show the greatest effect. Other factors such as land cost, working capital and utility cost showed the least effect on the minimum selling price.

8.2 Introduction

Hydrogen is an important commodity used for several applications including the production of platform chemicals, liquid hydrocarbon fuels, ammonia as well as upgrading of oils through hydrotreating, fuel cells, pharmaceutical and metallurgical utilities (Okolie et al., 2021). The demand for hydrogen increased from 20 metric tons in 1975 to 75 metric tons in 2018 globally (Noussan et al., 2020). Most of the bulk demand for hydrogen is supplied from fossil fuel precursors through steam reforming, which causes massive CO_2 emissions (Acar and Dincer, 2019). However, steam reforming technologies can be integrated with carbon capture and storage to curb the atmospheric accumulation of CO_2 (Al-Qahtani et al., 2021).

The issues of climate change and environmental pollution have stimulated interest in the production of green hydrogen from renewable resources and environmentally friendly processes. One such process is supercritical water gasification (SCWG). The process relies on the unique thermophysical properties of water at supercritical conditions (i.e., temperature $\geq$ 374 °C and pressure $\geq$ 22.1 MPa) including gas-like viscosity, liquid-like density and formation of ionic products and free radicals to decompose complex organic matter into hydrogen-rich syngas (Reddy

et al., 2014b). Considering the complexity of the technology and a few bottlenecks (i.e., reactor corrosion, high-pressure and high-temperature requirements, catalysts recycling, etc.), SCWG is still under developmental stages to be commercialized for large-scale applications unlike other thermochemical technologies (Gutiérrez Ortiz, 2020). However, a few academic and industrial firms have reported promising operations of pilot-scale SCWG plants. For example, the production capacities of General Atomics SCW partial oxidation plant in the U.S., Hiroshima University plant in Japan, Forschungszentrum Karlsruhe in Germany, and the State Key Laboratory of Multiphase Flow in Power Engineering in China are 200 kg/h (J. Chen et al., 2020), 1 ton/day (Nakamura et al., 2008), 100 L/h (Chen et al., 2020) and 1.03 ton/h, respectively.

Several studies have attempted to evaluate the economic feasibility of SCWG technology using different feedstocks. Özdenkçi et al. (2019) performed a TEA study of an integrated process with SCWG of black liquor and Kraft pulp mill. The authors compared the outcomes of using two different reactor materials i.e., stainless steel and Inconel. Inconel was found to be more profitable when compared to stainless steel. Besides, their findings show that SCWG technology can be effectively integrated into the pulp mill industry (Özdenkçi et al., 2019). However, the authors used the net present value (NPV) and the internal rate of return (IRR) to assess the profitability of the project without considering other indicators. Recently, Do et al. (2020) evaluated the economic feasibility of bio heavy-oil (BHO) produced from the gasification of sewage sludge in subcritical and supercritical water (SCW). The authors used the minimum selling price of BHO to evaluate the profitability of the project. However, their target product was not hydrogen, which is otherwise considered the main SCWG product in most cases.

A wide variety of feedstocks can be used to produce hydrogen from SCWG technology (Golecha, 2016), some of which include sewage sludge, algae, agricultural crop residues, forestry

biomass, energy crops, waste tires, cattle manure and waste cooking oil (Do et al., 2020; Okolie et al., 2020c). The type, availability and cost of feedstock used in SCWG technology affect the economic feasibility of the project (Gutiérrez Ortiz et al., 2012). Lignocellulosic biomass is inexpensive, readily available and a proven precursor for the production of hydrogen from SCWG technology (Okolie et al., 2020d). In phase 2, soybean straw and flax straw were reported as promising agricultural crop residues for hydrogen production from SCWG technology (Okolie et al., 2020c).Additionally, we developed a stable catalysts to elevate the product yield in the subsequent chapter. However, the economic viability must be assessed to make major decisions regarding its large-scale implementation.

To the best of our knowledge, there is no available study on the TEA of hydrogen production from SCWG of soybean straw and flax straw. Therefore, this study proposes a conceptual design to produce hydrogen from SCWG of soybean straw. The process is designed to be energetically self-sufficient with the reactor heat provided by the combustion of the flue gas. Furthermore, the CO_2 removal unit from the syngas has been integrated into the process. The TEA studies coupled with sensitivity analysis are used to evaluate the economic feasibility of the conceptual design and to determine the minimum selling price of hydrogen. Compared to other available studies on TEA of SCWG processes, the target product in this study is hydrogen. The break-even price of hydrogen was determined and compared with other hydrogen production routes. Furthermore, the present study provides a basis for the efficient utilization of soybean straw for hydrogen production.

8.3 Materials and Methods

8.3.1 Design basis

Although the developed model is used for the simulation of soybean straw, the model can be used to analyze several other lignocellulosic feedstocks. Soybean straw was selected as the base case for the following reasons. Firstly, due to its abundant availability in North America, especially in Canada, 7.7 million tons of soybean are produced annually (Abdulkhani et al., 2017). Secondly, soybean straw was used as a feedstock for SC WG in our recently published report in chapters 2 and 3 (Okolie et al., 2020d). Therefore, the extracted data and similar conditions were employed in this simulation. Moreover, lignocellulosic biomass is readily available and does not pose the threat of food versus fuel when compared with the first-generation feedstocks.

A plant with a capacity of 170 metric tons/day of soybean straw was designed and simulated with Aspen Plus v7.3 (AspenTech, Bedford, Massachusetts, USA). The plant was designed to process approximately 56,000 metric tons of lignocellulosic biomass per year. Aspen Plus contains an in-built array of different physical properties database that helps in the thermodynamics and energy calculations. The design procedure used to determine the TEA of SCWG of soybean straw is presented in Figure 8.1.

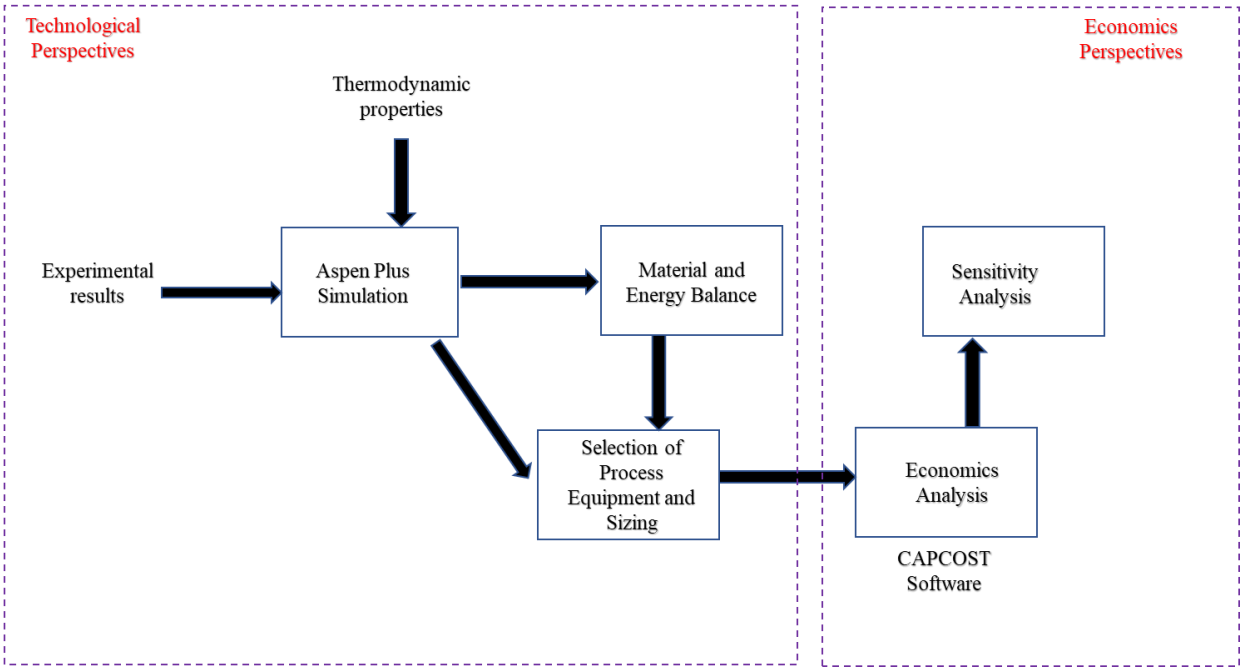

Figure 8.1: Schematics of the design procedure for the techno-economic analysis of SCWG of soybean straw.

8.3.2 Process description

The simplified block flow diagram and the process flow diagram in Aspen Plus for the supercritical water gasification of soybean straw are shown in Figure 8.2 and Figure 8.3 respectively.

The plant is assumed to process 170 metric tons/day of soybean straw at a biomass-to-water ratio of 1:10. The optimal process conditions obtained in our previous study were used to simulate the SCWG plant (Okolie et al., 2020c). The optimal conditions include a temperature of 500°C, a biomass-to-water ratio of 1:10, the biomass particle size of 0.13 mm and a reaction time of 45 min. The SCWG plant is assumed to run for 8000 hours per year with the remaining time set for maintenance. Table 8.1 in shows different assumptions used during the TEA studies.

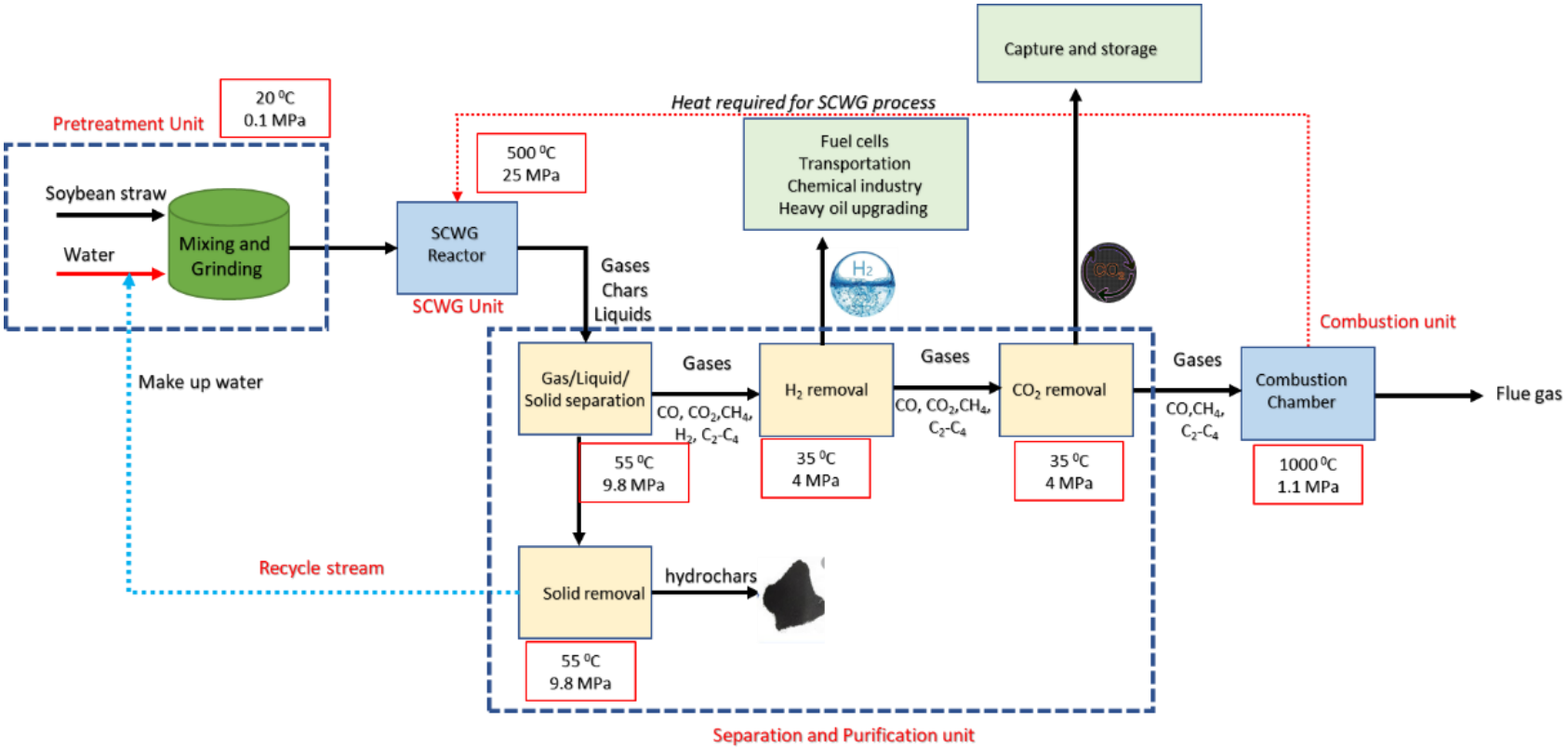

Figure 8.2: Block flow diagram for a conceptual process design for hydrogen production from SCWG of soybean straw

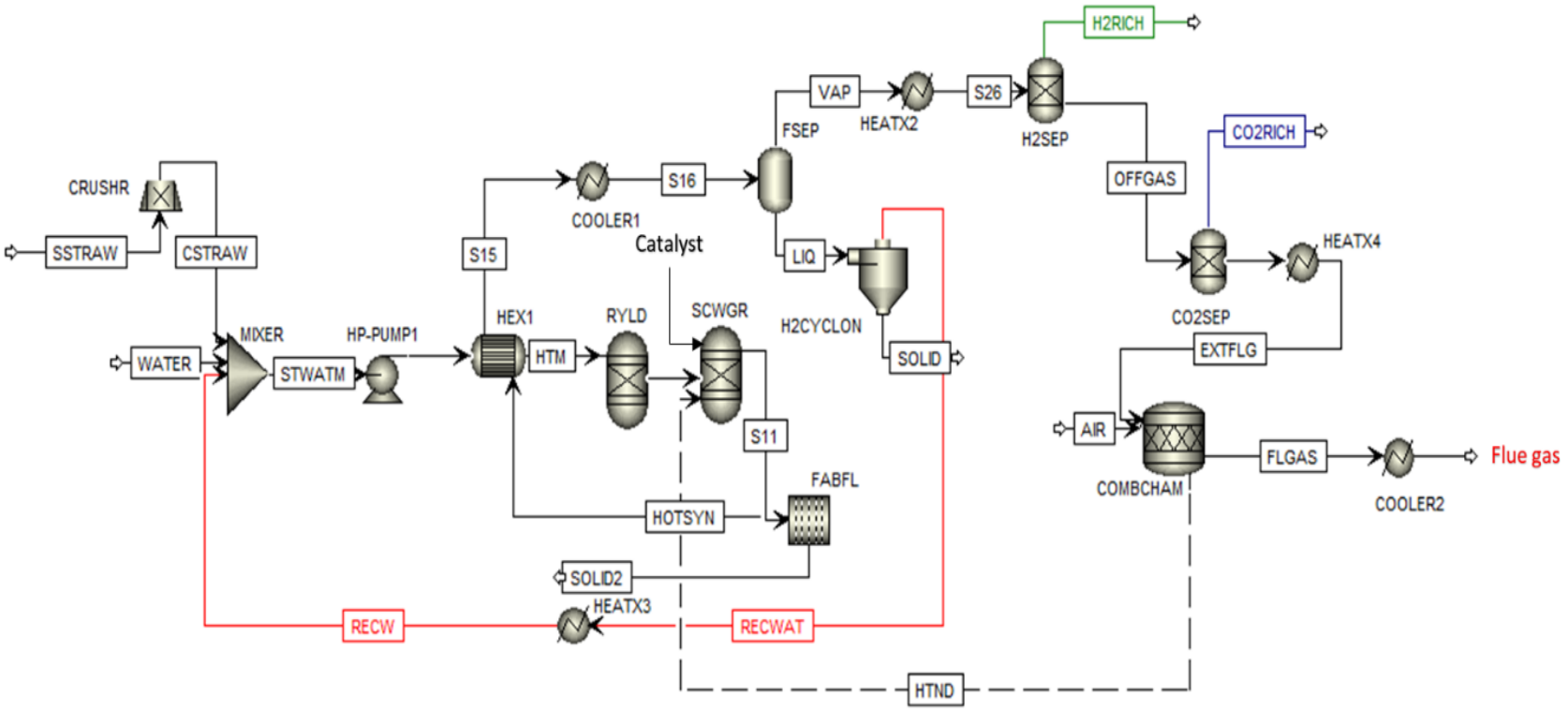

Figure 8.3: Process flow diagram for SCWG of 170 tons/day of soybean straw in the presence of Ni - Ce/ZrO_2 catalyst

Table 8.1: List of assumptions during the techno-economic analysis of soybean straw

Parameters	**Assumptions**
Hydrogen production plant capacity	170 metric tons/day of soybean straw
Biomass-to-water ratio	1:10
Annual plant operation	8000 h/year
Plant start-up time	4 months
Construction period	1 year
Depreciation period of plant	10 years
Plant life	20 years
Contractors fees	3% of total Module cost
Contingencies	15% of total module cost
Working capital	5% of FCI
Land cost	2% of FCI
Depreciation method	Straight line
Auxiliary facility fees	30% of BMC
Annual salary of process operators	U.S. $35,000/year
Cost of electricity	U.S. $0.14/KWh
Cost of process steam	U.S. $0.022/KWh
Cost of process water	U.S. $0.0011/KWh

References: Sinnott and Towler (2013); Turton et al. (2018); Ziyai et al. (2019)

During pretreatment, soybean straw is pulverized with a crusher (CRUSHR) to the desired particle size of 0.13 mm followed by mixing with water in the mixer (MIXER) to form a slurry, which enters the SCWG reactor. The pump (HP-PUMP1) was used to increase the discharge pressure of the water and biomass slurry. The pressurized stream is preheated using the HEX1 heat exchanger by utilizing the waste heat from recycled hot syngas (HSYN). It is important to note that the feed mixture was not heated directly to supercritical temperatures before being sent to the reactor to prevent salt and inorganic materials deposition in the pipelines (Özdenkçi et al., 2019). Therefore, the recycled liquid was cooled to a moderate temperature. This led to the mixture of the two inlet streams producing a temperature lower than the reaction temperature (500°C).

The reactor is designed as a vertical reactor to enable easy separation of solids and salt deposits. The configuration is similar to that of the VERENA pilot plant to ensure mitigation of plugging and salt precipitation (Boukis et al., 2007). The slurry feed mixture together with the high temperature recycled water is fed to the top of the reactor while the solid deposits and precipitated salts leave through the bottom of the reactor. The solid separator (FABFL) is used to separate the solid particles from reaction products.

Aspen Plus requires that the feed be defined together with the thermodynamic methods and yields. The solid biomass is modeled as a non-conventional solid (NC Solid) in Aspen Plus using the proximate and ultimate analyses. Furthermore, the density and the enthalpy methods are both specified as ‘DCOALIGT’ and ‘DCOALIGT’, respectively. The thermodynamic methods are defined by the Peng-Robinson equation of state. The non-conventional solid soybean straw was decomposed into its conventional components with the help of the RYield block (DECOMP). A calculator block was incorporated into the yield block with its function varied through a

FORTRAN subroutine statement. Another calculator block was used to specify the biomass-to-water ratio including that of the incoming recycle water stream (RECW).

The product exiting the RYield reactor enters the RGibbs (SCWG) reactor where the gasification reaction occurs at 500°C and 25 MPa, respectively. The thermodynamic calculations were carried out using data from the RGibbs reactor based on the minimization of Gibbs free energy method (Hantoko et al., 2018). In this approach, all the intermediate chemical reactions involved in the SCWG process do not need to be specified. Instead, calculations are performed to evaluate the product distribution that ensures that the system attains a state of minimum Gibbs energy.

The produced hot syngas is recycled to the heat exchanger (HEX1) to preheat the feed. The cold syngas stream (S16) containing the syngas and few solid precipitates that could not be removed by the fabric filter unit are fed to the gas-liquid separator (FSEP) and cooled at 70°C to separate the water stream (LIQ). The water stream (LIQ) was fed through the hydro cyclone (H2CYCLON) to further separate the solid precipitates. The pure liquid stream (RECWAT) leaving the cyclone is cooled and recycled to the feed mixture. Similarly, the vapor stream (VAP) is sent to the pressure swing adsorption (H2SEP) for hydrogen removal. The separator was modeled with the design specification of the Hysep Technology model (HYSEP Modul Type 1308, ECN, palladium membrane filter). The unit is operated at 35°C and 4 MPa (Hantoko et al., 2018). The high-pressure expanded gas is required for hydrogen-rich gas production in the pressure swing adsorption at the lowest possible temperature (Özdenkçi et al., 2019). It is worth emphasizing that the operating temperature and pressure of all process units have been indicated in the block diagram in Figure 8.2. The separated hydrogen is pressurized and transported to a storage station.

The OFFGAS stream leaving the H2SEP is passed through a low-pressure separator for CO_2 removal. The CO_2 removal efficiency was set at 90% while the absorbed CO_2 is sent to the storage station (Peters et al., 2011). The flue gas (EXTFLG) is fed to a combustion chamber (COMBCHAM) for burning to produce the required heat required to supply energy to the SCWG reactor. The combustion chamber was modeled in Aspen Plus with a stoichiometric reactor (Rstoic) operating at 1000°C under 1.1 MPa pressure. Four different combustion reactions (Equations 8.1 – 8.4) are incorporated into the Rstoic reactor based on the composition of EXTFLG.

$$CH_4 + 2O_2 \leftrightarrow CO_2 + 2H_2O \quad (8.1)$$

$$C_2H_4 + 3O_2 \leftrightarrow 2CO_2 + 2H_2O \quad (8.2)$$

$$C_2H_6 + 3.5O_2 \leftrightarrow 2CO_2 + 3H_2O \quad (8.3)$$

$$C_3H_8 + 5O_2 \leftrightarrow 3CO_2 + 4H_2O \quad (8.4)$$

The overall process is assumed to be energy self-sufficient. Furthermore, the heat integration approach helps to improve the overall energy of the process by reducing the energy demands. Therefore, external the use of external heat sources is minimized. Moreover, it is important to note that the compressors and pumps used some external energy sources in the form of electricity that would be accounted for during the estimation of capital cost as part of utility costs. Additionally, Table 8.2 in supplementary materials lists all the process units used in the simulation together with their specifications.

Table 8.2: Specification of the process units used for simulating SCWG of soybean straw for hydrogen production.

Process unit	Code	Specifications
Grinder	CRUSHR	Outlet biomass particle size is set to 0.13 mm
Mixer	MIXER	Negligible pressure drop
Pump	HP-PUMP1	Efficiency: 80%
Heat exchanger	HEX1	Shell and tube heat exchangers
Heat exchanger	COOLER1	Stream outlet temperature: 55°C
SCWG reactor	SCWGR	Operating temperature: 500-600°C Operating pressure: 25 MPa
Fabric filters	FABFL	Removes 95% of solids from hot syngas
Gas-liquid separators	FSEP	Adiabatic operation
Hydro cyclone	H2CYCLONE	Removes 90% of solids
Heat exchanger	HEATX3	Stream outlet temperature: 55 ^{0}C
Heat exchanger	HEATX2	Stream outlet temperature: 35 ^{0}C
Pressure swing adsorption	H2SEP	Removes 95% hydrogen from gaseous mixtures
Pressure swing adsorption	CO2SEP	Removes 95% CO_2 from gaseous mixtures
Heat exchanger	HEATX4	Stream outlet temperature: 1000°C
Combustion reactor	COMBCHAM	Operating temperature : 1000°C Operating pressure: 1.1MPa
Heat exchanger	COOLER2	Stream outlet temperature: 150°C

8.3.3 Estimation of the capital cost

After presenting a conceptual design and calculating the mass and energy balances, the next step is to design the equipment and evaluate the process economics (Figure 8.1). The total investment capital (TCI) defined as the overall cost related to the plant construction was calculated from the sum of the fixed capital investment (FCI), land cost (LC) and working capital investment (WCI) (Equation 8.5) (Ziyai et al., 2019).

$$\mathrm{TCI} = \mathrm{FCI} + \mathrm{LC} + \mathrm{WCI} \qquad (5)$$

The TCI can be divided into direct and indirect costs. The direct cost consists of all the expenses incurred during the plant installation including the cost of equipment, installation,

electrical systems and instrumentation and control (Gutiérrez Ortiz, 2020). On the contrary, the indirect cost includes the cost, which is not directly associated with the plant installation such as the legal fees due to land purchase or contractors fees (Gutiérrez Ortiz, 2020). Some costs associated with the indirect fixed capital investment were also evaluated. All contract fees and contingencies are assumed to be 3% and 7% of total module cost, respectively (Vlysidis et al., 2011). Furthermore, the working capital cost is calculated as 5% of the fixed capital cost while the LC is set at 2% of FCI (Lee et al., 2011).

FCI comprises the equipment purchase cost, which is also known as the bare module cost (BMC) together with any additional expenses associated with the construction of the plant (Vlysidis et al., 2011). The BMC includes all direct and indirect costs associated with the purchase and installation of equipment (Gutiérrez Ortiz, 2020). The CAPCOST software (Turton et al., 2018) and the online equipment cost estimator (Peters et al., 2021) were used to estimate the BMC. CAPCOST is a spreadsheet designed for the evaluation of the total investment cost by summing the total module cost and the cost of auxiliary facilities (Turton et al., 2018).

In the present study, the auxiliary facility fees are assumed to be 30% of the BMC (Borugadda et al., 2020). The additional cost is expressed as a fraction of the BMC cost based on some factors suggested by (Ulrich and Vasudevan, 2018). It is important to note that CAPCOST provides equipment purchase costs based on a literature survey with vendors from previous years with the most recent being year 2017. Therefore, the cost needs to be updated to the present year. The equipment purchase cost is adjusted to the Year 2019 by using the Chemical Engineering Plant Cost Index (CEPCI) as shown in Equation 8.6 (Sinnott and Towler, 2012).

$$C_{curent} = C_{reference}\left(\frac{CEPCI_{current}}{CEPCI_{reference}}\right) \tag{8.6}$$

8.3.4 Estimation of the operating cost and annual revenue

The operating cost includes the variable and fixed costs. The variable cost comprises raw materials cost (e.g., soybean straw, process water and catalysts cost) and utilities including the cost per KWh of cooling water and steam. On the other hand, the fixed operating cost, which includes maintenance and repair fees, labor cost, employee social benefits, supervision, overhead expenses, insurance and royalties, etc. is estimated as a percentage of the FCI using the assumptions suggested by (Vlysidis et al., 2011).

The operating labor cost is expressed as the product of the numbers of operators per shift, their wages per hour and the total operating hours per year. The number of operators required per shift is determined based on information provided by Ulrich and Vasudevan (2018). The SCWG plant of 56,000 metric tons/year capacity requires 10 operators for hydrogen production and 2 additional operators for the combustion unit and CO_2 separation unit. The average annual wage of the operator is assumed as U.S. $35,000/year.

The waste disposal cost is obtained from the annual ton of waste produced and the penalty required to be paid for every ton disposed of. Moreover, we assume that the waste generated is non-hazardous waste, which can offset the waste disposal cost. The cost of raw materials is calculated by multiplying the specified feed rate of each raw material per year with its price per kg. The utility cost is related to the annual energy consumption including steam and process water for heating and cooling, respectively. Equipment such as pumps also consumes electricity during operation. The energy balance results in the Aspen Plus simulation was used to calculate the heating and cooling while the utilities were evaluated by considering the energy price per unit of each piece of equipment. It is worth mentioning that the total annual production cost computed in

this study considers the fixed and variable operating cost together with the bare module cost and the rest of the investment cost is related to the waste disposal and additional expenses.

8.3.5 Economic evaluation and profitability index

The economic viability of an SCWG process with a capacity of 170 metric tons/day of soybean straw for hydrogen production was assessed by several indicators including the net present value (NPV), payback period (PBP), the net rate of return (NRR) and the discounted cash flow of the project (DCFR). Detailed information describing the mentioned terms has been mentioned elsewhere (Ulrich and Vasudevan, 2018). NPV indicates the profit of the plant for a particular period when considering the time value of money. It shows the sum of the present values of all cash flows, which includes the initial investment (Ulrich and Vasudevan, 2018). NPV can be evaluated by considering the overall sum of the current cash flow in a particular year over the total number of years. Therefore, it must be positive to consider the project acceptable. On the other hand, IRR refers to the discount rate that ensures NPV is zero (Gutiérrez Ortiz, 2020). The PBP refers to the duration it takes to pay off the initial investment with revenues generated from the beginning of the project. NRR is calculated using Equation 8.7 (Ulrich and Vasudevan, 2018).

$$\mathrm{NRR} = \frac{1.5 \text{ x } \mathrm{NPV}_{\text{i=capital cost}}}{\mathrm{C}_{\mathrm{T(i=capital\ cost)}} \text{x } \mathrm{n}^{\mathrm{i}}} \times 100 \qquad (8.7)$$

Where C_T is the total capital usually expressed at the start of the project. n^i is the operating lifetime of the project including one-half of the time since the project initiation. NRR is known to effectively illustrate the effect of the project lifetime.

To evaluate the profitability criteria for the SCWG of biomass, it is recommended that the project lifetime should be greater than 15 years but not too long due to the harsh operating conditions (Gutiérrez Ortiz, 2020). Therefore, the project life is set at 20 years. It is also assumed that the plant construction is completed at the end of the first year and that it starts operating at full capacity immediately after construction. A straight-line depreciation method was used while assuming a 100% equity financing. The project also assumes that no revenues are generated from selling the used property after the project lifetime (negligible salvage value). After estimating the total investment cost, fixed and variable operating cost a discounted cash flow analysis was employed to calculate the minimum selling price of hydrogen. The price is compared to hydrogen produced from other sources in the literature.

8.4 Results and discussions

8.4.1 Mass and Energy balance

Figure 8. 4 shows the mass and energy balance for SCWG of soybean straw for hydrogen production computed using Aspen Plus. They are used to assess the flow of mass and energy inputs and outputs, thereby facilitating the design of an alternative process. The mass balance results were expressed in metric tons per day as the plant was designed for processing 56,000 metric tons of biomass per year. Syngas yield of 30% was obtained from the SCWG process while 110 metric tons of hydrogen was produced per 170 metric tons of soybean straw processed daily. About 387 metric tons of the flue gas was combusted in the air to produce the heat required for the SCWG reactor.

The energy recovered in the product was also evaluated and the results are presented in Figure 8.3. The energy efficiency was calculated as the amount of useful energy output divided as the energy input of the system. It also includes the energy contained in the raw materials used for

SCWG (J. Chen et al., 2020). The energy balance results show that 33% of the energy contained in the feedstock was recovered in the final syngas product. On the other hand, the flue gas recovered 9% of the energy contained in the feedstock. The remaining energy is consumed by the process itself. Based on the overall energy recovery estimation, the process is estimated to possess about 63.5% energy efficiency assuming 95% combustion efficiency in the combustion chamber. While the process is designed to have energy self-sufficiency, it is noteworthy to mention that the reactor heat was supplied by the burning of flue gas in the combustion chamber. In addition, an external heat source was used to supplement the reactor heat to attain the desired process temperature. The high energy efficiency obtained in this study could be a result of the effective heat integration in the process. Furthermore, the combustion efficiency was assumed to be 95 % in the present study. This could also contribute to the increased energy efficiency.

The energy recovered from the produced syngas during the SCWG of soybean straw and the energy efficiency were compared with those reported in previous studies related to the thermochemical and biological conversion of waste biomass (Ortiz et al., 2012; Chen et al., 2020; Özdenkçi et al., 2019). Galara and Ortiz (2015) reported an energy efficiency of 36% and 35.8% during the autothermal SCW reforming and SCW reforming of glycerol, respectively. Both processes operated at 800°C using a glycerol feed concentration of 26.5 wt.% (Galera and Gutiérrez Ortiz, 2015). Naqi et al. (2019) reported a 37% energy recovery for diesel production from an integrated process including anaerobic digestion and biogas-to-liquid facility. The latter process involves a combination of biogas tri-reforming to produce syngas and Fischer-Tropsch synthesis. The authors reported an energy efficiency of 60% assuming an 80% combustion efficiency in the reforming reactor (Naqi et al., 2019).

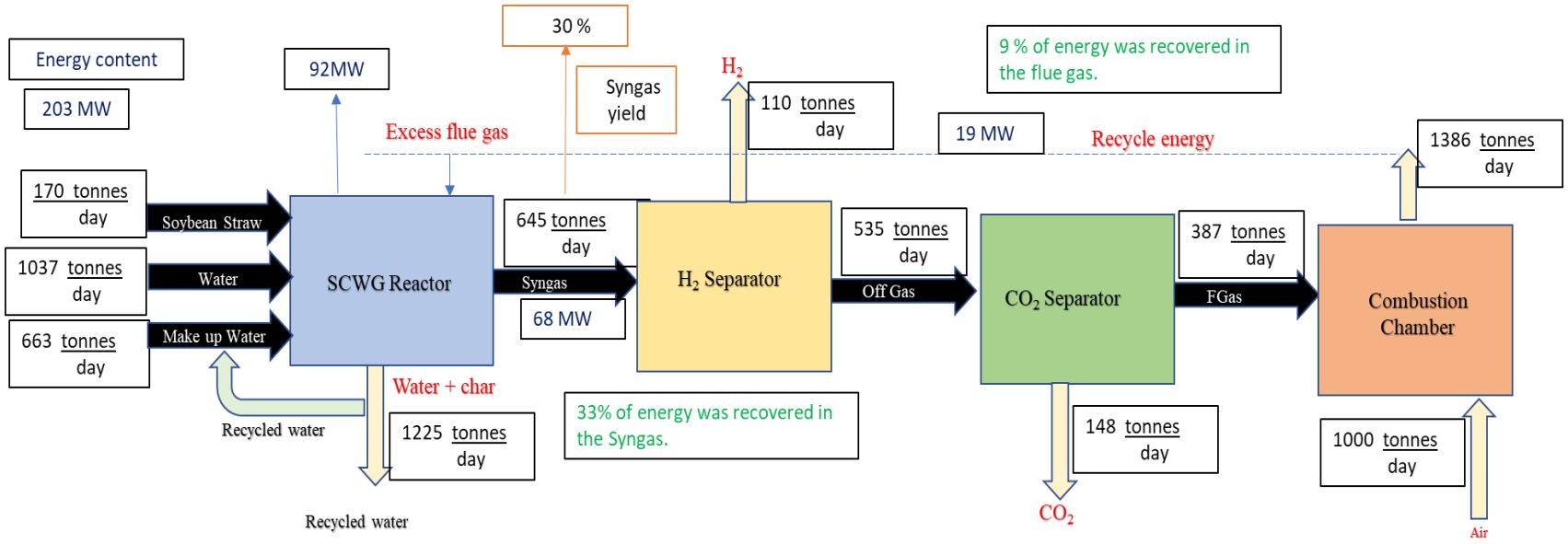

Figure 8.4: Overall mass balance and energy recovery during SCWG of soybean straw. The plant was designed with a capacity of 170 tons/day of soybean straw (56,000 tons/year) with a hydrogen yield of 110 tons/day. Note: 1 metric ton (tonne) is equivalent to 1000 kg.

8.4.2 Estimation of fixed capital investment, operating cost, and revenues

The FCI was evaluated with the data presented in Table 8.3. The grass root cost is estimated as the sum of the total module cost and the auxiliary facilities cost. On the other hand, the total module cost is expressed as the sum of the bare module cost, contingency and contractors fees (Gutiérrez Ortiz, 2020; Naqi et al., 2019). It is important to emphasize that all the amounts reported in Table 8.3 are expressed in millions of U.S.$ with the cost adjusted to 2019 using the CEPCI. Based on the results in Table 8.3, the FCI obtained during the SCWG of soybean straw is reported as U.S. $6.25M.

The operating cost evaluated in this study including the fixed and variable operating costs is reported in Table 8.4. The fixed operating cost does not depend on the production rate. Therefore, it is estimated using a fraction of the FCI. In contrast, the variable operating cost including the cost of raw materials and utility cost was calculated based on the production rate. As shown in Table 8.4, the total operating cost for processing 170 tons/day of soybean straw was estimated at U.S. $3.59M. This cost includes a fixed and variable operating cost of U.S. $1.43M and $2.16M, respectively. A breakdown of the FCI and the total annual production cost (AOE) of processing 56,000 tons/year of soybean straw is shown in Figure 8.5. The heat exchangers and separators account for most of the FCI, which is at 23.3% and 24.7% of FCI, respectively. This is mainly due to the heat exchangers required for heat recovery and effective heat integration in the process. Furthermore, the process contains a mixture of char containing water and hot syngas, which requires a gas-liquid (GL) separator. The SCWG reactor also accounts for 11.9% of the FCI. SCWG reactions occur at temperatures and pressures above the critical point of water. Therefore,

it is imperative to select a reactor material that can withstand harsh conditions with less susceptibility to corrosion (Okolie et al., 2019).

Table 8.3: Estimation of the fixed capital investment (FCI)

Process unit	**Total module cost (million U.S.$)**	**Auxiliary facilities cost (million U.S.$)**	**Grass root capital (million U.S.$)**
Grinder	0.10	0.03	0.13
Mixer	0.05	0.01	0.07
Pump	0.19	0.05	0.24
Heat exchanger	0.16	0.04	0.20
Heat exchanger	0.08	0.02	0.10
SCWG reactor	0.59	0.15	0.74
Fabric filters	0.10	0.02	0.12
Gas-liquid separators	1.23	0.31	1.54
Hydro-cyclone	0.09	0.02	0.11
Heat exchanger	0.02	0.00	0.02
Heat exchanger	0.02	0.01	0.03
Pressure swing adsorption	0.67	0.17	0.84
Pressure swing adsorption	0.41	0.10	0.51
Heat exchanger	0.75	0.19	0.95
Combustion reactor	0.40	0.10	0.50
Heat exchanger	0.12	0.03	0.15
Total	4.98	1.27	6.25

Inconel reactor is more expensive in comparison to stainless steel. However, Inconel was selected as the reactor material during economic analysis because it provides a better corrosion resistance (J. Chen et al., 2020). Furthermore, Inconel has the advantage of suppressing repolymerization reaction, which leads to the reduction in tar and char formation while increasing gas yields (De Blasio et al., 2016).

Two pressure swing adsorption (PSA) systems were employed during the SCWG process for the recovery of CO_2 and H_2 gas from the syngas mixture. The cost of the PSA system also accounts for 21.6% of the FCI. On the contrary, the SCWG system requires high pressure. Therefore, pumps and compressors are required in the process. The pumps and compressors are

used to attain the desired pressure cost of 3.8% of the FCI. On the other hand, solid separators are 3.2% of the FCI.

Table 8.4: Total operating cost estimation including the fixed and variable operating cost

Description	**Per unit cost**	**Total cost (million U.S.$)**	**References**
Feedstock (1)	U.S. $28/metric ton	1.22	Golecha (2016)
Catalyst (e.g., nickel) for SCWG process (2)	U.S. $798/metric ton	0.26	Millipore Sigma (2021)
Deionized Process water (3)	U.S. $1.6/metric ton	0.55	Galera and Ortiz (2015)
Cost of raw materials (4)	(4) = (1)+(2)+(3)	2.03	
Energy cost (U.S.$/KWh)			
Electricity (5)	U.S. $0.069/KWh	0.12	Naqi et al.(2019)
Process steam (6)	U.S. $0.022/KWh	0.02	Turton et al.(2018)
Cooling water (7)	U.S. $0.0011/KWh	0.00089	Turton et al.(2018)
Total utilities cost (8)	(8) = (5)+(6)+(7)	0.13	
Variable operating cost (9)	(9) = (8)+(4)	2.16	
Labor cost (10)	U.S. $35,000/year per operators, a total of 12 operators required	0.42	Borugadda et al. (2020)
Supervision cost (11)	(11) = 0.25*(10)	0.11	Vlysidis et al, (2011)
Maintenance and repair (12)	(12) = 0.03*(FCI)	0.19	Vlysidis et al, (2011); Chen et al.(2020)
Royalties, local tax and insurance (13)	(13) = 0.04*(FCI)	0.25	Vlysidis et al, (2011)
Plant overhead cost (14)	(14) = 0.5*[(10)+(11)+(12)]	0.36	Vlysidis et al, (2011)
Laboratory cost (15)	(15) = 0.1*(10)	0.042	Vlysidis et al, (2011)
Additional expenses (e.g., marketing, logistics, operation services, etc.) UNE (16)	(16) = 0.01*FCI	0.063	Chen et al.(2020)
Fixed operating cost (17)	(17) = (10)+(11)+(12)+(13)+(14)+(15)+(16)	1.43	
Waste disposal cost, WD (18)		0	
Total operating cost (19)	(19) = (9)+(17)	3.59	

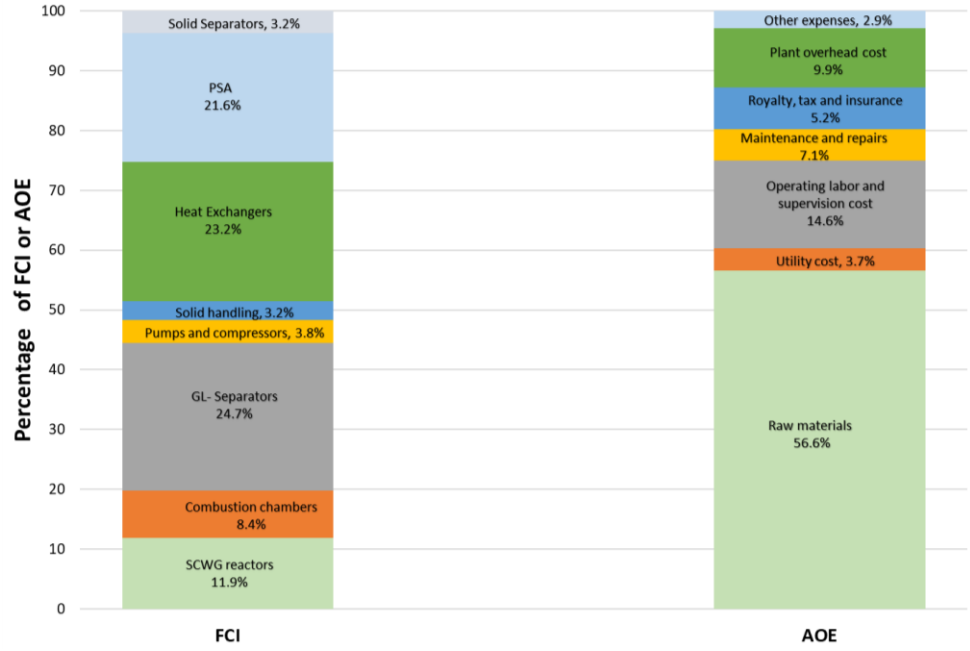

Figure 8.5: Breakdown of the percentage of the equipment cost involved in the fixed capital investment (FCI) and the fixed and variable expenses included in the annual operating expenses (AOE). Note that the FCI and AOE for the SCWG plant with an annual capacity of 56,000 metric tons of soybean straw per year are U.S. $6.25M and $3.59M, respectively.

As shown in Figure 8.5, the raw material cost accounts for more than half of the AOE (56.6%). This includes the cost of feedstock (soybean straw), catalysts (Ni-based) and process water. Included in the cost of the raw materials is the transportation and storage cost of the raw materials together with the catalysts. The cost for the recovery of heterogeneous catalysts was not included in the raw material cost. However, it is assumed to be part of the operating expenses. The operating labor and supervision cost accounts for a combined 14.6% of the AOE while the plant overhead and utility costs were 9.9% and 3.7% of the AOE, respectively.

The TCI including the FCI, WC and LC was estimated to be U.S. $6.69M. The annual revenue was also estimated as presented in Table 8.5.

Table 8.5: Total annual revenue cost estimation

Unit H_2 production cost (1)	U.S. $0.3/kg
Production rate of H_2 (2)	110,000 kg/day
Annual revenue from H_2 (3) = (1) × (2) × 334 days	U.S. $11.02M
Hydrochar cost (4) (Saba et al., 2019)	U.S. $0.117/kg
Production rate of hydrochar (5)	46,200 kg/day
Annual revenue from hydrochar (6) = (4) × (5) × 334 days	U.S. $1.81M
Cost of CO_2 emission storage (Schmelz et al., 2020) (7)	U.S. $0.052/kg
Production rate of CO_2 (8)	U.S. $148,000 kg/day
Annual CO_2 storage cost (9) = (7) × (8) × 334 days	U.S. $2.57M
Total annual revenue (10) = (3) + (6) – (9)	U.S. $10.26M

The total annual revenue includes the annual revenue from hydrogen (U.S. $11.02M), hydrochar (U.S. $1.81M) and the cost for CO_2 production and storage (U.S. $2.57M). Based on the data presented in Table 8.5, the annual revenue from SCWG was estimated at U.S. $10.26M. Moreover, the unit hydrogen production cost used to determine the yearly revenue was determined based on the total production cost and the hydrogen production capacity (Lee et al., 2020).

8.4.3 Cash flow (profitability) analysis

Profitability analysis, also known as the discounted cash flow analysis, was performed to evaluate the minimum selling price of the main product (i.e., hydrogen). Furthermore, this analysis was used to determine the economic feasibility of the project (Ulrich and Vasudevan, 2018). It should be mentioned that half of the TCI was paid at the beginning of the first year while the rest was paid at the end of the first year. The plant operated at 334 days per year with the remaining days set aside for maintenance downtime. Additional allowances or credits were also neglected. Although SCWG is a well-known technology with several experimental and pilot-scale studies, the commercial application is limited. Therefore, the sales income for the fourth year is assumed to be one-third of the maximum sales revenue.

Figure 8.6 shows the difference between the undiscounted and the discounted cash flow analyses. The discount rate is used to normalize the dollars to the same period based on an interest rate (i). In this case, the point in time considered is during the project initiation. The discount rate was varied from values of i in the range of 0–50%. The economic indicators including the NPV, PBP and DCFR for the SCWG process at the different discount rates were also calculated from Figure 8.6. Moreover, the estimated minimum selling price of hydrogen that produces an NPV value of 0 was U.S. $1.94/kg. This indicates that the process becomes profitable if the selling price of hydrogen is above this break-even point. The NPV of the undiscounted cash flow was U.S. $80.2M while the discounted cash flow has NPV ranging from U.S. $–0.63M (at i = 50%) to $45.2M (at i = 5%). It is worth emphasizing that the cash flow analysis was performed assuming 'year zero' was taken as the year of construction of the plant.

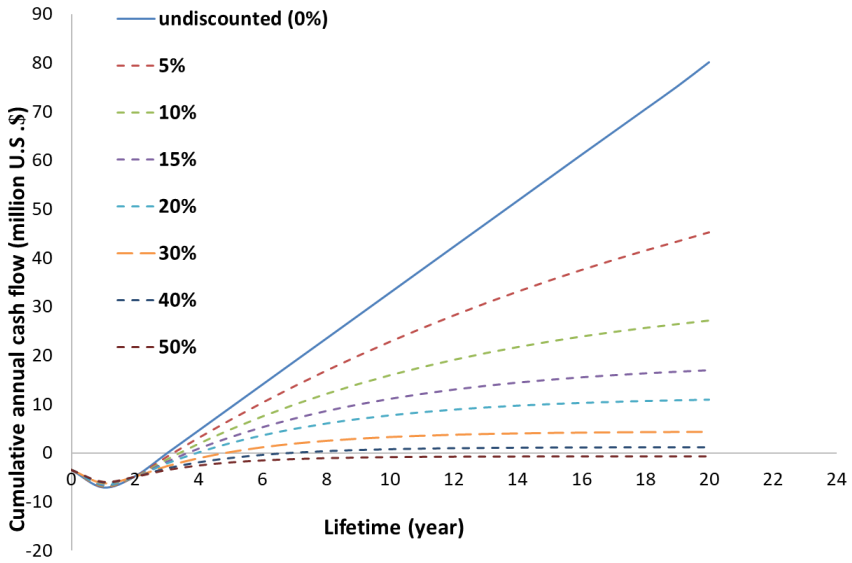

Figure 8.6: Cash flow analysis on hydrogen production from SCWG of soybean straw.

As illustrated in Figure 8.6, during year zero the cash flow is negative because of the money invested in the land purchase (2% of FCI) and the TCI. The working capital is included when the

project is about to proceed towards the end of the first year. Thus, the additional amount is set aside for the venture to spend safely. Moreover, this amount is kept differently from the capital cost. After plant construction and initiation of production, the funds received from sales and investments are recovered at an IRR rate of 10%. The payback period which indicates the time it takes to recover the initial amount invested in the project (discounting the land cost and working capital) was 2.5 years for the undiscounted case. It was obtained from the cash flow curve by tracing the point where the cumulative cash flow increases to the level of negative working capital. Moreover, the discounted case has a PBP ranging from 3.2 years (5%) to 5.4 years (50%). For the investment to be profitable, the PBP should always be less than the estimated project life. In the present study, the PBP for the undiscounted and discounted case is less than the project life. This indicates that the proposed SCWG plant for hydrogen production is profitable from an economic standpoint.

Although the PBP is an effective profitability index, it has the limitation of not explaining the performance of the project after the payback period. Therefore, the NPV and DCFR were used to complement the PBP in the present study. The DCFR estimated as the discount rate that produces zero NPV is 40.6%. The high DCFR indicates that the production is highly profitable. Like PBP, DCFR cannot predict whether the project is profitable. However, together they are frequently used to evaluate the profitability of a project. Regardless, DCFR also has some limitations. It does not indicate the financial risks or project size (Ulrich and Vasudevan, 2018). For instance, when considering two projects using DCFR, one would be inclined to select the one with higher DCFR without considering the individual capital investment required for each project which is dependent on the project size. The net rate of return (NRR), which combines NPV and DCFR is seen as the best profitability index (Ulrich and Vasudevan, 2018). Assuming a 10%

discounted rate, the NRR value estimated was 37.1%. A positive value of NRR indicates profit while a negative value indicates a loss. Based on the above results, the project is considered profitable.

8.4.4 Sensitivity analysis

Several parameters affect the unit production price of hydrogen obtained in this study together with the NPV. Some of these parameters include the cost of labor, working capital, land cost, cost of soybean straw and catalysts, depreciation time and utility cost. A sensitivity analysis was performed to evaluate how the changes in each of these parameters could influence the minimum selling price of hydrogen and the NPV. Besides, most of the parameters were varied to ±30.

Figure 8.7a and Figure 8.7b show the effects of the analyzed parameters on the undiscounted NPV and the unit production cost of hydrogen, respectively. The tax rate and cost of soybean straw had the greatest effect on the NPV. When the cost of soybean straw and the tax rate were decreased by 30%, the undiscounted NPV can be increased from U.S. $80.18M to $92.35M (with an increase in tax rate) and U.S. $68.02M (with an increase in the cost of soybean straw). Likewise, a 30% elevation in the tax rate and price of soybean straw also resulted in a decline in the undiscounted NPV from U.S. $80.18M to $68.02M (for tax rate) and U.S. $75.77M (for the cost of soybean straw). The labor cost is also sensitive towards the NPV. A 30% decline in the cost of labor produced about a 4.2% elevation in the NPV. A change in other factors such as the land cost and working capital did not significantly affect the NPV. With a 30% increase in the utility cost, there was a 0.3% increase in the NPV while a decrease did not affect the NPV. On the other hand, the cost of the catalyst had a minimal influence on the NPV. Increasing the catalyst

cost by 30% led to a decline in the NPV to U.S. $79.3M. Likewise, a 30% decrease produced an increase in the value of NPV to U.S. $80.19M.

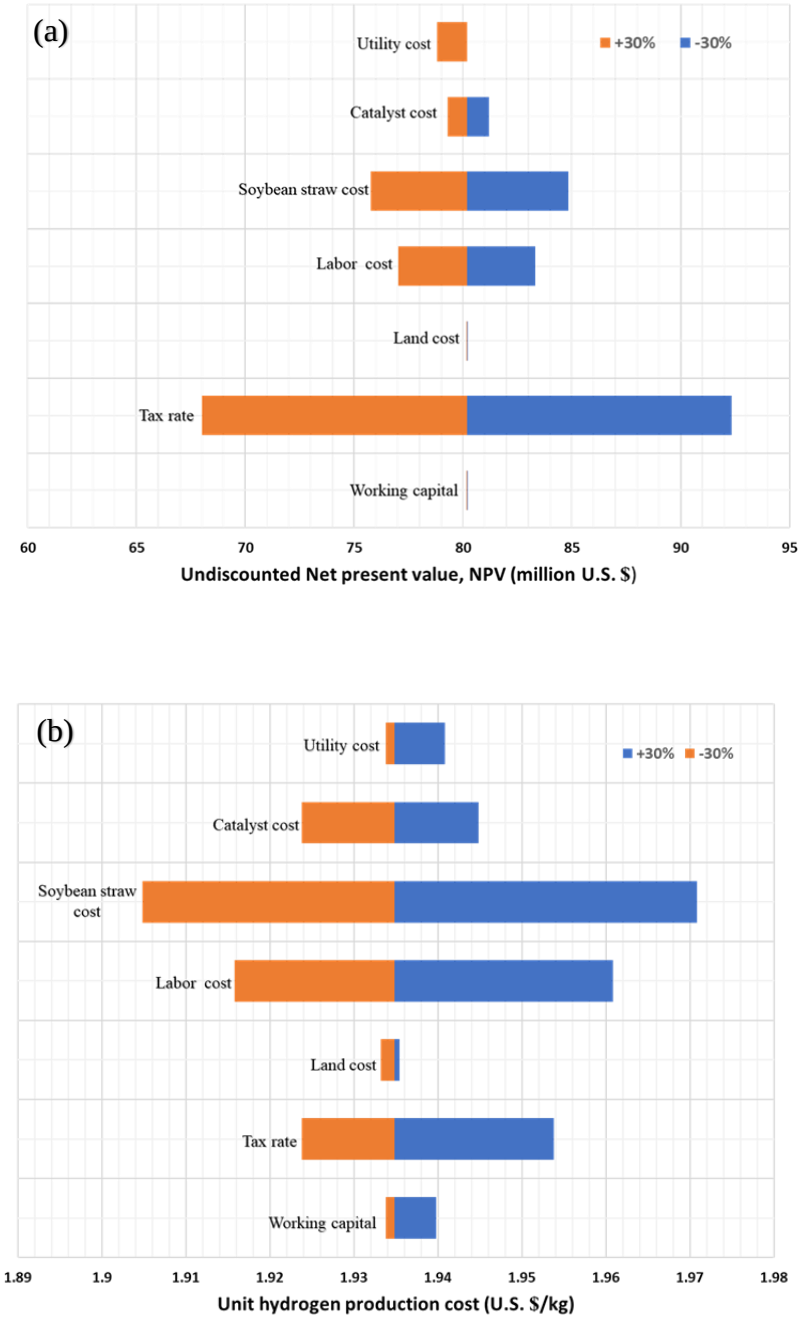

Figure 8.7: Sensitivity analysis showing the effect of several parameters on the (a) undiscounted net present value (NPV), and (b) unit production cost of hydrogen expressed in U.S.$/kg

As illustrated in Figure 8.7b, when compared to the undiscounted NPV, the unit hydrogen production cost varies with the parameters differently. The cost of soybean straw, catalysts and labor are sensitive to the unit hydrogen production cost. When the cost of soybean straw and catalysts decreased by 30%, the unit hydrogen production cost slightly reduced from U.S. $1.94/kg to $1.90/kg (soybean straw) and U.S. $1.93/kg (catalyst). Similarly, with a 30% rise in the cost of soybean straw and catalyst, the unit hydrogen production cost increased to U.S. $1.97/kg (soybean straw) and U.S. $1.95/kg (catalyst). Factors such as tax rate, utility cost and working capital are also sensitive to the unit hydrogen production cost. However, their influence was less pronounced when compared to the cost of soybean straw and catalyst. The land cost has the least influence on the unit hydrogen production price. When the land cost decreased by 30%, the unit production price also declined by 4.7%.

The sensitivity analysis shows that the costs of feedstock (soybean straw) and catalyst are important parameters affecting the minimum selling price of hydrogen. Soybean straw is a crop residue left behind after the harvesting and processing of soybean. Although it has fewer practical usage, it is mostly used as beddings for cattle or burnt in farmland. Therefore, its application for hydrogen production is perceived as a strategy to minimize waste disposal and environmental challenges. On the other hand, the cost of soybean straw is dependent on the logistics cost i.e., transportation from the farm to the plant site.

8.4.5 Key issues and bottlenecks in the implementation of the proposed design for hydrogen production

The TEA results for the conversion of 56,000 tons/year of soybean straw to hydrogen through SCWG shows a minimum selling price of hydrogen as U.S. $1.94/kg. This price is comparable to the selling price of hydrogen produced from other processes such as gasification, steam reforming, solar thermochemical cycle, and water electrolysis (Salkuyeh et al., 2018;

Schweitzer et al., 2018; Yates et al., 2020; Zhuang et al., 2020). Table 8.6 shows the minimum selling price of hydrogen from different processes reported in the literature. It should be noted that the articles cited in Table 8.6 applied different cost estimation methodology and the price stated is relevant to the publication date. Among all the processes, steam reforming of natural gas with carbon capture remains one of the cheapest sources of hydrogen with a minimum selling price of U.S. $1.26/kg (Al-Qahtani et al., 2021). The integration of carbon capture to steam reforming reaction minimizes the impact of the process on the environment and public health.

Other methods such as electrolysis coupled with renewable technologies (e.g., nuclear, solar, photovoltaics, etc.) are more expensive because of their high electricity consumption (Gutiérrez Ortiz et al., 2012). Therefore, the minimum hydrogen selling price derived from these processes could be dependent on electricity cost per kWh. The Cu-Cl hydrogen production cycle is a novel technology used to recycle industrial wastes combined with exhaust HCl for hydrogen production (Zhuang et al., 2020). However, the process still needs further research before implementation on a large scale.

The price of hydrogen is predicted to drop in the future because of the advancement in research. The higher price of hydrogen from other processes could be because of the increased feedstock cost, the relatively high capital cost involved in the construction and running of the plant and the cost of CO_2 removal. In comparison with other processes for producing clean hydrogen, SCWG remains competitive although the technology is still in its development stage and further research is needed to move from the pilot-scale to industrial-scale production.

Table 8.6: Minimum selling price of hydrogen from different production processes.

Hydrogen production process	**Minimum selling price (U.S.$/kg)**	**References**
Methane steam reforming with carbon capture	0.8-3	Acar and Dincer (2019): Al-Qahtani et al. (2021)
Methane steam reforming without carbon capture	1.88-2	Acar and Dincer (2019): Al-Qahtani et al. (2021)
Sorption enhanced reforming biomass gasification	10.93-11	Schweitzer et al. (2018)
Solar driven water electrolysis	2.89-4.67	Yates et al. (2020)
Cu-Cl hydrogen production cycle	2.8	Zhuang et al. (2020)
Fluidized bed gasification	3.1-4.0	Salkuyeh et al. (2018)
SCWG integrated with CO_2 removal unit and energy self-sufficient	1.94-1.97	This study
Dark fermentation	2.6	Salkuyeh et al. (2018)
Coal gasification with CO_2 sequestration	0.9-1.7	Acar and Dincer (2019)
Pyrolysis	1-2	Acar and Dincer (2019)
Coal gasification	0.8-1.3	Acar and Dincer (2019)

It is worth mentioning that there are few limitations in this study that needs to be considered by policymakers and stakeholders. The separation process is assumed to operate at 100% capacity while the heat loss is negligible. The cost of transportation, storage and distribution of hydrogen is not considered in the TEA study. These additional costs could increase the minimum selling price reported in the present study. On the contrary, tax exemption and biofuel subsidy implemented by several countries could contribute towards the reduction of hydrogen price. These aspects have not been considered in this study. However, most countries are known to offer such incentives to promote clean fuels. In addition, tipping fees and various environmental policies

offered by certain governmental bodies could elevate the economic viability of the process. Moreover, TEA results should be integrated with lifecycle assessment. Therefore, the economic and environmental risk assessment of any proposed design should be comprehensively studied to make major decisions regarding profitability, waste reduction and pollution abatement.

8.5 Conclusions

In this study, a conceptual SCWG process design was proposed for the conversion of 56,000 metric tons/year (or 170 metric tons/day) of soybean straw to hydrogen under SCWG conditions. The process was simulated based on the following operating conditions: temperature (500°C), pressure (25 MPa), biomass-to-water ratio (1:10) and biomass particle size (0.13). Aspen Plus process simulation software was used to prepare the simulation flowsheet and calculate the mass and energy balances. It was observed that for every 170 metric tons/day of soybean straw gasified in SCW, about 110 metric tons/day of hydrogen was produced. More importantly, 33% of the energy from the biomass was recovered by the produced syngas. On the other hand, the flue gas recovered 9% of the energy contained in the feedstock. The remaining energy was consumed by the process. Based on the overall energy recovery estimation, the process was estimated to possess about 63.5% energy efficiency.

A detailed TEA evaluation and sensitivity analysis were performed to determine the economic feasibility of the SCWG process. The undiscounted NPV value of U.S. $80.2M was obtained assuming the plant operates for 20 years with negligible salvage value. On the other hand, the NPV decreased to U.S. $27.1M with a discount rate of 10%. Besides, the NRR was 37.1%. The break-even price of hydrogen calculated at a zero NPV value was U.S. $1.94/kg. The relatively low price of hydrogen and the positive NPV and NRR values indicate that the proposed design is profitable. Sensitivity analysis was also performed to determine the influence of several parameters

on the NPV and the minimum selling price of hydrogen. The results suggest that the tax rate, raw material cost and labor cost are major factors that influence the NPV and the minimum selling price of hydrogen.

Chapter 9 Summary, Conclusions and Recommendation

9.1 Overall summary and conclusions

The research focused on evaluating the potential of lignocellulosic biomass as feedstock for hydrogen production using SCWG, optimize the operating conditions and propose strategies to minimize the selling price of hydrogen produced. Model compounds representing cellulose, xylose (hemicellulose) and lignin were used as feedstocks for SCWG. The response surface methodology based on the Box – Behnken design was used to study the effects of temperature (300–500 °C), reaction time (30–60 min) and feedstock concentration (10–30 wt%) on hydrogen yield and to optimize the process conditions. Maximum H_2 yield of 1.95 mmol/g was obtained at 500 °C with 12.5 wt.% feedstock concentration in 60 min of reaction time. A comparative evaluation of the SCWG of biomass model compounds representing cellulose, xylose and lignin shows that xylose had the highest H_2 yield of 2.26 mmol/g. Lignin had the lowest H_2 yield (0.73 mmol/g), which is attributed to its highly polymeric and recalcitrant chemical structure, difficult to decompose even at supercritical conditions.

Real biomass feedstocks (soybean straw and flax straw) were also tested to understand the effects of biomass heterogeneity on hydrogen yield during SCWG process. The two-feedstock showed different behaviour and produced different gaseous yields in SCW. Soybean straw and Flax straw produced hydrogen yield of 6.62 mmol/g and 3.82 mmol/g at 500 °C, 1:10 biomass to water ratio, particle size 0.13 mm for 45 min. The superior hydrogen yield of soybean straw was attributed to it low lignin content and high ash content. Moreover, the experimental results were compared with theoretical yields from thermodynamic calculations. It was observed that the experimental yield did not approach theoretical values. Therefore, heterogeneous catalyst was required to improve the hydrogen yield towards equilibrium values.

The deviation between experimental and theoretical results necessitated the need for a low-cost heterogeneous catalyst to improve the hydrogen yield and selectivity. Therefore, a comprehensive screening of different supports including activated carbon (AC), Carbon nanotubes (CNT), ZrO_2, Al_2O_3, SiO_2 and AL_2O_3-SiO_2 and promoters (K, Na and Ce) for Ni based catalysts was performed. The effectiveness of each support towards improving H_2 yield and selectivity was in the order: ZrO_2 > Al_2O_3 > AC > CNT > SiO_2 > $Al|_2O_3$ - SiO_2. In terms of H_2 yield, the performance of each promoters for Ni/ZrO_2 catalysts is in the order of Ce (10.91 mmol/g) > K (10.26 mmol/g) > Na (9.54 mmol/g). The improved performance of Ni – Ce/ZrO_2 catalysts was attributed to the high Ni dispersion and its ability to reduce carbon deposition.

Kinetic study was performed for the SCWG of soybean straw using the Ni – Ce/ZrO_2 catalysts. The kinetic studies helped to predict the evolution of the system over time and, therefore, calculate the dynamic mass and energy balances which are useful during techno – economic studies. The gas yield results obtained from the catalytic gasification of soybean straw at 500 °C, 1:10 biomass to water ratio, particle size 0.13 mm and 45 min residence time were used to fit the kinetic model while the rate constants were determined through minimizing the sum of the square of prediction errors. The results from the kinetics model fitted well with experimental observations. The model was used to successfully predict the gas yield as a function of time.

In the last phase of the study, the techno-economic feasibility of hydrogen production from the Ni – Ce/ZrO_2 catalyzed SCWG of soybean straw was studied. A novel energetic – self-sustaining process designed to process 56, 000 metric tons of soybean straw per year was proposed. The process used the heat from the produced flue gas to power the SCWG reactor. A minimum selling price of $1.94/kg of hydrogen was obtained from the study. This price is relatively low when compared to the hydrogen produced from other biomass conversion processes. Moreover, a

positive net rate of return (NRR) of 37.1% was obtained in this study. This shows that the project is profitable from an economic standpoint. Sensitivity analyses indicate that the minimum selling price of hydrogen is affected by the feedstock price, utility cost, tax rate and labor cost.

Important conclusions obtained from this research are provided below:

- For H_2 production from SCWG high temperature and long residence time is important.
- The performance of each lignocellulosic components for H_2 production from SCWG is in the order : xylose (hemicellulose) > cellulose > lignin.
- The optimum process conditions for SCWG of lignocellulosic biomass (soybean straw) is 500 °C, 1:10 biomass to water ratio, particle size 0.13 mm for 45 min.
- Higher H_2 yield is obtained from soybean straw (6.62 mmol/g) than flax straw (3.82 mmol/g).
- The effectiveness of each support towards improving H_2 yield and selectivity for Ni – based catalysts is in the order: ZrO_2 > Al_2O_3 > AC > CNT > SiO_2 > Al_2O_3 - SiO_2.
- The activity of Ni/ZrO_2 catalysts with different promoters is in the order: Ce > K > Na.
- Breakeven cost of H_2 obtained from a proposed SCWG plant for the processing of 56,000 metric tons/year of soybean straw was U.S. $1.94/kg excluding storage and transportation cost.

9.2 Contribution to knowledge

The contribution of this thesis in extending the knowledge of SCWG of biomass are listed below:

- Overall, the review articles in this study contributes towards the understanding of SCWG process by presenting a compilation of recent advances in the catalytic and non – catalytic gasification of lignocellulosic biomass, modelling and process optimization of SCWG process together with the challenges and future perspectives.
- The thesis provides a detailed understanding of the behavior of biomass model compounds and real lignocellulosic feedstock in SCW. Furthermore, a detailed reaction pathway of SCWG of lignocellulosic biomass was proposed in the study.
- Soybean straw and Flax straw as representative agricultural residues were proven to be promising feedstock for SCWG. Therefore, the study contributes to the knowledge of SCWG of lignocellulosic biomass and the physico – chemical properties of the hydrochars and liquid products.
- Detailed understanding of the stability and activity of Ni -Ce/ZrO_2 catalysts was presented in this study.
- The study contributes to the understanding of the kinetics model for predicting the gaseous yield and the variation of SCWG system with time.
- The tecno-economic feasibility of the hydrogen production from lignocellulosic biomass using SCWG shows that the process is economically feasible.

9.3 Recommendations

- Although high heating rate is favorable during SCWG it is often challenging to attain high heating rate in an autoclave batch reach reactor. This is because most batch reactors are heated by external heaters. To enhance the heating rate in such reactors the external heaters could be replaced with a molten salt bath or sand bath containing high thermal mass and superior heat transfer properties. Furthermore, concentrated feed at high temperature could be injected into the previously heated reactor through a very high – pressure pump.
- For future batch reactor studies, the effects of agitation should be studied to see if it would influence hydrogen yield and selectivity, since the presence of agitation could help eliminate the mass transfer resistance.
- The synergy between the model compounds representing cellulose, hemicellulose and lignin was not studied. Therefore, it is recommended that this effect should be studied in the future.
- The heterogeneous catalysts used in this study were prepared by co – impregnation method. However, future research should focus on comparing the performance of catalysts prepared from different methods such as the co – precipitation and impregnation methods.
- The mass balance from SCWG results shows that there is a loss in mass because of the challenges encountered during product collection. Therefore, future research should also focus on developing effective strategies for collecting and separating the reaction products to minimize product loss.
- For potential industrial applications of SCWG process, a detailed cost estimate should be combined with life cycle assessment to evaluate the economic and environmental impacts of the process. However, high quality data is needed to design a reliable life cycle assessment, this task requires a lot of time and effort.

REFERENCES

Abatzoglou, N., Fauteux-Lefebvre, C., 2016. Review of catalytic syngas production through steam or dry reforming and partial oxidation of studied liquid compounds. Wiley Interdiscip. Rev. Energy Environ. 5, 169–187. https://doi.org/10.1002/wene.167

Abdalla, A.M., Hossain, S., Nisfindy, O.B., Azad, A.T., Dawood, M., Azad, A.K., 2018. Hydrogen production, storage, transportation and key challenges with applications: A review. Energy Convers. Manag. https://doi.org/10.1016/j.enconman.2018.03.088

Abdulkhani, A., Alizadeh, P., Hedjazi, S., Hamzeh, Y., 2017. Potential of Soya as a raw material for a whole crop biorefinery. Renew. Sustain. Energy Rev. https://doi.org/10.1016/j.rser.2016.10.082

Acar, C., Dincer, I., 2019. Review and evaluation of hydrogen production options for better environment. J. Clean. Prod. 218, 835–849. https://doi.org/10.1016/j.jclepro.2019.02.046

Adamu, S., Binous, H., Razzak, S.A., Hossain, M.M., 2017. Enhancement of glucose gasification by Ni/La2O3-Al2O3 towards the thermodynamic extremum at supercritical water conditions. Renew. Energy 111, 399–409. https://doi.org/10.1016/j.renene.2017.04.020

Al-Qahtani, A., Parkinson, B., Hellgardt, K., Shah, N., Guillen-Gosalbez, G., 2021. Uncovering the true cost of hydrogen production routes using life cycle monetisation. Appl. Energy 281, 115958. https://doi.org/10.1016/j.apenergy.2020.115958

Anikeev, V.I., Fan, M., 2014. Supercritical Fluid Technology for Energy and Environmental

Applications, Supercritical Fluid Technology for Energy and Environmental Applications. https://doi.org/10.1016/C2012-0-00267-0

ASTM, 2004. E1755-01: Standard Test Method for Ash in Biomass. Annu. B. ASTM Stand. 3.

ASTM E871-82, 2006. Standard Test Method for Moisture Analysis of Particulate Wood Fuels. West Conshohocken, PA ASTM Int.

Azadi, P., Afif, E., Azadi, F., Farnood, R., 2012a. Screening of nickel catalysts for selective hydrogen production using supercritical water gasification of glucose. Green Chem. 14, 1766–1777. https://doi.org/10.1039/c2gc16378k

Azadi, P., Farnood, R., Vuillardot, C., 2011. Estimation of heating time in tubular supercritical water reactors. J. Supercrit. Fluids 55, 1038–1045. https://doi.org/10.1016/j.supflu.2010.09.025

Azadi, P., Khan, S., Strobel, F., Azadi, F., Farnood, R., 2012b. Hydrogen production from cellulose, lignin, bark and model carbohydrates in supercritical water using nickel and ruthenium catalysts. Appl. Catal. B Environ. 117–118, 330–338. https://doi.org/10.1016/j.apcatb.2012.01.035

Azargohar, R., Nanda, S., Dalai, A.K., 2018. Densification of agricultural wastes and forest residues: A review on influential parameters and treatments, in: Recent Advancements in Biofuels and Bioenergy Utilization. Springer Singapore, pp. 27–51. https://doi.org/10.1007/978-981-13-1307-3_2

Azargohar, R., Nanda, S., Dalai, A.K., Kozinski, J.A., 2019. Physico-chemistry of biochars

produced through steam gasification and hydro-thermal gasification of canola hull and canola meal pellets. Biomass and Bioenergy 120, 458–470. https://doi.org/10.1016/j.biombioe.2018.12.011

Azargohar, R., Nanda, S., Kozinski, J.A., Dalai, A.K., Sutarto, R., 2014. Effects of temperature on the physicochemical characteristics of fast pyrolysis bio-chars derived from Canadian waste biomass. Fuel 125, 90–100. https://doi.org/10.1016/j.fuel.2014.01.083

Badoga, S., Kamath, G., Dalai, A., 2020. Effects of promoters (Mn, Mg, Co and Ni) on the Fischer-Tropsch activity and selectivity of KCuFe/mesoporous-alumina catalyst. Appl. Catal. A Gen. 607, 117861. https://doi.org/10.1016/j.apcata.2020.117861

Bandura, A. V., Lvov, S.N., 2006. The ionization constant of water over wide ranges of temperature and density. J. Phys. Chem. Ref. Data 35, 15–30. https://doi.org/10.1063/1.1928231

Barbier, J., Charon, N., Dupassieux, N., Loppinet-Serani, A., Mahé, L., Ponthus, J., Courtiade, M., Ducrozet, A., Fonverne, A., Cansell, F., 2011. Hydrothermal conversion of glucose in a batch reactor. A detailed study of an experimental key-parameter: The heating time. J. Supercrit. Fluids 58, 114–120. https://doi.org/10.1016/j.supflu.2011.05.004

Basu, P., Mettanant, V., 2009. Biomass Gasification in Supercritical Water -- A Review. Int. J. Chem. React. Eng. 7. https://doi.org/10.2202/1542-6580.1919

Bej, B., Bepari, S., Pradhan, N.C., Neogi, S., 2017. Production of hydrogen by dry reforming of ethanol over alumina supported nano-NiO/SiO2 catalyst. Catal. Today 291, 58–66. https://doi.org/10.1016/j.cattod.2016.12.010

Borugadda, V.B., Kamath, G., Dalai, A.K., 2020. Techno-economic and life-cycle assessment of integrated Fischer-Tropsch process in ethanol industry for bio-diesel and bio-gasoline production. Energy 195, 116985. https://doi.org/10.1016/j.energy.2020.116985

Boukis, N., Galla, U., Müller, H., Dinjus, E., 2007. Biomass gasification in supercritical water. Experimental progress achieved with the Verena pilot plant., 15th European Biomass Conference & Exhibition, 7-11 May 2007, Berlin, Germany.

Brethauer, S., Studer, M.H., 2015. Biochemical conversion processes of lignocellulosic biomass to fuels and chemicals - A review. Chimia (Aarau). 69, 572–581. https://doi.org/10.2533/chimia.2015.572

Bühler, W., Dinjus, E., Ederer, H.J., Kruse, A., Mas, C., 2002. Ionic reactions and pyrolysis of glycerol as competing reaction pathways in near- and supercritical water. J. Supercrit. Fluids 22, 37–53. https://doi.org/10.1016/S0896-8446(01)00105-X

Buranov, A.U., Mazza, G., 2008. Lignin in straw of herbaceous crops. Ind. Crops Prod. https://doi.org/10.1016/j.indcrop.2008.03.008

Byrd, A.J., Kumar, S., Kong, L., Ramsurn, H., Gupta, R.B., 2011. Hydrogen production from catalytic gasification of switchgrass biocrude in supercritical water. Int. J. Hydrogen Energy 36, 3426–3433. https://doi.org/10.1016/j.ijhydene.2010.12.026

Byrd, A.J., Pant, K.K., Gupta, R.B., 2008. Hydrogen production from glycerol by reforming in supercritical water over Ru/Al2O3 catalyst. Fuel 87, 2956–2960. https://doi.org/10.1016/j.fuel.2008.04.024

Cai, J., He, Y., Yu, X., Banks, S.W., Yang, Y., Zhang, X., Yu, Y., Liu, R., Bridgwater, A. V., 2017. Review of physicochemical properties and analytical characterization of lignocellulosic biomass. Renew. Sustain. Energy Rev. https://doi.org/10.1016/j.rser.2017.03.072

Cao, C., Guo, L., Chen, Y., Guo, S., Lu, Y., 2011. Hydrogen production from supercritical water gasification of alkaline wheat straw pulping black liquor in continuous flow system. Int. J. Hydrogen Energy 36, 13528–13535. https://doi.org/10.1016/j.ijhydene.2011.07.101

Cao, W., Guo, L., Yan, X., Zhang, D., Yao, X., 2018. Assessment of sugarcane bagasse gasification in supercritical water for hydrogen production. Int. J. Hydrogen Energy 43, 13711–13719. https://doi.org/10.1016/j.ijhydene.2017.12.013

Carrier, M., Loppinet-Serani, A., Denux, D., Lasnier, J.M., Ham-Pichavant, F., Cansell, F., Aymonier, C., 2011. Thermogravimetric analysis as a new method to determine the lignocellulosic composition of biomass. Biomass and Bioenergy 35, 298–307. https://doi.org/10.1016/j.biombioe.2010.08.067

Castello, D., Fiori, L., 2011. Supercritical water gasification of biomass: Thermodynamic constraints. Bioresour. Technol. 102, 7574–7582. https://doi.org/10.1016/j.biortech.2011.05.017

Castello, D., Kruse, A., Fiori, L., 2015. Low temperature supercritical water gasification of biomass constituents: Glucose/phenol mixtures. Biomass and Bioenergy 73, 84–94. https://doi.org/10.1016/j.biombioe.2014.12.010

Chaubey, R., Sahu, S., James, O.O., Maity, S., 2013. A review on development of industrial

processes and emerging techniques for production of hydrogen from renewable and sustainable sources. Renew. Sustain. Energy Rev. 23, 443–462. https://doi.org/10.1016/j.rser.2013.02.019

Chen, J., Fan, Y., Jiaqiang, E., Cao, W., Zhang, F., Gong, J., Liu, G., Xu, W., 2019. Effects analysis on the gasification kinetic characteristics of food waste in supercritical water. Fuel 241, 94–104. https://doi.org/10.1016/j.fuel.2018.12.012

Chen, J., Liang, J., Xu, Z., E, J., 2020. Assessment of supercritical water gasification process for combustible gas production from thermodynamic, environmental and techno-economic perspectives: A review. Energy Convers. Manag. https://doi.org/10.1016/j.enconman.2020.113497

Chen, Y., Yi, L., Li, S., Yin, J., Jin, H., 2020. Catalytic gasification of sewage sludge in near and supercritical water with different catalysts. Chem. Eng. J. 388, 124292. https://doi.org/10.1016/j.cej.2020.124292

Cheng, L., Ye, X.P., 2010. Recent progress in converting biomass to biofuels and renewable chemicals in sub- or supercritical water. Biofuels. https://doi.org/10.4155/bfs.09.3

Chowdhury, M.B.I., Hossain, M.Z., Mazumder, J., Jhawar, A.K., Charpentier, P.A., 2018. La-based catalysts to enhance hydrogen production during supercritical water gasification of glucose. Fuel 217, 166–174. https://doi.org/10.1016/j.fuel.2017.12.105

Chuntanapum, A., Matsumura, Y., 2010. Char formation mechanism in supercritical water gasification process: A study of model compounds. Ind. Eng. Chem. Res. 49, 4055–4062. https://doi.org/10.1021/ie901346h

D3175-11, A., 2011. ASTM D3175-11: Standard test method for volatile matter in the analysis sample of coal and coke. ASTM Int. 6. https://doi.org/10.1520/D3175-11.2

Dahmoune, F., Spigno, G., Moussi, K., Remini, H., Cherbal, A., Madani, K., 2014. Pistacia lentiscus leaves as a source of phenolic compounds: Microwave-assisted extraction optimized and compared with ultrasound-assisted and conventional solvent extraction. Ind. Crops Prod. 61, 31–40. https://doi.org/10.1016/j.indcrop.2014.06.035

Damartzis, T., Vamvuka, D., Sfakiotakis, S., Zabaniotou, A., 2011. Thermal degradation studies and kinetic modeling of cardoon (Cynara cardunculus) pyrolysis using thermogravimetric analysis (TGA). Bioresour. Technol. 102, 6230–6238. https://doi.org/10.1016/j.biortech.2011.02.060

De Blasio, C., Järvinen, M., 2017. Supercritical Water Gasification of Biomass. Encycl. Sustain. Technol. 171–195. https://doi.org/10.1016/B978-0-12-409548-9.10098-3

De Blasio, C., Lucca, G., Özdenkci, K., Mulas, M., Lundqvist, K., Koskinen, J., Santarelli, M., Westerlund, T., Järvinen, M., 2016. A study on supercritical water gasification of black liquor conducted in stainless steel and nickel-chromium-molybdenum reactors. J. Chem. Technol. Biotechnol. 91, 2664–2678. https://doi.org/10.1002/jctb.4871

Demirbas, A., 2004. Hydrogen-rich gas from fruit shells via supercritical water extraction. Int. J. Hydrogen Energy 29, 1237–1243. https://doi.org/10.1016/j.ijhydene.2003.11.012

Deniz, I., Vardar-Sukan, F., Yüksel, M., Saglam, M., Ballice, L., Yesil-Celiktas, O., 2015. Hydrogen production from marine biomass by hydrothermal gasification. Energy Convers. Manag. 96, 124–130. https://doi.org/10.1016/j.enconman.2015.02.048

DeVlieger, D.J.M., Thakur, D.B., Lefferts, L., Seshan, K., 2012. Carbon Nanotubes: A Promising Catalyst Support Material for Supercritical Water Gasification of Biomass Waste. ChemCatChem 4, 2068–2074. https://doi.org/10.1002/cctc.201200318

Ding, N., Azargohar, R., Dalai, A.K., Kozinski, J.A., 2014. Catalytic gasification of glucose to H2 in supercritical water. Fuel Process. Technol. 127, 33–40. https://doi.org/10.1016/j.fuproc.2014.05.014

Do, T.X., Mujahid, R., Lim, H.S., Kim, J.K., Lim, Y. Il, Kim, J., 2020. Techno-economic analysis of bio heavy-oil production from sewage sludge using supercritical and subcritical water. Renew. Energy 151, 30–42. https://doi.org/10.1016/j.renene.2019.10.138

Elif, D., Nezihe, A., 2016. Hydrogen production by supercritical water gasification of fruit pulp in the presence of Ru/C. Int. J. Hydrogen Energy 41, 8073–8083. https://doi.org/10.1016/j.ijhydene.2015.12.005

Fang, Z., Minowa, T., Smith, R.L., Ogi, T., Koziński, J.A., 2004. Liquefaction and Gasification of Cellulose with Na2CO 3 and Ni in Subcritical Water at 350 °C. Ind. Eng. Chem. Res. 43, 2454–2463. https://doi.org/10.1021/ie034146t

Fang, Z., Sato, T., Smith, R.L., Inomata, H., Arai, K., Kozinski, J.A., 2008. Reaction chemistry and phase behavior of lignin in high-temperature and supercritical water. Bioresour. Technol. 99, 3424–3430. https://doi.org/10.1016/j.biortech.2007.08.008

Felfli, F.F., Mesa P, J.M., Rocha, J.D., Filippetto, D., Luengo, C.A., Pippo, W.A., 2011. Biomass briquetting and its perspectives in Brazil. Biomass and Bioenergy 35, 236–242. https://doi.org/10.1016/j.biombioe.2010.08.011

Ferreira, S.L.C., Bruns, R.E., Ferreira, H.S., Matos, G.D., David, J.M., Brandão, G.C., da Silva, E.G.P., Portugal, L.A., dos Reis, P.S., Souza, A.S., dos Santos, W.N.L., 2007. Box-Behnken design: An alternative for the optimization of analytical methods. Anal. Chim. Acta 597, 179–186. https://doi.org/10.1016/j.aca.2007.07.011

Fiori, L., Castello, D., 2014. Thermodynamic Analysis of the Supercritical Water Gasification of Biomass. pp. 99–129. https://doi.org/10.1007/978-94-017-8923-3_4

Fiori, L., Valbusa, M., Castello, D., 2012. Supercritical water gasification of biomass for H2 production: Process design. Bioresour. Technol. 121, 139–147. https://doi.org/10.1016/j.biortech.2012.06.116

Fougere, D., Nanda, S., Clarke, K., Kozinski, J.A., Li, K., 2016. Effect of acidic pretreatment on the chemistry and distribution of lignin in aspen wood and wheat straw substrates. Biomass and Bioenergy 91, 56–68. https://doi.org/10.1016/j.biombioe.2016.03.027

Friedl, A., Padouvas, E., Rotter, H., Varmuza, K., 2005. Prediction of heating values of biomass fuel from elemental composition. Anal. Chim. Acta 544, 191–198. https://doi.org/10.1016/j.aca.2005.01.041

Gadhe, J.B., Gupta, R.B., 2005. Hydrogen production by methanol reforming in supercritical water: Suppression of methane formation. Ind. Eng. Chem. Res. 44, 4577–4585. https://doi.org/10.1021/ie049268f

Galera, S., Gutiérrez Ortiz, F.J., 2015. Techno-economic assessment of hydrogen and power production from supercritical water reforming of glycerol. Fuel 144, 307–316. https://doi.org/10.1016/j.fuel.2014.12.033

Gökkaya, D.S., Saglam, M., Yuksel, M., Ballice, L., 2016. Hydrothermal gasification of xylose: Effects of reaction temperature, pressure, and K2CO3 as a catalyst on product distribution. Biomass and Bioenergy 91, 26–36. https://doi.org/10.1016/j.biombioe.2016.04.013

Golecha, R., 2016. Minimizing the Cost of Agriculture Waste for Cellulosic Biofuels. Strateg. Plan. Energy Environ. 36, 14–21. https://doi.org/10.1080/10485236.2016.11771073

Gong, M., Nanda, S., Hunter, H.N., Zhu, W., Dalai, A.K., Kozinski, J.A., 2017a. Lewis acid catalyzed gasification of humic acid in supercritical water. Catal. Today 291, 13–23. https://doi.org/10.1016/j.cattod.2017.02.017

Gong, M., Nanda, S., Romero, M.J., Zhu, W., Kozinski, J.A., 2017b. Subcritical and supercritical water gasification of humic acid as a model compound of humic substances in sewage sludge. J. Supercrit. Fluids 119, 130–138. https://doi.org/10.1016/j.supflu.2016.08.018

Goodwin, A.K., Rorrer, G.L., 2011. Modeling of supercritical water gasification of xylose to hydrogen-rich gas in a hastelloy microchannel reactor. Ind. Eng. Chem. Res. 50, 7172–7182. https://doi.org/10.1021/ie102482y

Grishina, E., Gelman, D., Belopukhov, S., Starosvetsky, D., Groysman, A., Ein-Eli, Y., 2016. Improvement of aluminum–air battery performances by the application of flax straw extract. ChemSusChem 9, 2103–2111. https://doi.org/10.1002/cssc.201600298

Guan, Q., Mao, T., Zhang, Q., Miao, R., Ning, P., Gu, J., Tian, S., Chen, Q., Chai, X.S., 2014. Catalytic gasification of lignin with Ni/Al2O3-SiO2 in sub/supercritical water. J. Supercrit. Fluids 95, 413–421. https://doi.org/10.1016/j.supflu.2014.10.015

Guan, Q., Wei, C., Savage, P.E., 2012. Kinetic model for supercritical water gasification of algae. Phys. Chem. Chem. Phys. 14, 3140–3147. https://doi.org/10.1039/c2cp23792j

Güngören Madenoğlu, T., Yildirir, E., Sağlam, M., Yüksel, M., Ballice, L., 2014. Improvement in hydrogen production from hard-shell nut residues by catalytic hydrothermal gasification. J. Supercrit. Fluids 95, 339–347. https://doi.org/10.1016/j.supflu.2014.09.033

Guo, L.J., Lu, Y.J., Zhang, X.M., Ji, C.M., Guan, Y., Pei, A.X., 2007. Hydrogen production by biomass gasification in supercritical water: A systematic experimental and analytical study. Catal. Today 129, 275–286. https://doi.org/10.1016/j.cattod.2007.05.027

Guo, S., Guo, L., Cao, C., Yin, J., Lu, Y., Zhang, X., 2012. Hydrogen production from glycerol by supercritical water gasification in a continuous flow tubular reactor. Int. J. Hydrogen Energy 37, 5559–5568. https://doi.org/10.1016/j.ijhydene.2011.12.135

Guo, S., Guo, L., Yin, J., Jin, H., 2013. Supercritical water gasification of glycerol: Intermediates and kinetics. J. Supercrit. Fluids 78, 95–102. https://doi.org/10.1016/j.supflu.2013.03.025

Gutiérrez Ortiz, F.J., 2020. Techno-economic assessment of supercritical processes for biofuel production. J. Supercrit. Fluids. https://doi.org/10.1016/j.supflu.2020.104788

Gutiérrez Ortiz, F.J., Ollero, P., Serrera, A., Galera, S., 2012. An energy and exergy analysis of the supercritical water reforming of glycerol for power production. Int. J. Hydrogen Energy 37, 209–226. https://doi.org/10.1016/j.ijhydene.2011.09.058

Gutiérrez Ortiz, F.J., Ollero, P., Serrera, A., Sanz, A., 2011. Thermodynamic study of the supercritical water reforming of glycerol. Int. J. Hydrogen Energy 36, 8994–9013.

https://doi.org/10.1016/j.ijhydene.2011.04.095

Han, J., Liang, Y., Hu, J., Qin, L., Street, J., Lu, Y., Yu, F., 2017. Modeling downdraft biomass gasification process by restricting chemical reaction equilibrium with Aspen Plus. Energy Convers. Manag. 153, 641–648. https://doi.org/10.1016/j.enconman.2017.10.030

Hansen, T.W., Delariva, A.T., Challa, S.R., Datye, A.K., 2013. Sintering of catalytic nanoparticles: Particle migration or ostwald ripening? Acc. Chem. Res. 46, 1720–1730. https://doi.org/10.1021/ar3002427

Hantoko, D., Su, H., Yan, M., Kanchanatip, E., Susanto, H., Wang, G., Zhang, S., Xu, Z., 2018. Thermodynamic study on the integrated supercritical water gasification with reforming process for hydrogen production: Effects of operating parameters. Int. J. Hydrogen Energy 43, 17620–17632. https://doi.org/10.1016/j.ijhydene.2018.07.198

Harry, I., Ibrahim, H., Thring, R., Idem, R., 2014. Catalytic subcritical water liquefaction of flax straw for high yield of furfural. Biomass and Bioenergy 71, 381–393. https://doi.org/10.1016/j.biombioe.2014.09.017

Hendriks, A.T.W.M., Zeeman, G., 2009. Pretreatments to enhance the digestibility of lignocellulosic biomass. Bioresour. Technol. 100, 10–18. https://doi.org/10.1016/j.biortech.2008.05.027

Hendry, D., Venkitasamy, C., Wilkinson, N., Jacoby, W., 2011. Exploration of the effect of process variables on the production of high-value fuel gas from glucose via supercritical water gasification. Bioresour. Technol. 102, 3480–3487. https://doi.org/10.1016/j.biortech.2010.11.003

Hossain, M.Z., Jhawar, A.K., Chowdhury, M.B.I., Xu, W.Z., Charpentier, P.A., 2018. Deactivation and regeneration studies of activated carbon during continuous decarboxylation of oleic acid in subcritical water. Fuel 231, 253–263. https://doi.org/10.1016/j.fuel.2018.05.068

Hu, F., Ragauskas, A., 2012. Pretreatment and Lignocellulosic Chemistry. Bioenergy Res. https://doi.org/10.1007/s12155-012-9208-0

Huang, X., Cao, J.P., Zhao, X.Y., Wang, J.X., Fan, X., Zhao, Y.P., Wei, X.Y., 2016. Pyrolysis kinetics of soybean straw using thermogravimetric analysis. Fuel 169, 93–98. https://doi.org/10.1016/j.fuel.2015.12.011

Issariyakul, T., Dalai, A.K., 2012. Comparative kinetics of transesterification for biodiesel production from palm oil and mustard oil. Can. J. Chem. Eng. 90, 342–350. https://doi.org/10.1002/cjce.20679

Jin, H., Guo, L., Guo, J., Ge, Z., Cao, C., Lu, Y., 2015a. Study on gasification kinetics of hydrogen production from lignite in supercritical water. Int. J. Hydrogen Energy 40, 7523–7529. https://doi.org/10.1016/j.ijhydene.2014.12.095

Jin, H., Guo, L., Guo, J., Ge, Z., Cao, C., Lu, Y., 2015b. Study on gasification kinetics of hydrogen production from lignite in supercritical water. Int. J. Hydrogen Energy 40, 7523–7529. https://doi.org/10.1016/j.ijhydene.2014.12.095

Jin, H., Guo, S., Guo, L., Cao, C., 2016. A mathematical model and numerical investigation for glycerol gasification in supercritical water with a tubular reactor. J. Supercrit. Fluids 107, 526–533. https://doi.org/10.1016/j.supflu.2015.06.028

Juan, J.C., Kartika, D.A., Wu, T.Y., Hin, T.Y.Y., 2011. Biodiesel production from jatropha oil by catalytic and non-catalytic approaches: An overview. Bioresour. Technol. 102, 452–460. https://doi.org/10.1016/j.biortech.2010.09.093

Kang, K., Azargohar, R., Dalai, A.K., Wang, H., 2017. Hydrogen generation via supercritical water gasification of lignin using Ni-Co/Mg-Al catalysts. Int. J. Energy Res. 41, 1835–1846. https://doi.org/10.1002/er.3739

Kang, K., Azargohar, R., Dalai, A.K., Wang, H., 2016a. Systematic screening and modification of Ni based catalysts for hydrogen generation from supercritical water gasification of lignin. Chem. Eng. J. 283, 1019–1032. https://doi.org/10.1016/j.cej.2015.08.032

Kang, K., Azargohar, R., Dalai, A.K., Wang, H., 2016b. Hydrogen production from lignin, cellulose and waste biomass via supercritical water gasification: Catalyst activity and process optimization study. Energy Convers. Manag. 117, 528–537. https://doi.org/10.1016/j.enconman.2016.03.008

Kang, K., Azargohar, R., Dalai, A.K., Wang, H., 2015. Noncatalytic gasification of lignin in supercritical water using a batch reactor for hydrogen production: An experimental and modeling study. Energy and Fuels 29, 1776–1784. https://doi.org/10.1021/ef5027345

Kou, J., Xu, J., Jin, H., Guo, L., Zhang, D., Cao, W., 2018. Evaluation of modified Ni/ZrO2 catalysts for hydrogen production by supercritical water gasification of oil-containing wastewater. Int. J. Hydrogen Energy 43, 13896–13903. https://doi.org/10.1016/j.ijhydene.2017.12.021

Kritzer, P., 2004. Corrosion in high-temperature and supercritical water and aqueous solutions: A

review. J. Supercrit. Fluids 29, 1–29. https://doi.org/10.1016/S0896-8446(03)00031-7

Kruse, A., 2008. Supercritical water gasification. Biofuels, Bioprod. Biorefining 2, 415–437. https://doi.org/10.1002/bbb.93

Kruse, A., Krupka, A., Schwarzkopf, V., Gamard, C., Henningsen, T., 2005. Influence of proteins on the hydrothermal gasification and liquefaction of biomass. 1. Comparison of different feedstocks. Ind. Eng. Chem. Res. 44, 3013–3020. https://doi.org/10.1021/ie049129y

Kumar, M., Olajire Oyedun, A., Kumar, A., 2018. A review on the current status of various hydrothermal technologies on biomass feedstock. Renew. Sustain. Energy Rev. 81, 1742–1770. https://doi.org/10.1016/j.rser.2017.05.270

Kumar, M., Olajire Oyedun, A., Kumar, A., 2016. A review on the current status of various hydrothermal technologies on biomass feedstock. Renew. Sustain. Energy Rev. https://doi.org/10.1016/j.rser.2017.05.270

Kumar, P., Sun, Y., Idem, R.O., 2008. Comparative study of Ni-based mixed oxide catalyst for carbon dioxide reforming of methane. Energy and Fuels 22, 3575–3582. https://doi.org/10.1021/ef800326q

Lee, I.G., Ihm, S.K., 2009. Catalytic gasification of glucose over Ni/activated charcoal in supercritical water. Ind. Eng. Chem. Res. 48, 1435–1442. https://doi.org/10.1021/ie8012456

Lee, I.G., Kim, M.S., Ihm, S.K., 2002. Gasification of glucose in supercritical water. Ind. Eng. Chem. Res. 41, 1182–1188. https://doi.org/10.1021/ie010066i

Lee, J.C., Lee, B., Ok, Y.S., Lim, H., 2020. Preliminary techno-economic analysis of biodiesel production over solid-biochar. Bioresour. Technol. 306, 123086. https://doi.org/10.1016/j.biortech.2020.123086

Lee, S., Posarac, D., Ellis, N., 2011. Process simulation and economic analysis of biodiesel production processes using fresh and waste vegetable oil and supercritical methanol. Chem. Eng. Res. Des. 89, 2626–2642. https://doi.org/10.1016/j.cherd.2011.05.011

Levin, D.B., Chahine, R., 2010. Challenges for renewable hydrogen production from biomass. Int. J. Hydrogen Energy 35, 4962–4969. https://doi.org/10.1016/j.ijhydene.2009.08.067

Levin, D.B., Pitt, L., Love, M., 2004. Biohydrogen production: Prospects and limitations to practical application. Int. J. Hydrogen Energy 29, 173–185. https://doi.org/10.1016/S0360-3199(03)00094-6

Li, G., Hu, L., Hill, J.M., 2006. Comparison of reducibility and stability of alumina-supported Ni catalysts prepared by impregnation and co-precipitation. Appl. Catal. A Gen. 301, 16–24. https://doi.org/10.1016/j.apcata.2005.11.013

Li, S., Lu, Y., Guo, L., Zhang, X., 2011. Hydrogen production by biomass gasification in supercritical water with bimetallic Ni-M/γAl2O3 catalysts (M = Cu, Co and Sn). Int. J. Hydrogen Energy 36, 14391–14400. https://doi.org/10.1016/j.ijhydene.2011.07.144

Li, S., Savage, P.E., Guo, L., 2019. Stability and activity maintenance of sol-gel Ni-MxOy (M=Ti, Zr, Ta) catalysts during continuous gasification of glycerol in supercritical water. J. Supercrit. Fluids 148, 137–147. https://doi.org/10.1016/j.supflu.2019.02.028

Louw, J., Schwarz, C.E., Burger, A.J., 2016. Catalytic supercritical water gasification of primary paper sludge using a homogeneous and heterogeneous catalyst: Experimental vs thermodynamic equilibrium results. Bioresour. Technol. 201, 111–120. https://doi.org/10.1016/j.biortech.2015.11.043

Lu, Y., Huang, J., Zheng, P., 2014a. Fluid hydrodynamic characteristics in supercritical water fluidized bed: A DEM simulation study. Chem. Eng. Sci. 117, 283–292. https://doi.org/10.1016/j.ces.2014.06.032

Lu, Y., Jin, H., Zhang, R., 2019. Evaluation of stability and catalytic activity of Ni catalysts for hydrogen production by biomass gasification in supercritical water. Carbon Resour. Convers. 2, 95–101. https://doi.org/10.1016/j.crcon.2019.03.001

Lu, Y., Li, S., Guo, L., 2014b. Catalysis in Supercritical Water Gasification of Biomass: Status and Prospects. pp. 343–371. https://doi.org/10.1007/978-94-017-8923-3_13

Lu, Y., Zhu, Y., Li, S., Zhang, X., Guo, L., 2014c. Behavior of nickel catalysts in supercritical water gasification of glucose: Influence of support. Biomass and Bioenergy 67, 125–136. https://doi.org/10.1016/j.biombioe.2014.04.038

Lu, Y., Zhu, Y., Li, S., Zhang, X., Guo, L., 2014d. Behavior of nickel catalysts in supercritical water gasification of glucose: Influence of support. Biomass and Bioenergy 67, 125–136. https://doi.org/10.1016/j.biombioe.2014.04.038

Lu, Y.J., Guo, L.J., Ji, C.M., Zhang, X.M., Hao, X.H., Yan, Q.H., 2006. Hydrogen production by biomass gasification in supercritical water: A parametric study. Int. J. Hydrogen Energy 31, 822–831. https://doi.org/10.1016/j.ijhydene.2005.08.011

Lu, Y.J., Jin, H., Guo, L.J., Zhang, X.M., Cao, C.Q., Guo, X., 2008. Hydrogen production by biomass gasification in supercritical water with a fluidized bed reactor. Int. J. Hydrogen Energy 33, 6066–6075. https://doi.org/10.1016/j.ijhydene.2008.07.082

Melia, P.M., Busquets, R., Ray, S., Cundy, A.B., 2018. Agricultural wastes from wheat, barley, flax and grape for the efficient removal of Cd from contaminated water. RSC Adv. 8, 40378–40386. https://doi.org/10.1039/C8RA07877G

Miller, A., Hendry, D., Wilkinson, N., Venkitasamy, C., Jacoby, W., 2012. Exploration of the gasification of Spirulina algae in supercritical water. Bioresour. Technol. 119, 41–47. https://doi.org/10.1016/j.biortech.2012.05.005

Modell, M., Reid, R., SI Amin - US Patent 4, 113, 446, 1978, U., 1978. Gasification process. Google Patents.

Mohanty, P., Nanda, S., Pant, K.K., Naik, S., Kozinski, J.A., Dalai, A.K., 2013. Evaluation of the physiochemical development of biochars obtained from pyrolysis of wheat straw, timothy grass and pinewood: Effects of heating rate. J. Anal. Appl. Pyrolysis 104, 485–493. https://doi.org/10.1016/j.jaap.2013.05.022

Muthukumar, M., Mohan, D., Rajendran, M., 2003. Optimization of mix proportions of mineral aggregates using Box Behnken design of experiments. Cem. Concr. Compos. 25, 751–758. https://doi.org/10.1016/S0958-9465(02)00116-6

Nakamura, A., Kiyonaga, E., Yamamura, Y., Shimizu, Y., Minowa, T., Noda, Y., Matsumura, Y., 2008. Gasification of catalyst-suspended chicken manure in supercritical water. J. Chem. Eng. Japan 41, 433–440. https://doi.org/10.1252/jcej.07WE289

Nalbant, M., Gökkaya, H., Sur, G., 2007. Application of Taguchi method in the optimization of cutting parameters for surface roughness in turning. Mater. Des. 28, 1379–1385. https://doi.org/10.1016/j.matdes.2006.01.008

Nanda, S., A. Kozinski, J., K. Dalai, A., 2015a. Lignocellulosic Biomass: A Review of Conversion Technologies and Fuel Products. Curr. Biochem. Eng. 3, 24–36. https://doi.org/10.2174/2213385203666150219232000

Nanda, S., Azargohar, R., Dalai, A.K., Kozinski, J.A., 2015b. An assessment on the sustainability of lignocellulosic biomass for biorefining. Renew. Sustain. Energy Rev. https://doi.org/10.1016/j.rser.2015.05.058

Nanda, S., Dalai, A.K., Berruti, F., Kozinski, J.A., 2016a. Biochar as an Exceptional Bioresource for Energy, Agronomy, Carbon Sequestration, Activated Carbon and Specialty Materials. Waste and Biomass Valorization 7, 201–235. https://doi.org/10.1007/s12649-015-9459-z

Nanda, S., Dalai, A.K., Gökalp, I., Kozinski, J.A., 2016b. Valorization of horse manure through catalytic supercritical water gasification. Waste Manag. 52, 147–158. https://doi.org/10.1016/j.wasman.2016.03.049

Nanda, S., Dalai, A.K., Kozinski, J.A., 2016c. Supercritical water gasification of timothy grass as an energy crop in the presence of alkali carbonate and hydroxide catalysts. Biomass and Bioenergy 95, 378–387. https://doi.org/10.1016/j.biombioe.2016.05.023

Nanda, Sonil, Gong, M., Hunter, H.N., Dalai, A.K., Gökalp, I., Kozinski, J.A., 2017a. An assessment of pinecone gasification in subcritical, near-critical and supercritical water. Fuel Process. Technol. 168, 84–96. https://doi.org/10.1016/j.fuproc.2017.08.017

Nanda, S., Isen, J., Dalai, A.K., Kozinski, J.A., 2016d. Gasification of fruit wastes and agro-food residues in supercritical water. Energy Convers. Manag. 110, 296–306. https://doi.org/10.1016/j.enconman.2015.11.060

Nanda, S., Li, K., Abatzoglou, N., Dalai, A.K., Kozinski, J.A., 2017. Advancements and confinements in hydrogen production technologies. Bioenergy Syst. Futur. Prospect. Biofuels Biohydrogen 373–418. https://doi.org/10.1016/B978-0-08-101031-0.00011-9

Nanda, S., Maley, J., Kozinski, J.A., Dalai, A.K., 2015c. Physico-chemical evolution in lignocellulosic feedstocks during hydrothermal pretreatment and delignification. J. Biobased Mater. Bioenergy 9, 295–308. https://doi.org/10.1166/jbmb.2015.1529

Nanda, S., Maley, J., Kozinski, J.A., Dalai, A.K., 2015d. Physico-chemical evolution in lignocellulosic feedstocks during hydrothermal pretreatment and delignification. J. Biobased Mater. Bioenergy 9, 295–308. https://doi.org/10.1166/jbmb.2015.1529

Nanda, S., Mohammad, J., Reddy, S.N., Kozinski, J.A., Dalai, A.K., 2014. Pathways of lignocellulosic biomass conversion to renewable fuels. Biomass Convers. Biorefinery. https://doi.org/10.1007/s13399-013-0097-z

Nanda, S., Mohanty, P., Pant, K.K., Naik, S., Kozinski, J.A., Dalai, A.K., 2013. Characterization of North American Lignocellulosic Biomass and Biochars in Terms of their Candidacy for Alternate Renewable Fuels. Bioenergy Res. 6, 663–677. https://doi.org/10.1007/s12155-012-9281-4

Nanda, S., Rana, R., Hunter, H.N., Fang, Z., Dalai, A.K., Kozinski, J.A., 2019a. Hydrothermal catalytic processing of waste cooking oil for hydrogen-rich syngas production. Chem. Eng.

Sci. 935–945. https://doi.org/10.1016/j.ces.2018.10.039

Nanda, Sonil, Rana, R., Zheng, Y., Kozinski, J.A., Dalai, A.K., 2017b. Insights on pathways for hydrogen generation from ethanol. Sustain. Energy Fuels 1, 1232–1245. https://doi.org/10.1039/C7SE00212B

Nanda, S., Reddy, S.N., Dalai, A.K., Kozinski, J.A., 2016e. Subcritical and supercritical water gasification of lignocellulosic biomass impregnated with nickel nanocatalyst for hydrogen production. Int. J. Hydrogen Energy 41, 4907–4921. https://doi.org/10.1016/j.ijhydene.2015.10.060

Nanda, S., Reddy, S.N., Hunter, H.N., Butler, I.S., Kozinski, J.A., 2015e. Supercritical Water Gasification of Lactose as a Model Compound for Valorization of Dairy Industry Effluents. Ind. Eng. Chem. Res. 54, 9296–9306. https://doi.org/10.1021/acs.iecr.5b02603

Nanda, S., Reddy, S.N., Hunter, H.N., Dalai, A.K., Kozinski, J.A., 2015f. Supercritical water gasification of fructose as a model compound for waste fruits and vegetables. J. Supercrit. Fluids 104, 112–121. https://doi.org/10.1016/j.supflu.2015.05.009

Nanda, S., Reddy, S.N., Hunter, H.N., Vo, D.V.N., Kozinski, J.A., Gökalp, I., 2019b. Catalytic subcritical and supercritical water gasification as a resource recovery approach from waste tires for hydrogen-rich syngas production. J. Supercrit. Fluids 154, 104627. https://doi.org/10.1016/j.supflu.2019.104627

Nanda, S., Reddy, S.N., Mitra, S.K., Kozinski, J.A., 2016f. The progressive routes for carbon capture and sequestration. Energy Sci. Eng. 4, 99–122. https://doi.org/10.1002/ese3.117

Nanda, S., Reddy, S.N., Vo, D.V.N., Sahoo, B.N., Kozinski, J.A., 2018. Catalytic gasification of wheat straw in hot compressed (subcritical and supercritical) water for hydrogen production. Energy Sci. Eng. 6, 448–459. https://doi.org/10.1002/ese3.219

Naqi, A., Kuhn, J.N., Joseph, B., 2019. Techno-economic analysis of producing liquid fuels from biomass via anaerobic digestion and thermochemical conversion. Biomass and Bioenergy 130, 105395. https://doi.org/10.1016/j.biombioe.2019.105395

Nikoo, M.K., Saeidi, S., Lohi, A., 2015. A comparative thermodynamic analysis and experimental studies on hydrogen synthesis by supercritical water gasification of glucose. Clean Technol. Environ. Policy 17, 2267–2288. https://doi.org/10.1007/s10098-015-0965-2

Norouzi, O., Safari, F., Jafarian, S., Tavasoli, A., Karimi, A., 2017. Hydrothermal gasification performance of Enteromorpha intestinalis as an algal biomass for hydrogen-rich gas production using Ru promoted Fe–Ni/Γ-Al2O3 nanocatalysts. Energy Convers. Manag. 141, 63–71. https://doi.org/10.1016/j.enconman.2016.04.083

Noussan, M., Raimondi, P.P., Scita, R., Hafner, M., 2020. The Role of Green and Blue Hydrogen in the Energy Transition—A Technological and Geopolitical Perspective. Sustainability 13, 298. https://doi.org/10.3390/su13010298

O'Sullivan, A.C., 1997. Cellulose: The structure slowly unravels. Cellulose 4, 173–207. https://doi.org/10.1023/A:1018431705579

Okolie, J.A., Nanda, S., Dalai, A.K., Berruti, F., Kozinski, J.A., 2020a. A review on subcritical and supercritical water gasification of biogenic, polymeric and petroleum wastes to hydrogen-rich synthesis gas. Renew. Sustain. Energy Rev.

https://doi.org/10.1016/j.rser.2019.109546

Okolie, J.A., Nanda, S., Dalai, A.K., Kozinski, J.A., 2020b. Optimization and modeling of process parameters during hydrothermal gasification of biomass model compounds to generate hydrogen-rich gas products. Int. J. Hydrogen Energy 45, 18275–18288. https://doi.org/10.1016/j.ijhydene.2019.05.132

Okolie, J.A., Nanda, S., Dalai, A.K., Kozinski, J.A., 2020c. Hydrothermal gasification of soybean straw and flax straw for hydrogen-rich syngas production: Experimental and thermodynamic modeling. Energy Convers. Manag. 208, 112545. https://doi.org/10.1016/j.enconman.2020.112545

Okolie, J.A., Nanda, S., Dalai, A.K., Kozinski, J.A., 2020d. Chemistry and Specialty Industrial Applications of Lignocellulosic Biomass. Waste and Biomass Valorization. https://doi.org/10.1007/s12649-020-01123-0

Okolie, J.A., Patra, B.R., Mukherjee, A., Nanda, S., Dalai, A.K., Kozinski, J.A., 2021. Futuristic applications of hydrogen in energy, biorefining, aerospace, pharmaceuticals and metallurgy. Int. J. Hydrogen Energy. https://doi.org/10.1016/j.ijhydene.2021.01.014

Okolie, J.A., Rana, R., Nanda, S., Dalai, A.K., Kozinski, J.A., 2019. Supercritical water gasification of biomass: A state-of-the-art review of process parameters, reaction mechanisms and catalysis. Sustain. Energy Fuels 3, 578–598. https://doi.org/10.1039/c8se00565f

Onwudili, J.A., Williams, P.T., 2009. Role of sodium hydroxide in the production of hydrogen gas from the hydrothermal gasification of biomass. Int. J. Hydrogen Energy 34, 5645–5656.

https://doi.org/10.1016/j.ijhydene.2009.05.082

Özdenkçi, K., De Blasio, C., Sarwar, G., Melin, K., Koskinen, J., Alopaeus, V., 2019. Techno-economic feasibility of supercritical water gasification of black liquor. Energy 189, 116284. https://doi.org/10.1016/j.energy.2019.116284

Papadikis, K., Gu, S., Bridgwater, A. V., Gerhauser, H., 2009. Application of CFD to model fast pyrolysis of biomass. Fuel Process. Technol. 90, 504–512. https://doi.org/10.1016/j.fuproc.2009.01.010

Parparita, E., Uddin, M.A., Watanabe, T., Kato, Y., Yanik, J., Vasile, C., 2015. Gas production by steam gasification of polypropylene/biomass waste composites in a dual-bed reactor. J. Mater. Cycles Waste Manag. 17, 756–768. https://doi.org/10.1007/s10163-014-0308-0

Peters, L., Hussain, A., Follmann, M., Melin, T., Hägg, M.B., 2011. CO 2 removal from natural gas by employing amine absorption and membrane technology-A technical and economical analysis. Chem. Eng. J. 172, 952–960. https://doi.org/10.1016/j.cej.2011.07.007

Peterson, A.A., Vogel, F., Lachance, R.P., Fröling, M., Antal, M.J., Tester, J.W., 2008. Thermochemical biofuel production in hydrothermal media: A review of sub- and supercritical water technologies. Energy Environ. Sci. 1, 32–65. https://doi.org/10.1039/b810100k

Pierella, L.B., Renzini, S., Anunziata, O.A., 2005. Catalytic degradation of high density polyethylene over microporous and mesoporous materials. Microporous Mesoporous Mater. 81, 155–159. https://doi.org/10.1016/j.micromeso.2004.11.015

Pińkowska, H., Wolak, P., Złocińska, A., 2011. Hydrothermal decomposition of xylan as a

model substance for plant biomass waste - Hydrothermolysis in subcritical water. Biomass and Bioenergy 35, 3902–3912. https://doi.org/10.1016/j.biombioe.2011.06.015

Prasad, S., Singh, A., Joshi, H.C., 2007. Ethanol as an alternative fuel from agricultural, industrial and urban residues. Resour. Conserv. Recycl. 50, 1–39. https://doi.org/10.1016/j.resconrec.2006.05.007

Promdej, C., Matsumura, Y., 2011. Temperature effect on hydrothermal decomposition of glucose in sub- and supercritical water. Ind. Eng. Chem. Res. 50, 8492–8497. https://doi.org/10.1021/ie200298c

Qian, Y., Zuo, C., Tan, J., He, J., 2007. Structural analysis of bio-oils from sub-and supercritical water liquefaction of woody biomass. Energy 32, 196–202. https://doi.org/10.1016/j.energy.2006.03.027

Qing, Q., Guo, Q., Zhou, L., Gao, X., Lu, X., Zhang, Y., 2017. Comparison of alkaline and acid pretreatments for enzymatic hydrolysis of soybean hull and soybean straw to produce fermentable sugars. Ind. Crops Prod. 109, 391–397. https://doi.org/10.1016/j.indcrop.2017.08.051

Rana, R., Nanda, S., Maclennan, A., Hu, Y., Kozinski, J.A., Dalai, A.K., 2019. Comparative evaluation for catalytic gasification of petroleum coke and asphaltene in subcritical and supercritical water. J. Energy Chem. 107–118. https://doi.org/10.1016/j.jechem.2018.05.012

Rana, R., Nanda, S., Reddy, S.N., Dalai, A.K., Kozinski, J.A., Gökalp, I., 2020. Catalytic gasification of light and heavy gas oils in supercritical water. J. Energy Inst. 93, 2025–2032. https://doi.org/10.1016/j.joei.2020.04.018

Reddy, S.N., Ding, N., Nanda, S., Dalai, A.K., Kozinski, J.A., 2014a. Supercritical water gasification of biomass in diamond anvil cells and fluidized beds. Biofuels, Bioprod. Biorefining 8, 728–737. https://doi.org/10.1002/bbb.1514

Reddy, S.N., Nanda, S., Dalai, A.K., Kozinski, J.A., 2014b. Supercritical water gasification of biomass for hydrogen production. Int. J. Hydrogen Energy. https://doi.org/10.1016/j.ijhydene.2014.02.125

Reddy, S.N., Nanda, S., Hegde, U.G., Hicks, M.C., Kozinski, J.A., 2015. Ignition of hydrothermal flames. RSC Adv. 5, 36404–36422. https://doi.org/10.1039/c5ra02705e

Reddy, S.N., Nanda, S., Kozinski, J.A., 2016. Supercritical water gasification of glycerol and methanol mixtures as model waste residues from biodiesel refinery. Chem. Eng. Res. Des. 113, 17–27. https://doi.org/10.1016/j.cherd.2016.07.005

Ren, R., Han, X., Zhang, H., Lin, H., Zhao, J., Zheng, Y., Wang, H., 2018. High yield bio-oil production by hydrothermal liquefaction of a hydrocarbon-rich microalgae and biocrude upgrading. Carbon Resour. Convers. 1, 153–159. https://doi.org/10.1016/j.crcon.2018.07.008

Resende, F.L.P., Neff, M.E., Savage, P.E., 2007. Noncatalytic gasification of cellulose in supercritical water. Energy and Fuels 21, 3637–3643. https://doi.org/10.1021/ef7002206

Resende, F.L.P., Savage, P.E., 2010. Kinetic model for noncatalytic supercritical water gasification of cellulose and lignin. AIChE J. 56, 2412–2420. https://doi.org/10.1002/aic.12165

Rocha, T.C.R., Hävecker, M., Knop-Gericke, A., Schlögl, R., 2014. Promoters in heterogeneous

catalysis: The role of Cl on ethylene epoxidation over Ag. J. Catal. 312, 12–16. https://doi.org/10.1016/j.jcat.2014.01.002

Rodriguez Correa, C., Kruse, A., 2018a. Supercritical water gasification of biomass for hydrogen production – Review. J. Supercrit. Fluids 133, 573–590. https://doi.org/10.1016/j.supflu.2017.09.019

Rodriguez Correa, C., Kruse, A., 2018b. Supercritical water gasification of biomass for hydrogen production – Review. J. Supercrit. Fluids 133, 573–590. https://doi.org/10.1016/j.supflu.2017.09.019

Roh, H.S., Jun, K.W., Dong, W.S., Chang, J.S., Park, S.E., Joe, Y. Il, 2002. Highly active and stable Ni/Ce-ZrO2 catalyst for H2 production from methane, in: Journal of Molecular Catalysis A: Chemical. Elsevier, pp. 137–142. https://doi.org/10.1016/S1381-1169(01)00358-2

Saba, A., McGaughy, K., Toufiq Reza, M., 2019. Techno-economic assessment of co-hydrothermal carbonization of a coal-Miscanthus blend. Energies 12. https://doi.org/10.3390/en12040630

Sadoun, O., Rezgui, F., G'Sell, C., 2018. Optimization of valsartan encapsulation in biodegradables polyesters using Box-Behnken design. Mater. Sci. Eng. C 90, 189–197. https://doi.org/10.1016/j.msec.2018.04.041

Salkuyeh, Y.K., Saville, B.A., MacLean, H.L., 2018. Techno-economic analysis and life cycle assessment of hydrogen production from different biomass gasification processes. Int. J. Hydrogen Energy 43, 9514–9528. https://doi.org/10.1016/j.ijhydene.2018.04.024

Samiee-Zafarghandi, R., Karimi-Sabet, J., Abdoli, M.A., Karbassi, A., 2018. Supercritical water gasification of microalga Chlorella PTCC 6010 for hydrogen production: Box-Behnken optimization and evaluating catalytic effect of MnO2/SiO2 and NiO/SiO2. Renew. Energy 126, 189–201. https://doi.org/10.1016/j.renene.2018.03.043

Santangelo, S., Messina, G., Faggio, G., Abdul Rahim, S.H., Milone, C., 2012. Effect of sulphuric-nitric acid mixture composition on surface chemistry and structural evolution of liquid-phase oxidised carbon nanotubes. J. Raman Spectrosc. 43, 1432–1442. https://doi.org/10.1002/jrs.4097

Sarangi, P.K., Nanda, S., Mohanty, P., 2018. Recent advancements in biofuels and bioenergy utilization, Recent Advancements in Biofuels and Bioenergy Utilization. https://doi.org/10.1007/978-981-13-1307-3

Sarker, T.R., Nanda, S., Dalai, A.K., Meda, V., 2021. A Review of Torrefaction Technology for Upgrading Lignocellulosic Biomass to Solid Biofuels. BioEnergy Res. 1–25. https://doi.org/10.1007/s12155-020-10236-2

Savage, P.E., 2009. A perspective on catalysis in sub- and supercritical water. J. Supercrit. Fluids 47, 407–414. https://doi.org/10.1016/j.supflu.2008.09.007

Schmelz, W.J., Hochman, G., Miller, K.G., 2020. Total cost of carbon capture and storage implemented at a regional scale: northeastern and midwestern United States. Interface Focus 10, 20190065. https://doi.org/10.1098/rsfs.2019.0065

Schweitzer, D., Albrecht, F.G., Schmid, M., Beirow, M., Spörl, R., Dietrich, R.U., Seitz, A., 2018. Process simulation and techno-economic assessment of SER steam gasification for

hydrogen production. Int. J. Hydrogen Energy 43, 569–579. https://doi.org/10.1016/j.ijhydene.2017.11.001

Shafiqah, M.N.N., Tran, H.N., Nguyen, T.D., Phuong, P.T.T., Abdullah, B., Lam, S.S., Nguyen-Tri, P., Kumar, R., Nanda, S., Vo, D.V.N., 2020. Ethanol CO2 reforming on La2O3 and CeO2-promoted Cu/Al2O3 catalysts for enhanced hydrogen production. Int. J. Hydrogen Energy 45, 18398–18410. https://doi.org/10.1016/j.ijhydene.2019.10.024

Shahkarami, S., Azargohar, R., Dalai, A.K., Soltan, J., 2015. Breakthrough CO2 adsorption in bio-based activated carbons. J. Environ. Sci. (China) 34, 68–76. https://doi.org/10.1016/j.jes.2015.03.008

Silva, V., 2018. Statistical Approaches With Emphasis on Design of Experiments Applied to Chemical Processes, Statistical Approaches With Emphasis on Design of Experiments Applied to Chemical Processes. https://doi.org/10.5772/65616

Simeonov, K., Kim, J.H., Ferrari, D., Huelsman, D., Budroni, G., Corthals, S., Pagán-Torres, Y.J., 2014. CoMoS/K catalysts for higher alcohol synthesis from syngas prepared by mechano-chemical activation of molybdenite. Catal. Sci. Technol. 4, 922–924. https://doi.org/10.1039/c3cy00865g

Sinağ, A., Kruse, A., Rathert, J., 2004. Influence of the Heating Rate and the Type of Catalyst on the Formation of Key Intermediates and on the Generation of Gases during Hydropyrolysis of Glucose in Supercritical Water in a Batch Reactor. Ind. Eng. Chem. Res. 43, 502–508. https://doi.org/10.1021/ie030475+

Singh, S., Kumar, R., Setiabudi, H.D., Nanda, S., Vo, D.V.N., 2018. Advanced synthesis

strategies of mesoporous SBA-15 supported catalysts for catalytic reforming applications: A state-of-the-art review. Appl. Catal. A Gen. 559, 57–74. https://doi.org/10.1016/j.apcata.2018.04.015

Sinnott, R.K., Towler, G., 2013. Chemical Engineering Design, Chemical Engineering Design. https://doi.org/10.1016/C2009-0-61216-2

Sivasangar, S., Zainal, Z., Salmiaton, A., Taufiq-Yap, Y.H., 2015. Supercritical water gasification of empty fruit bunches from oil palm for hydrogen production. Fuel 143, 563–569. https://doi.org/10.1016/j.fuel.2014.11.073

Soni, S.K., Goyal, N., Gupta, J.K., Soni, R., 2012. Enhanced production of α-amylase from bacillus subtilis subsp. spizizenii in solid state fermentation by response surface methodology and its evaluation in the hydrolysis of raw potato starch. Starch/Staerke 64, 64–77. https://doi.org/10.1002/star.201100119

Sun, J., Xu, L., Dong, G. hua, Nanda, S., Li, H., Fang, Z., Kozinski, J.A., Dalai, A.K., 2020. Subcritical water gasification of lignocellulosic wastes for hydrogen production with Co modified Ni/Al2O3 catalysts. J. Supercrit. Fluids 162, 104863. https://doi.org/10.1016/j.supflu.2020.104863

Sun, P., Heng, M., Sun, S.H., Chen, J., 2011. Analysis of liquid and solid products from liquefaction of paulownia in hot-compressed water. Energy Convers. Manag. 52, 924–933. https://doi.org/10.1016/j.enconman.2010.08.020

Susanti, R.F., Veriansyah, B., Kim, J.D., Kim, J., Lee, Y.W., 2010. Continuous supercritical water gasification of isooctane: A promising reactor design. Int. J. Hydrogen Energy 35,

1957–1970. https://doi.org/10.1016/j.ijhydene.2009.12.157

Swamy, G.J., Sangamithra, A., Chandrasekar, V., 2014. Response surface modeling and process optimization of aqueous extraction of natural pigments from Beta vulgaris using Box-Behnken design of experiments. Dye. Pigment. 111, 64–74. https://doi.org/10.1016/j.dyepig.2014.05.028

Tang, H., Kitagawa, K., 2005. Supercritical water gasification of biomass: Thermodynamic analysis with direct Gibbs free energy minimization. Chem. Eng. J. 106, 261–267. https://doi.org/10.1016/j.cej.2004.12.021

Tarley, C.R.T., Silveira, G., dos Santos, W.N.L., Matos, G.D., da Silva, E.G.P., Bezerra, M.A., Miró, M., Ferreira, S.L.C., 2009. Chemometric tools in electroanalytical chemistry: Methods for optimization based on factorial design and response surface methodology. Microchem. J. 92, 58–67. https://doi.org/10.1016/j.microc.2009.02.002

Tavasoli, A., Barati, M., Karimi, A., 2016. Sugarcane bagasse supercritical water gasification in presence of potassium promoted copper nano-catalysts supported on γ-Al2O3. Int. J. Hydrogen Energy 41, 174–180. https://doi.org/10.1016/j.ijhydene.2015.09.026

Taylor, A.D., DiLeo, G.J., Sun, K., 2009. Hydrogen production and performance of nickel based catalysts synthesized using supercritical fluids for the gasification of biomass. Appl. Catal. B Environ. 93, 126–133. https://doi.org/10.1016/j.apcatb.2009.09.021

Thamizhmanii, S., Saparudin, S., Hasan, S., 2007. Analyses of surface roughness by turning process using Taguchi method. J. Achiev. Mater. Manuf. Eng. 20, 503–505. https://doi.org/10.1007/s00170-006-0576-6

Thi Mai Hoa, L., 2018. Characterization of multi-walled carbon nanotubes functionalized by a mixture of HNO3/H2SO4. Diam. Relat. Mater. 89, 43–51. https://doi.org/10.1016/j.diamond.2018.08.008

Tiong, L., Komiyama, M., Uemura, Y., Nguyen, T.T., 2016. Catalytic supercritical water gasification of microalgae: Comparison of Chlorella vulgaris and Scenedesmus quadricauda. J. Supercrit. Fluids 107, 408–413. https://doi.org/10.1016/j.supflu.2015.10.009

Toor, S.S., Rosendahl, L., Rudolf, A., 2011. Hydrothermal liquefaction of biomass: A review of subcritical water technologies. Energy. https://doi.org/10.1016/j.energy.2011.03.013

Tumuluru, J.S., Wright, C.T., Hess, J.R., Kenney, K.L., 2011. A review of biomass densification systems to develop uniform feedstock commodities for bioenergy application. Biofuels, Bioprod. Biorefining 5, 683–707. https://doi.org/10.1002/bbb.324

Turton, R., Bailie, R., Whiting, W., Shaeiwitz, J., 1998. Analysis, synthesis, and design of chemical processes, Choice Reviews Online. https://doi.org/10.5860/choice.36-0974

Tushar, M.S.H.K., Dimaria, P.C., Al-Salem, S.M., Dutta, A., Xu, C.C., 2020. Biohydrogen Production by Catalytic Supercritical Water Gasification: A Comparative Study. ACS Omega 5, 15390–15401. https://doi.org/10.1021/acsomega.9b01782

Tushar, M.S.H.K., Dutta, A., Xu, C., 2015. Simulation and kinetic modeling of supercritical water gasification of biomass. Int. J. Hydrogen Energy 40, 4481–4493. https://doi.org/10.1016/j.ijhydene.2015.02.033

Ulrich, G.D., Vasudevan, P.T., 2018. Chemical Engineering Process Design and Economics: A Practical Guide, second ed.

Verma, R., Sam, A.A., Ghosh, P., 2015. CFD analysis of turbo expander for cryogenic refrigeration and liquefaction cycles. Phys. Procedia 67, 373–378. https://doi.org/10.1016/j.phpro.2015.06.043

Vlysidis, A., Binns, M., Webb, C., Theodoropoulos, C., 2011. A techno-economic analysis of biodiesel biorefineries: Assessment of integrated designs for the co-production of fuels and chemicals. Energy 36, 4671–4683. https://doi.org/10.1016/j.energy.2011.04.046

Wan, C., Zhou, Y., Li, Y., 2011. Liquid hot water and alkaline pretreatment of soybean straw for improving cellulose digestibility. Bioresour. Technol. 102, 6254–6259. https://doi.org/10.1016/j.biortech.2011.02.075

Wan, W., 2016. An innovative system by integrating the gasification unit with the supercritical water unit to produce clean syngas for solid oxide fuel cell (SOFC): System performance assessment. Int. J. Hydrogen Energy 41, 22698–22710. https://doi.org/10.1016/j.ijhydene.2016.09.146

Wang, J., Wan, W., 2009. Experimental design methods for fermentative hydrogen production: A review. Int. J. Hydrogen Energy 34, 235–244. https://doi.org/10.1016/j.ijhydene.2008.10.008

Wang, S., Lu, G.Q., 1998. Role of CeO2 in Ni/CeO2-Al2O3 catalysts for carbon dioxide reforming of methane. Appl. Catal. B Environ. 19, 267–277. https://doi.org/10.1016/S0926-3373(98)00081-2

Withag, J.A.M., Smeets, J.R., Bramer, E.A., Brem, G., 2012. System model for gasification of biomass model compounds in supercritical water - A thermodynamic analysis. J. Supercrit.

Fluids 61, 157–166. https://doi.org/10.1016/j.supflu.2011.10.012

Xu, D., Wang, S., Hu, X., Chen, C., Zhang, Q., Gong, Y., 2009. Catalytic gasification of glycine and glycerol in supercritical water. Int. J. Hydrogen Energy 34, 5357–5364. https://doi.org/10.1016/j.ijhydene.2008.08.055

Xu, X., Matsumura, Y., Stenberg, J., Antal, M.J., 1996. Carbon-catalyzed gasification of organic feedstocks in supercritical Water. Ind. Eng. Chem. Res. 35, 2522–2530. https://doi.org/10.1021/ie950672b

Xu, Z., Wang, Q., Jiang, Z.H., Yang, X. xin, Ji, Y., 2007. Enzymatic hydrolysis of pretreated soybean straw. Biomass and Bioenergy 31, 162–167. https://doi.org/10.1016/j.biombioe.2006.06.015

Xue, Q., Fox, R.O., 2014. Reprint of: Multi-fluid CFD modeling of biomass gasification in polydisperse fluidized-bed gasifiers. Powder Technol. 265, 23–34. https://doi.org/10.1016/j.powtec.2014.04.006

Yakaboylu, O., Harinck, J., Smit, K.G., de Jong, W., 2015. Supercritical water gasification of biomass: A literature and technology overview. Energies 8, 859–894. https://doi.org/10.3390/en8020859

Yang, H., Yan, R., Chen, H., Lee, D.H., Zheng, C., 2007. Characteristics of hemicellulose, cellulose and lignin pyrolysis. Fuel 86, 1781–1788. https://doi.org/10.1016/j.fuel.2006.12.013

Yanik, J., Ebale, S., Kruse, A., Saglam, M., Yüksel, M., 2007. Biomass gasification in supercritical water: Part 1. Effect of the nature of biomass. Fuel 86, 2410–2415.

https://doi.org/10.1016/j.fuel.2007.01.025

Yates, J., Daiyan, R., Patterson, R., Egan, R., Amal, R., Ho-Baille, A., Chang, N.L., 2020. Techno-economic Analysis of Hydrogen Electrolysis from Off-Grid Stand-Alone Photovoltaics Incorporating Uncertainty Analysis. https://doi.org/10.1016/j.xcrp.2020.100209

Yetilmezsoy, K., Demirel, S., Vanderbei, R.J., 2009. Response surface modeling of Pb(II) removal from aqueous solution by Pistacia vera L.: Box-Behnken experimental design. J. Hazard. Mater. 171, 551–562. https://doi.org/10.1016/j.jhazmat.2009.06.035

Yoshida, T., Matsumura, Y., 2009. Reactor Development for supercritical water gasification of 4.9 wt% glucose solution at 673 k by using computational fluid dynamics. Ind. Eng. Chem. Res. 48, 8381–8386. https://doi.org/10.1021/ie9002188

Yoshida, T., Matsumura, Y., 2001. Gasification of cellulose, xylan, and lignin mixtures in supercritical water, in: Industrial and Engineering Chemistry Research. American Chemical Society, pp. 5469–5474. https://doi.org/10.1021/ie0101590

Yoshida, T., Oshima, Y., Matsumura, Y., 2004. Gasification of biomass model compounds and real biomass in supercritical water. Biomass and Bioenergy 26, 71–78. https://doi.org/10.1016/S0961-9534(03)00063-1

Zhang, L., Champagne, P., Xu, C., 2011a. Screening of supported transition metal catalysts for hydrogen production from glucose via catalytic supercritical water gasification. Int. J. Hydrogen Energy 36, 9591–9601. https://doi.org/10.1016/j.ijhydene.2011.05.077

Zhang, L., Champagne, P., Xu, C., 2011b. Screening of supported transition metal catalysts for

hydrogen production from glucose via catalytic supercritical water gasification. Int. J. Hydrogen Energy 36, 9591–9601. https://doi.org/10.1016/j.ijhydene.2011.05.077

Zhang, L., Xu, C. (Charles), Champagne, P., 2010. Overview of recent advances in thermo-chemical conversion of biomass. Energy Convers. Manag. 51, 969–982. https://doi.org/10.1016/j.enconman.2009.11.038

Zhang, R., Jiang, W., Cheng, L., Sun, B., Sun, D., Bi, J., 2010. Hydrogen production from lignite via supercritical water in flow-type reactor. Int. J. Hydrogen Energy 35, 11810–11815. https://doi.org/10.1016/j.ijhydene.2010.01.029

Zhang, Y., Li, L., Xu, P., Liu, B., Shuai, Y., Li, B., 2019. Hydrogen production through biomass gasification in supercritical water: A review from exergy aspect. Int. J. Hydrogen Energy 44, 15727–15736. https://doi.org/10.1016/j.ijhydene.2019.01.151

Zhu, B., Li, S., Wang, W., Zhang, H., 2019. Supercritical water synthesized Ni/ZrO2 catalyst for hydrogen production from supercritical water gasification of glycerol. Int. J. Hydrogen Energy 44, 30917–30926. https://doi.org/10.1016/j.ijhydene.2019.10.044

Zhuang, R., Wang, X., Guo, M., Zhao, Y., El-Farra, N.H., Palazoglu, A., 2020. Waste-to-hydrogen: Recycling HCl to produce H2 and Cl2. Appl. Energy 259, 114184. https://doi.org/10.1016/j.apenergy.2019.114184

Ziyai, M.R., Mehrpooya, M., Aghbashlo, M., Omid, M., Alsagri, A.S., Tabatabaei, M., 2019. A techno-economic analysis of biodiesel biorefineries: Assessment of integrated designs for the co-production of fuels and chemicals. Int. J. Hydrogen Energy 44, 17845–17862. https://doi.org/10.1016/j.ijhydene.2019.05.017

Zöhrer, H., Vogel, F., 2013. Hydrothermal catalytic gasification of fermentation residues from a biogas plant. Biomass and Bioenergy 53, 138–148. https://doi.org/10.1016/j.biombioe.2012.12.030

Appendix A: GC Calibration data and Temperature and Pressure profile and mass balance calculations.

A.1: GC Calibration data

The concentration of the standard gases used for the calibration of our Agilent GC 7820A gas chromatography system is shown in Table A.1.

Table A.1: Concentration of standard gases used for GC calibration.

Gas	Concentration
Propane	0.2%
Acetylene	0.5%
Propylene	0.5%
Ethane	0.5%
Oxygen	2%
Ethylene	3%
Methane	6%
Carbon dioxide	7%
Carbon monoxide	8%
Hydrogen	10%
Nitrogen	Balance

A.2: Temperature profile

Figure A.1: Temperature profile of the SCWG batch reactor during heating.

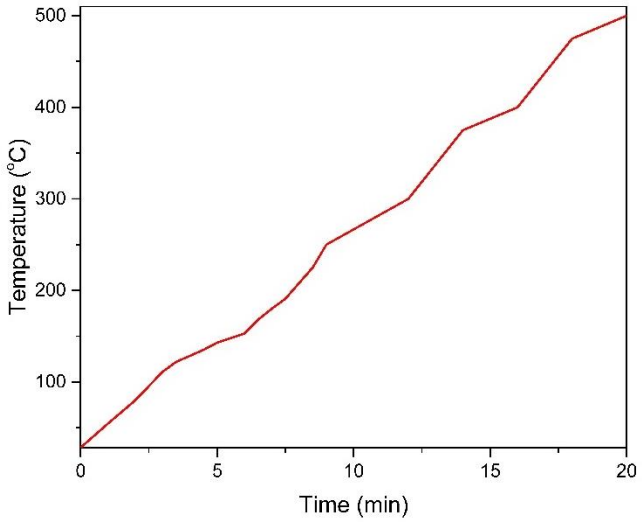

Figure A.2: Pressure profile of the SCWG batch reactor during heating.

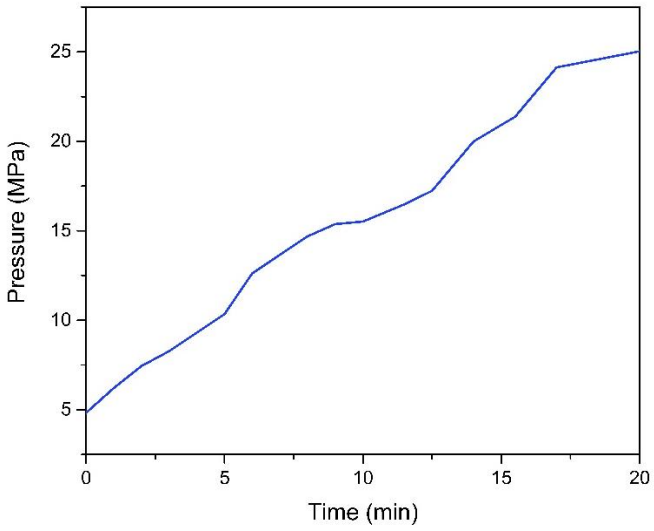

Figure A.3: Temperature profile of the SCWG batch reactor during holdup.

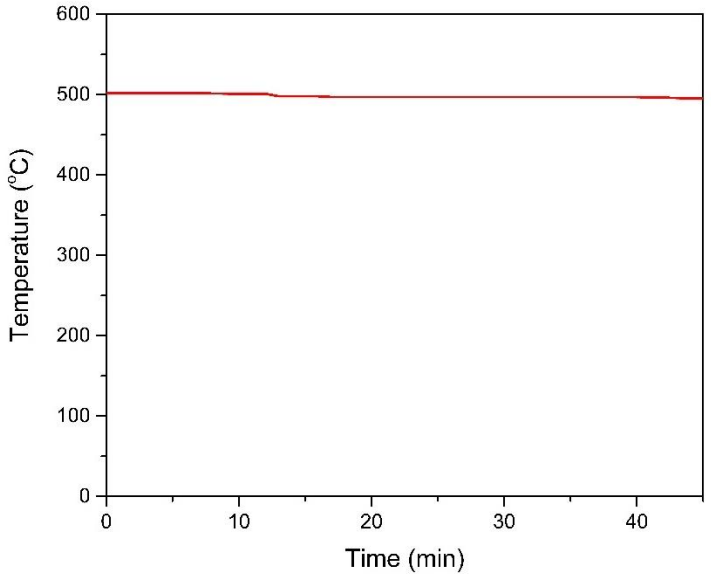

Figure A.4: Temperature profile of the SCWG batch reactor during holdup.

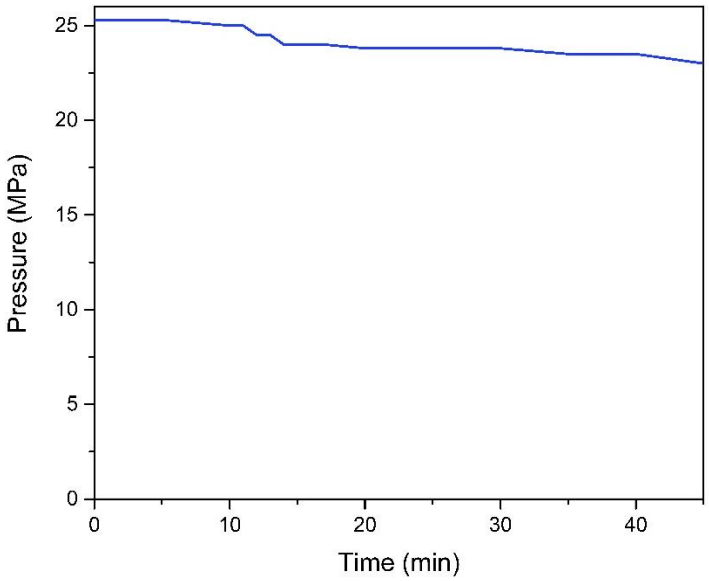

Mass balance calculations

The mass of the solid and liquid products was obtained by measuring the weight of the samples recovered after SCWG experiments. On the contrary, the mass of the gaseous products was calculated based on the individual gas yields and their molecular weight.

The mass of each samples recovered is expressed as a fraction of the mass of the biomass used for the experiment expressed in percentage. After obtaining the weight percentage of each SCWG products, the overall mass balance was estimated by adding the weight percentage of solid, liquid, and gaseous products.

For example, in experiment #1 of chapter 4 (Table 4.3): 1 g of biomass produces 0.186 g of hydrochars, 0.550 g of liquid products and 0.0.151 g of gaseous products. Then the overall mass balance would be calculated as follow:

Mass percentage of solid = 0.186/1 x 100 = 18.6%

Mass percentage of liquids = 0.550/1 x 100 = 55%

Mass percentage of gases = 0.151/1 x 100 = 15.1%

Overall mass balance = 18.6 + 55 + 15.1 = 88.7%.

Appendix B: Catalyst preparation calculations

B.1: Catalyst preparation calculations

For a pre-determined number of catalysts loading (L_{metal} in grams), the amount of precursors nNprecursor (g) required for the synthesis of the catalyst is determined from equation B.1

$$nNprecursor = \frac{m_{cat}\ X\ L_{metal}}{m_{metal}}\ x\ \frac{mm_{precursor}}{P_{purity}} \quad \text{(B.1)}$$

Where m_{cat} (g) is the mass of the catalysts to be synthesized

M_{metal} (g/mol) is the atomic weight of the metal in g/mol.

$MM_{precursor}$ is the molecular weight of Ni metal precursor.

P_{purity} is the purity of the metal precursor.

The amount of promoter precursor nP_{cursor} (g) required to synthesize a specified number of catalysts is determined from Equation A.2.

$$nPprecursor = \frac{m_{cat}\ X\ L_{metal}}{m_{metal}}\ x\ \frac{mp_{precursor}}{P_{xpurity}} \text{ x Ro/w} \quad \text{(B.2)}$$

Where Ro/w is the ratio of the promoter atom to the metal atom molar ratio and $P_{xpurity}$ is the purity of the promoter precursor. $Mp_{precursor}$ is the mass of promoter precursor.

The weight of catalysts support required for the preparation of a specific number of catalysts is calculated from Equation A.3.

$$Msupport = \ m_{cat}\ x\ \left(1 - \frac{L_{metal}}{100}\right) - (\frac{mp_{precursor}\ X\ pp_{purity}}{mp_{precursor}}\ x\ \frac{m_{promoter}}{m_{cat}}))$$

(B.3)

Where $M_{promoter}$ is the atomic weight of the promoter expressed in g/mol.

Appendix C: Additional data for Aspen Plus simulation

C.1: Details of Calculator block

Calculator name: DECOMP

Import variables: ULT, WATER.

Export variables: H_2O, ASH, CARB, H_2, AN2, SULF, O_2, MAXCC, PROXFC, PROXAS, ULTFC, ULTAS

Note:

ULT is defined as the vector that is used to assess the ultimate analysis of the biomass.

WATER is a defined variable that corresponds to the water content of proximate analysis of biomass.

CARB, AN2 and SULF represents the content of carbon, Nitrogen, and sulfur respectively.

MAXCC represents the carbon conversion efficiency.

PROXFC and PROXAS represents proximate analysis with unburnt carbon and ash, respectively.

ULTFC and ULTAS represents ultimate analysis with unburnt carbon and ash, respectively.

C2: Fortran subroutine statements

Table C.1: Fortran subroutine code used to decompose biomass.

```
c     fact is the factor to convert the ultimate analysis to
c     a wet basis
c     NB! water is the %moisture on a wet basis, but all the other
c          components are on a dry basis.
      fact = (100-water)/100
      h2o = water/100
      ash = ult(1) / 100 * fact
      carb = ult(2) / 100 * fact
      h2 = ult(3) / 100 * fact
      an2 = ult(4) / 100 * fact
      cl2 = ult(5) / 100 * fact
      sulf = ult(6) / 100 * fact
      o2 = ult(7) / 100 * fact
      WRITE (NTERM, 100) fact
  100 FORMAT ("Conversion Factor",4f10.2)
c     Changing ash to include some unburned carbon
C     Calculating the total masses leaving as carbon and ash (slag)
      unbc = (1-maxcc) * carb
      carb = carb - unbc
      ash = ash + unbc
C     Calculating the composition of the ash (slag)
C     For proximate and ultimate analysis...
C     Fixed carbon:
      IF (ash .GT. 0) THEN
        proxfc = unbc/ash*100
      ELSE
        proxfc = 100
      END IF
      ultfc = proxfc
C     Ash (as component of total ash mass):
      proxas = 100 - proxfc
      ultas = proxas
```

Table C2: Fortran code used to calculate the biomass-to-water (BTW) ratio

```
import variables
WATER
Export variables
```

SSTRAW
Code
SSTRAW = 0.1*WATER

Appendix D: Matlab Code

```
texp=[0 5 10 15 20 25 30 35 40 45 50 55 60];

%Define the error function

function  error = err(KI)

%run inputvalue which indicates the concentration versus time profile from
experiments.

run inputvalue;

%INPUT VALUE EXPORETED AND NAMED inputvalue as the concentration of gaseous
species from experimental data

% ************ Initial Guess for Rate Constants **************%

KI = [0.0011 0.000462 0.001283 0.000952 0.00376 0.000503 0.000094];

%first guess values of rate constants ki - k7


% Define initial concentration and experimental values

CExp = [CCO;  CH2; CCO2;  CCH4; CBIOMASS;  CLIQUID; CH2O];
Cini = CExp(:,2);
tspan = (0:5:60);


% ************ Solving Ordinary Differential Equations **************
[t,C] = ode45(@KinODE,tspan,Cini,[],KI);

%Display results of the ODEs


disp(C);
CCOc=C(:,1)';
CH2c=C(:,2)';
CCO2c=C(:,3)';
CCH4c=C(:,4)';
CBIOMASSc=C(:,5)';
CLIQUIDc=C(:,6)';
CH2Oc=C(:,7)';
```

```
CCOcal=[CCOc(t==0),CCOc(t==5),CCOc(t==10),
CCOc(t==15),CCOc(t==20),CCOc(t==25),CCOc(t==30),CCOc(t==35),CCOc(t==40),CCOc(
t==45),CCOc(t==50),CCOc(t==55),CCOc(t==60)];
CH2cal=[CH2c(t==0),CH2c(t==5),CH2c(t==10),
CH2c(t==15),CH2c(t==20),CH2c(t==25),CH2c(t==30),CH2c(t==35),CH2c(t==40),CH2c(
t==45),CH2c(t==50),CH2c(t==55),CH2c(t==60)];
CCO2cal=[CCO2c(t==0),CCO2c(t==5),CCO2c(t==10),CCO2c(t==15),CCO2c(t==20),CCO2c
(t==25),CCO2c(t==30),CCO2c(t==35),CCO2c(t==40),CCO2c(t==45),CCO2c(t==50),CCO2
c(t==55),CCO2c(t==60)];
CCH4cal=[CCH4c(t==0),CCH4c(t==5),CCH4c(t==10),CCH4c(t==15),CCH4c(t==20),CCH4c
(t==25),CCH4c(t==30),CCH4c(t==35),CCH4c(t==40),CCH4c(t==45),CCH4c(t==50),CCH4
c(t==55),CCH4c(t==60)];
CBIOMASScal=[CBIOMASSc(t==0),CBIOMASSc(t==5),CBIOMASSc(t==10),CBIOMASSc(t==15
),CBIOMASSc(t==20),CBIOMASSc(t==25),CBIOMASSc(t==30),CBIOMASSc(t==35),CBIOMAS
Sc(t==40),CBIOMASSc(t==45),CBIOMASSc(t==50),CBIOMASSc(t==55),CBIOMASSc(t==60)
];
CH2Ocal=[CH2Oc(t==0),CH2Oc(t==5),CH2Oc(t==10),CH2Oc(t==15),CH2Oc(t==20),CH2Oc
(t==25),CH2Oc(t==30),CH2Oc(t==35),CH2Oc(t==40),CH2Oc(t==45),CH2Oc(t==50),CH2O
c(t==55),CH2Oc(t==60)];
CLIQUIDcal=[CLIQUIDc(t==0),CLIQUIDc(t==5),CLIQUIDc(t==10),CLIQUIDc(t==15),
CLIQUIDc(t==20),CLIQUIDc(t==25),CLIQUIDc(t==30), CLIQUIDc(t==35),
CLIQUIDc(t==40), CLIQUIDc(t==45), CLIQUIDc(t==50), CLIQUIDc(t==55),
CLIQUIDc(t==60)];
Ccal = [CCOcal; CH2cal; CCO2cal;  CCH4cal; CBIOMASScal; CLIQUIDcal; CH2Ocal];


% ************ Define Error Parameter **************%
CError = abs(Ccal-Cexp)^2;
n=1;
error = sum(sum(CError))/n;

% ************ Reaction Time; Unit - Minutes **************

%Fmin search command to minimize the error function
[k,fval] = fminsearch(@err,KI);



function [f] = dCdt(Cinput)
%to calculate the reaction rate

run inputvalue;
C1 = Cinput(1); %CCO
C2 = Cinput(2); %CH2
C3 = Cinput(3); %CCO2
C4 = Cinput(4); %CCH4
C5 = Cinput(5); %CBIOMASS
C6 = Cinput(6); %CLIQUID
C7 = Cinput(7); %CWATER

% guessed k values
k1 = 0.0011;
k2 = 0.0462;
k3 = 0.1283;
k4 = 0.0956;
```

```
k5 = 0.376;
k6 = 0.0503;
k7 = 0.094;

dCCOdt = (2*k1*C5*C7)+(k2*C5)-(k5*C1*C7)-(k6*C1*C2);% FOR CO
dCH2dt = (1.58*k1*C5*C7)+(k5*C1*C7)-(3*k6*C1*C2); % FOR H2
dCCO2dt = (k3*C5)+(k5*C1*C7); %FOR CO2
dCH4dt = (k4*C5)+(k6*C1*C2); % FOR CH4
dCBIOMASSdt = (-2*k1*C5*C7)-(k2*C5)-(k3*C5)-(k4*C5)-(k7*C5); % for biomass
dCLIQUIDdt = (k7*C5);%for liquid
dCH2Odt = (-0.14*k1*C5*C7)-(k5*C1*C7)+(k6*C1*C2); % for water

f = [dCCOdt; dCH2dt; dCCO2dt; dCH4dt; dCBIOMASSdt; dCLIQUIDdt; dCH2Odt];
end



clear
run inputvalue
% ************ Initial Guess for Rate Constants **************
KI = [0.0025 0.0462 0.1283 0.0952 0.376 0.0503 0.00092];
% ************ Regression **************
%[k,fval] = fminsearch(@err,KI);
% ************ Optional Regression Command **************
%[k,fval] = fminunc(@err,KI);
% ************ Define Concentration and Step Time **************
CExp = [CCO; CH2;  CCO2;  CCH4; CBIOMASS; CLIQUID; CH2O;];
Cini = CExp(:,1);
tspan = (15:15:60);
% ************ Solving Ordinary Differential Equations **************
[t,C] = ode45(@KinODE,tspan,Cini,[],KI);
disp(C);
CCOc=C(:,1)';
CH2c=C(:,2)';
CCO2c=C(:,3)';
CCH4c=C(:,4)';
CBIOMASSc=C(:,5)';
CLIQUIDc=C(:,6)';
CH2Oc=C(:,7)';


CCOcal=[CCOc(t==15),CCOc(t==30),CCOc(t==45),CCOc(t==60)];
CH2cal=[CH2c(t==15),CH2c(t==30),CH2c(t==45),CH2c(t==60)];
CCO2cal=[CCO2c(t==15),CCO2c(t==30),CCO2c(t==45),CCO2c(t==60)];
CCH4cal=[CCH4c(t==15),CCH4c(t==30),CCH4c(t==45),CCH4c(t==60)];
CBIOMASScal=[CBIOMASSc(t==15),CBIOMASSc(t==30),CBIOMASSc(t==45),CBIOMASSc(t==
60)];
CLIQUIDcal=[CLIQUIDc(t==15), CLIQUIDc(t==30), CLIQUIDc(t==45),
CLIQUIDc(t==60)];
CH2Ocal=[CH2Oc(t==15),CH2Oc(t==30),CH2Oc(t==45),CH2Oc(t==60)];

Ccal = [CCOcal; CH2cal; CCO2cal; CCH4cal; CBIOMASScal; CLIQUIDcal; CH2Ocal];
```

Appendix E: Permissions to use manuscripts.

1. Permission to use published manuscript entitled " Okolie, J.A., Nanda, S., Dalai, A.K., Berruti, F. and Kozinski, J.A., 2020. A review on subcritical and supercritical water gasification of biogenic, polymeric and petroleum wastes to hydrogen-rich synthesis gas. Renewable and Sustainable Energy Reviews, 119, p.109546."

A review on subcritical and supercritical water gasification of biogenic, polymeric and petroleum wastes to hydrogen-rich synthesis gas

Author:

Jude A. Okolie,Sonil Nanda,Ajay K. Dalai,Franco Berruti,Janusz A. Kozinski

Publication:

Renewable and Sustainable Energy Reviews

Publisher:

Elsevier

Date:

March 2020

Journal Author Rights

Please note that, as the author of this Elsevier article, you retain the right to include it in a thesis or dissertation, provided it is not published commercially. Permission is not required, but please ensure that you reference the journal as the original source. For more information on this and on your other retained rights, please visit: https://www.elsevier.com/about/our-business/policies/copyright#Author-rights

BACK

CLOSE WINDOW

- Copyright Clearance Center, Inc.
- Privacy statement
- Terms and Conditions

2. Permission to use the published manuscript entitled “Okolie, J.A., Epelle, E.I., Nanda, S., Castello, D., Dalai, A.K. and Kozinski, J.A., 2021. Modeling and process optimization of hydrothermal gasification for hydrogen production: A comprehensive review. The Journal of Supercritical Fluids, p.105199”.

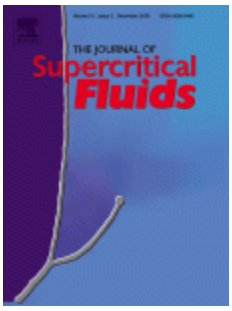

Modeling and process optimization of hydrothermal gasification for hydrogen production: A comprehensive review

Author:

Jude A. Okolie,Emmanuel I. Epelle,Sonil Nanda,Daniele Castello,Ajay K. Dalai,Janusz A. Kozinski

Publication:

The Journal of Supercritical Fluids

Publisher:

Elsevier

Date:

July 2021

Journal Author Rights

3. Permission to use the published manuscript entitled “Okolie, J.A., Rana, R., Nanda, S., Dalai, A.K. and Kozinski, J.A., 2019. Supercritical water gasification of biomass: a state-of-the-art review of process parameters, reaction mechanisms and catalysis. Sustainable energy & fuels, 3(3), pp.578-598”.

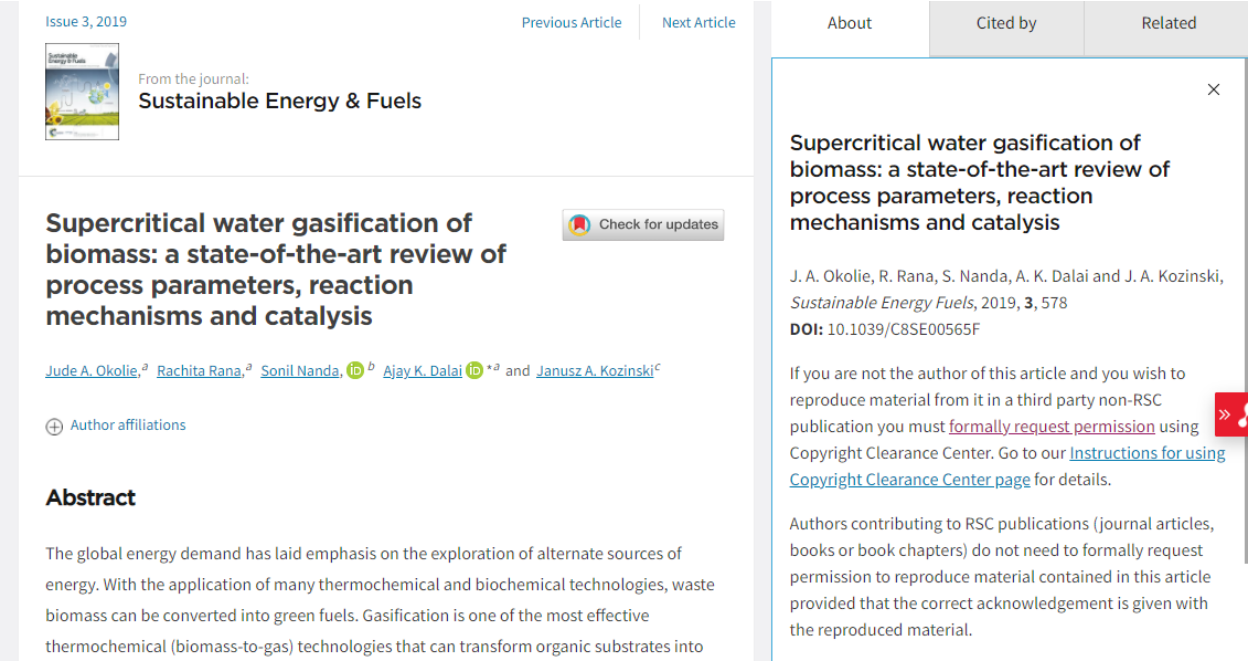

4. Permission to use the published manuscript entitled “Okolie, J.A., Nanda, S., Dalai, A.K. and Kozinski, J.A., 2020. Optimization and modeling of process parameters during hydrothermal gasification of biomass model compounds to generate hydrogen-rich gas products. International Journal of Hydrogen Energy, 45(36), pp.18275-18288”.

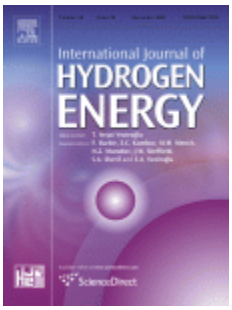

Optimization and modeling of process parameters during hydrothermal gasification of biomass model compounds to generate hydrogen-rich gas products

Author:

Jude A. Okolie,Sonil Nanda,Ajay K. Dalai,Janusz A. Kozinski

Publication:

International Journal of Hydrogen Energy

Publisher:

Elsevier

Date:

17 July 2020

Journal Author Rights

5. Permission to use published manuscript entitled “Okolie, J.A., Nanda, S., Dalai, A.K. and Kozinski, J.A., 2020. Hydrothermal gasification of soybean straw and flax straw for hydrogen-rich syngas production: Experimental and thermodynamic modeling. Energy Conversion and Management, 208, p.112545.”

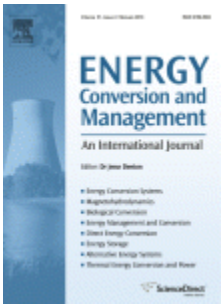

Hydrothermal gasification of soybean straw and flax straw for hydrogen-rich syngas production: Experimental and thermodynamic modeling

Author:

Jude A. Okolie,Sonil Nanda,Ajay K. Dalai,Janusz A. Kozinski

Publication:

Energy Conversion and Management

Publisher:

Elsevier

Date:

15 March 2020